UNIVERSITÀ DEGLI STUDI DI ROMA "TOR VERGATA"

UNIVERSIDAD AUTÓNOMA DE MADRID

Joining Corroles and Phthalocyanines in functional porphyrinoid arrays

Beatrice Berionni Berna

Supervisors:

Dr. Sara Nardis
Prof. Tomás Torres Cebada

Academic year 2016/2017

This work was developed as a joint PhD between the Department of Chemical Science and Technology of University of Rome Tor Vergata, under the supervision of Dr. Sara Nardis, and the Department of Organic Chemistry of The Autonomous University of Madrid, under the supervision of Prof. Dr. Tomás Torres Cebada.

This work was presented in the following articles:

- "Extending the corrole ring conjugation: preparation of β,β′-fused 2,3-[1′,2′-b]pyrazinocorroles". B. Berionni Berna, S. Nardis, F. Mandoj, F. R. Fronczek, K. M. Smith, R. Paolesse. *Org. Biomol. Chem*., **2016**,14, 2891-2897

- "β-Pyrrolopyrazino Annulated Corroles via a Pictet–Spengler Approach". B. Berionni Berna, S. Nardis, P. Galloni, A. Savoldelli, M. Stefanelli, F.R. Fronczek, K.M. Smith, R. Paolesse. *Org. Lett.*, **2016**, 18, 3318–3321

Pre-doctoral stay:

- Photophysical measurements were carried out in the group of Prof. Dirk M. Guldi in the Department of Chemistry and Pharmacy of Friedrich-Alexander-Universität of Erlangen-Nürnberg, Germany, May 2017.

Abbreviations and acronyms

Abbreviation and acronyms used in this thesis are listed in the "guidelines for authors" of *J. Org. Chem.* **2016**, and can be found in the journal webpage: http://pubs.acs.org/paragonplus/submission/joceah/joceah_authguide.pdf

A	Acceptor
AcOH	Acetic acid
Corr	Corrole
CR	Charge recombination
CS	Charge separation
CSR	Charge separation rate
CSS	Charge separation state
CT	Charge transfer
CV	Cyclic voltammetry
D	Donor
DBSA	p-dodecylbenzenesulfonic acid
DCTB	trans-2-[3-(4-tert-Butylphenyl)-2-methyl-2-propenylidene]malononitrile
DDQ	2,3-dichloro-5,6-dicyano-1,4-benzoquinone
DFT	Density functional theory
DPM	Dipyrromethane
DSSC	Dye-sensitized solar cell
ESI	Electrospray ionization
ε	Molar extinction coefficient
FAB	Fast atom bombardment
G	Guest
H	Host
HOMO	Highest occupied molecular orbital
λ	Wavelength
L	Linker
LUMO	Lowest unoccupied molecular orbital
MALDI	Matrix-assisted laser desorption ionization
o-DCB	*o*-Dichlorobenzene

Φ	Quantum Yield
Pc	Phthalocyanine
PET	Photoinduced electron transfer
PHT	Photoinduced hole transfer
Por	Porphyrin
TBAH	Tetrabutylammonium hexafluorophosphate
TBAP	Tetrabutylammonium perchlorate
TFA	Trifluoroacetic acid
THF	Tetrahydrofurane
TMS	Trimethylsilyl

Table of Contents

Summary

In the compendium of porphyrinoids, corroles have experienced increasing attention in the past two decades, starting from the disclosure in 1999 of simple routes for the synthesis of *meso*-triarylcorroles.[1,2] Since then, they have been successfully used in various contexts ranging from catalysis[3,4] to dye-sensitized solar cells.[5,6]

Peripheral modifications are important to modulate corrole properties and make them suitable for these applications. In this view, the synthetic availability of triarylcorroles has allowed a more detailed investigation of the corrole ring functionalization. Research under this heading will focus in particular on the synthesis and functionalization of new free base- and metallo-corrole derivatives.

The synopsis presented here reports a concise overview of the design, synthesis, structural, photophysical, electrochemical, and molecular modelling characterization of:

1. Expanded Corroles by β-fused aromatic rings.
2. Design and synthesis of new Phthalocyanine-Corrole hybrid conjugates for application in light harvesting systems.

This thesis consists of a general introduction and two chapters.

Introduction

In the introduction, a general description of corrole structure, reactivity and photophysical properties is presented. The main synthetic strategies to achieve symmetric and asymmetric corrole derivatives are briefly discussed, as well as their applications in different research fields. Lastly, general objectives of the present thesis are there highlighted.

Chapter 1

Among the different corrole functionalizations, we focused on the fusion of aromatic substituents at the macrocyclic β-positions. It is well known that in the case of porphyrins, the introduction of fused π-conjugated units strongly modifies the electronic character of the

---

(1) Gross, Z.; Galili, N.; Saltsman, I. The First Direct Synthesis of Corroles from Pyrrole. *Angew. Chem. Int. Ed.* **1999**, *38* (10), 1427–1429.

(2) Paolesse, R.; Mini, S.; Sagone, F.; Boschi, T.; Jaquinod, L.; Nurco, D. J.; Smith, K. M. 5,10,15-Triphenylcorrole: A Product from a Modified Rothemund Reaction. *Chem. Commun.* **1999**, *14*, 1307–1308.

(3) Saltsman, I.; Simkhovich, L.; Balazs, Y.; Goldberg, I.; Gross, Z. Synthesis, Spectroscopy, and Structures of New Rhodium(I) and Rhodium(III) Corroles and Catalysis Thereby. *Inorganica Chim. Acta* **2004**, *357* (10), 3038–3046.

(4) Zdilla, M. J.; Abu-Omar, M. M. Mechanism of Catalytic Aziridination with Manganese Corrole: The Often Postulated High-Valent Mn(V) Imido Is Not the Group Transfer Reagent. *J. Am. Chem. Soc.* **2006**, *128* (51), 16971–16979.

(5) Sudhakar, K.; Giribabu, L.; Salvatori, P.; Angelis, F. D. Triphenylamine-Functionalized Corrole Sensitizers for Solar-Cell Applications. *Phys. Status Solidi A* **2015**, *212* (1), 194–202.

(6) Wróbel, D. From Natural Photosynthesis to Molecular Photovoltaics. *Mol. Cryst. Liq. Cryst.* **2016**, *627* (1), 4–22.

resulting chromophores, allowing porphyrin systems with unique optical and electrochemical properties.[7,8]

Starting from the same substrate, a variety of π-extended corroles were obtained using two different synthetic pathways. The first methodology exploited a one-pot reaction of 2,3-diaminocorroles (or 2,3,17,18-tetraaminocorroles) with different diones, affording new corrole derivatives with *β*-fused pyrazino rings (**Figure 1**). X-ray crystallographic characterization and electronic absorption spectra highlight interesting features of these derivatives. An easy demetallation procedure allowed us to obtain the corresponding free base derivatives, opening the door to the preparation of different metal complexes, with the possible modulation of the related photophysical characteristics and potentially making these species suitable for optoelectronic applications.

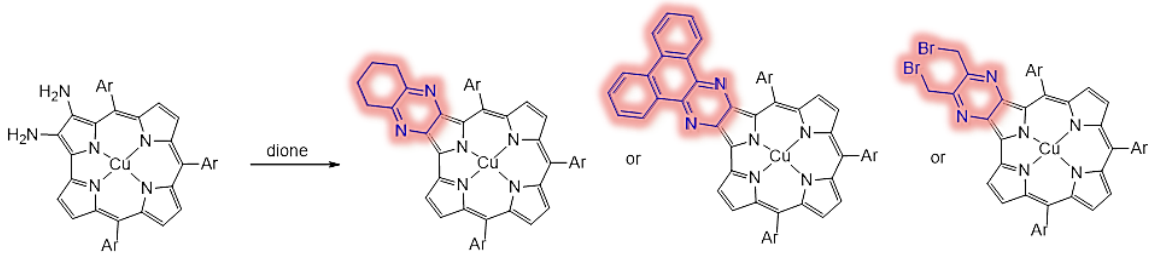

Figure 1. Synthesis of new *β*-annulated corrole derivatives *via* one-pot reduction and condensation with different diones.

The obtained results prompted us to investigate the development of other synthetic routes leading to π-expanded corroles with annulated pyrazino units. These groups are interesting because it has been shown that heterocycles containing a pyrrolo[1,2-a]pyrazino moiety (highlighted in purple in **Figure 2**) can play an important role in pharmacological terms.[9–13]

---

(7) Sessler, J. L.; Gebauer, A.; Vogel, E. Expanded Porphyrins. In *The Porphyrin Handbook*; Kadish, K. M.; Smith, K. M.; Guilard, R., 2000; Vol. II.

(8) Saegusa, Y.; Ishizuka, T.; Komamura, K.; Shimizu, S.; Kotani, H.; Kobayashi, N.; Kojima, T. Ring-Fused Porphyrins: Extension of π-Conjugation Significantly Affects the Aromaticity and Optical Properties of the Porphyrin π-Systems and the Lewis Acidity of the Central Metal Ions. *Phys. Chem. Chem. Phys.* **2015**, *17* (22), 15001–15011.

(9) Fisher, T. E.; Kim, B.; Staas, D. D.; Lyle, T. A.; Young, S. D.; Vacca, J. P.; Zrada, M. M.; Hazuda, D. J.; Felock, P. J.; Schleif, W. A.; et al. 8-Hydroxy-3,4-Dihydropyrrolo[1,2-a]Pyrazine-1(2H)-One HIV-1 Integrase Inhibitors. *Bioorg. Med. Chem. Lett.* **2007**, *17* (23), 6511–6515.

(10) Rault, S.; Lancelot, J. C.; Prunier, H.; Robba, M.; Renard, P.; Delagrange, P.; Pfeiffer, B.; Caignard, D. H.; Guardiola-Lemaitre, B.; Hamon, M. Novel Selective and Partial Agonists of 5-HT3 Receptors. Part 1. Synthesis and Biological Evaluation of Piperazinopyrrolothienopyrazines. *J. Med. Chem.* **1996**, *39* (10), 2068–2080.

(11) Dawidowski, M.; Chońska, J.; Mika, W.; Turło, J. Novel Fluorinated Pyrrolo[1,2-a]Pyrazine-2,6-Dione Derivatives: Synthesis and Anticonvulsant Evaluation in Animal Models of Epilepsy. *Bioorg. Med. Chem.* **2014**, *22* (19), 5410–5427.

(12) Arban, R.; Bianchi, F.; Buson, A.; Cremonesi, S.; Di Fabio, R.; Gentile, G.; Micheli, F.; Pasquarello, A.; Pozzan, A.; Tarsi, L.; et al. Pyrrolo[1,2-a]Pyrazine and Pyrazolo[1,5-a]Pyrazine: Novel, Potent, and Selective Series of Vasopressin 1b Receptor Antagonists. *Bioorg. Med. Chem. Lett.* **2010**, *20* (17), 5044–5049.

(13) Micheli, F.; Bertani, B.; Bozzoli, A.; Crippa, L.; Cavanni, P.; Di Fabio, R.; Donati, D.; Marzorati, P.; Merlo, G.; Paio, A.; et al. Phenylethynyl-Pyrrolo[1,2-a]Pyrazine: A New Potent and Selective Tool in the MGluR5 Antagonists Arena. *Bioorg. Med. Chem. Lett.* **2008**, *18* (6), 1804–1809.

In this reaction, already performed on porphyrins,[14] corrole reveals once again an unusual reactivity pattern, affording the unsubstituted pyrrolopyrazino substituent by an unprecedented reaction pathway. All the new derivatives were fully characterized, by means of ^{1}H NMR, UV-vis, electrochemical and X-ray techniques.

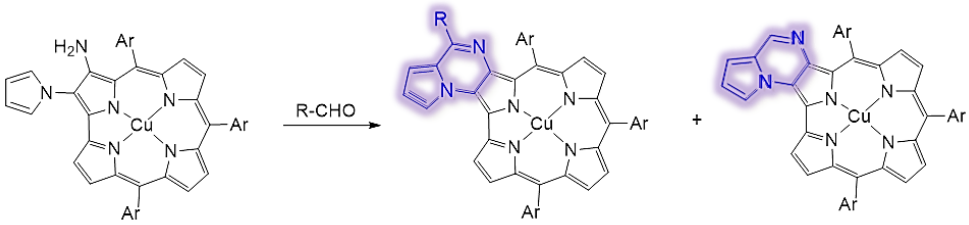

Figure 2. Synthesis of new *β*–annulated corrole derivatives *via* Pictet-Spengler reaction with different arylaldehydes.

Chapter 2

Chapter 2 focuses on the design, synthesis and photophysical studies of new functional materials for light harvesting applications.

In the last decade great attention has been focused on the preparation of porphyrin derivatives characterized by an expanded aromatic system, which causes a decrease in the HOMO-LUMO gap that leads to improved harvesting of solar energy in a broad spectral region.[15] These molecules are very promising as dyes in the study of photoinduced electron and energy transfer. Most of these artificial systems are made up of oligomeric species, where the porphyrin (or phthalocyanine) units are linked by bridges, such as for example ethynes, that allow macrocyclic conjugation.[16] To the best of our knowledge, no multicomponent systems based on corrole-phthalocyanine (Corr-Pc) have been described.

In the first section of this Chapter, we successfully synthesized two different corrole-phthalocyanine covalent dyes (**Figure 3**,left). The presence of a greater number of methoxy moieties in the corrole framework was expected to improve the electron-donor properties of the macrocycle and enhance the electron transfer to the linked zinc phthalocyanine bearing electron-withdrawing groups. The newly prepared multicomponent systems have been studied performing spectral, computational and electrochemical measurements. Transient absorption spectroscopy showed the appearance of a fast-forming and short-living charge separated states

---

(14) Singh, D. K.; Nath, M. Ambient Temperature Synthesis of β,B′-Fused Nickel(II) Pyrrolo[1,2-a]Pyrazinoporphyrins via a DBSA-Catalyzed Pictet–Spengler Approach. *Org. Biomol. Chem.* **2015**, *13* (6), 1836–1845.

(15) Hsieh, C.-P.; Lu, H.-P.; Chiu, C.-L.; Lee, C.-W.; Chuang, S.-H.; Mai, C.-L.; Yen, W.-N.; Hsu, S.-J.; Diau, E. W.-G.; Yeh, C.-Y. Synthesis and Characterization of Porphyrin Sensitizers with Various Electron-Donating Substituents for Highly Efficient Dye-Sensitized Solar Cells. *J. Mater. Chem.* **2010**, *20* (6), 1127–1134.

(16) Anderson, H. L. Building Molecular Wires from the Colours of Life: Conjugated Porphyrin Oligomers. *Chem. Commun.* **1999**, No. 23, 2323–2330.

constituted by the radical cation of corrole and radical anion of the phthalocyanine.

In the second part of the chapter, we have prepared a donor-acceptor ensemble built on metal-ligand coordination between a zinc(II) phthalocyanine derivative, bearing electron withdrawing groups at its periphery, and an electron-donor corrole, featuring a pyridyl moiety in position 10 (**Figure 3**,right). Binding studies were performed by means of NMR and photophysical techniques, in order to determine thermodynamic and kinetic constants.

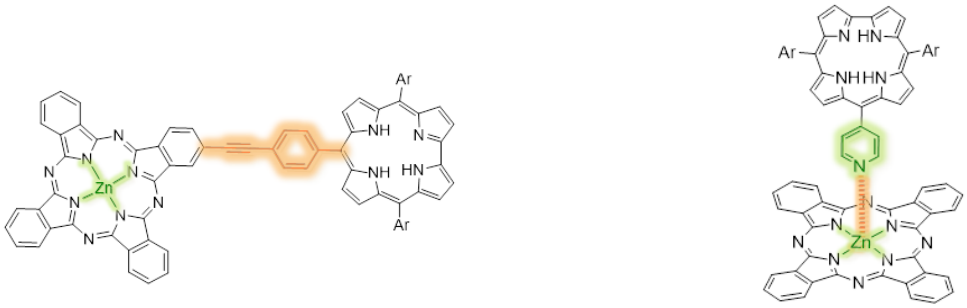

Figure 3. Schematic representation of covalently and supramolecular conjugated Corr-Pc that will be presented in Chapter 2.

Riassunto

All'interno della famiglia dei porfirinoidi, i corroli sono stati oggetto di crescente interesse da parte della comunità scientifica negli ultimi due decenni, da quando, nel 1999, sono state scoperte nuove strategie sintetiche per la sintesi di *meso*-triarilcorroli.[1,2]

Da allora, sono stati ampiamente utilizzati in differenti contesti e per diverse applicazioni, dalla catalisi[3,4] allo sviluppo di *dye-sensitized solar cells*.[5,6]

Al fine di rendere i corroli buoni candidati verso l'applicazione concreta, è necessario effettuare modifiche del macrociclo con opportuni sostituenti. La disponibilità sintetica di triarilcorroli a partire da aldeidi commercialmente disponibili ha reso possibile uno studio dettagliato sulla funzionalizzazione dell'anello centrale. In tale contesto si inserisce questa tesi, incentrata in particolar modo sulla sintesi e funzionalizzazione di nuovi derivati corrolici, come base libera o come complessi metallici.

Il riassunto qui presentato riporta una panoramica concisa su sintesi e caratterizzazioni strutturali, fotofisiche, elettrochimiche e computazionali di:

1. Corroli espansi mediante annulazione delle posizioni β-pirroliche.
2. Sintesi di nuovi sistemi Corrolo-Ftalocianina per applicazioni fotovoltaiche.

La suddetta tesi è costituita da un'introduzione generale e due capitoli.

Introduzione

La parte introduttiva fornisce una descrizione generale sui corroli, sulle relative caratteristiche di reattività e proprietà fotofisiche. Vengono inoltre presentate le strategie sintetiche più utilizzate per la sintesi di corroli simmetrici ed asimmetrici. Una sottosezione è dedicata alle applicazioni di tale macrociclo nei diversi ambiti di ricerca.

Infine, vengono presentati gli obiettivi generali di questo lavoro di tesi.

Capitolo 1

Tra le possibili funzionalizzazioni del macrociclo tetrapirrolico, ci siamo focalizzati sulla sintesi di sistemi aromatici fusi nelle posizioni β-pirroliche.

Nel caso delle porfirine è stato dimostrato come l'introduzione di sistemi π-fusi modifichi

---

(1) Gross, Z.; Galili, N.; Saltsman, I. The First Direct Synthesis of Corroles from Pyrrole. *Angew. Chem. Int. Ed.* **1999**, *38* (10), 1427–1429.

(2) Paolesse, R.; Mini, S.; Sagone, F.; Boschi, T.; Jaquinod, L.; Nurco, D. J.; Smith, K. M. 5,10,15-Triphenylcorrole: A Product from a Modified Rothemund Reaction. *Chem. Commun.* **1999**, *14*, 1307–1308.

(3) Saltsman, I.; Simkhovich, L.; Balazs, Y.; Goldberg, I.; Gross, Z. Synthesis, Spectroscopy, and Structures of New Rhodium(I) and Rhodium(III) Corroles and Catalysis Thereby. *Inorganica Chim. Acta* **2004**, *357* (10), 3038–3046.

(4) Zdilla, M. J.; Abu-Omar, M. M. Mechanism of Catalytic Aziridination with Manganese Corrole: The Often Postulated High-Valent Mn(V) Imido Is Not the Group Transfer Reagent. *J. Am. Chem. Soc.* **2006**, *128* (51), 16971–16979.

(5) Sudhakar, K.; Giribabu, L.; Salvatori, P.; Angelis, F. D. Triphenylamine-Functionalized Corrole Sensitizers for Solar-Cell Applications. *Phys. Status Solidi A* **2015**, *212* (1), 194–202.

(6) Wróbel, D. From Natural Photosynthesis to Molecular Photovoltaics. *Mol. Cryst. Liq. Cryst.* **2016**, *627* (1), 4–22.

fortemente il carattere elettronico del macrociclo, conferendo a tali sistemici nuove ed interessanti proprietà dal punto di vista ottico ed elettrochimico.[7,8]

A partire dallo stesso substrato, è stata ottenuta una rosa di differenti corroli π-espansi mediante due diversi approcci sintetici.

Nel primo caso è stata sfruttata una reazione di condensazione tra 2,3-diamminocorroli (o 2,3,17,18-tetraamminocorroli) e diversi dioni. Tale sintesi ha portato alla formazione di nuovo derivati corrolici caratterizzati da un'unità pirazinica di collegamento, annulata all'anello β-pirrolico (**Figura 1**). Tali strutture hanno mostrato interessanti proprietà, rilevate grazie a studi fotofisici e tecniche di diffrazione ai raggi X. Attraverso un semplice passaggio sintetico, è stato possibile demetallare i complessi, fornendo specie con nuove proprietà fotofisiche, che le rendono particolarmente adatte ad applicazioni in ambito optoelettronico.

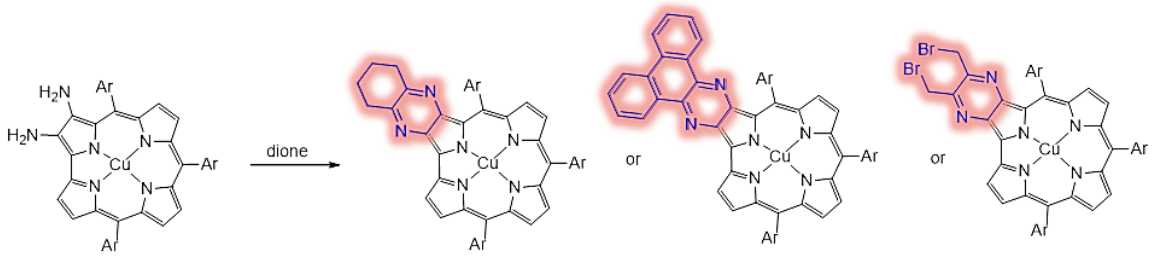

Figura 1. Sintesi di derivati corrolici *β*-fusi, mediante reazione di condensazione con diversi dioni.

I risultati ottenuti ci hanno spinto a continuare lo studio in questo ambito, alla ricerca di ulteriori strategie sintetiche che portassero alla formazione di corroli π-espansi annulati con funzionalità piraziniche. È stato inoltre dimostrato come eterocicli contenenti gruppi pirrolo[1,2-a]pyrazina

---

(7) Sessler, J. L.; Gebauer, A.; Vogel, E. Expanded Porphyrins. In *The Porphyrin Handbook*; Kadish, K. M.; Smith, K. M.; Guilard, R., 2000; Vol. II.

(8) Saegusa, Y.; Ishizuka, T.; Komamura, K.; Shimizu, S.; Kotani, H.; Kobayashi, N.; Kojima, T. Ring-Fused Porphyrins: Extension of π-Conjugation Significantly Affects the Aromaticity and Optical Properties of the Porphyrin π-Systems and the Lewis Acidity of the Central Metal Ions. *Phys. Chem. Chem. Phys.* **2015**, *17* (22), 15001–15011.

(9) Fisher, T. E.; Kim, B.; Staas, D. D.; Lyle, T. A.; Young, S. D.; Vacca, J. P.; Zrada, M. M.; Hazuda, D. J.; Felock, P. J.; Schleif, W. A.; et al. 8-Hydroxy-3,4-Dihydropyrrolo[1,2-a]Pyrazine-1(2H)-One HIV-1 Integrase Inhibitors. *Bioorg. Med. Chem. Lett.* **2007**, *17* (23), 6511–6515.

(10) Rault, S.; Lancelot, J. C.; Prunier, H.; Robba, M.; Renard, P.; Delagrange, P.; Pfeiffer, B.; Caignard, D. H.; Guardiola-Lemaitre, B.; Hamon, M. Novel Selective and Partial Agonists of 5-HT3 Receptors. Part 1. Synthesis and Biological Evaluation of Piperazinopyrrolothienopyrazines. *J. Med. Chem.* **1996**, *39* (10), 2068–2080.

(11) Dawidowski, M.; Chońska, J.; Mika, W.; Turło, J. Novel Fluorinated Pyrrolo[1,2-a]Pyrazine-2,6-Dione Derivatives: Synthesis and Anticonvulsant Evaluation in Animal Models of Epilepsy. *Bioorg. Med. Chem.* **2014**, *22* (19), 5410–5427.

(12) Arban, R.; Bianchi, F.; Buson, A.; Cremonesi, S.; Di Fabio, R.; Gentile, G.; Micheli, F.; Pasquarello, A.; Pozzan, A.; Tarsi, L.; et al. Pyrrolo[1,2-a]Pyrazine and Pyrazolo[1,5-a]Pyrazine: Novel, Potent, and Selective Series of Vasopressin 1b Receptor Antagonists. *Bioorg. Med. Chem. Lett.* **2010**, *20* (17), 5044–5049.

(13) Micheli, F.; Bertani, B.; Bozzoli, A.; Crippa, L.; Cavanni, P.; Di Fabio, R.; Donati, D.; Marzorati, P.; Merlo, G.; Paio, A.; et al. Phenylethynyl-Pyrrolo[1,2-a]Pyrazine: A New Potent and Selective Tool in the MGluR5 Antagonists Arena. *Bioorg. Med. Chem. Lett.* **2008**, *18* (6), 1804–1809.

(evidenziati in viola in **Figura 2**) rivestano un ruolo di indubbia importanza in termini farmaceutici.[9–13]

In questa reazione, riportata precedentemente sulle porfirine,[14] i corroli mostrano ancora una volta una reattività inusuale, portando a derivati recanti unità pirrolo-pirazina mediante meccanismi di reazione del tutto caratteristici. Studi elettrochimici, di risonanza magnetica nucleare, di assorbimento UV-vis e di diffrazione ai raggi X, hanno permesso una completa caratterizzazione di tutti i composti sintetizzati.

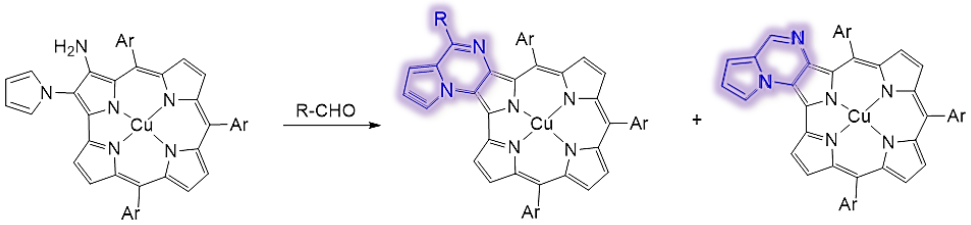

Figura 2. Sintesi di derivati corrolici annulati nelle posizioni *β*-pirroliche mediante reazione di Pictet-Spengler con diverse ariladeidi.

Capitolo 2

Il secondo capitolo della presente tesi si incentra sulla sintesi di nuovi materiali per fotovoltaico organico e sui relativi studi fotofisici.

Nell'ultimo decennio sono stati studiati in maniera approfondita sistemi porfirinici caratterizzati da un sistema aromatico espanso. L'espansione causa una diminuzione dell'intervallo energetico HOMO-LUMO, portando a sistemi che assorbono in maniera più efficiente la radiazione luminosa, in una vasta regione spettrale.[15] Tali molecole risultano estremamente promettenti come cromofori per lo studio di trasferimento energetico e/o elettronico fotoindotto. La maggior parte di questi sistemi sono costituiti da specie oligomeriche, come ad esempio unità porfiriniche (o ftalocianine) unite da ponti che ne permettano la coniugazione (es: gruppi acetilene).[16]

Ad oggi, nessun sistema basato su corrolo-ftalocianina (Corr-Pc) è stato ancora descritto in questo contesto.

Nella prima sezione di questo capitolo, sono state sintetizzate due diadi covalenti corrolo-

---

(14) Singh, D. K.; Nath, M. Ambient Temperature Synthesis of β,B'-Fused Nickel(II) Pyrrolo[1,2-a]Pyrazinoporphyrins via a DBSA-Catalyzed Pictet–Spengler Approach. *Org. Biomol. Chem.* **2015**, *13* (6), 1836–1845.

(15) Hsieh, C.-P.; Lu, H.-P.; Chiu, C.-L.; Lee, C.-W.; Chuang, S.-H.; Mai, C.-L.; Yen, W.-N.; Hsu, S.-J.; Diau, E. W.-G.; Yeh, C.-Y. Synthesis and Characterization of Porphyrin Sensitizers with Various Electron-Donating Substituents for Highly Efficient Dye-Sensitized Solar Cells. *J. Mater. Chem.* **2010**, *20* (6), 1127–1134.

(16) Anderson, H. L. Building Molecular Wires from the Colours of Life: Conjugated Porphyrin Oligomers. *Chem. Commun.* **1999**, No. 23, 2323–2330.

ftalocianina (**Figura 3** , sinistra).

È stata studiata l'influenza delle diverse unità metossi presenti nel corrolo sull'efficienza di trasferimento elettronico verso la zinco ftalocianina, recante gruppi elettron-attrattori.

Tali sistemi sono stati studiati mediante analisi fotofisiche, computazionali ed elettrochimiche. Inoltre, studi di spettroscopia ad assorbimento transiente hanno mostrato la formazione di specie a separazione di carica, costituite dal corrolo radicale catione e dalla corrispondente ftalocianina radicale anione.

Nella seconda parte del capitolo, è stato preparato un complesso donatore-accettore costituito da un corrolo recante gruppi elettron-donatori, e una zinco ftalocianina con funzionalità ad attrazione elettronica. Il suddetto complesso è stato formato in soluzione mediante coordinazione assiale tra lo zinco della ftalocianina e un gruppo piridinico presente nella posizione 10 del macrociclo corrolico (**Figura 3**, destra). Sono stati effettuati studi di binding mediante risonanza magnetica nucleare e tecniche fotofisiche, con il fine di stimare le costanti cinetiche e termodinamiche che governano il processo di formazione del complesso.

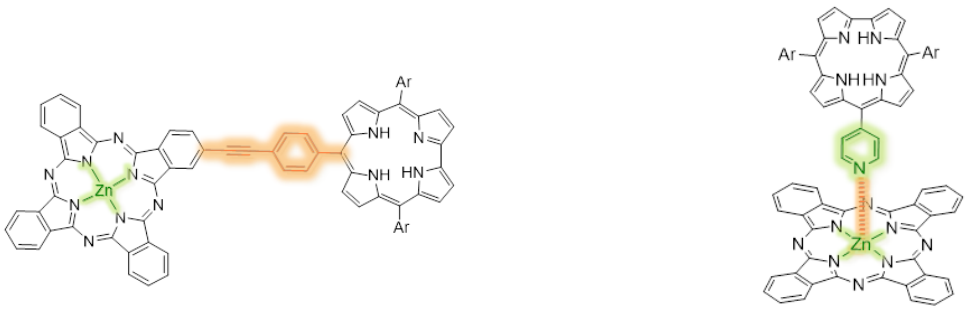

Figura 3. Rappresentazione schematica delle diadi covalente (a sinistra) e supramolecolare (destra) illustrate nel capitolo 2 della presente tesi.

Resumen

Dentro de la familia de los porfirinoides, los corroles han sido objeto de estudio en las últimas dos décadas, desde que, en el 1999, fueron descubiertas nuevas estrategias sintéticas para la síntesis de *meso*-triarilcorroles.[1,2] Desde entonces, dichas moléculas han sido ampliamente utilizadas en distintos ámbitos para diversas aplicaciones, desde catálisis, hasta el desarrollo de *dye-sensitized solar cells*.[5,6]

Con el fin de convertir a los corroles en buenos candidatos para su aplicación concreta, es necesario modificar el macrociclo mediante la introducción de sustituyentes apropiados.

La disponibilidad sintética de triarilcorroles a partir de aldehídos comercialmente accesibles, ha hecho sí que empezase un estudio detallado sobre la funcionalización del anillo central de dicho macrociclo. En este contexto se enmarca esta tesis, que se centra de un modo especial en la síntesis y funcionalización de nuevos derivados corrólicos, como base libre o como complejos metálicos.

Este resumen presenta una panorámica concisa acerca de la síntesis y caracterización estructural, fotofísica, electroquímica y computacional de:

1. Corroles expandidos mediante fusión de las posiciones β-pirrólicas.
2. Síntesis de nuevos sistemas Corrol-Ftalocianina para aplicaciones fotovoltaicas.

Dicha tesis consta de una introducción general y dos capítulos.

Introducción

La introducción proporciona una descripción general sobre los corroles, sobre las relativas características de reactividad y propiedades fotofísicas. Se presentan las estrategias sintéticas más utilizadas para la síntesis de corroles tanto simétricos como asimétricos. Una de sus secciones está dedicada a las aplicaciones de estos macrociclos en las distintas áreas de investigación.

A continuación, se presentan los objetivos generales de este trabajo de tesis.

Capítulo 1

Entre las posibles funcionalizaciones del macrociclo tetrapirrólico, nos hemos centrado en la síntesis de sistemas aromáticos fusionados en las posicione β-pirrolicas.

---

(1) Gross, Z.; Galili, N.; Saltsman, I. The First Direct Synthesis of Corroles from Pyrrole. *Angew. Chem. Int. Ed.* **1999**, *38* (10), 1427–1429.

(2) Paolesse, R.; Mini, S.; Sagone, F.; Boschi, T.; Jaquinod, L.; Nurco, D. J.; Smith, K. M. 5,10,15-Triphenylcorrole: A Product from a Modified Rothemund Reaction. *Chem. Commun.* **1999**, *14*, 1307–1308.

(3) Saltsman, I.; Simkhovich, L.; Balazs, Y.; Goldberg, I.; Gross, Z. Synthesis, Spectroscopy, and Structures of New Rhodium(I) and Rhodium(III) Corroles and Catalysis Thereby. *Inorganica Chim. Acta* **2004**, *357* (10), 3038–3046.

(4) Zdilla, M. J.; Abu-Omar, M. M. Mechanism of Catalytic Aziridination with Manganese Corrole: The Often Postulated High-Valent Mn(V) Imido Is Not the Group Transfer Reagent. *J. Am. Chem. Soc.* **2006**, *128* (51), 16971–16979.

(5) Sudhakar, K.; Giribabu, L.; Salvatori, P.; Angelis, F. D. Triphenylamine-Functionalized Corrole Sensitizers for Solar-Cell Applications. *Phys. Status Solidi A* **2015**, *212* (1), 194–202.

(6) Wróbel, D. From Natural Photosynthesis to Molecular Photovoltaics. *Mol. Cryst. Liq. Cryst.* **2016**, *627* (1), 4–22.

En el caso de las porfirinas, se ha demostrado que la introducción de sistemas π-fundidos modifica notablemente el carácter electrónico del macrociclo, otorgando a dichos sistemas nuevas y interesantes propiedades desde un punto de vista óptico y electroquímico.[7,8] A partir del mismo substrato, se han obtenido distintos corroles π-expandidos mediante dos estrategias sintéticas distintas. En el primer caso, hemos utilizado una reacción de condensación entre 2,3-diaminocorroles (o 2,3,17,18-tetraaminocorroles) y distintas dionas. Dicha síntesis conlleva la formación de nuevos derivados corrólicos, caracterizados por una unidad pirazínica de enlace, fundida al anillo *β*-pirrólico (**Figura 1**). Estas estructuras han mostrado propiedades interesantes, detectadas gracias a estudios fotofísicos y técnicas de difracción de rayos X. A través de un único y sencillo paso sintético, ha sido posible demetalar los complejos, obteniendo especies con nuevas propiedades fotofísicas, que las hacen particularmente adecuadas para aplicaciones en el ámbito optoelectrónico.

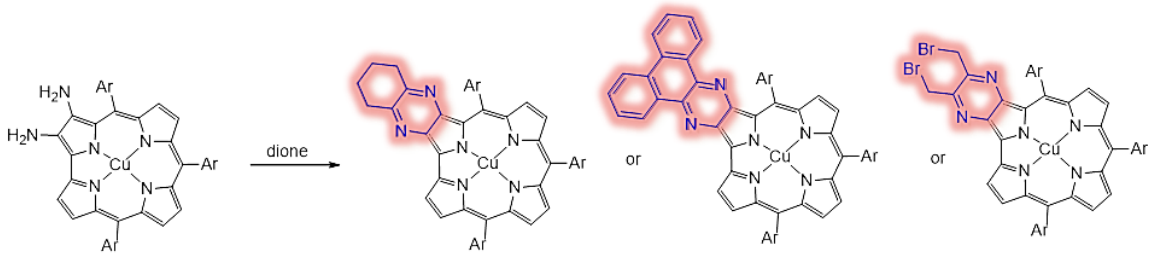

Figura 1. Síntesis de nuevos derivados de corroles mediante reacción de condensación con distintas dionas.

Los resultados obtenidos nos han animado a continuar con el estudio en este ámbito, en la búsqueda de estrategias sintéticas ulteriores para la formación de corroles π-expandidos, fundidos con funcionalizaciones pirazínicas. Además, ha sido descrito que heterociclos con grupos pirrol [1,2-a] pirazina (mostrado en morado en **Figura 2**) podrían tener un papel importante en términos farmacéuticos.[9–13]

---

(7) Sessler, J. L.; Gebauer, A.; Vogel, E. Expanded Porphyrins. In *The Porphyrin Handbook*; Kadish, K. M.; Smith, K. M.; Guilard, R., 2000; Vol. II.

(8) Saegusa, Y.; Ishizuka, T.; Komamura, K.; Shimizu, S.; Kotani, H.; Kobayashi, N.; Kojima, T. Ring-Fused Porphyrins: Extension of π-Conjugation Significantly Affects the Aromaticity and Optical Properties of the Porphyrin π-Systems and the Lewis Acidity of the Central Metal Ions. *Phys. Chem. Chem. Phys.* **2015**, *17* (22), 15001–15011.

(9) Fisher, T. E.; Kim, B.; Staas, D. D.; Lyle, T. A.; Young, S. D.; Vacca, J. P.; Zrada, M. M.; Hazuda, D. J.; Felock, P. J.; Schleif, W. A.; et al. 8-Hydroxy-3,4-Dihydropyrrolo[1,2-a]Pyrazine-1(2H)-One HIV-1 Integrase Inhibitors. *Bioorg. Med. Chem. Lett.* **2007**, *17* (23), 6511–6515.

(10) Rault, S.; Lancelot, J. C.; Prunier, H.; Robba, M.; Renard, P.; Delagrange, P.; Pfeiffer, B.; Caignard, D. H.; Guardiola-Lemaitre, B.; Hamon, M. Novel Selective and Partial Agonists of 5-HT3 Receptors. Part 1. Synthesis and Biological Evaluation of Piperazinopyrrolothienopyrazines. *J. Med. Chem.* **1996**, *39* (10), 2068–2080.

(11) Dawidowski, M.; Chońska, J.; Mika, W.; Turło, J. Novel Fluorinated Pyrrolo[1,2-a]Pyrazine-2,6-Dione Derivatives: Synthesis and Anticonvulsant Evaluation in Animal Models of Epilepsy. *Bioorg. Med. Chem.* **2014**, *22* (19), 5410–5427.

(12) Arban, R.; Bianchi, F.; Buson, A.; Cremonesi, S.; Di Fabio, R.; Gentile, G.; Micheli, F.; Pasquarello, A.; Pozzan, A.; Tarsi, L.; et al. Pyrrolo[1,2-a]Pyrazine and Pyrazolo[1,5-a]Pyrazine: Novel, Potent, and Selective Series of Vasopressin 1b Receptor Antagonists. *Bioorg. Med. Chem. Lett.* **2010**, *20* (17), 5044–5049.

(13) Micheli, F.; Bertani, B.; Bozzoli, A.; Crippa, L.; Cavanni, P.; Di Fabio, R.; Donati, D.; Marzorati, P.; Merlo, G.; Paio, A.; et al. Phenylethynyl-Pyrrolo[1,2-a]Pyrazine: A New Potent and Selective Tool in the MGluR5 Antagonists Arena. *Bioorg. Med. Chem. Lett.* **2008**, *18* (6), 1804–1809.

En esta reacción, conseguida primero en porfirinas,[14] los corroles muestran de nuevo una reactividad inusual, formando derivados que llevan una unidad pirrol-pirazina a través de mecanismos de reacción característicos. Estudios electroquímicos, de resonancia magnética nuclear, de espectroscopia UV-vis y de difracción de rayos X han permitido la completa caracterización de todos los compuestos sintetizados.

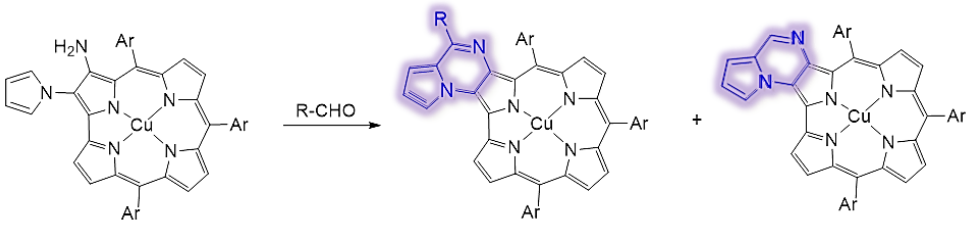

Figura 2. Síntesis de derivados de corroles *β*–fusionados mediante reacción de Pictet-Spengler con distintos ariladehídos.

.

Capítulo 2

El segundo capítulo de la presente tesis se centra en la síntesis de nuevos materiales para aplicaciones fotovoltaicas y en su consecuente estudio fotofísico.

En la última década se han estudiado en profundidad sistemas porfirínicos caracterizados por un sistema aromático expandido. Dicha expansión provoca una disminución del gap HOMO-LUMO, llevando a la formación de sistemas que absorben de manera más eficiente la radiación lumínica, en una amplia región espectral.[15]

Estas moléculas resultan extremadamente prometedoras como cromóforos para el estudio de transferencia energética o electrónica fotoinducida. La mayoría de dichos sistemas están constituidos por especies oligoméricas, como por ejemplo unidades de porfirinas (o ftalocianinas), unidas a través de puentes que permitan la conjugación del sistema (grupos acetilenos por ejemplo).[16]

Hasta donde sabemos, ningún sistema basado en corrol-ftalocianina (Corr-Pc) ha sido descrito en este contexto.

---

(14) Singh, D. K.; Nath, M. Ambient Temperature Synthesis of β,B'-Fused Nickel(II) Pyrrolo[1,2-a]Pyrazinoporphyrins via a DBSA-Catalyzed Pictet–Spengler Approach. *Org. Biomol. Chem.* **2015**, *13* (6), 1836–1845.

(15) Hsieh, C.-P.; Lu, H.-P.; Chiu, C.-L.; Lee, C.-W.; Chuang, S.-H.; Mai, C.-L.; Yen, W.-N.; Hsu, S.-J.; Diau, E. W.-G.; Yeh, C.-Y. Synthesis and Characterization of Porphyrin Sensitizers with Various Electron-Donating Substituents for Highly Efficient Dye-Sensitized Solar Cells. *J. Mater. Chem.* **2010**, *20* (6), 1127–1134.

(16) Anderson, H. L. Building Molecular Wires from the Colours of Life: Conjugated Porphyrin Oligomers. *Chem. Commun.* **1999**, No. 23, 2323–2330.

En la primera sección de este capítulo, se han sintetizado dos díadas covalentes corrol-ftalocianina (**Figura 3**, izquierda).

Hemos estudiado la influencia de distintas unidades metoxi, presentes en el corrol, sobre la eficiencia de transferencia electrónica hacia la ftalocianina de zinc, que lleva grupos atractores de electrones. Dichos sistemas han sido estudiados a través de análisis fotofísicos, computacionales y electroquímicos. Además, estudios de espectroscopía resuelta en el tiempo han evidenciado la formación de especies a separación de carga, formadas por el corrol radical catión y la correspondiente ftalocianina radical anión.

En la segunda parte del capítulo, se ha preparado un complejo dador-aceptor que consta de un corrol con grupos dadores de electrones y una ftalocianina de zinc con grupos atractores. Dicho complejo ha sido formado en disolución a través de coordinación axial entre el zinc de la ftalocianina y un grupo piridínico presente como funcionalización corrólica en posición 10 del anillo (**Figura 3**, derecha). Se han realizado estudios de binding a través de resonancia magnética nuclear y de técnicas fotofísicas, con la finalidad de evaluar las constantes cinéticas y termodinámicas que regulan el proceso de formación del complejo.

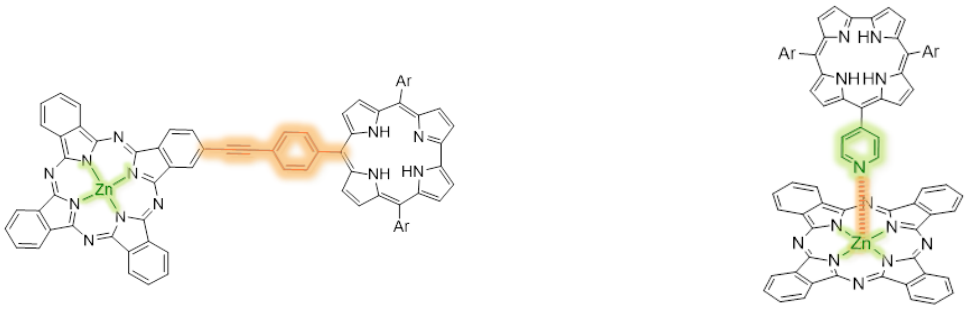

Figura 3. Representación esquemática de díadas Corr-Pc covalentes (izquierda) y supramoleculares (derecha).

Introduction

Corroles

The history of corroles begins in the second decade of the 20th century with George Whipple, who studied the influence of diet on regeneration of hemoglobin in dogs with anemia, with particular attention to liver-rich diets. In 1926, with this aim in mind, George Minot and William Murphy applied the liver diet to patients with pernicious anemia and they observed that the same diet rich in raw liver restored the normal red blood cell level. This new therapy, called "liver therapy", applied to the treatment of pernicious anemia, earned G. Minot, G. Whipple and W. Murphy jointly the Nobel Prize for Physiology and Medicine in 1934.[1]

In those years the scientific community focused on the discovery of the active principle of this new method. In the late 1940s, Rickes *et al.*, isolated a red crystalline pigment from the liver, which was designated as vitamin B_{12}.[2] In 1949, Pierce *et al*. isolated two crystalline forms of vitamin B_{12}, equally effective in combating pernicious anemia: cyanocobalamin and hydroxycobalamin.[3] In 1956, Dorothy Crowfoot-Hodgkin, through X-ray diffraction studies, elucidated the structure of cyanocobalamin and its coenzyme forms.[4] The Nobel Prize in Chemistry 1964 was awarded to Hodgkin "for her determinations by X-ray techniques of the structures of important biochemical substances".[5] These studies identified for the first time a new type of macrocycle called Corrin. With the aim of discovering new strategies for the preparation of corrins, Jonhson and Price discovered a synthetic route to prepare various metal derivatives of a macrocycle containing eleven double bonds, which was called Corrole (**Figure 1, Structure I**).[6] Five years later, Jonhson and Kay corrected the 1st structure and suggested the term corrole to designate the macrocycle (**Figure 1, Structure II**) containing ten double bonds.[7] This structure was unambiguously confirmed by Harrison

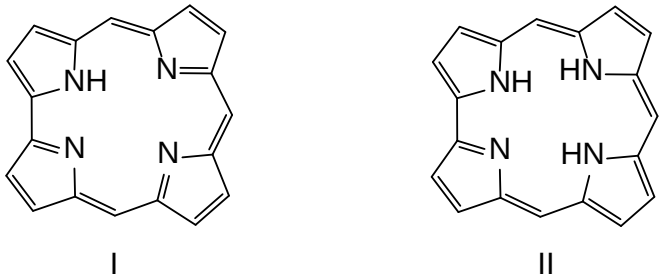

I II

Figure 1. Proposed structures of corrole.

et al., through the X-ray diffraction of the 8,12-diethyl-2,3,7,13,17,18-hexamethylcorrole.[8]

Despite being discovered over fifty years ago, for a long time corroles chemistry has not been investigated as much as porphyrins one. One of the reasons for this lack of interest was probably due to the multi-step, lengthy and laborious preparation of the macrocycle, which precluded the study of corrole to researchers not familiar with pyrrole chemistry. Since 1999, corrole-related research has experienced an impressive growth, when simple synthetic routes for the preparation of *meso*-triarylcorroles, starting from the commercially available pyrrole and arylaldehydes, were reported, thus allowing a more detailed characterization of the chemistry of the macrocycle.[9–12]

From 1999 onwards, the number of publications has dramatically increased, paving the way for new research areas in corrole chemistry (**Figure 2**).

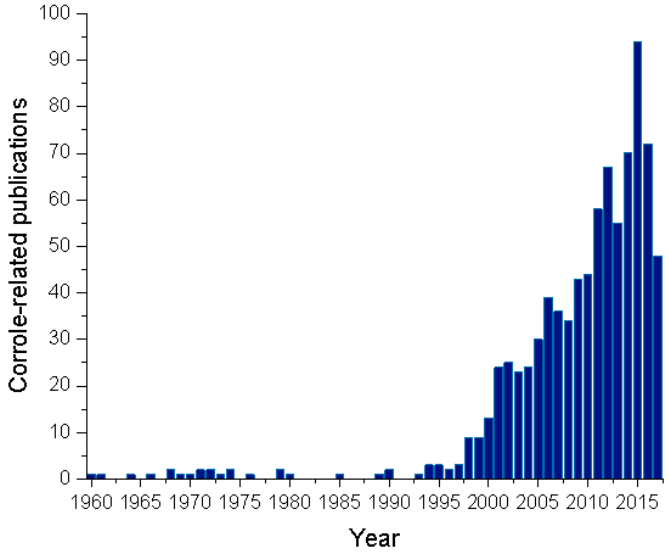

Figure 2. Number of corrole-related publications from 1960 to 2017.

General behaviour and synthesis of free bases or metal complexes of triarylcorroles bearing either the same or different substituents on the *meso* positions (A_3 or A_2B corroles, respectively), have been reported in the very next sections (**Figure 9**).

Structure and General Properties

Corroles are aromatic tetrapyrrole macrocycles bearing a direct pyrrole-pyrrole link, thereby constituting a bridge between porphyrins and corrins. Contrary to what happens with other tetrapyrroles, like porphyrins, chlorins, and bacteriochlorins, which play vital functions in nature, corroles are not natural compounds. The corrole macrocycle is structurally related to the corrin, with a 19-atom carbon skeleton, and maintains the 18-electron π aromatic system such as porphyrin, i.e. only nine of the ten double bonds in the macrocycle contribute to the aromatic character. IUPAC nomenclature of corroles has been derived from that of the porphyrins and, to retain comparability, position 20 has been omitted. The 5, 10 and 15 positions on the ring are referred to *meso*-positions, while the 2, 3, 7, 8, 12, 13, 17 and 18 ring positions are referred to *β*-pyrrole. Inner core N-atoms denoted to be 21, 22, 23 and 24 (**Figure 3**).[13–16]

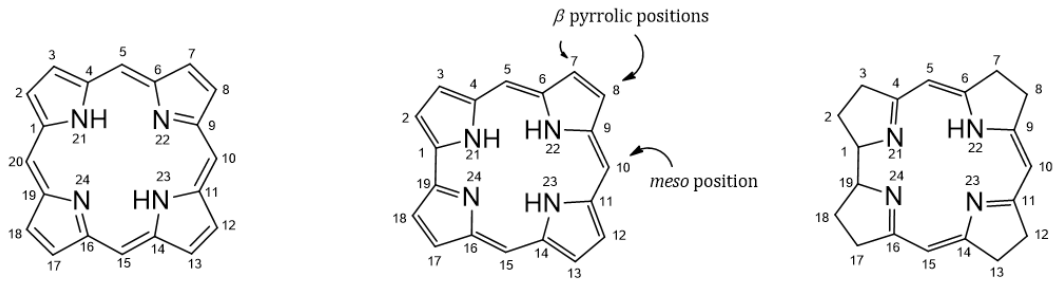

Figure 3. Porphyrin, corrole and corrin numbering systems.

According to the studies carried out by Dyke *et al*.[17] the imino nitrogen atom in the corrole inner core is preferably located at position 22. However, in 1997, Ghosh and Jynge performed a theoretical study that suggested the existence of different tautomers, with no real difference in energy among the possible isomers. This, coupled with the presence of short strong N-H···N hydrogen bonds, suggests that N-H tautomerism in free-base corrole isomers should be considerably faster than that in porphyrins (**Scheme 1**).[18]

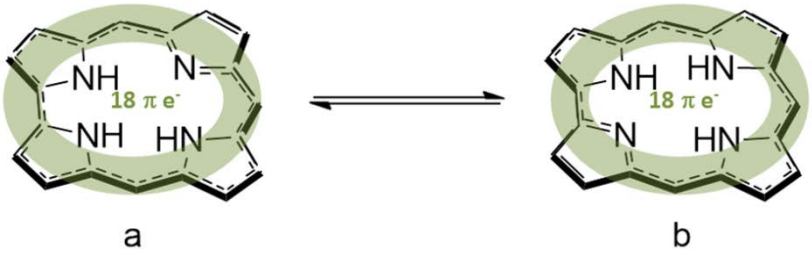

Scheme 1. Two tautomers of corroles where NH protons are assigned to different rings.

In this work, the structure **b** will be used as representative structure of the corrole macrocycle.

Despite nearly 50 years of corrole research, only few unsubstituted free-base corrole crystal structures have been published.[8,12,19–22]. As shown by X-ray analysis of 5,10,15-triphenylcorrole (H_3TPC) (**Figure 4**), the steric repulsion between inner protons causes a deviation from planarity, with one pyrrole ring tilted out of the mean plan of the macrocycle.[20] However corroles have an unexpected flexibility of molecular structure, which retains a quite planar conformation even if all the peripheral positions are substituted.

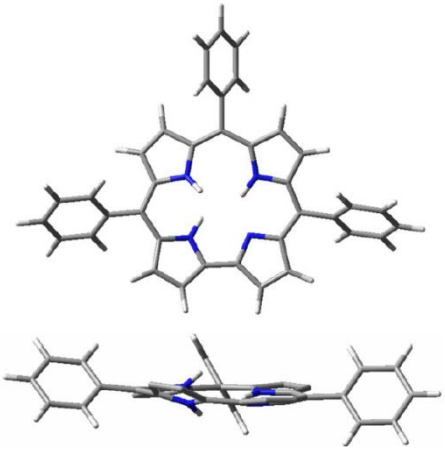

Figure 4. Structure of H_3TPC; Top: plane view; Bottom: side view (H-atoms on *β*-pyrrole are omitted for clarity).

Corrole derivatives show similar photophysical properties as porphyrins, such as visible light absorption. Their UV-vis spectra show an intense band (ε = 120000 $M^{-1}cm^{-1}$) in the region of 400-440 nm, which is considered to arise from a combination of the second $\pi \rightarrow \pi^*$ transition and its vibrational components, and weaker absorption bands between

500-700 nm (ε = 10000-15000 $M^{-1}cm^{-1}$). By analogy with in the porphyrins, they are designed as Soret and Q bands, respectively, thus confirming the presence of an aromatic system (**Figure 5**).

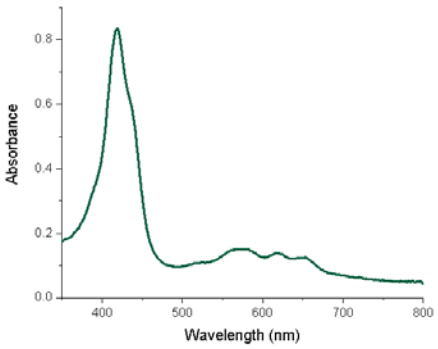

Figure 5. UV-vis spectrum of triarylcorroles.

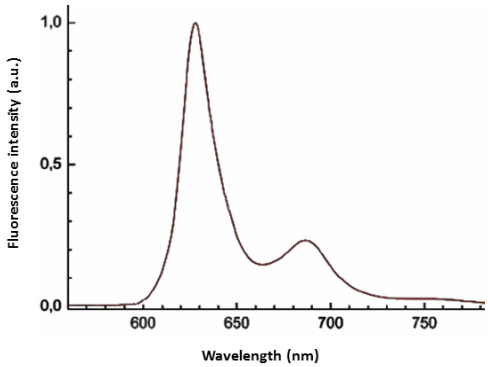

Figure 6. Emission spectrum of triarylcorroles.

The absorption spectra of corroles, particularly *meso*-triaryl corroles, exhibit two important differences with respect to the absorption spectra of porphyrins: a greater variation in the optical bands upon changing substitution on the phenyl groups and a significant solvent dependent shift in their absorption bands. In polar solvents, this dependence is justified by the internal hydrogen bonding interactions between the NH groups and the solvent.[23,24]

Corroles display an intense luminescence band (**Figure 6**) around 670-710 nm; lifetime is in the nanoseconds region with a very small Stokes shift[12] and a quantum yield of 0.07-0.08; this band could be assign to the singlet of the lowest π→π* transition observed in the absorption spectrum. For *meso*-arylcorroles noticeable changes are observed in intensity and position of the bands on changing the nature of the solvent. For example, fluorescence quantum yield of 5,10,15-triphenylcorrole decreases when dielectric constant of solvents increases while 5,10,15-tris (pentafluorophenyl) corrole doubles its value in polar solvents.[23,24]

By means of ^{1}H NMR spectroscopy the aromatic character of the corroles is confirmed.

The presence of the typical ring current leads to a high field shift NH inner protons, showing negative values of chemical shifts, (around -2 ppm) although this signal is usually not observed due to the rapid tautomeric exchange. *β*-pyrrolic protons resonate at low-field, usually in the range between 7 to 9 ppm.

Although the structure is not completely planar, and due to its reduced symmetry, ^{1}H NMR spectrum of corroles shows a macrocycle with a C_{2v} symmetry, that is, the parts [A-B] and [C-D] are magnetically and chemically equivalent due to the rapid exchange of protons between rings B and C (**Figure 7**).[14,25,26]

Moreover, while fully symmetric porphyrins show one singlet for pyrrolic protons, corroles have 4 doublets, each of them referred to two protons. These signals appear in this order moving from low to high field: (H2,18) > (H7,13) > (H3,17) ≈ (H8,12), even if the presence of other substituents may affects their chemical shifts.

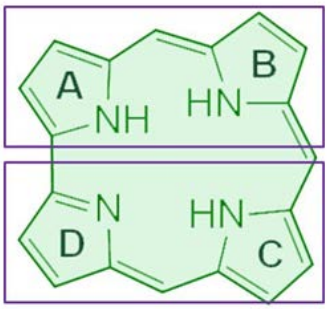

Figure 7. Corrole structure showing C_{2v} symmetry.

Corroles free base exhibit an amphoteric character.[15] They are stronger acids than the porphyrins, due to the greater stereo tension created by the three groups NH within the inner core. Free base derivatives readily form monoanionic species in dilute basic solutions (**Scheme 2**); which retain their aromatic behaviour and the Soret band in their electronic absorption spectra.

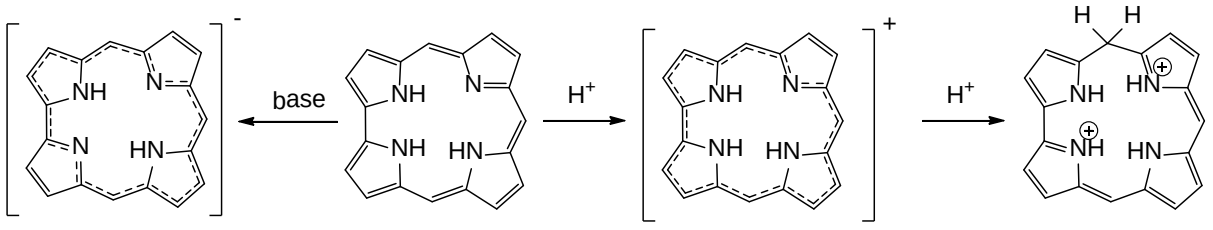

Scheme 2. Acid-base equilibria of corrole free base.

By treatment with weak acid, corroles generate monoprotonated derivatives. These monocationic species are still aromatic, indicating that the addition of a proton occurs at the inner core nitrogen atom.

Both charged forms are aromatic and have in their absorption spectra more intense Q-bands than the respective neutral forms. The presence of electron withdrowing or donating groups in the aryl moieities of the *meso* positions also influences the formation of these species.[27,28]

Stronger acid conditions result in the disappearance of the Soret band, since the conjugated aromatic π system is interrupted due to the formation of a dicationic species. Spectroscopic analysis indicates that the protonation occurred at the C-5 carbon (or 15) (**Scheme 2**).[14,15,29]

The three NH groups within the ring make the corrole a tetradentate trianionic ligand, different from corrins and porphyrins which are, respectively, monoanionic and dianionic ligands.

Corrolate ligand supports unusually high metal oxidation states, such as Cr (V), Fe (III) and Fe (IV), Co (IV) and Co (V), Mn (III). Acting as trianionic ligands, and being their internal cavity smaller than that of porphyrin, it is able to stabilize metallic ions with lower ionic radius and with a higher oxidation state.[30] Generally, the most stable oxidation number in the metallocorrolates is the oxidation state three. According to Density Functional Theory (DFT) calculations , gallium ion with oxidation state of +*3*, Ga (III), is the metal ion that best fits in the inner cavity of the corrol,[18] thus being considered the prototype of metallocorroles, as 5,10,15,20-tetraphenylporphyrinato-zinc(II) (ZnTPP), is the model for metalloporphyrin.[31] The synthetic method *par excellence* for the synthesis of metallocorrole involves the direct complexation of the macrocycle from divalent metal salts, therefore involving the oxidation of the metal center.[31]

Corroles, regardless of the substitution pattern, are less stable in solution toward light and air than the corresponding porphyrins.[32] It is well established that corroles, especially free base, are photosensitive. The lack of a *meso* carbon makes the inner cavity smaller, and hence, the average electron density is higher. Therefore, the first oxidation potential of corroles is lower than that of porphyrins possessing the same substituents pattern.

Subsequently, several studies pointed out that the oxidative pathway is strongly dependent on the corrole structural features and reaction conditions.[33–38] The most typical decomposition pathway includes the hydroxylation to form hydroxyisocorrole and further ring opening to form biliverdin type structures (**Figure 8**).[32,38,39]

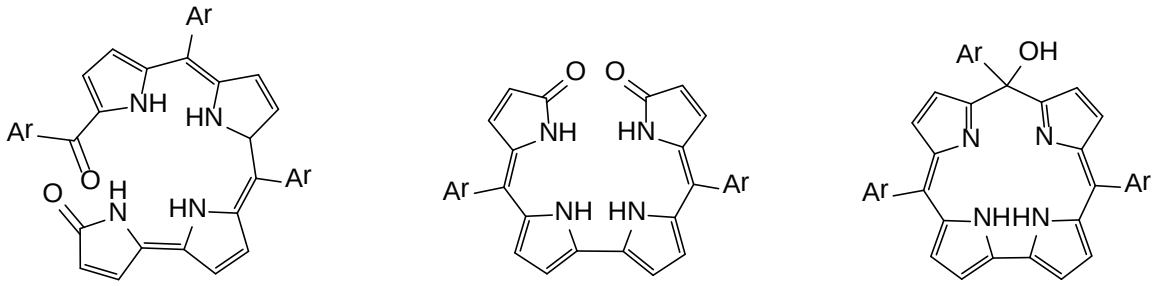

Figure 8. Exemplary products of oxidation of aryl-corroles.

The rate of corroles decomposition is solvent dependent, being higher in acetonitrile than in other organic solvents.[38] Moreover, corrole stability is strongly related to the influence of the substituents at both the *β* and the *meso* positions.[40] The presence of electron-donating substituents can decrease the stability the macrocycle, while electron-withdrawing groups can prevent oxidation.[38,41]

Synthesis of meso-substituted A_3 Corroles

In analogy to the broadly accepted nomenclature for *meso*-substituted porphyrins, corroles bearing three identical substituents at all three *meso* positions are called A_3 corroles (**Figure 9**).

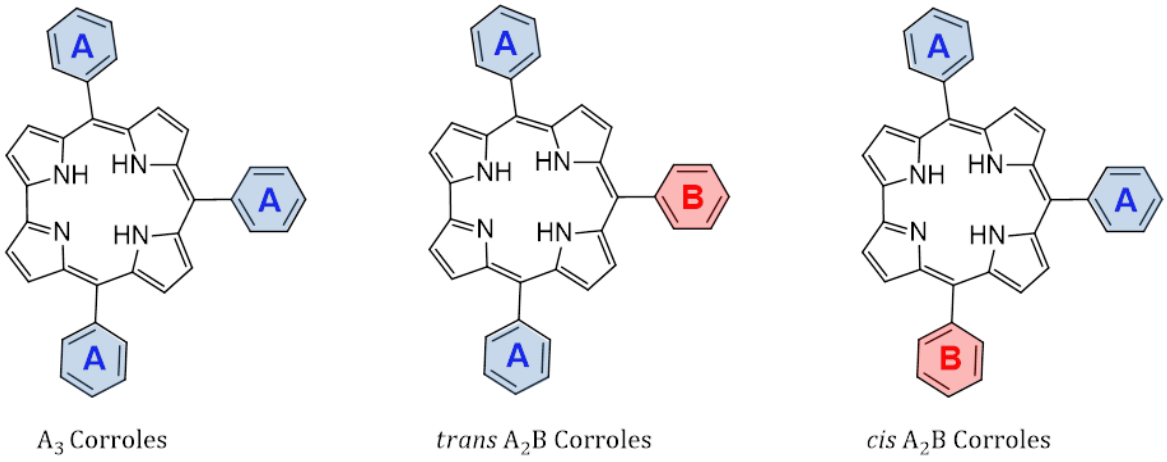

Figure 9. Types of *meso*-substituted corroles.

A_3 Corroles can be synthesized by any of the methods shown on **Scheme 3**, with the formation of bilane (or tetrapyrrane) and its macrocyclization *via* oxidation. Several synthetic approaches can be performed to obtain bilane: directly from pyrrole and aldehydes; from dipyrromethanes (or dipyrranes) and aldehydes; and from dipyrromethanes –diols and pyrrole[42–45] (**Scheme 3**).

Although significant efforts have been devoted to optimization of different synthetic strategies, nowadays only direct condensation of pyrrole with aldehydes prevails in the literature. Consequently, only this strategy has been described in this section.

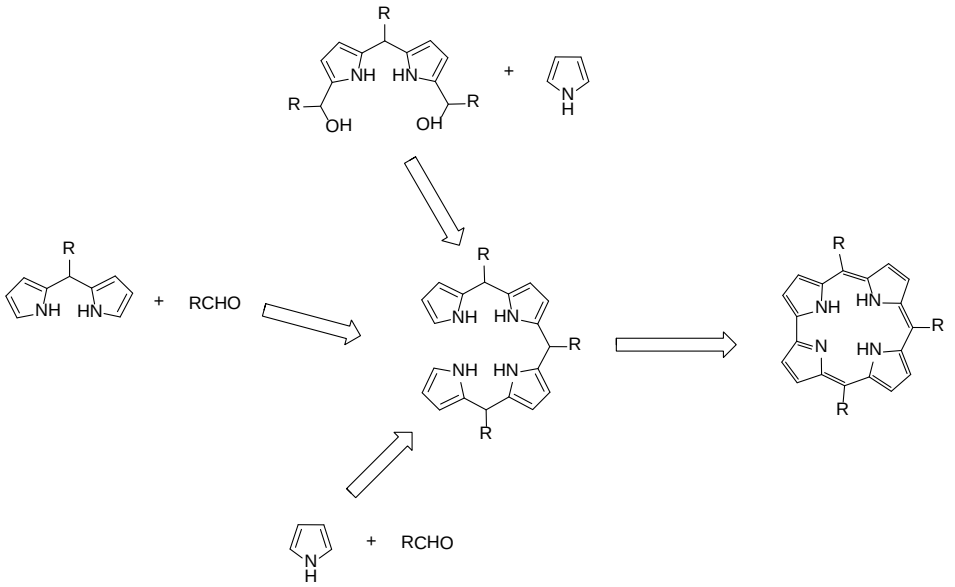

Scheme 3. Synthetic strategies leading to *meso*-substituted corroles *via* bilanes as intermediates.

Synthesis Using Al_2O_3 as a Solid Support

Gross *et al*. performed the reaction of pyrrole and the aldehyde on a solid support, with Al_2O_3 in the absence of solvent.

Heating mixture of pentafluorobenzaldehyde with pyrrole on Al_2O_3 for 4 h, followed by suspending it in CH_2Cl_2 and adding 2,3-dichloro-5,6-dicyano-1,4-benzoquinone (DDQ), the desired corrole was obtained in 11% yield. The yields of the reaction were satisfactory in the presence of fluorinated benzaldehydes, while in the presence of less reactive aldehydes a significant reduction of yields or the complete failure of the reaction was observed.[9]

In 2003 Collman and Decréau suggested another modification by using microwaves for heating of the reaction mixture. Starting from electron-withdrawing aldehydes, several A_3-corroles were obtained, but yield improvements achieved by microwaves *vs* classical heating was rather small.[46]

Modified Rothemund method[47]

This procedure is quite similar to Rothemund method for arylporphyrins synthesis, modified in order to promote corrole formation: the ratio of pyrrole/aldehyde was changed from 1:1 to 3:1.[10,48] By reacting pyrrole and aromatic aldehyde in refluxing acetic or propionic acid, a mixture of corrole and porphyrin is generally obtained, which represents the nuisance in this procedure. As a consequence, the overall yield is reduced due to an inefficient separation; indeed corrole and porphyrin have a quite similar R_f factor.
However, in the case of 4-nitrobenzaldehyde (22% yield), no traces of porphyrin were evidenced; making this methodology the best option for the synthesis of 5,10,15-tris(4-nitrophenyl)corrole over the last 15 years.[49,50]

Modified Lindsey method[12]

This method applies particularly to planar aromatic aldehydes possessing a large molecular mass that cannot dissolve in pyrrole or in boiling acetic acid.
This approach, which can be considered a modification of the Lindsey procedure for the preparation of tetraarylporphyrins involves a two-step reaction. In the first step a tenfold excess of pyrrole and aldehyde in CH_2Cl_2 using trifluoroacetic acid (TFA) as a catalyst; dilution with solvent increases the formation of bilane from pyrrolic Fragments. The final step, oxidative ring closure, was carried out with chloranil, affording corrole in satisfactory yields, while the corresponding porphyrin was not present or was observed only in traces among reaction products. The results obtained showed good generality for the use of several aldehydes bearing different substitution pattern.[51]

Very recently, Virgil and co-workers revisited the mechanism of corrole oligomerization and cyclization steps in an effort to achieve a scalable synthesis with an increased yield.[52–54] They purified bilane and, under optimized conditions, afforded a favourable yield of 84% starting from pentafluorobenzaldehyde. Furthermore, they discovered that evaporation of pyrrole before adding DDQ reduced the formation of polymeric byproducts and simplified purification. Moreover they were able to perform a scalable synthesis directly from aldehyde and pyrrole without intermediate purification, afforded 17% of the corrole over two steps on the impressive scale of 4.6 g.

Modified Král method

Gryko approach starts from the results obtained by Kral's work on dipyrromethanes.[55] The reaction was performed in a mixture of water and methanol and catalysed by HCl.
This procedure is based on the different solubility of pyrrole and aldehyde, either soluble in H_2O, and dipyrromethanes which is not soluble, so it forms a white suspension. Gryko starting point was a careful optimization of pyrrole-aldehyde and water-organic solvent ratios to force reaction toward longer pyrrolic compound like bilane. In the published procedure for the synthesis of A_3 corroles, a twofold excess of pyrrole and aldehyde (10:5 mmol) were dissolved in a mixture water-methanol, followed by the addiction of a catalytic amount of HCl; immediately the more lipophilic tetrapyrrane precipitated from the reaction mixture, which was then diluted with chloroform, and oxidized with chloranil. This procedure is therefore particularly suited to aryl-aldehydes bearing substituents without strong electron releasing or withdrawing effects, giving the corresponding corroles in good yields.

Synthesis of meso-substituted trans A_2B Corroles

In agreement with the nomenclature used for porphyrins, corroles with the same substituents at positions 5 and 15, and a different substituent at position 10 are called *trans*-A_2B-corroles, while corroles with two identical substituents at positions 5 (or 15) and 10 and a different substituent at position 15 (or 5) are called *cis*-A_2B corroles.

Although both *cis*-A_2Bcorroles and *trans*-A_2B-corroles are equally possible, the latter is considerably more popular because of synthetic accessibility (**Figure 9**). A summary of procedures until now elaborated includes:

- Synthesis from Aldehydes and Dipyrromethanes
- Synthesis from 2,2'-Bipyrrole and Dipyrromethanes–Diols
- Synthesis from Alkyl Oxalyl Chlorides and Dipyrromethanes
- Synthesis from Dipyrromethanes–Diols and Pyrrole

The most general procedure involves the synthesis directly from aldehydes and dipyrromethanes. In this scenario, several approaches and modification to the set of conditions already published for *trans* A_2B_2 porphyrins porphyrins were performed.[56–58] However, the concomitant scrambling represented the nuisance in the *trans* A_2B corrole synthesis.

By scrambling is meant the undesired rearrangement of substituted dipyrromethanes or bilanes leading to a mixture of products bearing different types and/or patterns of substituents at the perimeter of the macrocycle (**Scheme 4**).

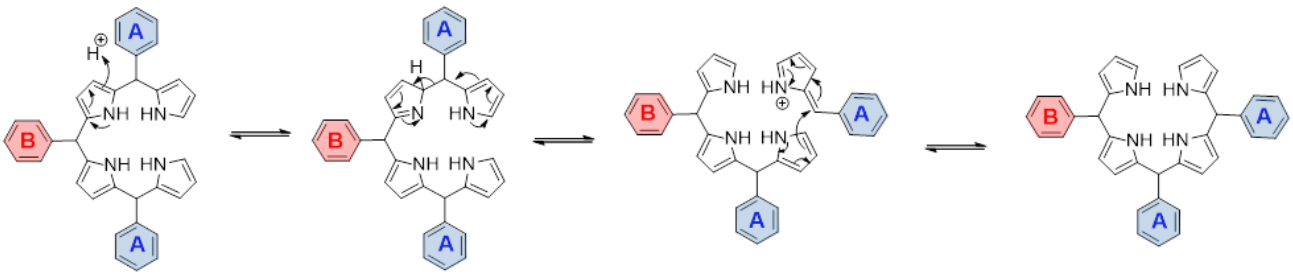

Scheme 4. Scrambling mechanism.

Several synthetic approaches have been optimized during the last two decades in order to prevent this secondary effect.

The first example of this approach was reported in 2001 by Gryko;[11] the reaction of mesityl dipyrromethane with fluoro substituted benzaldehydes afforded the corresponding A_2B corroles in moderate yields (4-19%). In the preliminary communication the reaction has been reported to be successful only with activated liquid aldehydes and was carried out without the addition of acid as a catalyst. Later, it

was discovered that the acid catalysis is necessary for the success of the reaction; at the beginning the catalysis was performed by the presence of small amounts of benzoic acids present as contaminants in the liquid aldehydes. Later, it was found that an increase in the concentration of acid (TFA) up to 13 mM represented an efficient method for the synthesis of A_2B corroles without scrambling for the sterically hindered dipyrromethanes, reducing considerably the reaction time.[59] Aromatic and lipophilic aldehydes react preferably in CH_2Cl_2 in the presence of TFA and DDQ as oxidant. Different sets of conditions were proposed for hindered or unhindered aldehydes, by varying the amount of aldehyde ,TFA, along with the time of acid-catalyzed step.[59–61]

In 2006, Gryko and Koszarna extended the methodology used for A_3 Corroles to A_2B corroles in same paper.[62] Particularly suited to small and hydrophilic aldehydes and dipyrromethanes, the reaction was performed in a mixture of water and methanol in the presence of HCl, giving the corresponding corroles in good yields with no scrambling.

Corrole-based applications

Taking advantage of all the optimized synthetic methodologies, the scientific interest in corroles has continuously increased, as witnessed by the abundance of studies dealing with the theoretical[63,64] as well as more application-related aspects (**Figure 10**). The very first review on corrole applications was put forward in 2007 by Aviv and Gross.[65] Since then, particularly in recent years, several research groups have considered corrole derivatives as their research targets.

As a result, it became known that such compounds can play an important role in oxidation or group transfer catalysis,[66] specifically in the areas of cyclopropanation,[67,68] C-H insertion, N-H insertion,[65] and aziridination.[69,70] They have been widely exploited in dye-sensitized solar cells (DSSCs),[71–73] photoactive arrays,[74] sensing applications,[75–79] molecular spintronics[80] and nonlinear optics.[63,81,82]

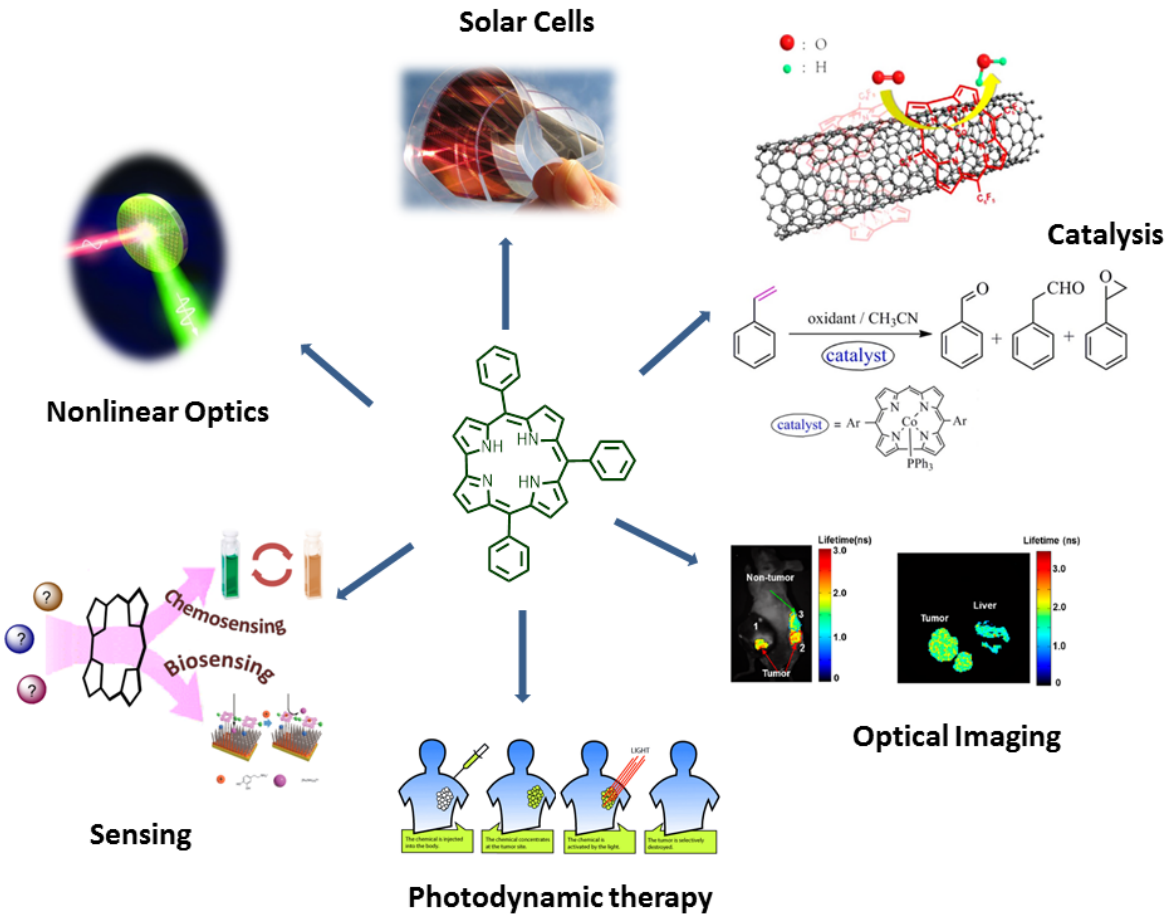

Figure 10. Examples of some of the most important applications of Corroles.

More recently, corrole has been proven to be an outstanding electrocatalyst for the reduction of O_2, with a better long-term durability compared to commercially used high-cost Pt/C catalyst.[83–86]

Another well documented application is the corrole's use in photodynamic therapy (PDT), where, compared with a variety of porphyrins, corroles demonstrated superior efficiency in inhibition of endothelial cell proliferation, as well as tumour progression and metastasis.[87,88]

The potential applications already demonstrated are very significant and point to new developments and further studies in all those areas.

References

(1) Presentation Speech - Nobel Prize in Physiology or Medicine 1934 https://www.nobelprize.org/nobel_prizes/medicine/laureates/1934/press.html (accessed Aug 29, 2017).

(2) Rickes, E. L.; Brink, N. G.; Koniuszy, F. R.; Wood, T. R.; Folkers, K. Crystalline Vitamin B12. *Science* **1948**, *107* (2781), 396–397.

(3) Pierce, J. V.; Page, A. C.; Stokstad, E. L. R.; Jukes, T. H. CRYSTALLIZATION OF VITAMIN B12b. *J. Am. Chem. Soc.* **1949**, *71*, 2952.

(4) Hodgkin, D. C.; Kamper, J.; Mackay, M.; Pickworth, J.; Trueblood, K. N.; White, J. G. Structure of Vitamin B12. *Nature* **1956**, *178* (4524), 64–66.

(5) Presentation Speech - Nobel Prize in Chemistry 1964 https://www.nobelprize.org/nobel_prizes/chemistry/laureates/1964/press.html (accessed Aug 29, 2017).

(6) Johnson, A. W.; Price, R. 331. The Synthesis of Derivatives of Corrole (Pentadehydrocorrin). *J. Chem. Soc.* **1960**, 1649–1653.

(7) Johnson, A. W.; Kay, I. T. 306. Corroles. Part I. Synthesis. *J. Chem. Soc.* **1965**, 1620–1629.

(8) Harrison, H. R.; Hodder, O. J. R.; Hodgkin, D. C. Crystal and Molecular Structure of 8,12-Diethyl-2,3,7,13,17,18-Hexamethylcorrole. *J. Chem. Soc. B* **1971**, 640–645.

(9) Gross, Z.; Galili, N.; Saltsman, I. The First Direct Synthesis of Corroles from Pyrrole. *Angew. Chem. Int. Ed.* **1999**, *38* (10), 1427–1429.

(10) Paolesse, R.; Mini, S.; Sagone, F.; Boschi, T.; Jaquinod, L.; Nurco, D. J.; Smith, K. M. 5,10,15-Triphenylcorrole: A Product from a Modified Rothemund Reaction. *Chem. Commun.* **1999**, *14*, 1307–1308.

(11) Gryko, D. T. A Simple, Rational Synthesis of Meso-Substituted A2B-Corroles. *Chem. Commun.* **2000**, *22*, 2243–2244.

(12) Paolesse, R.; Marini, A.; Nardis, S.; Froiio, A.; Mandoj, F.; Nurco, D. J.; Prodi, L.; Montalti, M.; Smith, K. M. Novel Routes to Substituted 5,10,15-Triarylcorroles. *J. Porphyr. Phthalocyanines* **2003**, *07* (01), 25–36.

(13) Milgrom, L. R. *The Colours of Life*, Oxford University Press.; 1997.

(14) Rodríguez-Morgade; de la Torre, G.; Torres, T. Design and Synthesis of Low-Symmetry Phthalocyanines and Related Systems. In *The Porphyrin Handbook*; Kadish, K. M.; Smith, K. M.; Guilard, R., 2003; Vol. 15, p 125.

(15) Johnson, A. W. Structural Analogs of Porphyrins. In *Porphyrins and Metalloporphyrins*; 1975.

(16) Smith, K. M. General Features of the Structure and Chemistry of Porphyrin Compounds. In *Porphyrins and Metalloporphyrins*; 1975.

(17) Dyke, J. M.; Hush, N. S.; Williams, M. L.; Woolsey, I. S. Bond Lengths and Location of the Inner-Ring Protons in the Corrole Molecule. *Mol. Phys.* **1971**, *20* (6), 1149–1152.

(18) Ghosh, A.; Jynge, K. Molecular Structures and Energetics of Corrole Isomers: A Comprehensive Local Density Functional Theoretical Study. *Chem. – Eur. J.* **1997**, *3* (5), 823–833.

(19) Paolesse, R.; Jaquinod, L.; Senge, M. O.; Smith, K. M. Functionalization of Corroles: Formylcorroles. *J. Org. Chem.* **1997**, *62* (18), 6193–6198.

(20) Paolesse, R.; Nardis, S.; Venanzi, M.; Mastroianni, M.; Russo, M.; Fronczek, F. R.; Vicente, M. G. H. Vilsmeier Formylation of 5,10,15-Triphenylcorrole: Expected and Unusual Products. *Chem. – Eur. J.* **2003**, *9* (5), 1192–1197.

(21) Gross, Z.; Galili, N.; Simkhovich, L.; Saltsman, I.; Botoshansky, M.; Bläser, D.; Boese, R.; Goldberg, I. Solvent-Free Condensation of Pyrrole and Pentafluorobenzaldehyde: A Novel Synthetic Pathway to Corrole and Oligopyrromethenes. *Org. Lett.* **1999**, *1* (4), 599–602.

(22) Simkhovich, L.; Goldberg, I.; Gross, Z. First Syntheses and X-Ray Structures of a Meso-Alkyl-Substituted Corrole and Its Ga(III) Complex. *J. Inorg. Biochem.* **2000**, *80* (3–4), 235–238.

(23) Ventura, B.; Esposti, A. D.; Koszarna, B.; Gryko, D. T.; Flamigni, L. Photophysical Characterization of Free-Base Corroles, Promising Chromophores for Light Energy Conversion and Singlet Oxygen Generation. *New J. Chem.* **2005**, *29* (12), 1559–1566.
(24) Ding, T.; Alemán, E. A.; Modarelli, D. A.; Ziegler, C. J. Photophysical Properties of a Series of Free-Base Corroles. *J. Phys. Chem. A* **2005**, *109* (33), 7411–7417.
(25) Erben, C.; Will, S.; Kadish, K. M. Metallocorroles: Molecular Structure, Spectroscopy and Electronic States. In *The Porphyrin Handbook*; Kadish, K. M.; Smith, K. M.; Guilard, R., 2000; Vol. II.
(26) Nardis, S.; Monti, D.; Paolesse, R. Novel Aspects of Corrole Chemistry. *Mini-Rev. Org. Chem.* **2005**, *2* (4), 355–374.
(27) Shen, J.; Shao, J.; Ou, Z.; E, W.; Koszarna, B.; Gryko, D. T.; Kadish, K. M. Electrochemistry and Spectroelectrochemistry of Meso-Substituted Free-Base Corroles in Nonaqueous Media: Reactions of (Cor)H3, [(Cor)H4]+, and [(Cor)H2]-. *Inorg. Chem.* **2006**, *45* (5), 2251–2265.
(28) Ou, Z.; Shen, J.; Shao, J.; E, W.; Gałęzowski, M.; Gryko, D. T.; Kadish, K. M. Protonated Free-Base Corroles: Acidity, Electrochemistry, and Spectroelectrochemistry of [(Cor)H4]+, [(Cor)H5]2+, and [(Cor)H6]3+. *Inorg. Chem.* **2007**, *46* (7), 2775–2786.
(29) Gryko, D. T. Recent Advances in the Synthesis of Corroles and Core-Modified Corroles. *Eur. J. Org. Chem.* **2002**, *2002* (11), 1735–1743.
(30) Gross, Z. High-Valent Corrole Metal Complexes. *JBIC J. Biol. Inorg. Chem.* **2001**, *6* (7), 733–738.
(31) Bendix, J.; Dmochowski, I. J.; Gray, H. B.; Mahammed, A.; Simkhovich, L.; Gross, Z. Structural, Electrochemical, and Photophysical Properties of Gallium(III) 5,10,15-Tris(Pentafluorophenyl)Corrole. *Angew. Chem. Int. Ed.* **2000**, *39* (22), 4048–4051.
(32) Tardieux, C.; Gros, C. P.; Guilard, R. On Corrole Chemistry. An Isomerization Study and Oxidative Cleavage of the Corrole Macroring to a Biliverdin Structure. *J. Heterocycl. Chem.* **1998**, *35* (4), 965–970.
(33) Geier, I.; Chick, J. F. B.; Callinan, J. B.; Reid, C. G.; Auguscinski, W. P. A Survey of Acid Catalysis and Oxidation Conditions in the Two-Step, One-Flask Synthesis of Meso-Substituted Corroles via Dipyrromethanedicarbinols and Pyrrole. *J. Org. Chem.* **2004**, *69* (12), 4159–4169.
(34) Nardis, S.; Pomarico, G.; Fronczek, F. R.; Vicente, M. G. H.; Paolesse, R. One-Step Synthesis of Isocorroles. *Tetrahedron Lett.* **2007**, *48* (49), 8643–8646.
(35) Paolesse, R.; Sagone, F.; Macagnano, A.; Boschi, T.; Prodi, L.; Montalti, M.; Zaccheroni, N.; Bolletta, F.; Smith, K. M. Photophysical Behaviour of Corrole and Its Symmetrical and Unsymmetrical Dyads. *J. Porphyr. Phthalocyanines* **1999**, *3* (5), 364–370.
(36) Gros, C. P.; Barbe, J.-M.; Espinosa, E.; Gullard, R. Room-Temperature Autoconversion of Free-Base Corrole into Free-Base Porphyrin. *Angew. Chem. - Int. Ed.* **2006**, *45* (34), 5642–5645.
(37) Barata, J. F. B.; Neves, M. G. P. M. S.; Tomé, A. C.; Faustino, M. A. F.; Silva, A. M. S.; Cavaleiro, J. A. S. How Light Affects 5,10,15-Tris(Pentafluorophenyl)Corrole. *Tetrahedron Lett.* **2010**, *51* (12), 1537–1540.
(38) Świder, P.; Nowak-Król, A.; Voloshchuk, R.; Lewtak, J. P.; Gryko, D. T.; Danikiewicz, W. Mass Spectrometry Studies on Meso-Substituted Corroles and Their Photochemical Decomposition Products. *J. Mass Spectrom.* **2010**, *45* (12), 1443–1451.
(39) Wojaczyński, J.; Duszak, M.; Latos-Grazyński, L. Photooxidation of Unhindered Triarylcorroles. *Tetrahedron* **2013**, *69* (48), 10445–10449.
(40) Narayanan, S. J.; Sridevi, B.; Chandrashekar, T. K.; Englich, U.; Ruhlandt-Senge, K. Core-Modified Smaragdyrins: First Examples of Stable Meso-Substituted Expanded Corrole. *Org. Lett.* **1999**, *1* (4), 587–590.
(41) Iris, A.-H.; Gross, Z. Aura of Corroles. *Chem. - Eur. J.* **2009**, *15* (34), 8382–8394.
(42) Decréau, R. A.; Collman, J. P. Corrole Synthesis by Dipyrromethane–dicarbinol and 2,2′-Bipyrrole Condensation. *Tetrahedron Lett.* **2003**, *44* (16), 3323–3327.
(43) Geier, G. R.; Grindrod, S. C. Meso-Substituted [34]Octaphyrin(1.1.1.0.1.1.1.0) and Corrole Formation in Reactions of a Dipyrromethanedicarbinol with 2,2'-Bipyrrole. *J. Org. Chem.* **2004**, *69* (19), 6404–6412.

(44) Guilard, R.; Gryko, D. T.; Canard, G.; Barbe, J.-M.; Koszarna, B.; Brandès, S.; Tasior, M. Synthesis of Corroles Bearing up to Three Different Meso Substituents. *Org. Lett.* **2002**, *4* (25), 4491–4494.
(45) Gryko, D. T.; Tasior, M.; Koszarna, B. Parallel Synthesis of Meso-Substituted Corroles and Meso-Substituted [22]Pentaphyrins(1.1.1.0.0) from Diacyl-Dipyrromethanes. *J. Porphyr. Phthalocyanines* **2003**, *07* (04), 239–248.
(46) Collman, J. P.; Decréau, R. A. Microwave-Assisted Synthesis of Corroles. *Tetrahedron Lett.* **2003**, *44* (6), 1207–1210.
(47) Lindsey, J. S. Syntheses of Meso-Substituted Porphyrins. In *The Porphyrin Handbook*; Kadish, K. M.; Smith, K. M.; Guilard, R., 2000; Vol. I.
(48) Paolesse, R.; Nardis, S.; Sagone, F.; Khoury, R. G. Synthesis and Functionalization of Meso-Aryl-Substituted Corroles. *J. Org. Chem.* **2001**, *66* (2), 550–556.
(49) Fu, B.; Huang, J.; Ren, L.; Weng, X.; Zhou, Y.; Du, Y.; Wu, X.; Zhou, X.; Yang, G. Cationic Corrole Derivatives: A New Family of G-Quadruplex Inducing and Stabilizing Ligands. *Chem. Commun.* **2007**, No. 31, 3264–3266.
(50) Fryxelius, J.; Eilers, G.; Feyziyev, Y.; Magnuson, A.; Sun, L.; Lomoth, R. Synthesis and Redox Properties of a [Meso-Tris(4-Nitrophenyl) Corrolato]Mn(III) Complex. *J. Porphyr. Phthalocyanines* **2005**, *9* (6), 379–386.
(51) Rose, E.; Kossanyi, A.; Quelquejeu, M.; Soleilhavoup, M.; Duwavran, F.; Bernard, N.; Lecas, A. Synthesis of Biomimetic Heme Precursors: The "Double Picket Fence" 5,10,15,20-Tetrakis(2′,6′-Dinitro-4′-Tert-Butylphenyl) Porphyrin. *J. Am. Chem. Soc.* **1996**, *118* (6), 1567–1568.
(52) Blumenfeld, C.; Fisher, K. J.; Henling, L. M.; Grubbs, R. H.; Gray, H. B.; Virgil, S. C. Control of Oligomerization and Oxidation Steps in the Synthesis of Tris(Pentafluorophenyl)Corrole. *Eur. J. Org. Chem.* **2015**, *2015* (14), 3022–3025.
(53) Wasbotten, I. H.; Wondimagegn, T.; Ghosh, A. Electronic Absorption, Resonance Raman, and Electrochemical Studies of Planar and Saddled Copper(III) Meso-Triarylcorroles. Highly Substituent-Sensitive Soret Bands as a Distinctive Feature of High-Valent Transition Metal Corroles. *J. Am. Chem. Soc.* **2002**, *124* (27), 8104–8116.
(54) Dogutan, D. K.; McGuire, R.; Nocera, D. G. Electocatalytic Water Oxidation by Cobalt(III) Hangman β-Octafluoro Corroles. *J. Am. Chem. Soc.* **2011**, *133* (24), 9178–9180.
(55) Kral, V.; Vasek, P.; Dolensky, B. Green Chemistry for Preparation of Oligopyrrole Macrocycles Precursors: Novel Methodology for Dipyrromethanes and Tripyrromethanes Synthesis in Water. *Collect. Czechoslov. Chem. Commun.* **2004**, *69* (5), 1126–1136.
(56) Lee, C.-H.; S., L. One-Flask Synthesis of Meso-Substituted Dipyrromethanes and Their Application in the Synthesis of Trans-Substituted Porphyrin Building Blocks. *Tetrahedron* **1994**, *50* (39), 11427–11440.
(57) Littler, B. J.; Ciringh, Y.; Lindsey, J. S. Investigation of Conditions Giving Minimal Scrambling in the Synthesis of Trans-Porphyrins from Dipyrromethanes and Aldehydes. *J. Org. Chem.* **1999**, *64* (8), 2864–2872.
(58) Rao, P. D.; Littler, B. J.; Geier, I.; Lindsey, J. S. Efficient Synthesis of Monoacyl Dipyrromethanes and Their Use in the Preparation of Sterically Unhindered Trans-Porphyrins. *J. Org. Chem.* **2000**, *65* (4), 1084–1092.
(59) Gryko, D. T.; Koszarna, B. Refined Methods for the Synthesis of Meso-Substituted A3- and Trans-A2B-Corroles. *Org. Biomol. Chem.* **2003**, *1* (2), 350–357.
(60) Gryko, D. T.; Jadach, K. A Simple and Versatile One-Pot Synthesis of Meso-Substituted Trans-A2B-Corroles. *J. Org. Chem.* **2001**, *66* (12), 4267–4275.
(61) Gryko, D. T.; Koszarna, B. Refined Synthesis of Meso-Substituted Trans-A2B-Corroles Bearing Electron-Withdrawing Groups. *Synthesis* **2004**, *2004* (13), 2205–2209.
(62) Koszarna, B.; Gryko, D. T. Efficient Synthesis of Meso-Substituted Corroles in a H2O-MeOH Mixture. *J. Org. Chem.* **2006**, *71* (10), 3707–3717.
(63) Ying, X.; Long, X.-Y.; Mahmood, M. H.; Hu, Q.-Y.; Liu, H.-Y.; Chang, C.-K. Second Order Nonlinear Optical Properties of Corroles: Experimental and Theoretical Investigations. *J. Porphyr. Phthalocyanines* **2012**, *16* (12), 1276–1284.

(64) Thomas, K. E.; Alemayehu, A. B.; Conradie, J.; Beavers, C. M.; Ghosh, A. The Structural Chemistry of Metallocorroles: Combined X-Ray Crystallography and Quantum Chemistry Studies Afford Unique Insights. *Acc. Chem. Res.* **2012**, *45* (8), 1203–1214.
(65) Aviv, I.; Gross, Z. Corrole-Based Applications. *Chem. Commun.* **2007**, *0* (20), 1987–1999.
(66) Gross, Z.; Gray, H. B. Oxidations Catalyzed by Metallocorroles. *Adv. Synth. Catal.* **2004**, *346* (2–3), 165–170.
(67) Simkhovich, L.; Goldberg, I.; Gross, Z. The Effects of Bulky Ortho-Aryl Substituents in Corroles, Tested by X-Ray Crystallography of the Rhodium Complexes and Catalysis Thereby. *J. Porphyr. Phthalocyanines* **2002**, *06* (06), 439–444.
(68) Saltsman, I.; Simkhovich, L.; Balazs, Y.; Goldberg, I.; Gross, Z. Synthesis, Spectroscopy, and Structures of New Rhodium(I) and Rhodium(III) Corroles and Catalysis Thereby. *Inorganica Chim. Acta* **2004**, *357* (10), 3038–3046.
(69) Simkhovich, L.; Gross, Z. Iron(IV) Corroles Are Potent Catalysts for Aziridination of Olefins by Chloramine-T. *Tetrahedron Lett.* **2001**, *42* (45), 8089–8092.
(70) Zdilla, M. J.; Abu-Omar, M. M. Mechanism of Catalytic Aziridination with Manganese Corrole: The Often Postulated High-Valent Mn(V) Imido Is Not the Group Transfer Reagent. *J. Am. Chem. Soc.* **2006**, *128* (51), 16971–16979.
(71) Walker, D.; Chappel, S.; Mahammed, A.; Brunschwig, B. S.; Winkler, J. R.; Gray, H. B.; Zaban, A.; Gross, Z. Corrole-Sensitized TiO2 Solar Cells. *J. Porphyr. Phthalocyanines* **2006**, *10* (11), 1259–1262.
(72) Sudhakar, K.; Giribabu, L.; Salvatori, P.; Angelis, F. D. Triphenylamine-Functionalized Corrole Sensitizers for Solar-Cell Applications. *Phys. Status Solidi A* **2015**, *212* (1), 194–202.
(73) Wróbel, D. From Natural Photosynthesis to Molecular Photovoltaics. *Mol. Cryst. Liq. Cryst.* **2016**, *627* (1), 4–22.
(74) Flamigni, L.; Gryko, D. T. Photoactive Corrole-Based Arrays. *Chem. Soc. Rev.* **2009**, *38* (6), 1635–1646.
(75) Barbe, J.-M.; Canard, G.; Brandès, S.; Guilard, R. Organic-Inorganic Hybrid Sol-Gel Materials Incorporating Functionalized Cobalt(III) Corroles for the Selective Detection of CO. *Angew. Chem. Int. Ed Engl.* **2005**, *44* (20), 3103–3106.
(76) Barbe, J.-M.; Canard, G.; Brandès, S.; Jérôme, F.; Dubois, G.; Guilard, R. Metallocorroles as Sensing Components for Gas Sensors: Remarkable Affinity and Selectivity of Cobalt(III) Corroles for CO vs. O2 and N2. *Dalton Trans. Camb. Engl. 2003* **2004**, No. 8, 1208–1214.
(77) Capuano, R.; Pomarico, G.; Paolesse, R.; Di Natale, C. Corroles-Porphyrins: A Teamwork for Gas Sensor Arrays. *Sensors* **2015**, *15* (4), 8121–8130.
(78) Paolesse, R.; Nardis, S.; Monti, D.; Stefanelli, M.; Di Natale, C. Porphyrinoids for Chemical Sensor Applications. *Chem. Rev.* **2017**, *117* (4), 2517–2583.
(79) Savoldelli, A.; Magna, G.; Di Natale, C.; Catini, A.; Nardis, S.; Fronczek, F. R.; Smith, K. M.; Paolesse, R. ß-Acrolein-Substituted Corroles: A Route to the Preparation of Functionalized Poly-Acrolein Microspheres for Chemical Sensor Applications. *Chem. Weinh. Bergstr. Ger.* **2017**.
(80) Wu, F.; Liu, J.; Mishra, P.; Komeda, T.; Mack, J.; Chang, Y.; Kobayashi, N.; Shen, Z. Modulation of the Molecular Spintronic Properties of Adsorbed Copper Corroles. *Nat. Commun.* **2015**, *6*, ncomms8547.
(81) Hamad, S.; Tewari, S. P.; Giribabu, L.; Rao, S. V. Picosecond and Femtosecond Optical Nonlinearities of Novel Corroles. *J. Porphyr. Phthalocyanines* **2012**, *16* (01), 140–148.
(82) Garai, A.; Kumar, S.; Sinha, W.; Purohit, C. S.; Das, R.; Kar, S. A Comparative Study of Optical Nonlinearities of Trans-A2B-Corroles in Solution and in Aggregated State. *RSC Adv.* **2015**, *5* (36), 28643–28651.
(83) Schechter, A.; Stanevsky, M.; Mahammed, A.; Gross, Z. Four-Electron Oxygen Reduction by Brominated Cobalt Corrole. *Inorg. Chem.* **2012**, *51* (1), 22–24.
(84) Zhang, W.; Lai, W.; Cao, R. Energy-Related Small Molecule Activation Reactions: Oxygen Reduction and Hydrogen and Oxygen Evolution Reactions Catalyzed by Porphyrin- and Corrole-Based Systems. *Chem. Rev.* **2017**, *117* (4), 3717–3797.

(85) Samireddi, S.; Shown, I.; Shen, T.-H.; Huang, H.-C.; Wong, K.-T.; Chen, L.-C.; Chen, K.-H. Hybrid Bimetallic-N4 Electrocatalyst Derived from a Pyrolyzed Ferrocene–Co-Corrole Complex for Oxygen Reduction Reaction. *J. Mater. Chem. A* **2017**, *5* (19), 9279–9286.
(86) Tang, J.; Ou, Z.; Guo, R.; Fang, Y.; Huang, D.; Zhang, J.; Zhang, J.; Guo, S.; McFarland, F. M.; Kadish, K. M. Functionalized Cobalt Triarylcorrole Covalently Bonded with Graphene Oxide: A Selective Catalyst for the Two- or Four-Electron Reduction of Oxygen. *Inorg. Chem.* **2017**, *56* (15), 8954–8963.
(87) Pandey, R. K.; Kessel, D.; Dougherty, T. J. *Handbook of Photodynamic Therapy: Updates on Recent Applications of Porphyrin-Based Compounds*; World Scientific, 2016.
(88) Teo, R. D.; Hwang, J. Y.; Termini, J.; Gross, Z.; Gray, H. B. Fighting Cancer with Corroles. *Chem. Rev.* **2017**, *117* (4), 2711–2729.

General Objectives

Thesis distribution

The aim of this Thesis is the preparation and characterization of new corrole-based expanded systems and it has been organized in two parts.

Chapter 1 is centered on the design and synthesis of annulated corroles bearing a pyrazino functionality as a linker (**Figure 11**). Special emphasis is made on the state of the art of this field and on the different types of functionalization performed to achieve the goal. This chapter is, at the same time, divided in two sections, according to the two main synthetic protocols we used to obtain different complexes.

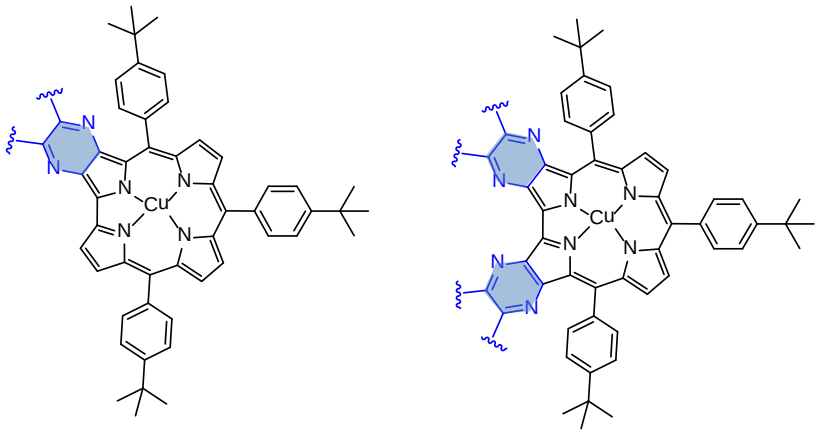

Figure 11. Schematic representation of the target corroles bearing annulated pyrazine moieties in their β-positions that will be studied in Chapter 1.

Chapter 2 is centered on the use of phthalocyanines for the construction of hybrids with corroles and their preliminary study as photoactive materials for their application in solar technologies. This chapter is, at the same time, divided in two sections. The first one is dealing with covalent systems of phthalocyanines and corroles, bearing different types of donor and acceptor units.

The second section is centered on supramolecular corrole-phthalocyanine conjugates, in which the phthalocyanine was designed to act as the electron acceptor group. Two different corroles were prepared, that we expected them to act as the electron donor counterpart. Their electron donor behaviour towards the phthalocyanine was herein studied (**Figure 12**).

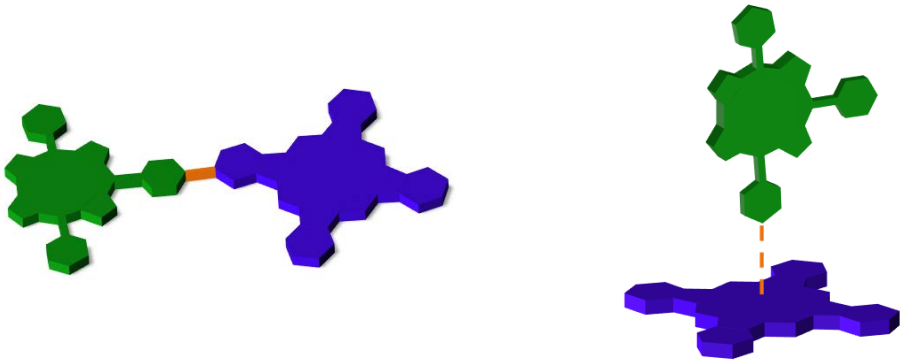

Figure 12. Schematic representation covalently and supramolecular conjugated Corr_Pc that will be studied in Chapter 2.

Specific objectives to be met in the research will be listed in each chapter.

Chapter I

Expanded Corroles by β-fused aromatic rings

State of the Art

Studies related to the chemistry of tetrapyrrolic macrocycles have as their objective not only to develop strategies and methods of synthesis of these compounds, but also their transformation, modeling them together with their properties, for the most diverse areas that are intended to be applied for.

That is why it is important to elaborate synthetic modifications that can finely tune the corrole properties to match the target application. In this scenario, both the lower symmetry (than porphyrin) of the corrole and its frequently unpredictable reactivity make it difficult to optimize simple protocols for the functionalization of the corrole ring, leaving this chemistry far less developed than that of porphyrins. Although the synthetic availability of corrole has been greatly improved in the last few years by the optimization of different synthetic routes, the preparation of corrole conjugated arrays has been sparsely explored.

Among the different corrole functionalization, in recent years we have been interested in the fusion of aromatic substituents at the *β*-positions, thus expanding the conjugation of the system. It is well known that in the case of porphyrins, the introduction of fused *π*-conjugated units strongly modifies the electronic character of the resulting chromophores, affording porphyrin systems with unique optical and electrochemical properties.[1,2]

To the best of our knowledge, corrole *β*-pyrrolic post-functionalization remains less explored than that of *meso*-aryl positions. Furthermore, most of the examples reported in the literature are fitted for 5,10,15-tris(pentafluorophenyl) corrole and does not work for other arylcorroles. In this regard, several methods involving different types of functionalization have been used for the synthesis of a wide range of *β*-substituted corrole macrocycles. The most recent procedures to perform *β*-annulated corroles will be highlighted.

The first example of corroles with annulated aromatic rings was described by Cavaleiro and co-workers in 2004 as an extension of their studies in the porphyrin field.[3]. It was shown that 5,10,15-tris (pentafluorophenyl)corrole, in the presence of pentacene in 1,2,4-trichlorobenzene at 200 °C can act either as a 2π- or as a 4π component in Diels–Alder reactions. After 6 h, the corresponding dehydrogenated Diels–Alder [4+2]

cycloadducts and the symmetry-forbidden [4+4] cycloadduct, were obtained in moderate yields (**Scheme 1.1**).[4]

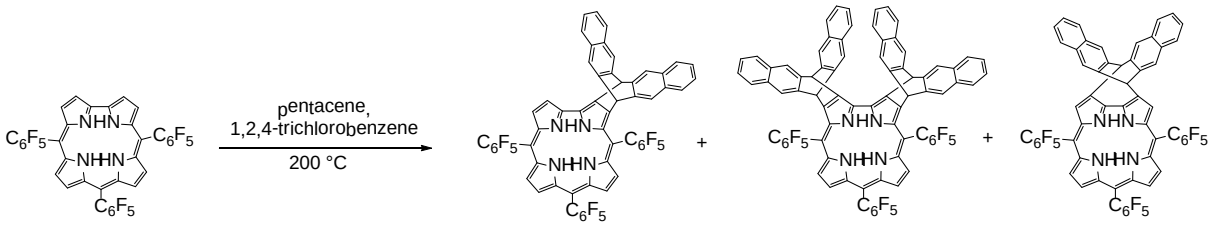

Scheme 1.1. Cycloaddition reactions of 5,10,15-tris-(pentafluorophenyl)corrole with pentacene.

Different dehydrogenated Diels–Alder [4+2] cycloadducts were obtained using other polycyclic aromatic dienes, such as anthracene, tetracene, 9,10-dimethylanthracene, and naphtho[2,3-*a*]pirene (**Scheme 1.2 a,b,c,d** respectively).

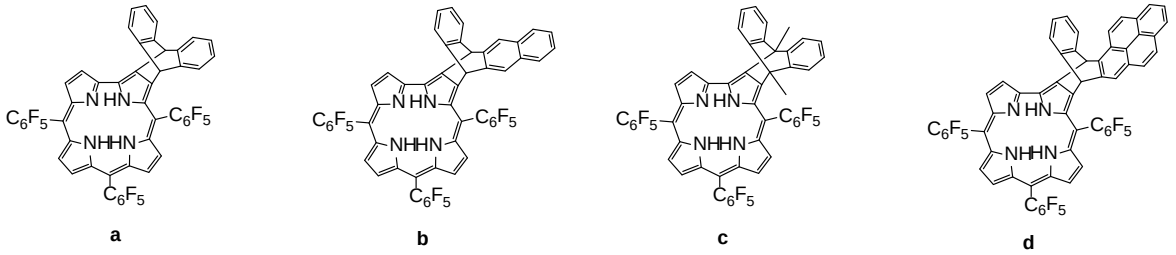

Scheme 1.2. Different dehydrogenated cycloadducts obtained by cycloaddition reactions.

Kräutler and co-workers synthesize from *β,β'*-sulfolenopyrrole and di-*tert*butylbenzaldehyde the corresponding dipyrromethane. By condensation with p-tolualdehyde they obtained the tetra-*β,β'*-sulfoleno-corrole and used it as 4π dienes in Diels–Alder reactions (**Scheme 1.3**).

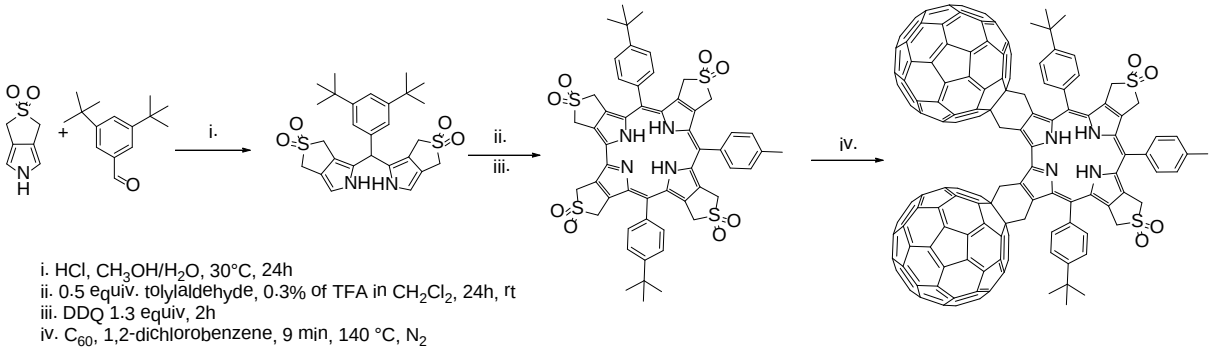

Scheme 1.3. Preparation of difullero-corrole derivative.

The regioselective extrusion of SO_2 in pyrroles rings A and D was obtained performing the reaction in 1,2-dichlorobenzene at 140°C in a large excess of C_{60} (30 equivalents). After 9 min the difullereno-corrole was obtained in high yields (83%).[5]

The possibility of using *β*-vinylcorroles as dienes in Diels–Alder reaction was also investigated.[6]

By introducing of a vinyl group in the corrole macrocycle through a Wittig-modified reaction on the 3-formyl derivative of gallium(III) complex of 5,10,15-tris(pentafluorophenyl)-corrole, the corresponding of 3-vinyl derivative was obtained (**Scheme 1.4**).[7]

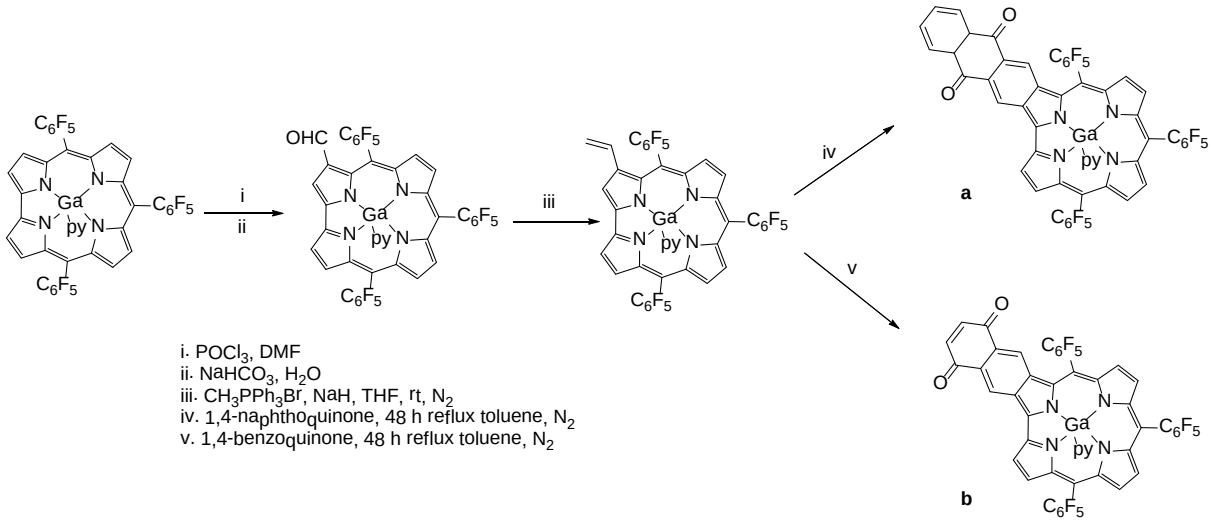

Scheme 1.4. Preparation of 3-Vinyl-corrole derivative as diene in Diels-Alder reactions.

The reaction was performed in the presence of 1,4-benzoquinone and 1,4-naphthoquinone in refluxing toluene, affording the corresponding dehydrogenated cycloadducts in high yields (64% and 76%, respectively,) which were characterized as compounds **1.4.a** and **1.4.b**.[6]

Furthermore, it was shown that compound **1.4.b** could be used as chemosensor for anions and amines, showing good affinity for fluoride, nicotine, and caffeine in water samples (**Figure 1.1**).[6]

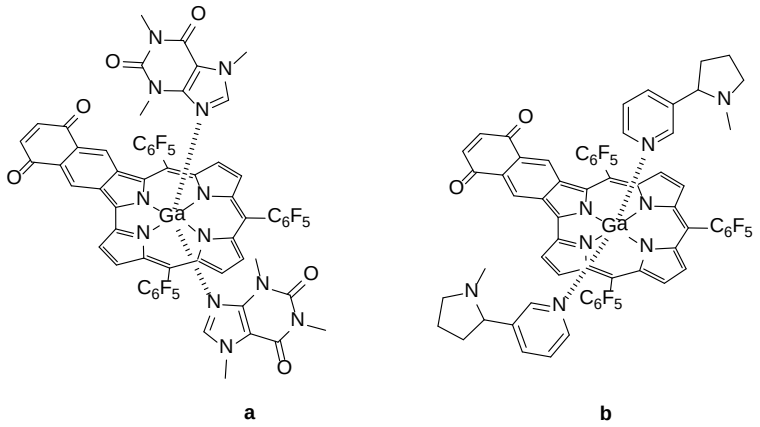

Figure 1.1. Chemosensor capability of the corrole ring: Interaction with caffeine (a) and nicotine (b).

Using the same substrate, the 3-vinyl-corrolato gallium(III)pyridine, **1.4.a** other π-extended quinone-fused corroles were obtained by Cavaleiro and co-workers through the synthesis of an azomethine ylide.

The reaction was performed using the 3-viniyl derivative with N-methylglycine in refluxing toluene. In the study the reaction of azomethine ylide with several dipolarophile (C_{60}, dimethyl fumarate, dimethyl acetylenedicarboxylate and different quinines) was described. In the particular case of 1,4-naphthoquinone and 1,4-anthraquinone, besides the expected dehydrogenated cycloadducts, the quinone-fused corroles have been isolated, in moderate yields (18% and 46%, respectively), (**Scheme 1.5**).[8]

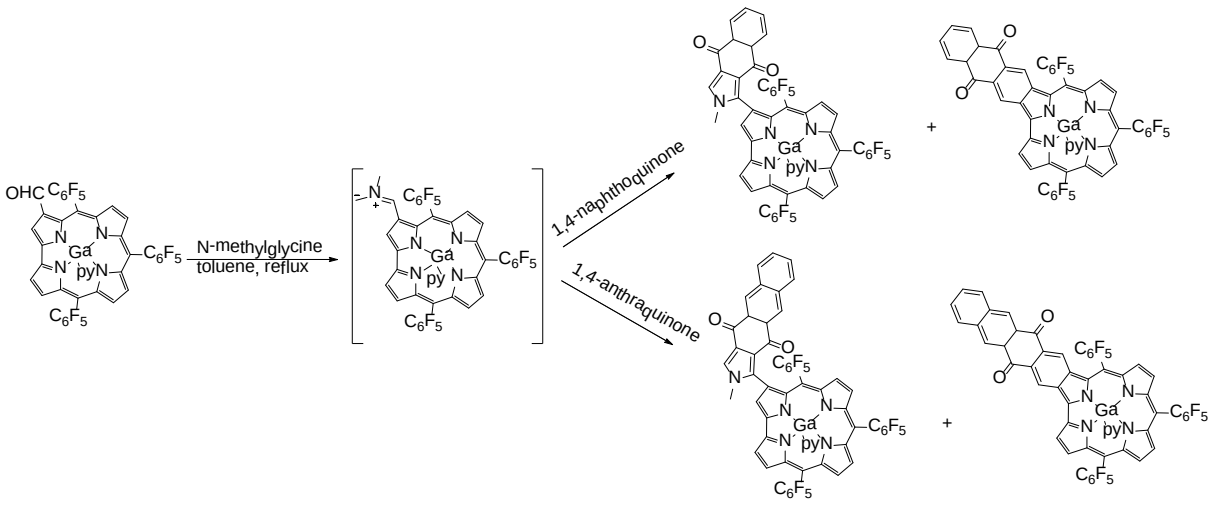

Scheme 1.5. Preparation of corrole azomethine ylide and 1,3-dipolar cycloaddition reaction with 1,4-naphthoquinone and 1,4-anthraquinone.

Same result was obtained with the 2-formyl derivative 1,4-naththoquinone: the expected dehydrogenated cycloadduct was once more accompanied by the π-extended chromophore (**Scheme 1.6**) [9]

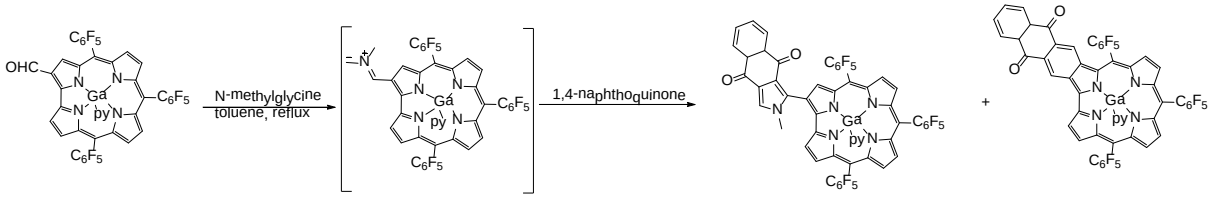

Scheme 1.6. 1,3-dipolar cycloaddition reaction obtained from a Ga(III) 2-formylcorrole via the corresponding azomethine ylide.

Other examples of more symmetric annulations are given by tetrabenzocorroles (TBC). Reported for the first time by Paolesse and co-workers, one of the possible synthetic strategies followed the most common way for the benzoporphyrin syntheses,[10–13] where substituted pyrroles are used to prepared the functionalized corrole ring. The reaction involved the condensation of a benzaldehyde with tetrahydroisoindole, leading to the formation of the tetrabenzocorrole in very moderate yields, upon oxidation of the intermediate tetrabutanocorrole (**Scheme 1.7**).[14]

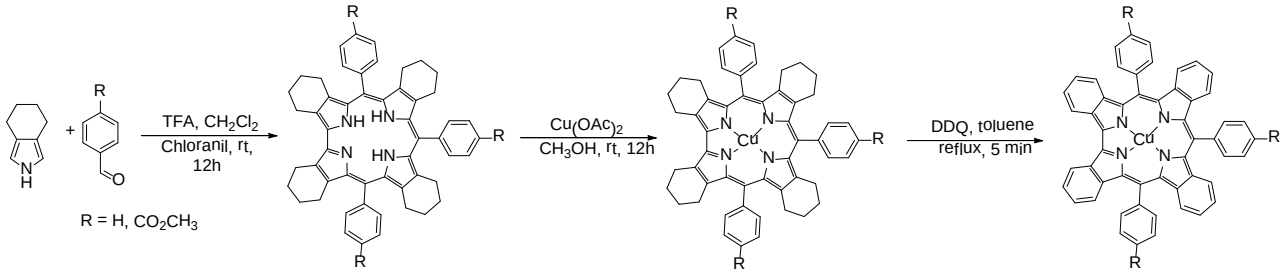

Scheme 1.7. Synthesis of triaryl-tetrabutanecorrole, further complexation and oxidation to get the tetrabenzocorrole derivative.

More recently, Shen and co-workers obtained a Cu-TBC from a copper bicyclo[2.2.2]octadiene (BCOD)-fused corrole through a retro Diels-Alder approach (**Scheme 1.8**).[15] In the procedure, 4,7-dihydro-4,7-ethano-2H-isoindole and benzaldehyde were dissolved in a mixture of H_2O and CH_3OH, followed by a small amount of HCl 36%. Further oxidation with chloranil and complexation with Cu(II) acetate afforded the desired Cu-BCOD in moderate yields (19%). Heating the macrocycle at 250 °C under vacuum (2 mmHg) for 20 min leads to the elimination of four ethylene molecules and the formation of Cu-tetrabenzocorrole in quantitative yield.

Cu-TBC was also obtained by sublimation onto an Au(111) substrate under ultrahigh vacuum conditions at ca. 300 °C. This derivative demonstrated to be a good candidate for molecular spintronics, since π-extended corroles complex can modulate spin states as a result of the modification to the d–π interaction between the metal and ligand.

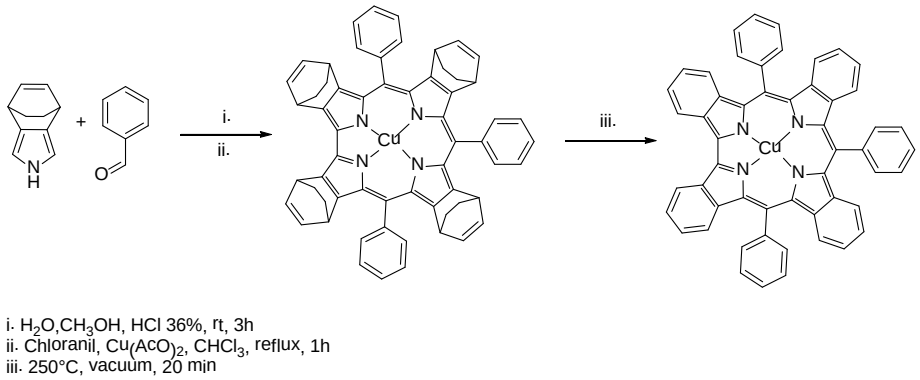

Scheme 1.8. TBC obtained by a retro Diels-Alder reaction from copper bicyclo[2.2.2]octadiene-fused corrole.

In the case of porphyrins, *β*-fused *π*-conjugated systems were mostly obtained through transition metal-catalyzed cross coupling reactions.[16,17] For these reactions, the most common starting material is the halogen-substituted macrocycle, and it is therefore mandatory to regioselectively insert the halogen atom into the porphyrin ring. Several halogenation procedures for the insertion of halogen atoms (Br^-, I^-, Cl^-) into the *β*-pyrrolic positions of the corrole macrocycle have been exploited. These strategies are typically based on the use of conventional halogenating reagents: Cl_2, Br_2, I_2 or the corresponding N-halosuccinimides.

In the case of corroles this route presents some difficulties: the lower symmetry of the corrole compared with porphyrin leads to the potential formation of a huge number of different regioisomers.[18–20]

While for several functionalization reactions corroles show a surprisingly high regioselectivity, with pyrroles A and D being more reactive than their B and C counterparts[21] the halogenation reaction is far less regioselective, affording a mixture of mono- and poly-halogenated isomers, which are difficult to separate, either as free bases or as metal complexes.

For this reason, when the preparation of corroles with *β*-fused benzene rings using a cross-coupling methodology, based on the Heck procedure, was attempted,[14,22] the approach was limited to the preparation of tetrabenzocorroles, using octabromocorrole

as the starting material. This procedure was reported by Paolesse and co-workers for the synthesis of TBC as alternative strategy to the condensation of benzaldehyde with tetrahydroisoindole. The reaction involved the octabrominated corroles and methyl acrylate in toluene/DMF at 125 °C, for 3 days, in the presence of $Pd(OAc)_2$, PPh_3 and K_2CO_3 (**Scheme 1.9**).

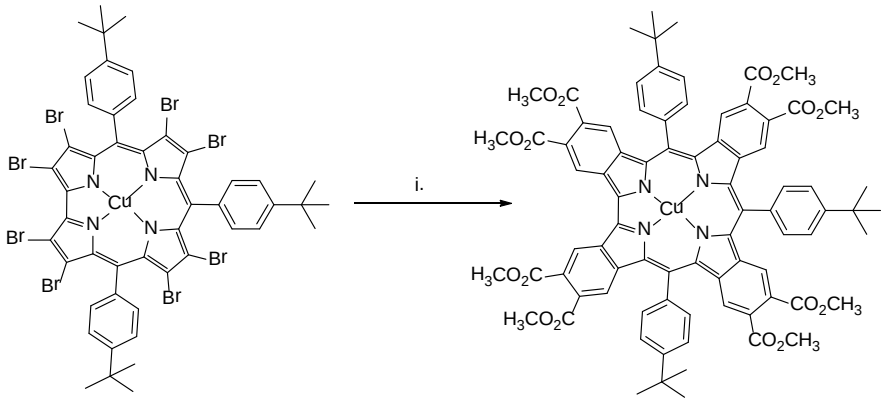

i. Methyl acrylate, $Pd(AcO)_2$, PPh_3, K_2CO_3, toluene/DMF, 125°C, 3 days

Scheme 1.9. Synthesis of TBC through Heck cross-coupling reaction.

Functionalization of aminocorroles

With the aim to prepare mono- or di-benzocorroles, our work has focused on the exploration of a different synthetic route for the fusion of aromatic moieties to corrole macrocycles, by using condensation reactions of suitable groups. Mono- or di-benzocorroles could be of particular interest for the investigation of the influence of the annulated rings on their physicochemical properties, thus offering a way to modulate them by selective functionalization of the corrole π-aromatic system.

The specific objective of this chapter is the design, synthesis and characterization of a series of β-fused annulated corroles. As explained above, the lack of effective synthetic strategies for corrole regioselective modification is still a nuisance, even if considerable efforts have been made to develop selective methods that allow the effective functionalization of the macrocycle. Moreover, the presence of two vicinal moieties in

the corrole β positions is mandatory for the construction of annulated systems. This makes the synthesis even more difficult.

To circumvent these limitations, the preparation of corroles bearing a nitro and a vicinal amino moiety was chosen as the most suitable strategy for further developments. Synthetic methodologies available for the insertion of the above mentioned functionalizations are discussed briefly in the following sections.

Nitration

Among the possible β-corrole modifications, nitration is considered particularly appealing, since the nitro group is a useful starting function for further developments. Several protocols have been developed to give access to corroles bearing one or more nitro groups directly linked to β-pyrrolic positions.[23,24]

The nitration of the Ga(III) complex of 5,10,15-tris(pentafluorophenyl)corrole was firstly reported by Gross and co-workers in 2002. The reaction was performed with an excess $NaNO_2$ in acetonitrile, followed by the addition of tris(4-bromophenyl)-aminium hexachloroantimonate, a one electron oxidant. Depending on the amount of oxidant used (75, 200 and 300 mol %), the reaction gives the 3-nitro-, the 3,17-dinitro-, and the 2,3,17-trinitrocorrole derivatives as the main products (84%, 94% and 58%, respectively) (**Scheme 1.10**). Most important, all three products were obtained as single isomers, that is, only one out of four possible mono-, one out of 16 di-, and one out of 28 tri-nitro corroles.

Moreover, the authors suggested that under these reaction conditions (very large excess of $NaNO_2$), the hexachloroantimonate oxidizes NO_2^- to NO_2, rather than the corrole to its π-cation radical.

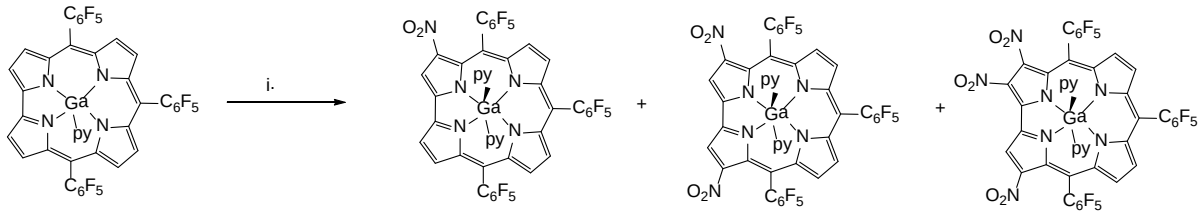

Scheme 1.10. Selective nitration of gallium(III) complex of 5,10,15-tris(pentafluorophenyl)corrole.

Paolesse and co-workers also studied the nitration of germanium(IV) complex of 5,10,15-triphenylcorrole using two different methods.

In the first one, the presence of the mild nitrating system as $LiNO_3$/ Ac_2O/AcOH led to the formation of the Ge(IV) 3-nitrocorrole monomer and the corresponding Ge(IV) 3-nitrocorrole μ-oxo dimer. The other approach involved the use of $NaNO_3$ in Ac_2O/AcOH, a more severe nitrating mixture, aiming to obtain polysubstituted products. In this case, the two main products identified were the μ-oxo dimers of the dinitro corrole. Upon the addition of dilute HCl, the dimers were converted into the monomeric species, bearing Cl^- and OH^- as axial ligands (**Scheme 1.11**). Crystallization of the monomeric corroles from CH_2Cl_2/MeOH gave the methoxy derivatives. Also in this case, the substitution is highly regioselective in each case, giving only the 3-nitro or 3,17-dinitro derivatives among the different possible isomers.[25]

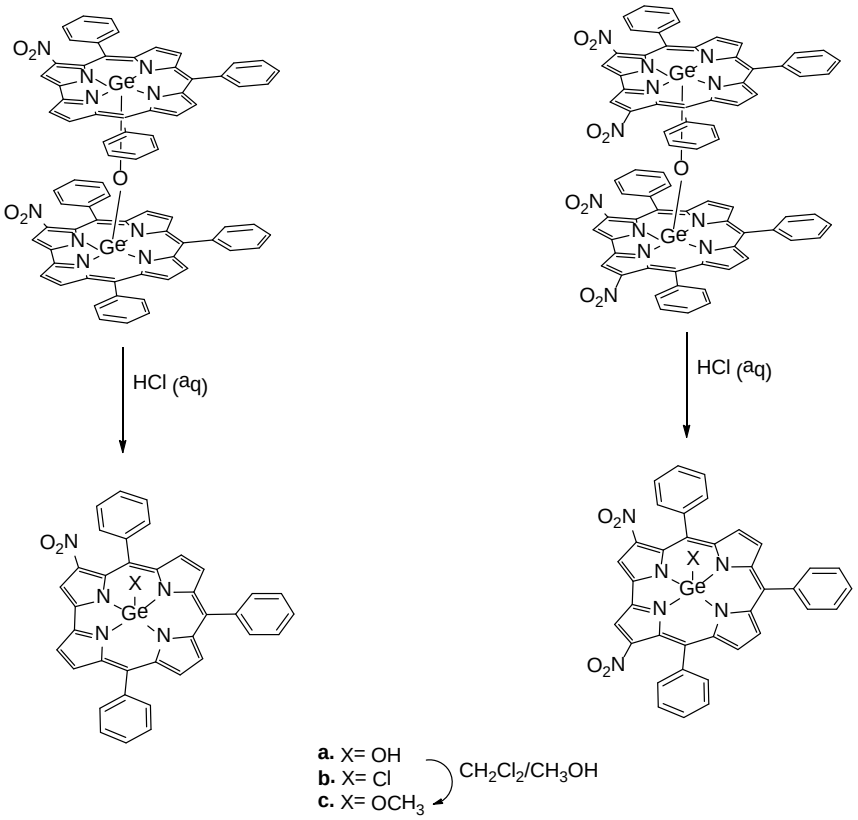

Scheme 1.11. Germanium(IV) μ-oxo dimer and the corresponding monomer.

Paolesse and co-workers studied the efficiency of various nitrating agents for the nitration of free base corroles and metallo corroles. It was verified that in the presence of a large excess of $AgNO_2$, the nitration and metallation of the macrocycle occurred simultaneously, affording the corresponding Ag(III) 3-nitrocorrole and the Ag(III)complex of the starting corrole (**Scheme 1.12**).

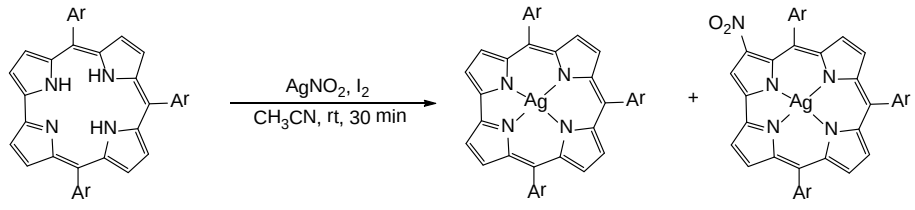

a. Ar = C_6F_5
b. Ar = C_6H_5
c. Ar = 4-$CH_3(C_6H_4)$
d. Ar = 4-$(CH_3)_3C(C_6H_4)$
e. Ar = 3,5-$F_2C_6H_3$

b. Ar = C_6H_5
c. Ar = 4-$CH_3(C_6H_4)$
d. Ar = 4-$(CH_3)_3C(C_6H_4)$

Scheme 1.12. Nitration of *meso*-triarylcorroles with $AgNO_2/I_2$.

Furthermore, it was found that electron-releasing *meso*-aryl groups favoured the nitration while electron-withdrawing aryl groups promoted the decomposition of the corrole ring, with the formation of ring-opened derivatives. It was observed that, although not being necessary for the success of nitration, addition of I_2 increases the rate of the reaction, while the presence of the silver ion is crucial for the success of the reaction. The role of the silver ion for the nitration at the *meso* position of *β*-octaalkylporphyrins was previously elucidated.[26]

The authors proposed a reaction pathway, where the nitrating agent is the NO_2- ion, which attacks the Ag(III) π-cation radical, formed by oxidation with excess of the Ag^+ ion. Then, a second one-electron oxidation takes place, and the loss of a proton restores the corrole aromaticity (**Scheme 1.13**).

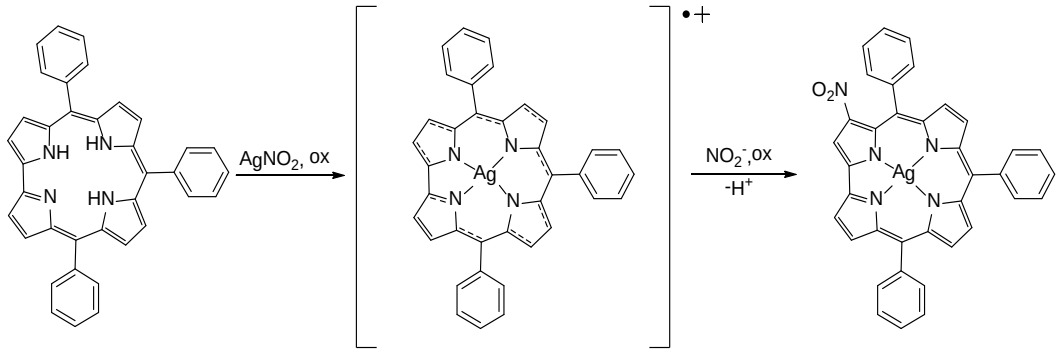

Scheme 1.13. Proposed nitration pathway.

The following reductive demetallation procedure under basic conditions (DBU/THF) led to free base 3-(NO_2) corrole derivative.[27]

Further studies revealed that the reaction with the $AgNO_2$/$NaNO_2$ system was regioselective and gave mono- and dinitrocorrole derivatives when the stoichiometry was carefully controlled. Using the ratio of 1:1:9 for corrole/$AgNO_2$/ $NaNO_2$ the 3-nitro derivative was obtained as the main product (52% yield) and 2-nitrocorrole as a minor one (**Scheme 1.14**). Changing the molar ratio to 1:2:8 (corrole/$AgNO_2$/$NaNO_2$), the 3,17-dinitrocorrole becomes the main product (20% yield). In the same paper, another approach to obtain selectively the 3,17-dinitrocorrole was reported. Free base corrole and $Cu(OAc)_2$ were dissolved in pyridine, followed by a huge excess of $AgNO_2$ (1:50), affording the dinitro derivative in a 52% yield.

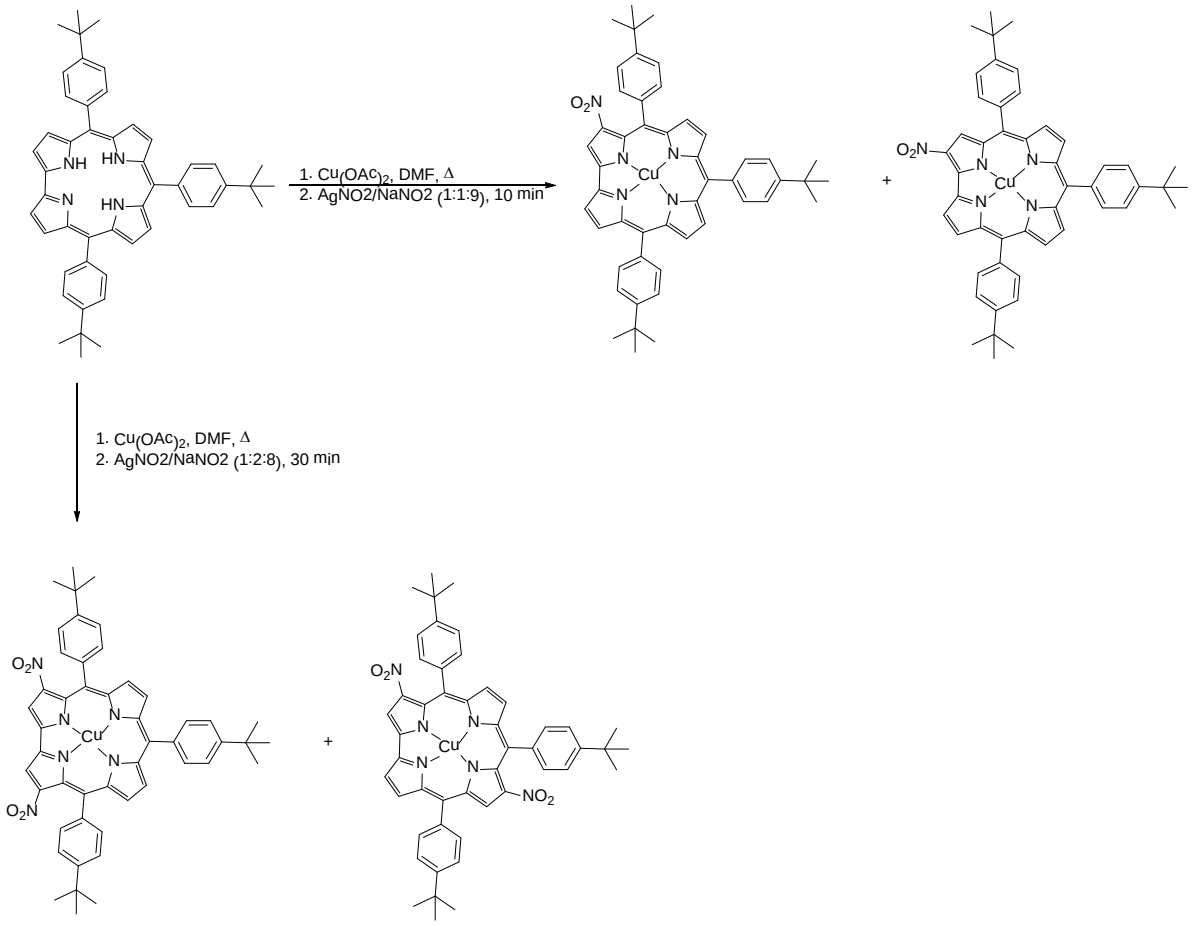

Scheme 1.14. Preparation of *β*-nitro corrole derivatives.

Amination

In analogy with the work developed in the porphyrin field,[28] several procedures leading to the insertion of amino moieties are based on the reduction of nitro groups. In 2005, Collman and Decréau[29] exploited this approach starting from 5,10,15-tris (2-aminophenyl)corrole, for the synthesis of a series of free base hemoprotein corrole derivatives. The reduction of 5,10,15-tris(*o*-nitrophenyl)corrole was achieved in 80% yield by treatment with 9 equiv $SnCl_2 \cdot 2H_2O$ in HCl at 70°C, followed by neutralization and extraction with ethyl acetate. The desired amino-derivative was obtained as a mixture of atropisomers (αβα, ααβ, ααα) (**Scheme 1.15**).

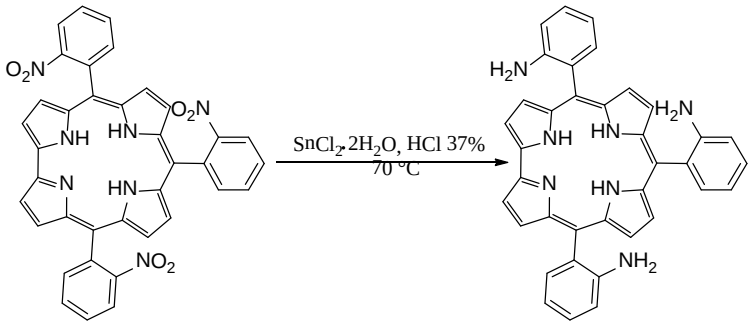

Scheme 1.15. Synthesis of meso-substituted amino corroles.

The same group applied the methodology to other aryl-corroles complexes bearing electron withdrawing substituents at their *meso* positions.[30] Another approach was described by Guilard and co-workers, in their study on the synthetic design of organic–inorganic hybrid materials.[31] In their attempt to introduce a (propyl)triethoxysilane in *para* positions of the phenyl substituent, they reduced the nitro group with H_2/Pd/C, followed by the reaction with (3-isocyanatopropyl)triethoxysilane in acetonitrile. After 4 days, the desired compound was obtained in 68% yield (**Scheme 1.16**).

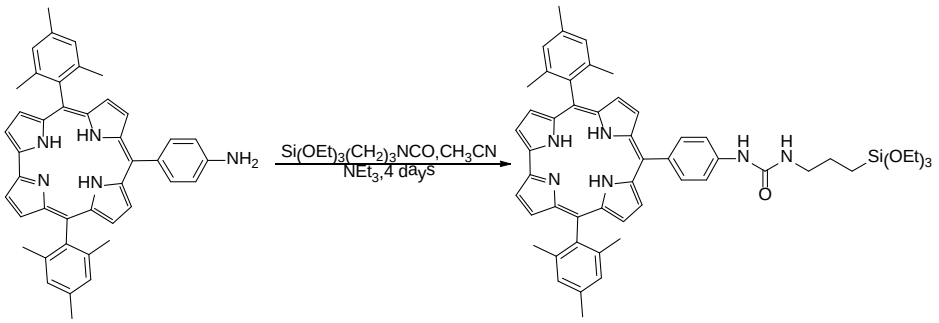

Scheme 1.16. Functionalization of *meso*-substituted amino corroles.

The same group[32] obtained corroles bearing a benzylamino group at the *meso*-position by reduction of an azido moiety. The corrole was dissolved in THF, followed by a dropwise addition of triphenylphosphine in THF. Further hydrolysis afforded the amino-derivative in 52% yield (**Scheme 1.17**).

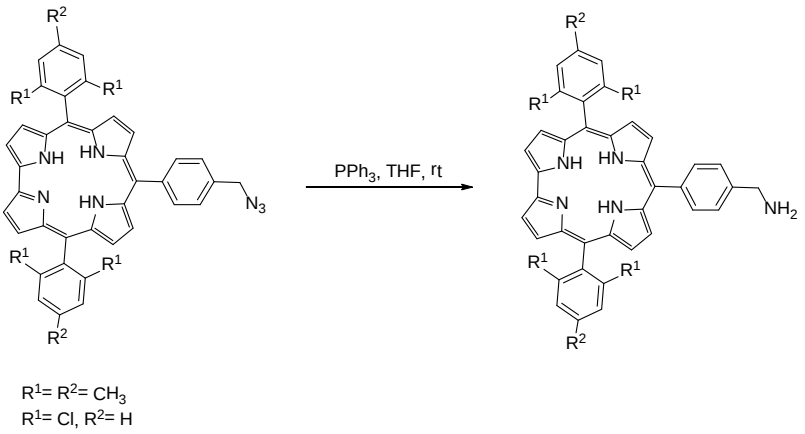

Scheme 1.17. Synthesis of corrole derivatives bearing benzylamino group.

In 2011 Paolesse and co-workers investigated the role of corroles toward SNAr reactions at free *β*-positions. According to the protocol employed for the preparation of 2-amino-3-nitroporphyrins,[33] they discovered that the *β*-nitro group activate nucleophilic substitution on the vicinal positions of the corrole ring. Performing the reaction on the copper complex of 3-nitrocorrole with 4-amino-4H-1,2,4-triazole in the presence of NaOH using a molar ratio of 1:12:5, the desired 2-amino-3-nitrocorrole was obtained after 45 min (**Scheme 1.18**).

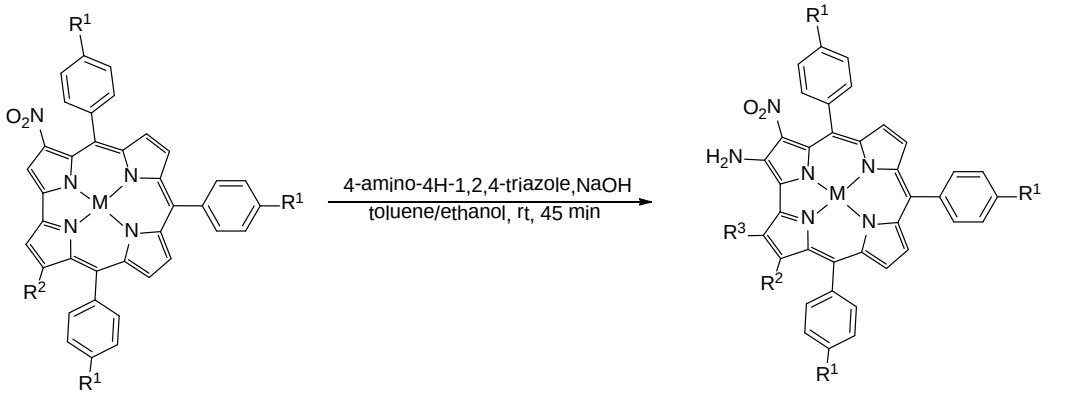

a) R^1= $C(CH_3)_3$, R^2= H, M=Cu
b) R^1= $C(CH_3)_3$, R^2= NO_2, M=Cu
c) R^1= H, R^2= H, M=$Ge(OCH_3)$

d) R^1= $C(CH_3)_3$, R^2= R^3= H, M=Cu
e) R^1= $C(CH_3)_3$, R^2= NO_2, R^3=NH_2, M=Cu
f) R^1= H, R^2= R^3= H, M=$Ge(OCH_3)$

Scheme 1.18. Amination on *β*-nitrocorrole derivatives with 4-amino-4H-1,2,4-triazole.

The extension of such experimental conditions to 3,17-dinitro derivative afforded the tetra-substituted 2,18-diamino-3,17-dinitrocorrole (**Scheme 1.18**). A similar reaction profile is observed with a Ge(IV) 3-nitrocorrole, giving the 2-amino-3-nitrocorrolate in 50% yield.

Since the preparation of corroles bearing vicinal substituents is the first necessary step toward new highly conjugated fused oligomeric systems, these derivatives (bearing vicinal amino and nitro moieties) have been chosen as building blocks for further developments in this work.

Results and discussion

Since diamagnetic copper complexes of triarylcorroles are good substrates for the nitration reaction and the subsequent amination, we decided to use copper complex of tris-(5,10,15-*tert*-butylphenyl)corrole [*t*BuTPC]Cu as starting material. This substrate underwent nitration reaction, followed by a vicarious nucleophilic substitution with 4-amino-4H-1,2,4-triazole leading to [2-(NH_2)-3-(NO_2)-*t*BuTPC]Cu (**1**) and 2,18-(NH_2)$_2$-3,17-(NO_2)$_2$-*t*BuTPC] Cu (**2**).[33] The first route for the preparation of corroles with annulated aromatic rings exploits the reduction of the nitro group to get the diamino (or tetraamino) moiety and the further one-pot condensation with an *α*-dione. The other procedure exploit a Pictet-Spengler reaction to obtain a *β,β′*-pyrrolo(1,2-*a*)pyrazino-fused corrole. Both synthetic approaches led up to corroles characterized by having a pyrazine unit in the linker.

Functionalization by one- pot reduction and condensation

A widely extended method to obtain new expanded porphyrin derivatives relies on the condensation of vicinal diketones with an *o*-diamino derivative. It could be achieved by following two main synthetic approaches: whereas in the former case a *o*-damino porphyrin is reacted with an α- dione (diethyl oxalate, 1,2-cyclohexanedione) (**Scheme 1.19a**); as far as the second case is concerned, a porphyrin derivative bearing an *α*-dione moiety is reacted with a aromatic *o*-diamines (3,4-diaminothiophene, diaminomaleonitrile, 2,3,5,6-tetraamino-1,4-benzoquinone) (**Scheme 1.19b**).
In the case of corrole, all the attempts to obtain the corresponding dione failed, probably due to the facile oxidative decomposition of this macrocycle. This is the reason why condensation reactions merely involve *α*-diaminocorrolates as substrates.

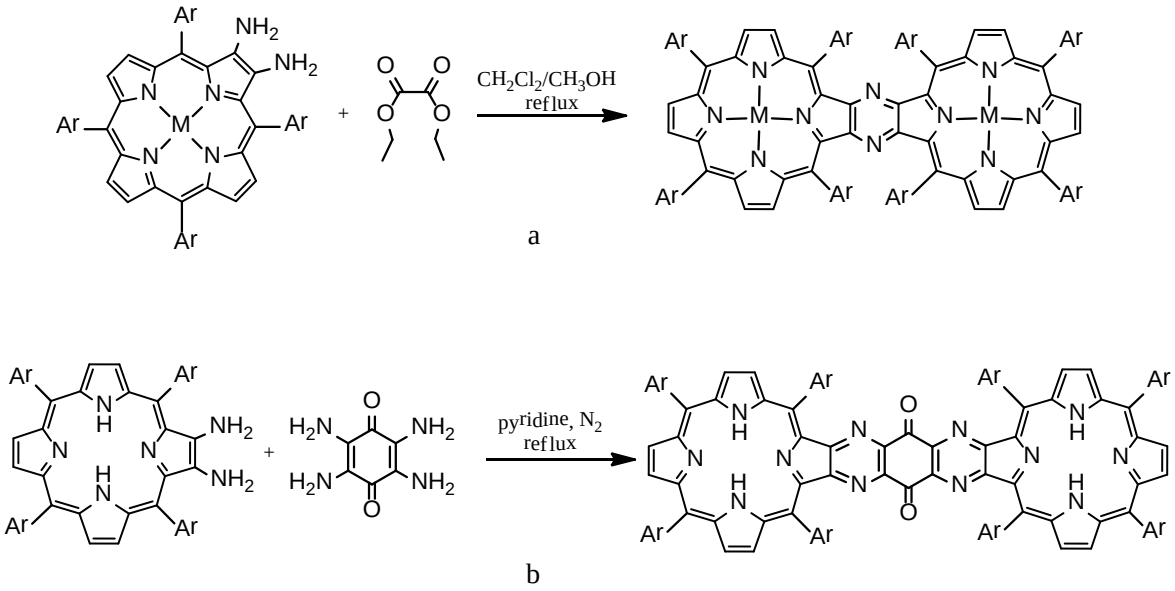

Scheme 1.19. Synthesis of *β*-pyrazino-fused tetrarylporphyrins by condensation with diethyl oxalate (**a**) and with 2,3,5,6-tetraamino-1,4-benzoquinone (**b**).

Reaction with 1,2-cyclohexanedione

At the outset for the standardization of the reaction conditions for the synthesis of the desired *β*-fused copper[1,2-*b*] pyrazinocorrolates, we selected 1,2-cyclohexanedione as a model dione because it could be easily detected using ^{1}H NMR analysis, considering that its protons resonate in the aliphatic region (**Scheme 1.20**).

For such a purpose the 2,3-diamino copper complexes of the *t*BuTPC has been prepared by reduction of the corresponding mononitro-monoamino derivatives:[33] as well as in the case of porphyrins, the reaction has been carried out in a solvent mixture (CH_2Cl_2/MeOH 4:1$_{v/v}$) by using Pd/C 10%$_{wt}$ as catalyst and $NaBH_4$ as reducing agent.[34]

Unlike porphyrins, the diamino derivative is not stable, so it should be used as soon as prepared, without a prior purification. For this reason the reaction was performed one-pot, reducing the nitro group and immediately carrying out the condensation.

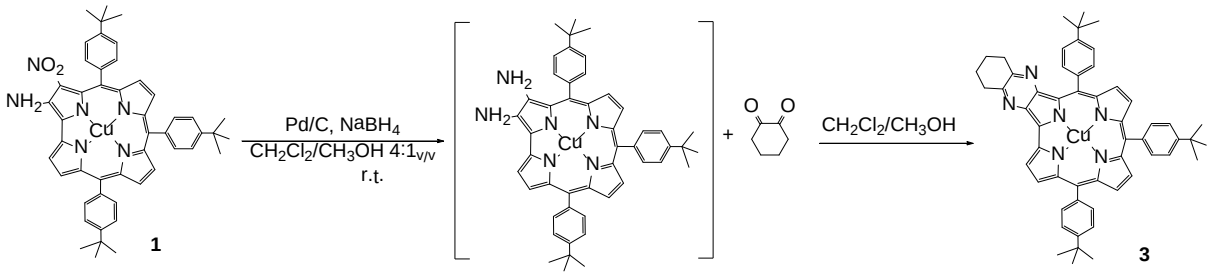

Scheme 1.20. Synthetic route to 2,3-[1'2'-*b*]pyrazinocorrolatoCu(II) (**3**).

The diamino complex was reacted with the dione for 1 h, controlling the reaction progress by TLC; when no more starting material was detected, a brownish spot with the highest R_f appeared together with some degradation products. The reaction work-up and the chromatographic separation afforded the first fraction as the desired corrole **3** in moderate yields (26%).

The ^{1}H NMR showed broad signals, however it has been possible to observe three signals with different integration values in the aliphatic zone, which underscore the presence of the annulated cyclohexane ring (**Figure 1.2**).

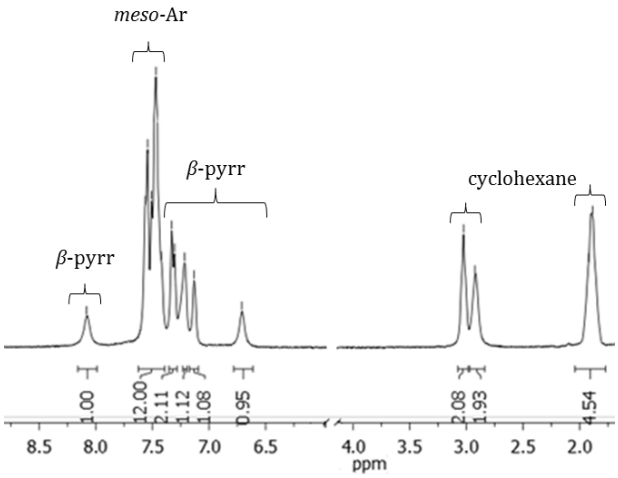

Figure 1.2. ^{1}H NMR spectrum of **3.**

The low resolution observed for the ^{1}H NMR spectrum was more serious in the case of the ^{13}C NMR spectrum, where only the signals of the peripheral *tert*-butyl and cyclohexane groups can be observed. This broadening can be reasonably due to aggregation phenomena, which also reduced the solubility of these complexes.

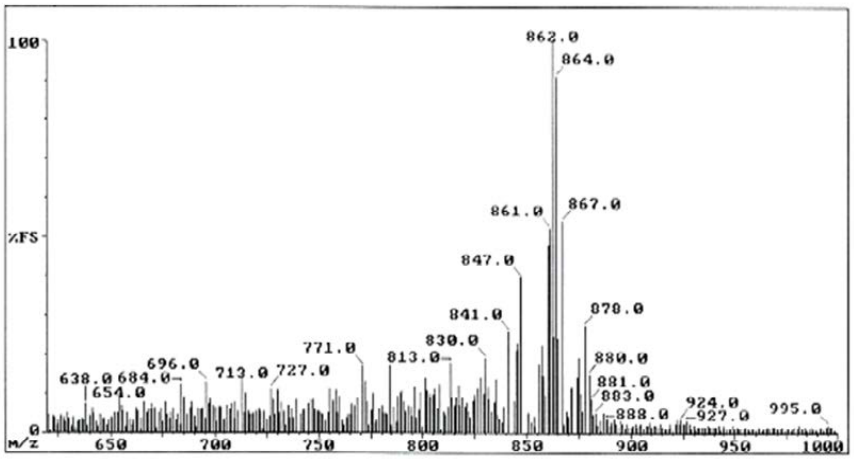

Figure 1.3. FAB spectrum of **3.**

The molecular ion peak in the FAB spectrum at m/z 862 was compatible with structure **3** (**Figure 1.3**), which was then unequivocally characterized by X-ray analysis (**Figure 1.4**) carried out on single crystals obtained from slow diffusion of methanol into a chloroform solution of **3**.

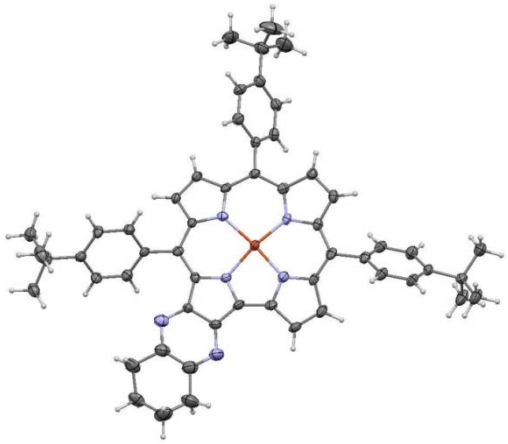

Figure 1.4. Crystal structure of **3**, with 50% ellipsoids.

Cu–N distances are in the range 1.898(5)–1.911(5) Å, the longest to the pyrrole fused to pyrazine. The Cu atom lies 0.080 Å out of the best plane of the 23-atom corrole core, which has a saddle distortion with a mean deviation of 0.148 Å from coplanarity. The pyrazino plane is nearly coplanar with the corrole, forming a dihedral angle of 6.0° with it.

The successful preparation of **3** led us to explore the possibility of synthesizing the corresponding corrole bearing two annulated pyrazino rings, using the same synthetic protocol considering the availability of the starting complex **2**. In this case the starting complex was also reduced and then condensed with two equivalents of 1,2-cyclohexanedione to obtain the target complex **4** (**Scheme 1.21**).

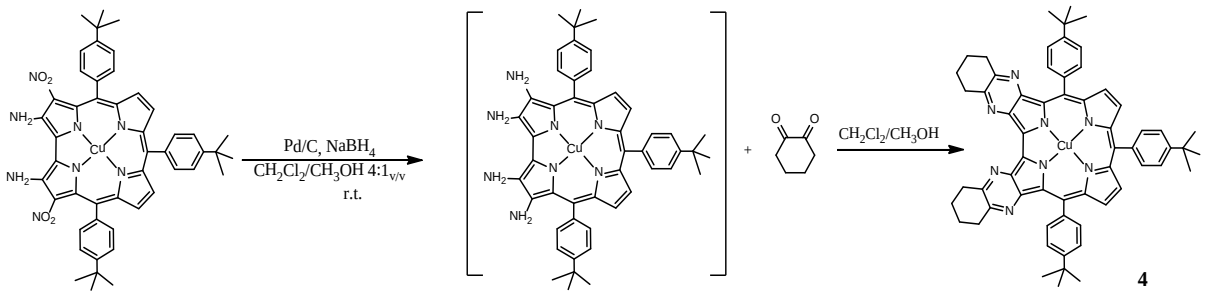

Scheme 1.21. Synthetic route to 2,3,17,18-bis-[1',2'b]pyrazinocorrolatoCu(II) (**4**).

The UV-vis spectrum of the compound had a pattern comparable with the monocondensed species; the Soret band exhibited a slight red shift (from 431 nm to 442 nm), as shown in **Figure 1.5.** Each condensed system contributed with an 11 nm bathochromic shift of the Soret band, it can be adequately explained by the expanded π-aromatic system owing to pyrazine moiety.

The magnitude of the shift is in agreement with the data already reported in the literature.[14,35,36]

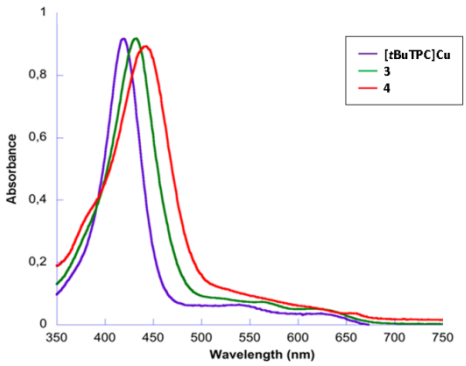

Figure 1.5. UV-vis spectra of **[*t*BuTPC]Cu** (purple), **3** (green), **5** (red).

Due to the higher symmetry of the molecule, only two doublets were observed in the ^{1}H NMR spectrum (**Figure 1.6**), which also showed the severe line broadening observed for **3**. FAB result was consistent with the formation of the above-mentioned complex, giving a ion peak at 969 m/z (**Figure 1.7**).

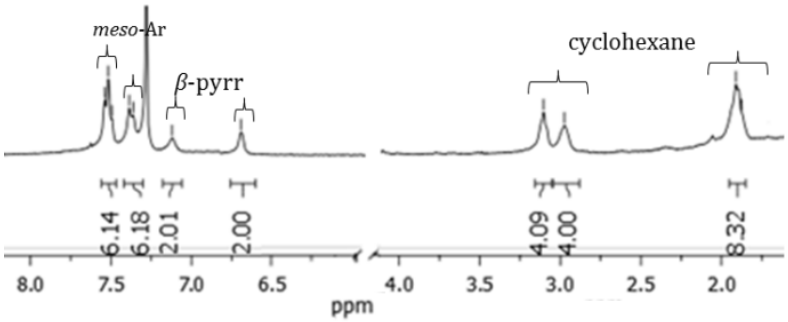

Figure 1.6. ^{1}H NMR spectrum **4.**

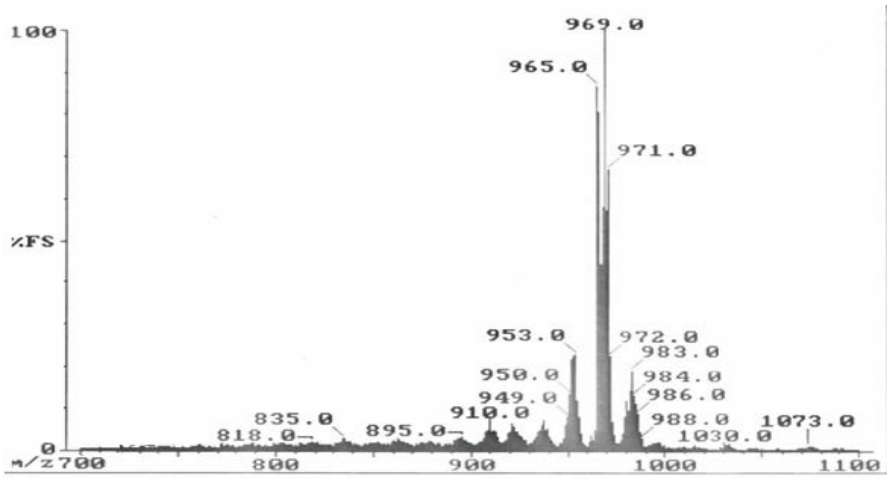

Figure 1.7. FAB spectrum of **4.**

We were also able to obtain a single crystal suitable for X-ray crystallographic analysis, which confirmed the formation of the above-mentioned complex (**Figure 1.8**). The compound crystallizes with four independent molecules in the asymmetric unit, with Cu–N distances in the range 1.890(3)–1.931(3) Å and mean value 1.908 Å. For all four molecules, the longest Cu–N distance is to a pyrrole fused to pyrazine, mean value 1.926 Å.

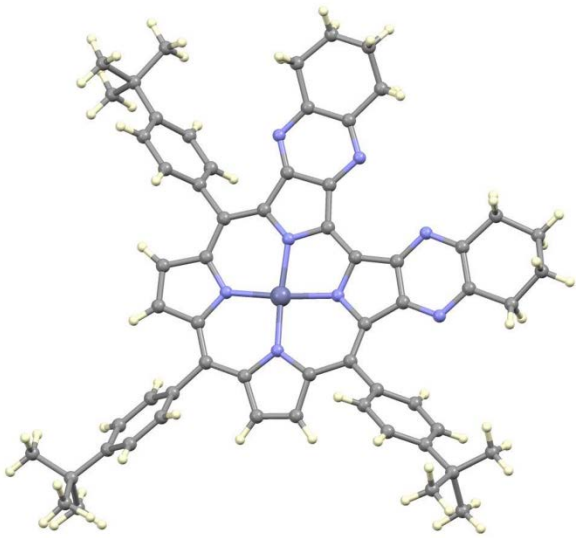

Figure 1.8. Crystal structure of **4**, with 50% ellipsoids.

The coordination geometry of the Cu center is square planar with a slight tetrahedral distortion, the N atoms lying alternately above and below the CuN_4 plane by a mean (of 16) value of 0.178 Å. The N atoms also lie in an average distance of 0.180 Å from the best plane of the corrole core, while the 19 C atoms are somewhat more coplanar, exhibiting a mean deviation of 0.076 Å. The pyrazine planes are tipped out of the corrole planes by variable amounts, forming dihedral angles in the range 1.6–12.9°, mean (of 8) 7.5°.

Reaction with 1,4-dibromo-2,3-butanedione and further functionalization

As mentioned in the general introduction of this thesis, the functionalization of the corrole core *via* cycloaddition reactions is another important approach that can give access to a wide variety of novel corrole derivatives. Up to now in the literature only 5,10,15-tris(pentafluorophenyl)corrole (and the corresponding *β*-vinylcorrole) was reported, acting either as a 2π or as a 4π component in the presence of pentacene .[37,38] To test the scope of the Diels-Alder reaction with other corrole derivatives and with the aim to obtain a functionalized macrocycle, we studied the reaction between the [2-(NH_2)3-(NO_2)-*t*BuTPC]Cu complex and 1,4-dibromobutanedione, following the same procedure used for the previous diones (**Scheme 1.22**).

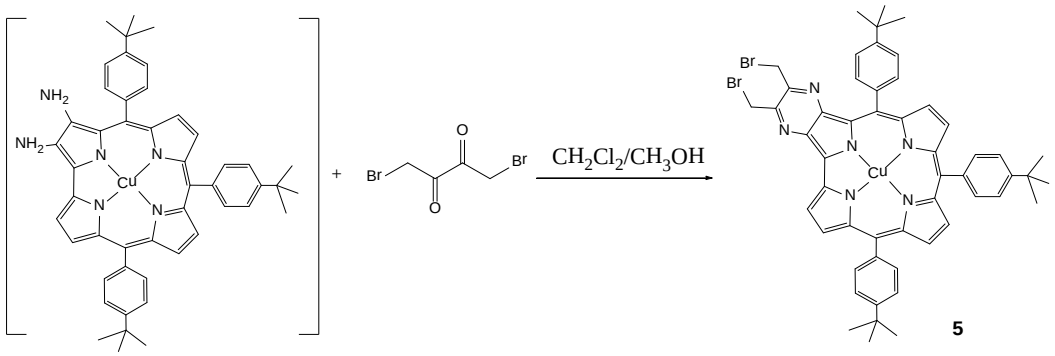

Scheme 1.22. Synthetic route to **5.**

The annulated system was obtained with a 30% yield and it was characterized by UV-vis, ^{1}H NMR and mass analyses. ^{1}H NMR showed also in this case a severe line broadening, making the assignment more difficult. Nevertheless, it has been possible to observe two peaks, at 4.95 and 4.64 ppm, corresponding to the CH_2 fused to the pyrazino moiety (**Figure 1.9**). UV-vis spectrum of **5** (**Figure 1.10**) showed a pattern comparable with complex **3**, with a red shifted and broad Soret band (if compared with [*t*BuTPC]Cu) and an unsolved Q bands at 638 nm.

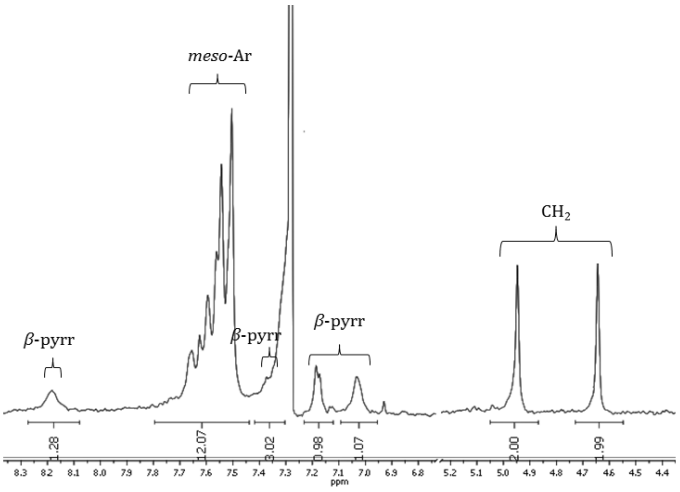

Figure 1.9. ^{1}H NMR spectrum **5.**

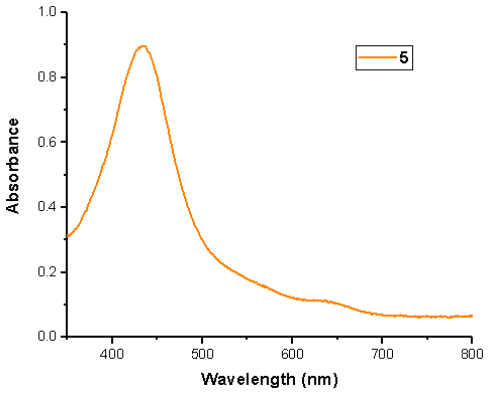

Figure 1.10. UV-vis spectrum of **5.**

FAB mass spectrum shows the molecular ion peak at 994 m/z, consistent with the desired species. Moreover, losses from the molecular ion of bromine atoms are shown at 917 and 833 m/z, respectively (**Figure 1.11**).

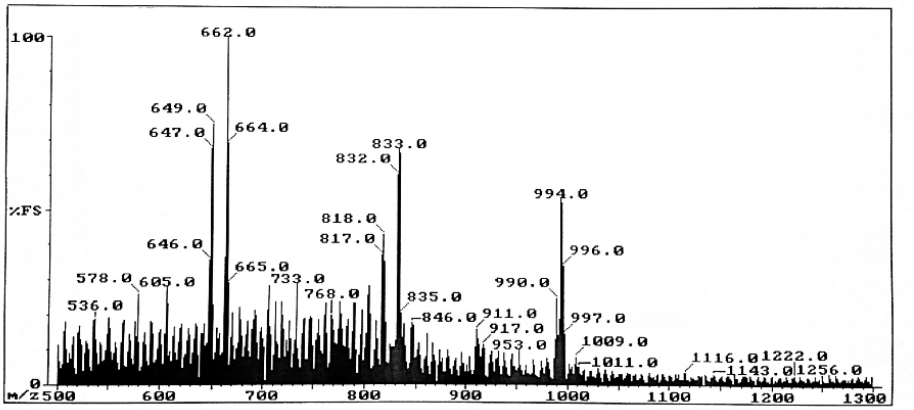

Figure 1.11. FAB spectrum of **5.**

We decided to use the approach reported for tetraphenylporphyrins with a pyrazine *o*-quinodimethane derivative providing *β*-fused annulated systems. The pyrazine *o*-quinodimethane was generated in situ from the corresponding 2,3-bis(bromomethyl)pyrazine derivative in the presence of porphyrins by adding NaI.[39] In our case we choose as dienophile 5,10,15,20-tetrakis(pentafluorophenyl) porphyrin (TF_5PP), that was prepared following the procedure reported in the literature.[40] TF_5PP and complex **5** were dissolved in 1,2,4-trichlorobenzene, followed by the addiction of KI. The reaction was followed by TLC analysis and UV-vis spectroscopy. After 7 hours three main fractions were collected by chromatographic column. The first one corresponded to the TF_5PP copper complex, the second one was the TF_5PP free base while the last fraction exhibited a corrolic feature, although the quantity of such a species did not permit a thorough characterization. Moreover, many degradation products were evinced (**Scheme 1.23**).

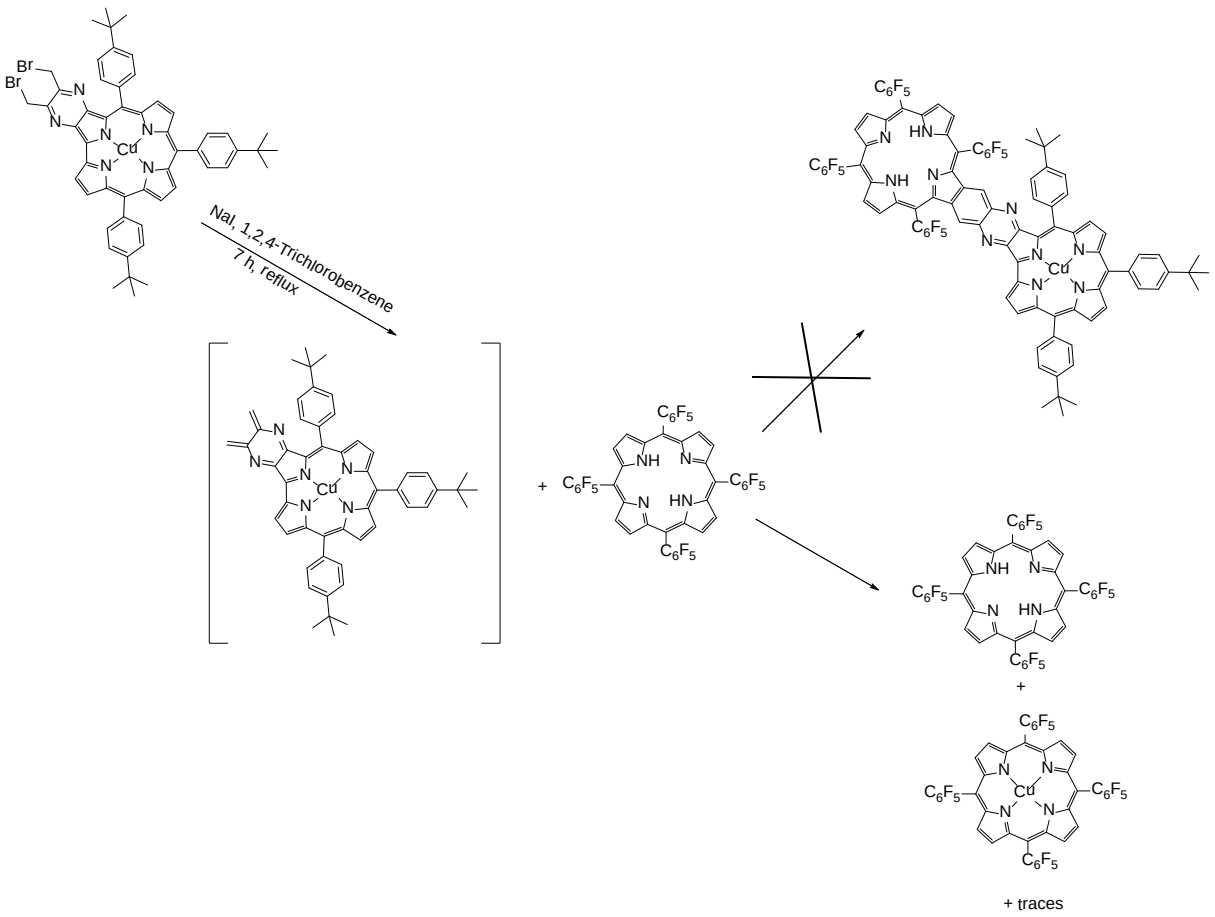

Scheme 1.23. Attempt of Diels Alder reaction.

We tried the same approach with a smaller dienophile in order to avoid steric hindrance. For such a purpose we chose methyl acrylate. Even with this type of approach no products were evidenced, and after 3 hours TLC analysis and UV-vis analyses showed the presence of the no reacted starting material and many degradation products (**Scheme 1.24**).

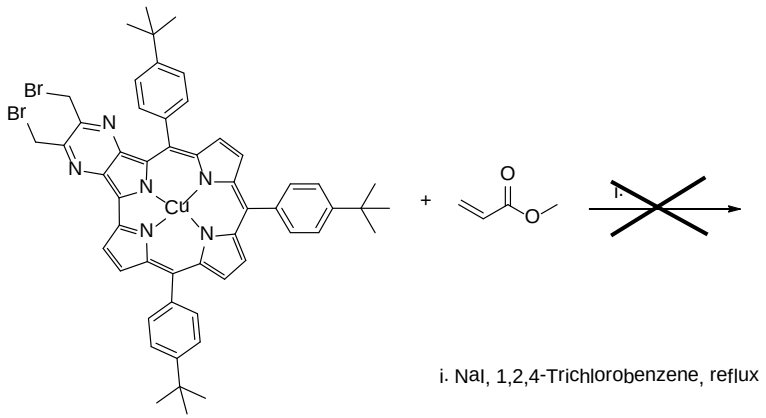

Scheme 1.24. Attempt of Diels Alder reaction.

The failure of the reaction both with TF_5PP and methyl acrylate could be reasonably explained considering the oxidative environment due to the presence of NaI and the reaction conditions of high temperature, that make the copper corrole susceptible to degradation.

Reaction with 9,10-phenanthrenequinone

We directed our own efforts towards the fusion of an aromatic substituent at the macrocycle *β*-position, in order to enhance the expansion of the π-aromatic system of the macrocycle and the resulting optical features. With this aim in mind, we chose the 9,10-phenanthrenequinone as the dione for the coupling reaction (**Scheme 1.25**).

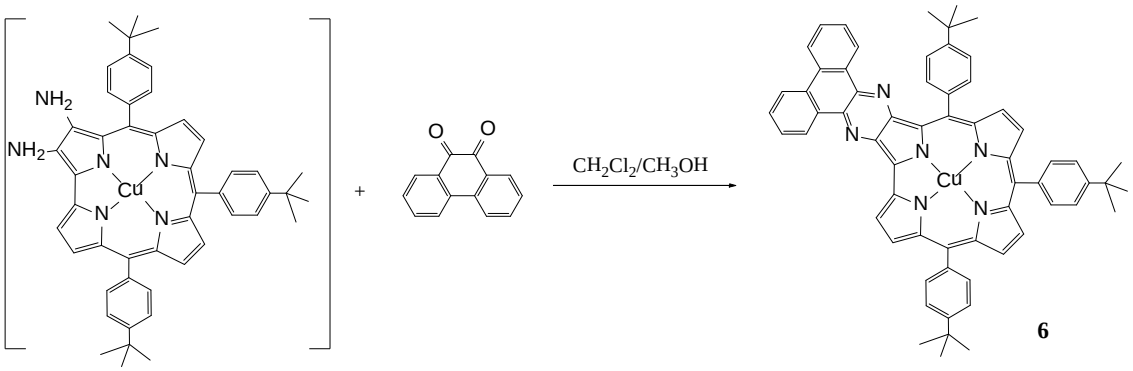

Scheme 1.25. Synthetic route to **6.**

Following the same procedure used for **3** and **5**, starting from the 2,3-diamino copper complex, we obtain compound **6** in 44% yield. Also in this case, the desired complex was fully characterized. ^1H NMR spectrum was not particularly indicative, since all the phenanthrene signals resonated in the same region of the *meso*- functionalities, with a partial overlapping between 7 and 7.5 ppm (**Figure 1.12**).

FAB value of 957 m/z matched with **6**. Moreover, we have been able to obtain single crystals suitable for X-ray crystallographic characterization (**Figure 1.13**).

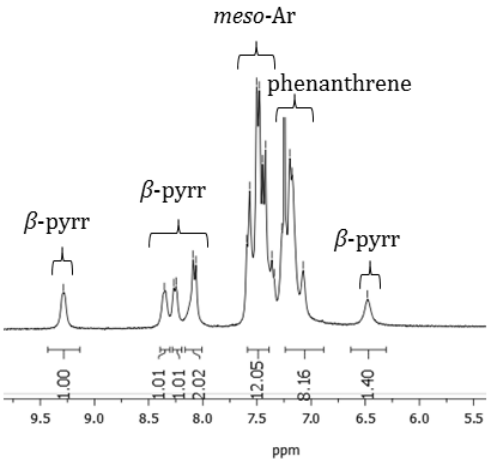

Figure 1.12. ^{1}H NMR spectrum **6.**

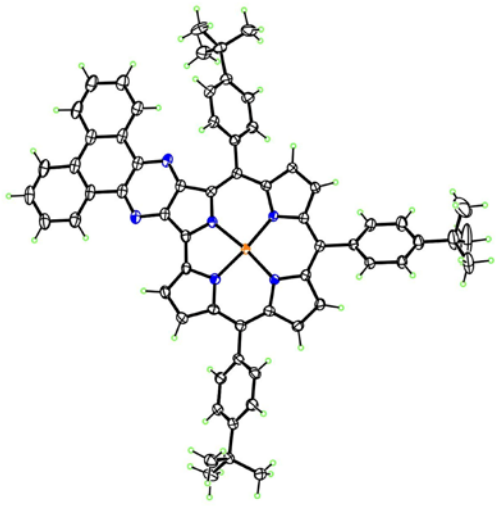

Figure 1.13. Crystal structure of **6**, with 50% ellipsoids.

The structure is very similar to that of **4**, with Cu–N distances in the range 1.895(2)–1.912(2) Å, the longest to the pyrrole fused to pyrazine. The Cu atom has slightly tetrahedrally- distorted coordination, with N atoms alternating a mean distance of 0.140 Å above and below the CuN4 plane. Cu lies 0.022 Å out of the best plane of the 23-atom corrole core, which has a saddle distortion with a mean deviation of 0.171 Å from coplanarity. The phenanthrene pyrazino plane is tilted slightly from the corrole plane, forming a dihedral angle of 4.1° with it.

The same reaction was performed on **2** (**Scheme 1.26**), affording compound **7** in low yields (8%).

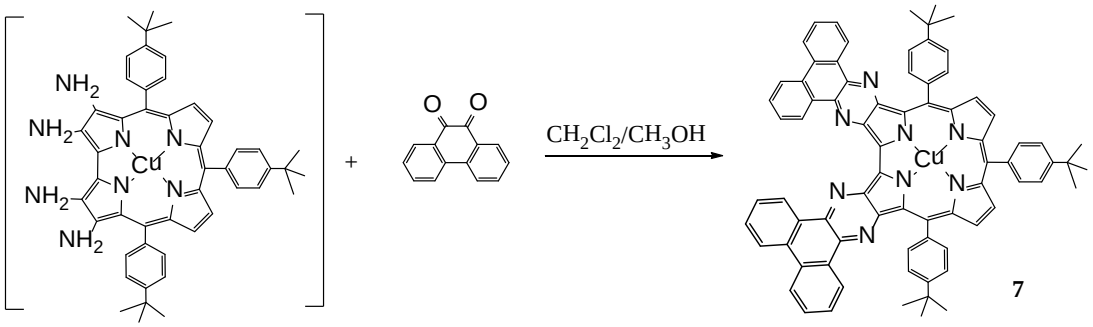

Scheme 1.26. Synthetic route to 7.

^{1}H NMR of **7** showed a severe line broadening, making impossible both the integration and the assignment of each peak. Nevertheless, we were able to observe a FAB peak at

1160 m/z, which corresponds to the desired species. UV-vis comparison between complexes **6** and **7** is shown in **Figure 1.14**.

Once again, bathochromic shifts of the Soret band were evidenced, by comparing [*t*BuTPC]Cu with the analogous monoannulated (**6**) and diannulated (**7**) derivatives. However, UV-vis comparison of **7** with [*t*BuTPC]Cu and **6** is not possible, due to its tendency to form aggregates. This gives rise to a broad Soret band and to scattering phenomena, as it is clear from the high baseline absorbance.

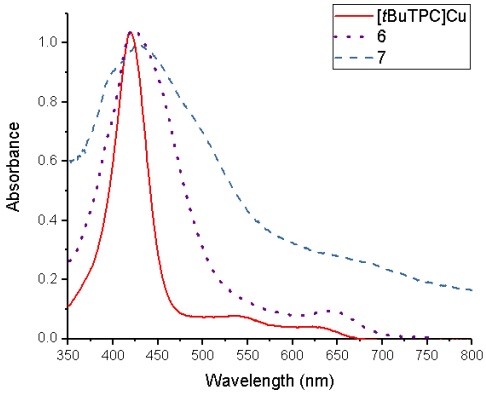

Figure 1.14. UV-vis spectra of **[*t*BuTPC]Cu** (red full line), **6** (purple dotted line) and **7** (blue dashed line).

Demetalation

It is well known the temperature-dependent magnetic behavior of copper corrolates, which was ascribed to an equilibrium between a diamagnetic Cu(III) corrole and a paramganetic Cu(II) corrole π-cation radical of higher energy. Thus, ^{1}H NMR spectra of these complexes exhibited broaded and not so well solved signals, because of the overlapped signals of *β*-pyrrolic and phenyl protons. Moreover, so as to appreciate the real bathochromic shift from the *t*BuTPC free base, we decided to remove the copper ion from the macrocycle, following the procedure reported in literature.[41]

By treating complex **6** with concentrated sulfuric acid in $CHCl_3$ at room temperature, the desired corrole free base **8** was obtained after 10 minutes with moderate yield (27%). FAB peak at 897 m/z was consistent with **8**, and ^{1}H NMR showed an increased peak resolution, if compared with the analogous copper complex.

UV-vis absorption spectra of *t*BuTPC and the selected condensed-corrole free base in CH_2Cl_2 are shown in **Figure 1.15.**

These corrole molecules absorb the whole visible spectra region and display characteristic Soret bands, which are found to be drastically red shifted as compared to the starting material, thereby confirming the increase of π-conjugation in these corrole analogues.

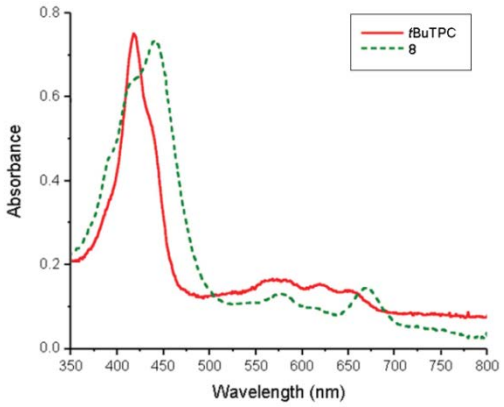

Figure 1.15. UV-vis spectra of ***t*BuTPC** (red full line) and compound **8** (green dashed line).

Catalytic hydrogenation and condensation

We noticed that the condensation proceeded almost quantitatively, but the crucial factor for the overall yields of the reaction was the reduction step. The *β*-aminocorroles are in fact very sensitive to decomposition and most of these intermediates decomposed during the reduction reaction. For this reason, we decided to investigate the possibility of exploiting reducing systems other than sodium borohydride, with the aim of optimizing both a milder reaction and purification conditions that can eliminate the decomposition of the di- or tetra-amino species.

We decided to carry out the catalytic hydrogenation with H_2 gas and 10% Pd/C in dry THF. Unfortunately, the application of this methodology to **1** was not productive, since most of the starting materials was left unreacted and no *β*-fused system was detected when the condensation reaction was attempted. In the case of **2**, we performed the reaction firstly with 1,2-cyclohexanedione. To a solution containing corrole **2** in dry THF, the catalyst was added, and the reaction was allowed to stir at room temperature under an excess of hydrogen for 1h 40 min. Then, the hydrogen was removed and the desired dione added, letting it react overnight. The isolated product was not the

expected corrole derivative, but the monofunctionalized species **9**, which retained a nitro and an amino moieties (**Scheme 1.27**).

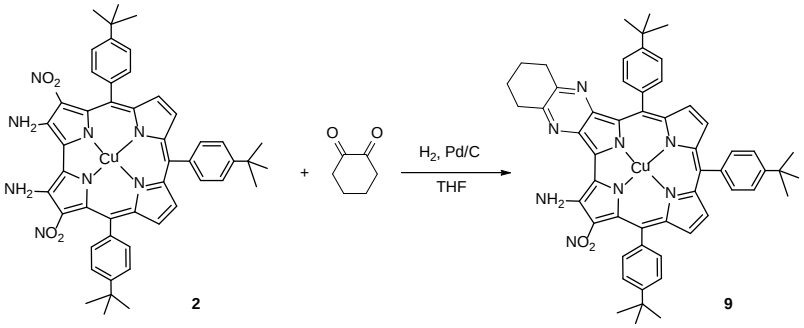

Scheme 1.27. Hydrogenation of complex **2** and further condensation with 1,2-cyclohexanedione.

Complex **9** was characterized by FAB spectrometry, that gave the molecular peak at 921 m/z, in accordance with the molecular weight of the aforementioned compound. Moreover, the peak at 874 m/z is congruous with the NO_2 loss from the macrocycle (**Figure 1.16**).

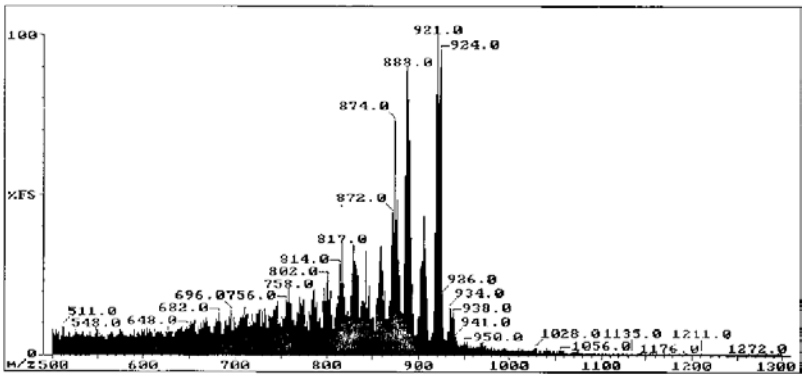

Figure 1.16. FAB spectrum of **9.**

^{1}H NMR showed two 4H integration peaks in the aliphatic range, and two 1H integration peaks at 6.23 and 6.72 ppm, corresponding to the two NH_2 protons, thus confirming the formation of **9**. Moreover, the symmetry reduction of the system provoked a splitting in the *tert*-butyl signals, which resonate at three different chemical shift values, namely 1.29, 1.36 and 1.41 ppm (**Figure 1.17**).

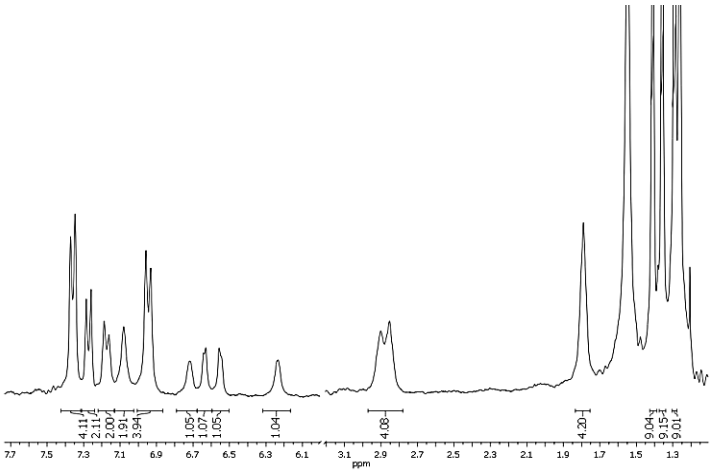

Figure 1.17. ^{1}H NMR of **9.**

The same reaction was performed using 1,4-dibromobutanedione, affording the same monofunctionalized species, bearing the nitro and amino moieties at position 17 and 18 of the macrocycle (**Scheme 1.28**).

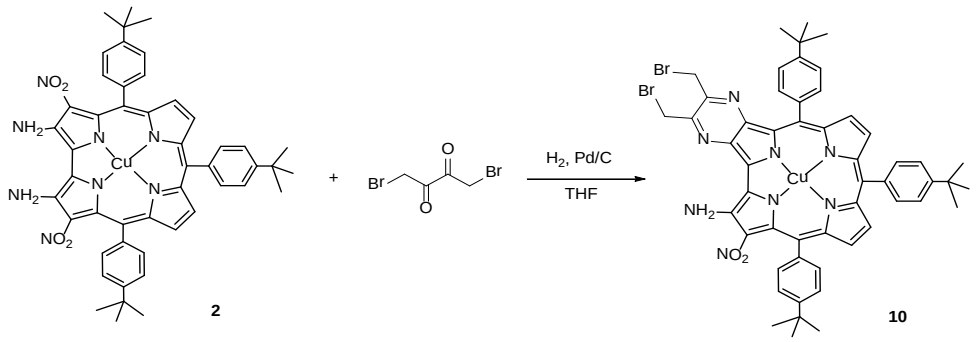

Scheme 1.28. Hydrogenation of complex **2** and further condensation with 1,4-dibromobutanedione.

^{1}H NMR spectrum showed the same integration pattern of 9, with two 2H integration peaks in the aliphatic range, corresponding to the CH_2 fused to the pyrazino moiety.

FAB spectrum was congruous with the desired complex and showed, also in this case, a peak imputable to the loss of the NO_2 moiety at 1007m/z; moreover, losses from the molecular ion of bromine atoms are shown at 974 and 892 m/z, respectively (**Figure 1.18**).

UV-vis comparison between complexes **9** and **10** is shown in **Figure 1.19**. Both compounds show a comparable pattern, although a 8 nm bathochromic shift for the Soret band of complex **9** was evidenced, if compared with **10**. This suggests that the presence of electron-donating (**9**) or withdrawing groups (**10**) strongly influence absorption features, even if these substituents are far away from the corrole core. This

change constitutes a significant data, considering that the molecular orbitals system of copper-corrole complexes makes them very sensitive to the nature of the substituent placed on *meso*- position and less to ones on *beta*-positions.[42]

In both cases, a shoulder at 374 nm was evidenced, due to the presence of a nitro functionality in corrole β-position, in agreement with the data already reported in the literature.[33,43]

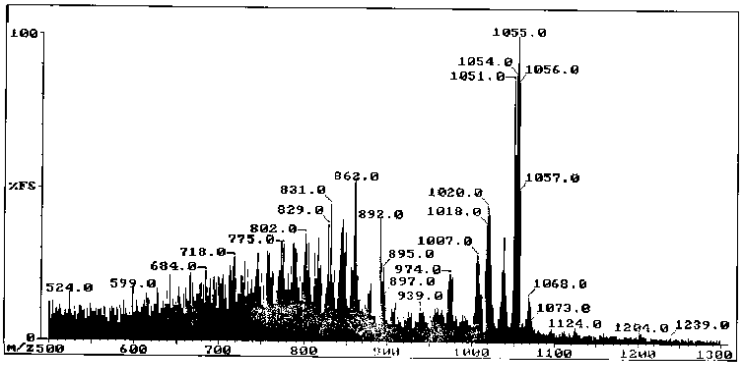

Figure 1.18. FAB spectrum of **10.**

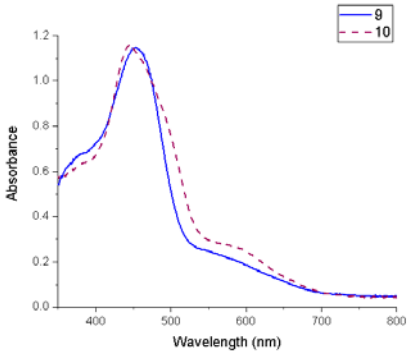

Figure 1.19. UV-vis spectra of **9** (blue full line) and **10** (purple dashed line).

All the attempts to obtain the exhaustive reduction of **2** by Pd/H_2 were unsuccessful, since no more than one nitro group ever reacted. Although this methodology was not useful to increase the yields of the desired difunctionalized species, it should be noted that this approach gave complexes **9** and **10** in good yields, opening the door for the preparation of β-fused corrole systems bearing two different groups annulated at the β-pyrrole positions. The NO_2 moiety can be reduced with sodium borohydride, and then the reaction of the two amino groups with a suitable dione could give the desired product.

All the expected products with their relative yields are shown in **Table 1.1**.

Table 1.1. Relative Yields for the Synthesis of annulated corrolates (complexes **1**,**2**,**3**,**4**,**5**,**6**,**7**,**9**,**10**).

Substrate	Dione	Reducing Agent	Product	Yield
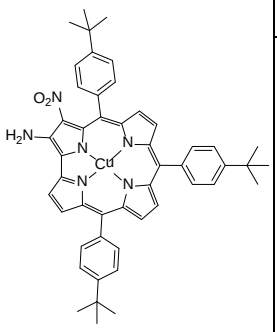	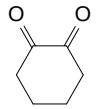	Pd/C, $NaBH_4$	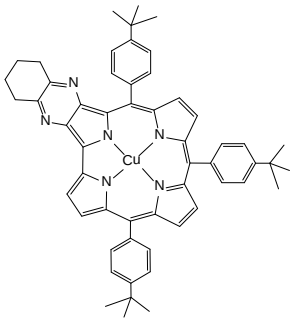	26%
	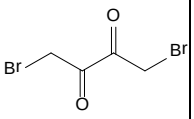	Pd/C, $NaBH_4$	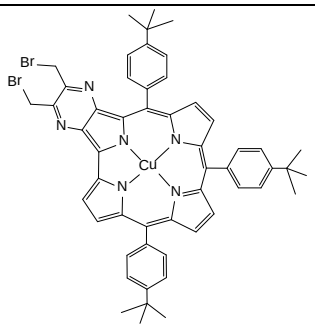	30%
	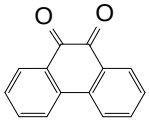	Pd/C, $NaBH_4$	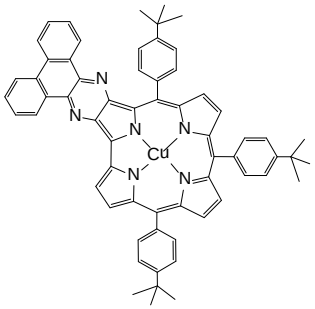	44%
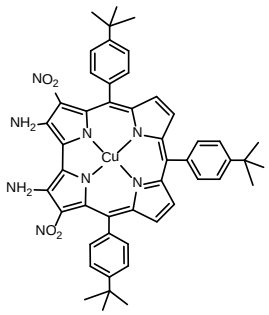	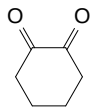	Pd/C, $NaBH_4$	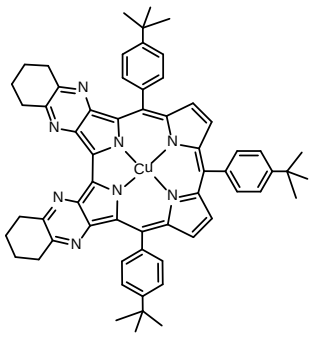	11%
	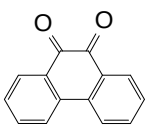	Pd/C, $NaBH_4$	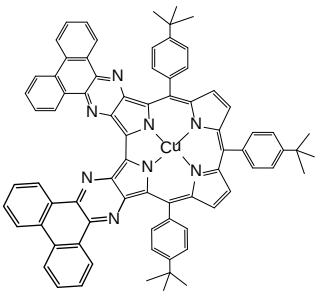	8%

Substrate	Dione	Reducing Agent	Product	Yield
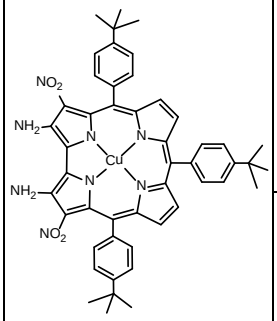	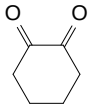	$Pd/C,H_2$	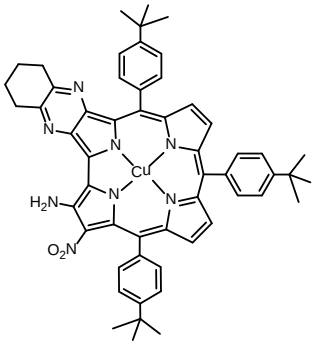	27%
	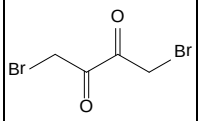	$Pd/C,H_2$	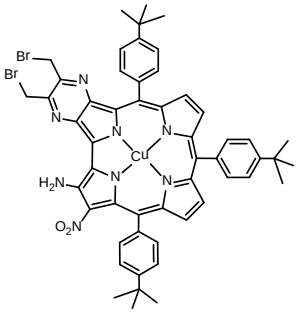	32%

Functionalization via Pictet–Spengler approach

Heterocycles containing a pyrrolo[1,2-*a*]pyrazine ring system display numerous pharmacological profiles such as HIV-1 integrase inhibitors,[44] $5HT_3$ receptor agonists,[45] anticonvulsants,[46] $Vasopressin_{1b}$ receptor antagonists [47] and selective non-competitive mGluR5 antagonists.[48] This moiety is also useful for making luminescent materials for various applications.[18] By considering the biological significance of these two classes of heteroaromatics, we envisaged an efficient strategy to couple a pyrrolo[1,2-*a*]pyrazine unit at the corrole *β*,*β*′-positions.

Very recently, the preparation of a *β*,*β*′-fused nickel(II) pyrrolo[1,2-*a*]pyrazino tetraphenylporphyrin by application of the Pictet–Spengler reaction conditions was reported.[49] These results led us to explore the application of the same route in the case of corrole using, also in this case, the copper complex **1** of 2-amino- 3-nitrotris(5,10,15-tert-butylphenyl)corrole as starting material.

Synthesis of a pyrrole moiety via a Clauson–Kaas reaction

The first step of the study involved the synthesis of a N-substituted pyrrole in position *β* of the macrocycle through a Clauson-Kaas reaction. This functionalization represent a widely used synthetic pathway in organic chemistry for the synthesis of pyrroles starting from primary amines with 2,5-dialkoxytetrahydrofurans.[50]

Complex **1** was dissolved in a mixture of acetic acid and toluene (6:1) in the presence of 2,5-dimethoxytetrahydrofuran. The solution was heated at reflux for 45 min under a nitrogen atmosphere. TLC of the reaction mixture showed the complete disappearance of the starting material, and a new product with higher R_f was apparent. The solvent was evaporated, and the compound was purified by column chromatography using CH_2Cl_2 as the eluent. The main fraction corresponded to the desired complex **11**, obtained in 90% yield (**Scheme 1.29**).

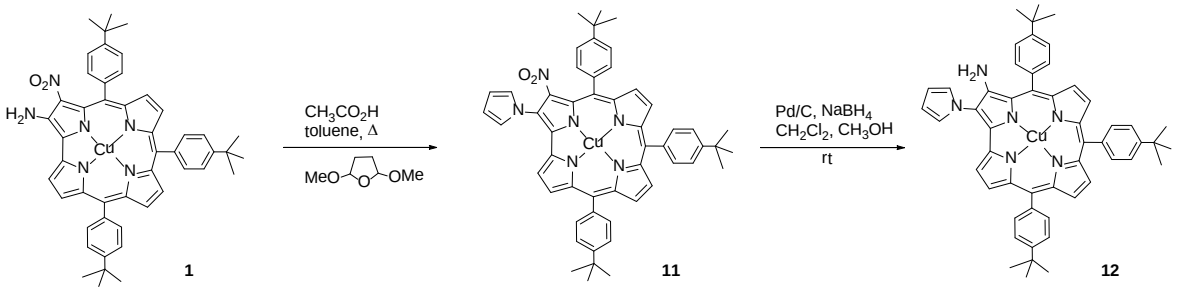

Scheme 1.29. Synthesis of Compound **11** and further reduction.

Spectroscopic characterization of **11** was in agreement with the proposed structure. Although the ^{1}H NMR spectrum exhibited severe line broadening, with overlapped signals of the *β*-pyrrolic and phenyl protons, it was possible to observe two multiplets, with double integration value, centered at 7.16 and 6.40 ppm (**Figure 1.20**), which underscore the presence of pyrrole in position 2 of the macrocycle, in agreement with the chemical shifts observed in the case of porphyrin functionalization.[49]

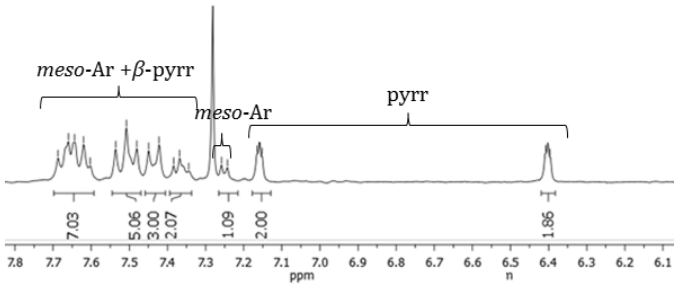

Figure 1.20. ^{1}H NMR spectrum of **11**, aromatic range.

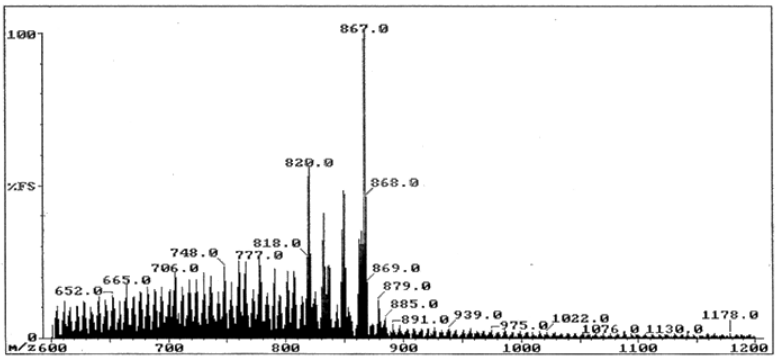

Figure 1.21. FAB spectrum of **11.**

The molecular ion peak in the FAB spectrum at 867 m/z was congruous with such a structure (**Figure 1.21**), which was unequivocally characterized by X-ray analysis,

carried out on single crystals obtained from slow diffusion of methanol in dichlorometane solution of **11** (**Figure 1.22**).

The Cu atom in **11** had slight tetrahedrally distorted square-planar coordination, with the four N atoms an average of 0.154 Å above and below their best plane and Cu–N distances in the range of 1.879(5)–1.906(6) Å. The corrole core has a saddle distortion with β-C atoms an average of 0.394 Å from the 23 atom best plane. The pyrrole and nitro substituents at the 2 and 3 positions are twisted out of the plane of the core pyrrole on which they are substituted, forming dihedral angles of 41.1 and 49.2° respectively, with it.

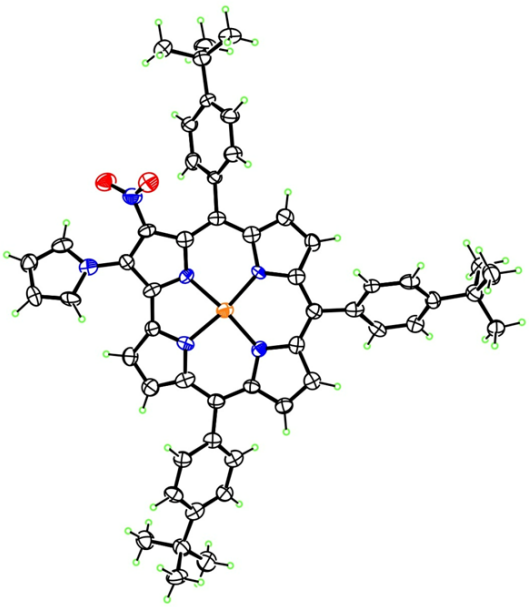

Figure 1.22. Crystal structure of **11.**

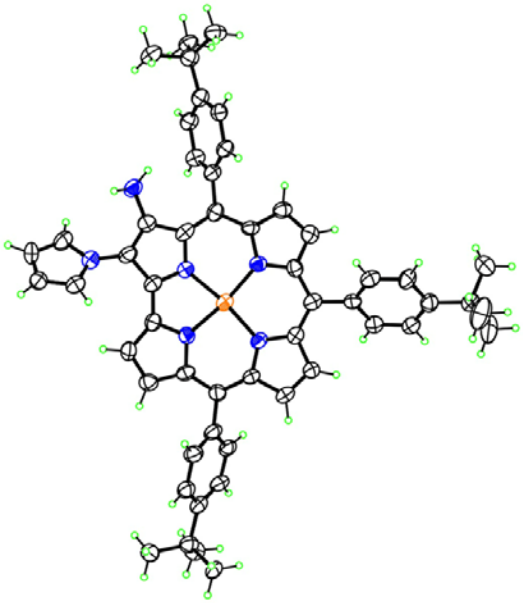

Figure 1.23. Crystal structure of **12.**

Corrole **11** was successfully reduced, using 10% Pd/C-$NaBH_4$ in a 4:1 mixture of CH_2Cl_2/CH_3OH to produce [2-(pyrrol-1- yl),3-(NH_2)-*t*BuTPC]Cu (**12**) (Scheme 1.29) in 83% yield. In this case, crystallization from a dichloromethane/methanol solution provided crystals for X-ray characterization of **12** (**Figure 1.23**). The molecular structure of **12**, as the chloroform solvate, is very similar to that of **11**, with a slightly greater tetrahedral distortion from the square-planar Cu coordination (mean deviation of four N atoms 0.177 Å) and Cu–N distances in the range of 1.889(5)– 1.909(5) Å. The corrole core has a slightly less pronounced saddle distortion, with β-C atoms an average of 0.228 Å from the 23 atom best plane. The out-of-plane twist of the pyrrole substituent is comparable at 44.8°. As already experienced for complex **11**, the ^1H NMR spectrum

showed broad signals, but it was possible to observe a signal at 2.97 ppm, attributable to the NH_2 protons (**Figure 1.24**).

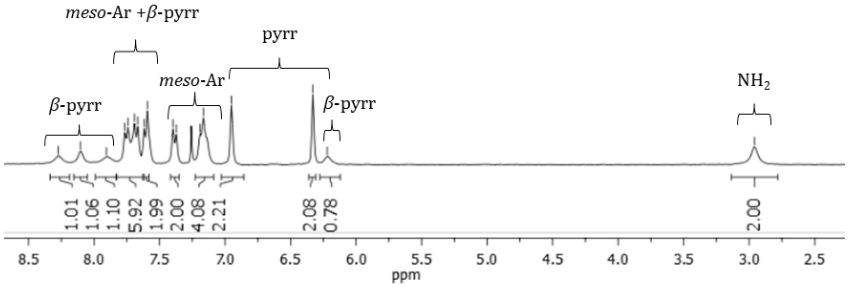

Figure 1.24. ^{1}H NMR spectrum of **12.**

It is interesting to note that both complexes **11** and **12** were obtained in yields higher than those for the analogous porphyrins, an unusual feature for corrole functionalizations.

π-extended β,β'-copper (II) pyrrolo[1,2-a]pyrazinocorrolates via a Pictet-Spengler reaction

In the Pictet-Spengler reaction dodecylbenzenesulfonic acid (DBSA) catalyzes the conversion of a *β*-arylenylamine (NH_2 moiety in corrole C3 position) to a pyrazino unit in the presence of an aldehyde.[51,52] We selected *p*-tolualdehyde as model substrate because it could be easily detected using ^{1}H NMR analysis.

To a solution of **12** and aldehyde in 1,4-dioxane (4 mL), dodecylbenzenesulfonic acid (DBSA, 10% molar ratio) was added and the reaction mixture was stirred at room temperature. Progress of the reaction was monitored by TLC, which showed incomplete conversion of the starting corrole. We tried to improve the reaction of **12** by prolonging the reaction time, but this attempt led to an increase of decomposition products, while an increase of the DBSA amount was unsuccessful. For these reasons, we decided to stop the reaction after 2 h. TLC analysis of the crude mixture showed, apart from the starting material, two reaction products. Chromatographic separation of the corresponding bands afforded the expected *β,β'*-pyrrolo[1,2-*a*]pyrazino-fused corrole **13** as a fast moving fraction in moderate yields (32%, **Scheme 1.30**).

Spectroscopic characterization of **13** was in agreement with the proposed structure, FAB spectrum showing a molecular peak at 934 m/z, and the ^{1}H NMR spectrum showing

a 3-proton singlet at 2.43 ppm, in keeping with the presence of the CH_3 moiety (**Figure 1.25**).

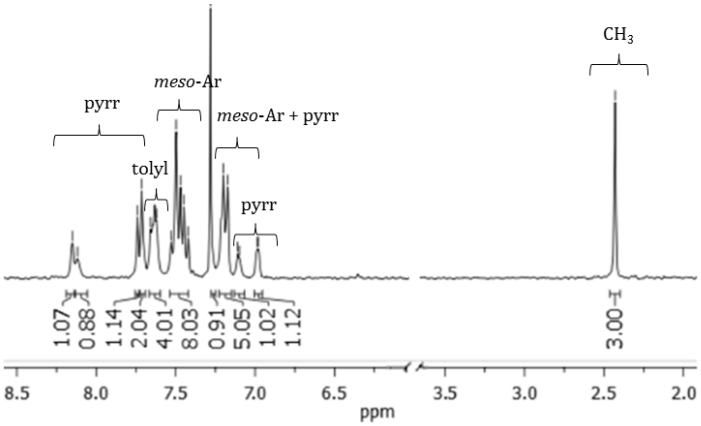

Figure 1.25. ^{1}H NMR of **13.**

The second fraction was obtained in lower amount than **13** and the ^{1}H NMR spectrum of the compound showed the absence of the resonances attributable to the 4-methylphenyl substituent, while an additional singlet at 8.56 was present (**Figure 1.26**). The FAB mass spectrum also indicated a molecular peak at 849 m/z, confirming the absence in the product of the peripheral 4- methylphenyl unit.

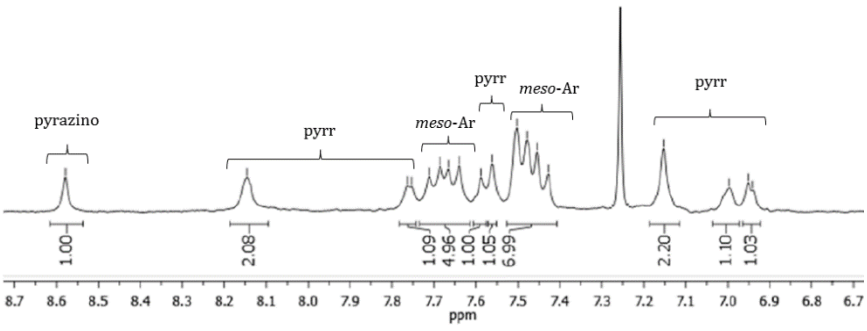

Figure 1.26. ^{1}H NMR of 14, aromatic range.

These features led us to hypothesize the formation of **14** (**Scheme 1.30**), which was unambiguously confirmed by X-ray characterization (**Figure 1.27**).

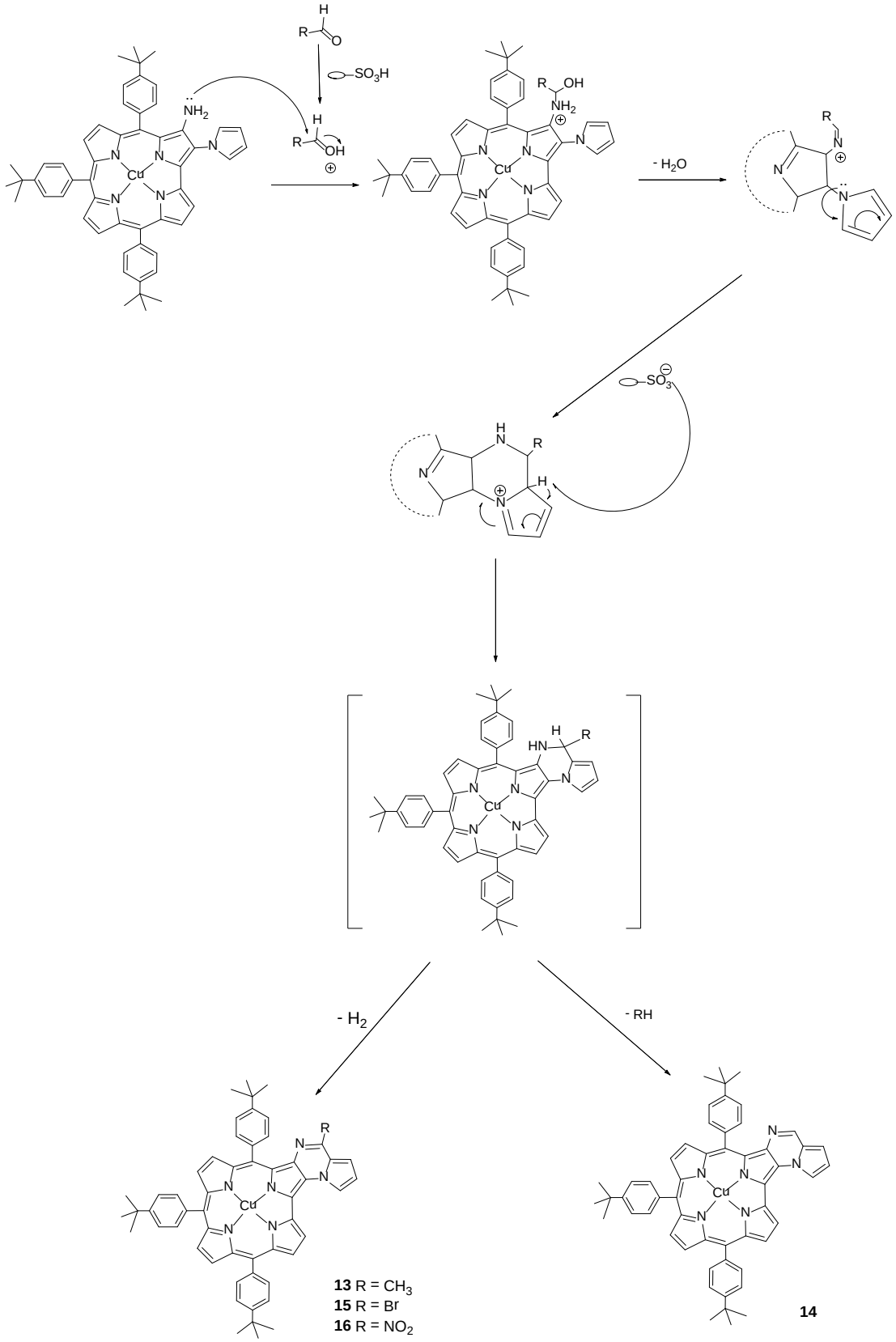

Scheme 1.30. Proposed mechanism for the DBSA-catalyzed synthesis of β,β′-fused copper(II) pyrrolo[1,2-*a*]pyrazinocorrolates (**13**-**16**).

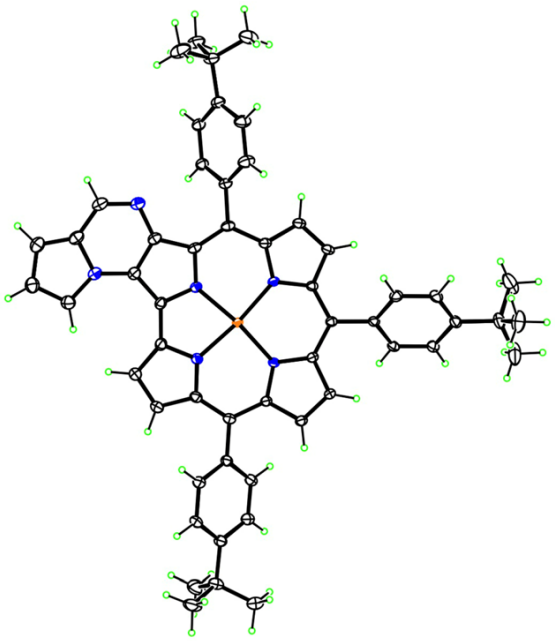

Figure 1.27. Crystal structure of **14**.

The structure of **14** as the chloroform solvate is very similar to those of **11** and **12**. Coordination geometry of the Cu atom is also square-planar with a small tetrahedral distortion, with the N atoms lying alternately an average of 0.145 Å above and below their best plane. The Cu–N distances are experimentally indistinguishable, in the range of 1.903(2)–1.905(2) Å. The corrole core has a saddle distortion with β-C atoms an average of 0.391 Å from the 23 atom best plane. Cyclization prevents the pyrrolopyrazino substituent from deviating much from coplanarity with the core pyrrole to which it is fused, with the dihedral angle between those moieties being 3.5°. To the best of our knowledge, the formation of **14** is novel for the Pictet–Spengler reaction, and a similar pathway has not been observed in the reaction of Ni tetraphenylporphyrin.[53] Formation of **14** probably occurs after the formation of the cyclic adduct, with the subsequent aromatization occurring with the competing elimination of H_2 or toluene, leading to **13** or **14** (**Scheme 1.30**).

To investigate the generality of this reaction and the relative influence of benzaldehyde substituents on the product pattern, we reacted **12** with two additional benzaldehydes, bearing at the 4- position a strongly or a weakly electron-withdrawing group, namely *4*-nitrobenzaldehyde and 4-bromobenzaldehyde, to complete the series with the electron-donating character of the methyl group.

In all cases, the expected products (**15**, **16**) were obtained with formation of **14** (**Table 1.2**).

The highest yields were obtained with 4-methylbenzaldehyde; this result seems to indicate that electron-rich benzaldehydes can favour the formation of **14**.

FAB spectrum of derivatives **15** and **16** showed a major peak at 1000 and 969 m/z respectively, corresponding to the molecular ion. Moreover, ^{1}H NMR spectra of the aforesaid derivatives exhibited pattern similar to **13**. UV/vis absorption spectra of [*t*BuTPC]Cu, complexes **13**,**15**,**16** and compound **14** are shown in **Figure 1.28**.

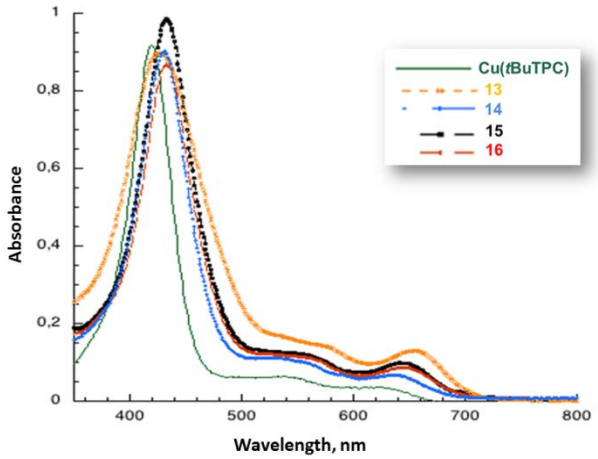

Figure 1.28. Electronic absorption spectra of **[*t*BuTPC]Cu** and corroles **13**-**16**, in CH_2Cl_2 solution.

Table 1.2. Relative Yields for the Synthesis of **13**-**16**[a]

R	Product	Yield
p-$CH_3C_6H_4$	**13**	32%
	14	19%
p-BrC_6H_4	**15**	21%
	14	16%
p-$NO_2C_6H_4$	**16**	29%
	14	9%

[a]Calculated based on unreacted starting material.

These molecules displayed characteristic Soret bands between λ_{max} 425 and 433 nm, which are red-shifted compared to the starting complex (Soret band at λ_{max} 418 nm). Bathochromic shifts observed for these complexes are similar to those observed for the analogous corroles bearing *β*-annulated aromatic rings,[14] thereby confirming the increase in π-conjugation in these corrole analogues.

To further elucidate the influence of the *β*-annulation on the corrole properties, we carried out the cyclic voltammetry of **13** and **14** (**Figure 1.29**)

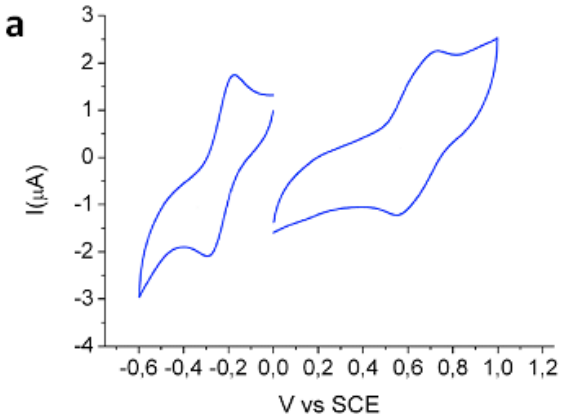

a) Cyclic voltammogram of **13.**

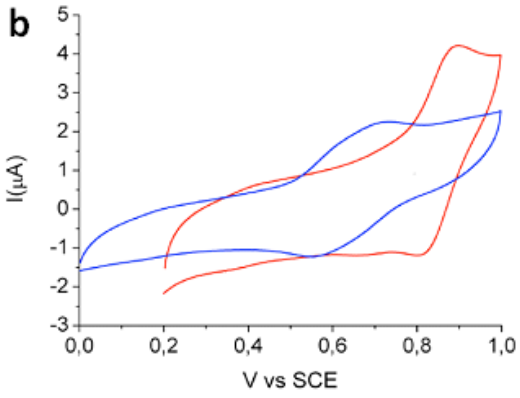

b) Cyclic voltammogram of **13** (blue line), and upon addition of one drop of TFA (red line).

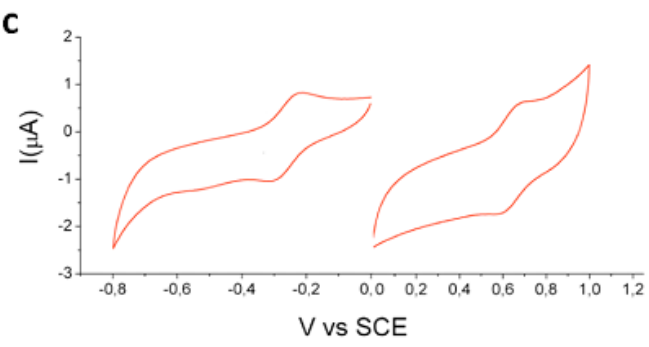

c) Cyclic voltammogram of **14.**

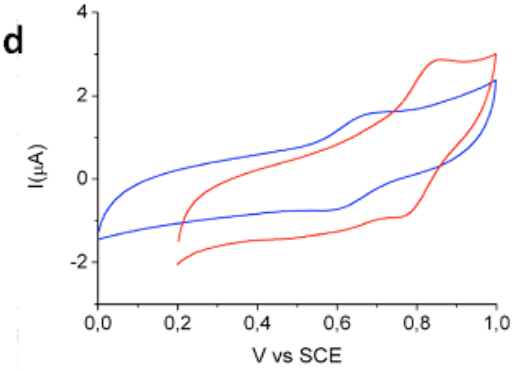

d) Cyclic voltammogram of **14** (blue line), and upon addition of one drop of TFA (red line).

Figure 1.29. Cyclic voltammograms of **13** (**a**,**b**) and **14**(**b**,**c**), in CH_2Cl_2 (0.1 M TBAH) at room temperature using a glassy carbon electrode measured at 100 mV/s. Potentials *vs* SCE.

For both compounds, we observed an appreciable shift of the first oxidation potential to values lower than that of [*t*BuTPC]Cu,[33] which is further confirmation of the π-conjugation increase operated by the annulated pyrrolopyrazino ring (**Table 1.3**). Furthermore, we did not observe a second oxidation process up to 1.5 V, where an irreversible reaction occurs. Since for [*t*BuTPC]Cu the second oxidation process occurs at 1.31 V,[33] this result further indicates a strong influence operated by the annulated ring. It is also interesting to note that this influence can be modulated by acids. A drop of TFA, inducing the protonation of the fused pyrrolopyrazino ring, strongly reduces the π- conjugation of the *β*-annulated aromatic ring, resulting in the blue shift of the corrole Soret bands in the UV–vis spectrum (**Figure 1.30**), which becomes similar to that of [*t*BuTPC]Cu. For the same reason, in the cyclic voltammogram, we observe a significant increase of about 200 mV of the first oxidation potential for both **13** and **14**. The

presence of the charged pyrazino ring induces a shift similar to that of a peripheral nitro group.[33]

The process is reversible because, with the addition of a base, the original spectral features are recovered.

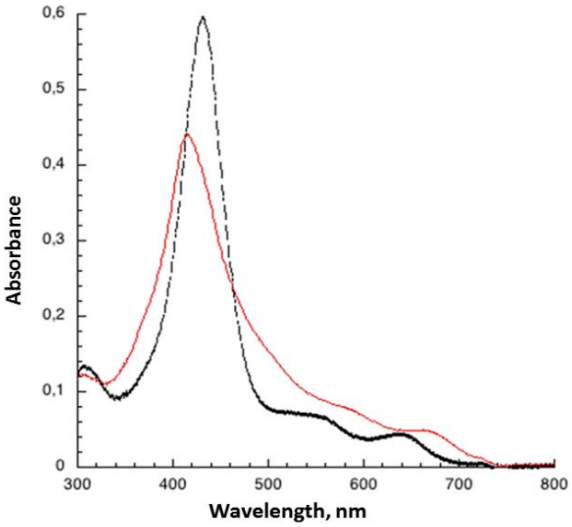

Figure 1.30. Electronic absorption spectra of **14** (black dotted line) and **14** upon addition of a few drops of TFA (red solid line) in CH_2Cl_2 solution.

Table 1.3. Half-Wave Potentials (V vs SCE) of Cu Corroles in CH_2Cl_2 Containing 0.1 M TBAH.

R	E_{ox}	E_{red}
[*t*BuTPC]Cu	0.71	-0.17
13	0.64	-0.22
	0.86[a]	
14	0.64	-0.24
	0.85[a]	

[a]Upon TFA addition.

Vilsmeier-Haack formilation of 2-(pyrrol-1-yl)-3-nitro corrolate

The opportunity to obtain easily with high yield new corrole derivatives bearing an (pyrrol-1-yl) moiety (compounds **11** and **12**) opens a novel opportunity to further corrole modifications.

To widen the scope of corrole functionalization, we have been particularly interested in the formylation reaction, because it represents the easiest way to introduce a carbon atom at a macrocyclic peripheral position, thus constituting an useful starting point for further developments. Moreover, in the case of corroles, the efficiency of the Vilsmeier–Haack reaction is well established, giving access functionalized species in excellent yields.[9,54–56]

Complex **11** was chosen as the best candidate for this reaction. Although it disposes of eight *β*- and two α- pyrrolic positions available for the functionalization, it is reasonable to assume that α positions could be preferred. The intermediate formed by α attack is more resonance stabilized, and the activation energy leading to it will be reduced.

The synthesis was performed using the procedure already reported in the literature for the formylation on corroles *β*-positions.[55] The reaction was carried out by adding the Vilsmeier reagent $POCl_3$/DMF (1:110 molar ratio) to a solution of **11** in dry dichloromethane, at room temperature under an inert atmosphere. The expected corrole complex **17** was obtained as the only product with 50% yields (**Scheme 1.31**).

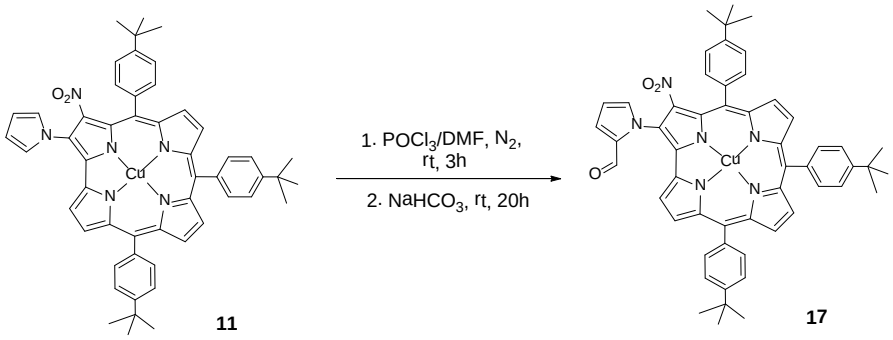

Scheme 1.31. Vilsmeier formylation on **11.**

The ESI spectrum of derivative **17** showed a major peak at 892 m/z corresponding to the molecular ion, together with some small peaks at lower intensities due to fragmentation. Moreover ^{1}H NMR spectrum showed 1-proton singlet at 9.61 ppm, in keeping with the presence of only one formyl group.

UV-vis spectra of compounds **11** and **17** showed a pattern comparable (**Figure 1.31**), with a red shift of both Soret and Q bands. Whilst the bathochromic shift of the Soret band is negligible (3 nm), the second Q band exhibited a more drastic shift (15nm). Moreover, both compounds retain a peak at 374 nm, corresponding to the NO_2 functionality.

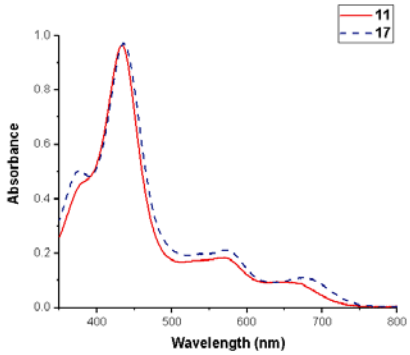

Figure 1.31. Electronic absorption spectra of **11** (red solid line) and **17** (blue dotted line) in CH_2Cl_2 solution.

Further evidence of this functionalization was obtained by X-ray analysis, confirming the position of the formyl group on pyrrole α position (**Figure 1.32**).

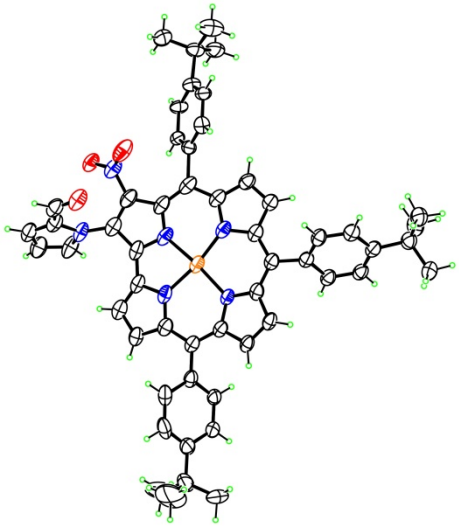

Figure 1.32. Crystal structure of **17.**

Summary and conclusions

In the first part of this Chapter, we synthesized and characterized new families of *β*-fused corroles through a simple one-pot reduction and condensation reaction. The influence of the pyrazino units and of the different substituents in the optical properties of corroles has been studied. The X-ray crystallographic characterization and electronic absorption spectra highlight interesting features of these derivatives. Peripheral conjugated substituents produce large bathochromic shifts in both Soret e Q-bands. Considering the Soret band, the extent of this red shift is of 11 nm per pyrazino unit. None of the newly prepared copper complexes showed any fluorescence emission. An easy demetallation procedure also allows us to obtain the corresponding free base derivatives, opening the door to the preparation of different metal complexes, with the possible modulation of the related photophysical characteristics and potentially making these species suitable for optoelectronic applications.

In the second part of this Chapter, we developed a simple synthetic route by which we obtained *β,β′*-fused copper(II) pyrrolo[1,2-a]pyrazinocorroles. The annulated aromatic group opens a novel opportunity to modulate the photophysical and redox properties of corroles. In this reaction, corrole reveals once again an unusual reactivity pattern, affording the unsubstituted pyrrolopyrazino substituent by an unprecedented reaction pathway. This route is very encouraging for the development of new π-extended corrole architectures, particularly appealing as useful functional materials

Experimental section

Materials and Instruments

Chemical reagents and solvents (Sigma-Aldrich, Alfa Aesar, Fluka Chemie and Carlo Erba Reagenti) were of the highest grade available and were used without further purification. Additionally, some solvents were further dried by distillation with $LiAlH_4$ (THF,Toluene), or with previously activated molecular sieves (3 or 4 Å), or with a solvent purifying system by Innovative Technology Inc. MD-4-PS. Air- and moisture sensitive experiments were carried out using standard Schlenk line techniques.

Chromatography: Thin layer chromatography (TLC) analyses were performed on aluminum sheets coated with silica gel 60 F_{254} or neutral alumina 60 F_{254} (Merck).

TLCs analyses were carried out with an UV lamp of 254 and 365 nm.

Column chromatography was carried out using silica gel Merck-60 (230-400 mesh, 60 Å), Sigma-Aldrich (70–230 mesh, 60 Å) and and neutral alumina (Merk, Brockmann Grade III) as the solid support. Eluents and relative proportions are indicated for each particular case.

Nuclear magnetic resonance (NMR): ^{1}H and ^{13}C NMR spectra were measured on a Bruker AV300 (300 MHz), or a Bruker AC-300 (300 MHz) spectrometer, locked on deuterated solvents. Chemical shifts are given in ppm relative to residual solvents using literature reference of δ ppm values.[57]

Mass-spectrometry (MS): mass spectra were recorded employing Electrospray ionization (ESI), or Fast Atom Bombardment (FAB), using a VG Quattro spectrometer in the positive-ion mode for FAB. The different matrixes employed are indicated for each spectrum. Mass spectrometry data are expressed in *m/z* units.

Ultraviolet-visible spectroscopy: UV–vis spectra were recorded on a Varian Cary 50 spectrophotometer. using spectroscopic grade solvents in 1 cm path length quartz cell.

Electrochemistry: cyclic voltammetry (CV) experiments were performed with a Palmsens potentiostat, using a standard calomel electrode (SCE) as the reference electrode, a platinum wire as the auxiliary electrode and a platinum disk (1 mm diameter) as working electrode. The experiments were performed in anhydrous CH_2Cl_2 and THF using tetrabutylammonium hexafluorophosphate (TBAH,

Aldrich,electrochemical grade) as supporting electrolyte at 100 mV/s scan rate. Prior to each voltammetric measurement, the cell was degassed by bubbling with nitrogen for about 20 min. Electrochemical measurements were performed using a concentration of approximately 1×10^{-3} M for the compound in question. Compensation for internal resistance was not applied.

X-Ray diffraction: X-ray data were collected at low temperature with CuKα or MoKα radiation on a Bruker Kappa Apex-II DUO diffractometer.

Synthetic procedures

2-amino-3-nitro-5,10,15-tris(4-tert-butyl)corrolato-Cu (**1**) and 2,18-diamino-3,17-dinitro-5,10,15-tris(4-tert-butyl)corrolato-Cu (**3**) were prepared following a literature procedure.[33]

General procedure for the syntheses of β-fused 2,3-[1',2'-b]pyrazinocorrolato-Cu(II)

Corrole **1** (35 mg, 0.043 mmol) was dissolved in a mixture of CH_2Cl_2 (24 mL) and CH_3OH (6 mL) and allowed to stir under nitrogen for 10 min. 10% Pd on activated carbon (35 mg, 0.329 mmol) and $NaBH_4$ (32 mg, 0.860 mmol) were added and the mixture was stirred under nitrogen for 10 min. The solution immediately turned bright green and TLC monitoring showed almost quantitative consumption of the starting complex. The reduction was considered complete when a Soret band at 420 nm was evident and the shoulder at 370 nm had disappeared. Then the appropriate dione (1.076 mmol) was added, and the mixture was stirred at room temperature for 1 h. The reaction progress was followed using TLC, observing the appearance of a brown streak with a larger R_f. UV-vis spectroscopy showed a bathochromic shift of the Soret band. Once the reaction was complete, the mixture was filtered through Celite. The filtrate was collected and evaporated under reduced pressure. The crude product was purified on a silica gel column using CH_2Cl_2 as the eluent. The characterization data of all the newly prepared compounds are given below.

*2,3-[1'-2'-Cyclohexane(b)pyrazino]-5,10,15-tris(4-tert-butylphenyl)corrolato-Cu (**3**)*

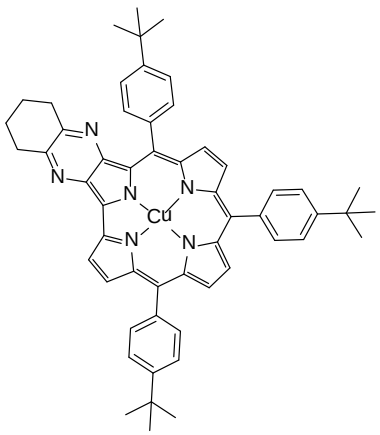

Yield: 26%, brown solid, mp >300 °C; ^{1}H NMR (CD_2Cl_2, 300 MHz, δ ppm): 1.39 (s, 9H, *p*-*t*Bu), 1.42 (s, 9H *p*-*t*Bu), 1.43 (s, 9H, *p*-*t*Bu), δ 1.92–1.88 (br m, 4H, cyclohexane), 2.92 (br t, 2H, cyclohexane H), 3.02 (br t, 2H, cyclohexane), 6.71 (br d, 1H, *β*-pyrr), 7.13 (br d, 1H, *β*-pyrr), 7.22 (br d, 1H, *β*-pyrr), 7.32 (d, 2H, J = 7.42Hz, *β*-pyrr), 7.56–7.42 (m, 12H, *meso*-Ar), 8.08 (br d, 1H, *β*-pyrr); Anal. Calcd for $C_{55}H_{53}CuN_6$: C, 76.67; H, 6.20; N, 9.75; found: C, 76.61; H, 6.12; N, 9.83; MS (FAB, m/z): 862 (M+); UV-vis (CH_2Cl_2): λ_{max} nm (log ε): 431 (4.04), 623 (3.77).

*2,3-[1'-2'-bis(bromomethyl)(b)pyrazino]-5,10,15-tris(4-tert-butylphenyl)corrolato-Cu (**5**)*

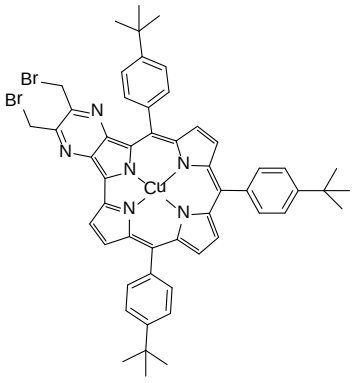

Yield: 30%, brown solid, mp >300 °C; ^{1}H NMR (CD_2Cl_2, 300 MHz, δ ppm): 1.42 (s, 9H, *p*-*t*Bu), 1.43 (s, 9H, *p*-*t*Bu), 1.48 (s, 9H, *p*-*t*Bu), 4.64 (s, 2H, CH_2), 4.95 (s, 2H, CH_2), 7.03 (br d, 1H, *β*-pyrr), 7.17 (br d, 1H, *β*-pyrr), δ 7.32-7.37 (br m, 3 H, *β*-pyrr), δ 7.48–7.66 (br m, 12H, *meso*-Ar), 8.17 ((br d, 1H, *β*-pyrr); Anal. Calcd for $C_{53}H_{49}Br_2CuN_6$: C, 64.08; H, 4.97; N, 8.46; found: C, 64.19; H, 4.92; N, 8.49; MS (FAB, m/z): 994 (M+); UV-vis (CH_2Cl_2): λ_{max} nm (log ε): 431 (4.68), 643 (sh).

*2,3-[1'-2'-phenanthrene(b)pyrazino]-5,10,15-tris(4-tert-butylphenyl)corrolato-Cu (**6**)*

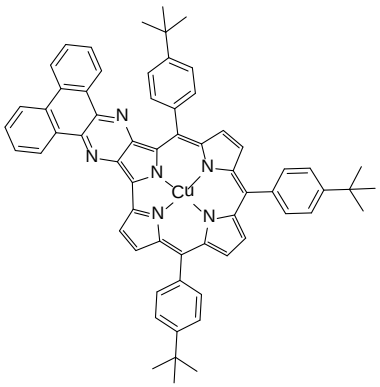

Yield: 44%, brown solid, mp >300 °C; ^{1}H NMR (CD_2Cl_2, 300 MHz, δ ppm): 1.39 (s, 9H, *p*-*t*Bu), 1.43 (s, 9H, *p*-*t*Bu), 1.58 (s, 9H, *p*-*t*Bu), 6.48 (br d, 1H, *β*-pyrr), δ 7.18–7.27 (br m, 8H, phenanthrene), δ 7.34–7.59 (br m, 12H, *meso*-Ar), 8.08 (d, 2H, J = 7.50 Hz, *β*-pyrr), 8.26 (br d, 1H, *β*-pyrr), 8.35 (br d, 1H, *β*-pyrr), 9.29 (br d, 1H, *β*-pyrr); Anal. Calcd for $C_{63}H_{53}CuN_6$: C, 79.01; H, 5.58; N, 8.78; found: C, 79.10; H, 5.50; N, 8.74; MS (FAB, m/z): 957 (M+); UV-vis (CH_2Cl_2): λ_{max} nm (log ε): 423 (4.72), 643 (3.65).

General procedure for the syntheses of β-fused 2,3,17,18-bis-[1',2'-b] pyrazinocorrolato-Cu(II)

Corrole **2** (50 mg, 0.057 mmol) was dissolved in a mixture of CH_2Cl_2 (32 mL) and CH_3OH (8 mL) and allowed to stir under nitrogen for 10 min. 10% Pd on activated carbon (50 mg, 0.470 mmol) and $NaBH_4$ (65 mg, 1.713 mmol) were added and the mixture was stirred under nitrogen for 10 min. The solution immediately became bright green in colour and TLC monitoring showed almost quantitative consumption of the starting complex. The reduction was considered complete when a Soret band at 400 nm was evident and the shoulder at 366 nm had disappeared. Then the appropriate dione (2.856 mmol) was added and the mixture was stirred at room temperature for 1 h. The reaction progress was followed using TLC, monitoring the appearance of a brown streak with a larger R_f. UV-vis spectroscopy showed a bathochromic shift of the Soret band. Once the reaction was complete, the mixture was filtered through Celite. The filtrate was collected and evaporated under reduced pressure. The crude product was purified on a silica gel column using CH_2Cl_2 as the eluent. The characterization data of all the newly prepared compounds are given below.

*2,3,17,18-bis[1'-2'-cyclohexane(b)pyrazino]-5,10,15-tris(4-tert-butylphenyl) corrolato-Cu (**4**)*

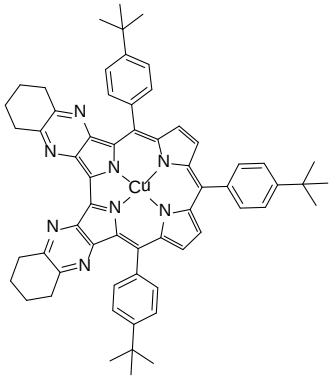

Yield: 11%, brown solid, mp >300 °C; ^{1}H NMR ($CDCl_3$, 300MHz, δ ppm): 1.38 (s, 9H, *p*-*t*Bu), 1.43 (s, 18H, *p*-*t*Bu), δ 1.91–1.87 (br m, 8H, cyclohexane H), 2.97 (br t, 4H, cyclohexane H), 3.10 (br t, 4H, cyclohexane H), 6.69 (br d, 2H, *β*-pyrr), 7.12 (br d, 2H, *β*-pyrr),), δ 7.39–7.36 (m, 6H, *meso*-Ar), δ 7.54–7.49 (m, 6H, *meso*-Ar); Anal. Calcd for $C_{61}H_{59}CuN_8$: C, 75.71; H, 6.14; N, 11.58; found: C, 75.64; H, 6.07; N, 11.66; MS (FAB, m/z): 969 (M+); UV-vis (CH_2Cl_2): λ_{max} nm (log ε): 442 (4.82), 656 (3.24).

*2,3,17,18-bis[1'-2'-phenanthrene(b)pyrazino]-5,10,15-tris(4-tert-butylphenyl)corrolato-Cu (**7**)*

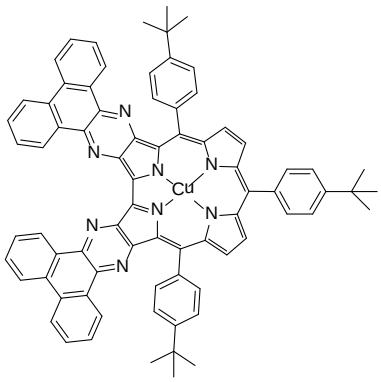

Yield: 8%, brown solid, mp >300 °C; ^{1}H NMR ($CDCl_3$, 300MHz, δ ppm): 1.38 (br m, 27H, *p*-*t*Bu), 7.56 (br d, 2H, *meso*-Ar), 7.59 (br d, 2H, *meso*-Ar), δ 7.61–7.63 (br m, 4H, phenanthrene), 7.65 (br d, 2H, *meso*-Ar), 7.68 (br d, 2H, *meso*-Ar), 7.73 (s, 4H, phenanthrene), 7.87 (br d, 2H, phenanthrene), 7.90 (br d, 2H, phenanthrene), 8.67 (br d, 2H, *β*-pyrr), 8.70 (br d, 2H, *β*-pyrr); Anal. Calcd for $C_{77}H_{59}CuN_8$: C, 79.73; H, 5.13; N, 9.66; found: C, 75.68; H, 5.11; N, 9.61; MS (FAB, m/z): 1160 (M+); UV-vis (CH_2Cl_2): λ_{max} nm (log ε): 430 (4.78), 668 (sh).

*2,3-[1'-2'-Phenanthrene(b)pyrazino]-5,10,15-tris(4-tert-butylphenyl)corrole (**8**)*

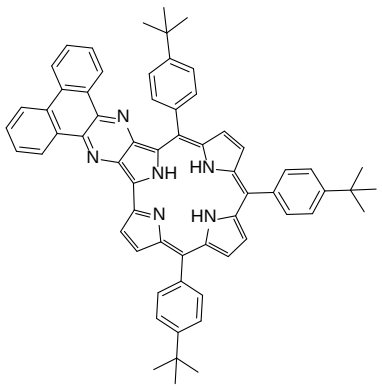

To a chloroform solution (15 mL) of complex 5 (20 mg, 0.021 mmol) was added conc. sulfuric acid (H_2SO_4; 1.5 mL). The mixture was stirred at room temperature for 10 min following the progress of the demetalation by TLC analysis and UV-vis spectroscopy (by diluting an aliquot of the reaction mixture in CH_3OH). Then, distilled water (20 mL) was added and the organic phase was extracted by adding $CHCl_3$. The organic phase was washed twice with water, then neutralized twice with saturated aqueous $NaHCO_3$ and dried over anhydrous Na_2SO_4. After evaporation of the solvent, the crude product was purified on a short column of silica gel eluting with CH_2Cl_2/hexane 1 : 1. The first brown fraction was collected and crystallized from CH_2Cl_2/methanol affording complex 8 as a dark brown powder (5 mg, 0.006 mmol; 27% yield). ^{1}H NMR ($CDCl_3$, 300 MHz, δ ppm): 9.53 (d, 1H, J = 2.57 Hz, *β*-pyrr), 8.98 (br d, 1H, *β*-pyrr), 8.77 (br d, 1H, *β*-pyrr), 8.69 (br d, 1H, *β*-pyrr), 8.62 (br d, 1H, *β*-pyrr), 8.54 (br d, 1H, *β*-pyrr), 8.19 (d, 2H, J = 7.23 Hz, *meso*-Ar), 8.02 (d, 2H, J = 7.10 Hz, *meso*-Ar), 7.92 (d, 2H, J = 8.77 Hz, *meso*-Ar), 7.83 (d, 2H, J = 7.05 Hz, *meso*-Ar), δ 7.64–7.58 (br m, 4H, phenanthrene), δ 7.47–7.39 (br m, 4H, phenanthrene), 1.82 (s, 9H, *p*-*t*Bu), 1.64 (s, 18H, *p*-*t*Bu). Anal. Calcd for $C_{77}H_{62}N_8$: C, 84.34; H, 6.29; N, 9.37; found: C, 84.31; H, 6.25; N, 9.42; MS (FAB, m/z): 897 (M+); UV-vis (CH_2Cl_2): λ_{max} nm (log ε) 391 (sh), 417 (4.52), 442 (4.62), 571 (3.98), 669 (4.05).

General procedure for the syntheses of β-fused 2,3,-[1',2'-b]]-17-NO_2-18- NH_2-pyrazinocorrolato-Cu(II)

To a mixture of corrole **2** (45 mg, 0.051 mmol) and 10% Pd on activated carbon (45 mg) in dry THF (10 mL), an excess of hydrogen was added and allowed to stir at room temperature for 1 h 40 min. The reaction progress was followed using TLC by observing the appearance of a green streak at the baseline. Then, the hydrogen gas was removed and the mixture was degassed with nitrogen before the addition of the appropriate dione (2.568 mmol). The mixture was left stirring at room temperature overnight, monitoring the course via UV-vis spectrometry and TLC analysis. After completion of the reaction, the mixture was filtered through Celite. The filtrate was collected and evaporated under reduced pressure. The residue obtained was dissolved with CH_2Cl_2

and passed through a silica gel column eluted with CH_2Cl_2/hexane (3:1). The characterization data of all the newly prepared compounds are given below.

*2,3-[1′-2′-cyclohexane(b)pyrazino]-17-NO_2-18- NH_2-5,10,15-tris(4-tert-butylphenyl)corrolato-Cu (**9**)*

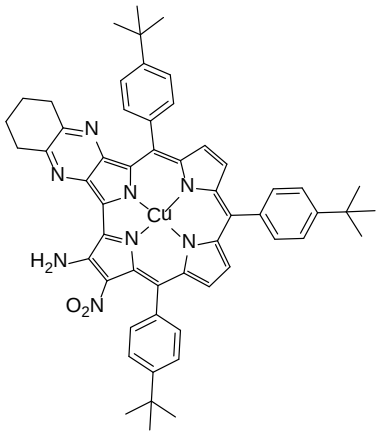

The first brown fraction eluted by column chromatography was collected and crystallized from CH_2Cl_2/CH_3OH to give the title corrole (13 mg, 27% yield) as a brown solid, mp >300 °C; ^{1}H NMR (CD_2Cl_2, 300 MHz, δ ppm): 1.29 (s, 9H, *p*-*t*Bu), 1.36 (s, 9H, *p*-*t*Bu), 1.41 (s, 9H, *p*-*t*Bu), 1.79 (br m, 4H, cyclohexane H), 2.88 (br m, 4H, cyclohexane H), 6.23 (br s, 1H, NH_2), 6.56 (br d, 1H, *β*-pyrr), 6.63 (br d, 1H, *β*-pyrr), 6.72 (br s 1H, NH_2), 6.94 (d, 4H, J = 7.74 Hz, *meso*-Ar), 7.08 (br s, 2H, *β*-pyrr), 7.17 (d, 2H, J = 7.80 Hz, *meso*-Ar), 7.27 (d, 2H, J = 7.88 Hz, *meso*-Ar), 7.36 (d, 4H, J = 7.48 Hz, *meso*-Ar); Anal. Calcd for $C_{55}H_{53}CuN_8O_2$: C, 71.68; H, 5.80; N, 12.16; O, 3.47; found: C, 71.62; H, 5.73; N, 12.22; MS (FAB, m/z): 921 (M+); UV-vis (CH_2Cl_2): λ_{max} nm (log ε): 370 (4.40), 456 (4.66), 543 (4.00).

*2,3-[1′-2′- bis(bromomethyl)(b)pyrazino]-17-NO_2-18- NH_2-5,10,15-tris(4-tert-butylphenyl)corrolato-Cu (**10**)*

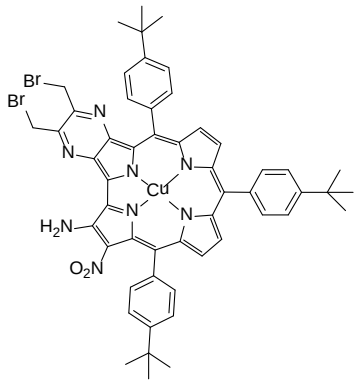

Yield: 32%, brown solid, mp >300 °C; ^{1}H NMR ($CDCl_3$, 300 MHz, δ ppm): 1.35 (s, 9H, *p*-*t*Bu), 1.37 (s, 9H, *p*-*t*Bu), 1.43 (s, 9H, *p*-*t*Bu), 4.53 (s, 2H, CH_2), 4.75 (s, 2H, CH_2), 6.55 (d, 1H, J=3 Hz, *β*-pyrr), 6.62 (d, 1H, J=3 Hz, *β*-pyrr), 6.81 (br s 1H, NH_2), 6.86 (br d, 2H, *meso*-Ar), 7.09 (br d, 1H, *β*-pyrr), 7.13 (d, 2H, J=6 Hz, *meso*-Ar), 7.25 (br d, 1H, *β*-pyrr), δ 7.28-7.36 (m, 6H, *meso*-Ar), 7.42 (d, 2H, J= 6 Hz, *meso*-Ar); Anal. Calcd for $C_{53}H_{49}Br_2CuN_8O_2$: C, 60.43; H, 4.69; N, 10.64; found: C, 60.29; H, 4.76; N, 10.60; MS (FAB, m/z): 1055 (M+); UV-vis (CH_2Cl_2): λ_{max} nm (log ε): 447 (4.62), 762 (3.01).

*2-(pyrrol-1-yl)-3-nitro-3-5,10,15-tris(4-tert-butyl-phenyl)corrolato-Cu (**11**)*

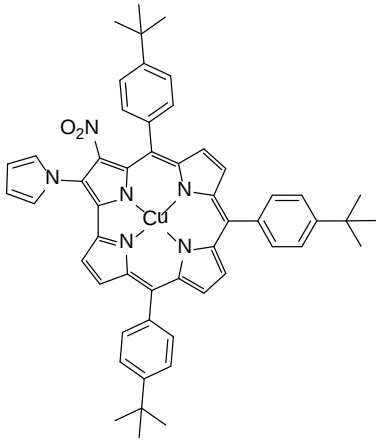

Corrole **1** (30 mg, 0.037 mmol) was dissolved in a mixture of acetic acid (7 mL) and toluene (1 mL). 2,5-Dimethoxytetrahydrofuran (9.5 µL, 0.074 mmol) was added; the mixture was refluxed under nitrogen and the course of the reaction was monitored by TLC and UV−vis measurements. After 45 min TLC monitoring showed almost quantitative formation of a brown band with higher R_f and a total consumption of the starting complex. The reaction mixture was cooled, and the solvent removed under reduced pressure. The residue was dissolved in CHCl3 and washed twice with water. The organic phase was collected, dried over anhydrous Na2SO4 and evaporated under reduced pressure to dryness. Chromatographic purification of the reaction crude was performed on a silica gel column, eluting with CH_2Cl_2. Yield: 90%, 27 mg, brown solid, mp >300 °C. ^{1}H NMR (300 MHz, $CDCl_3$, δ ppm): 1.41 (s, 9H, *p*-*t*Bu), 1.45 (s, 18H, *p*-*t*Bu), 6.40 (t, 2H, *J* = 3 Hz, pyrr),7.16 (t, 2H, *J* = 3 Hz, pyrr), 7.25 (d, 1H, *J* = 6 Hz, *meso*-Ar), δ 7.34-7-38 (br m, 2H, *β*-pyrr), δ 7.42-7.45 (br m, 3H, *meso*-Ar + *β*-pyrr), δ 7.60-7.69 (br m, 7H, *meso*-Ar + *β*- pyrr). ^{13}C NMR (300 MHz, CDCl3, δ ppm): 31.27, 35.14, 109.96, 122.68, 123.01, 125.39, 125.60, 128.02, 129.62, 130.12, 132.03, 134.59, 135.65, 136.87, 138.15, 139.58, 144.97, 147.45, 151.03, 152.33, 152.70. Anal. Calcd for $C_{53}H_{49}CuN_6O_2$: C, 73.55; H, 5.71; N, 9.71; found: C, 73.83; H, 5.59; N, 9.85; MS (FAB, *m/z*): 867 (M+); UV-vis (CH2Cl2): λmax nm (log ε): 378 (sh), 433 (4.64), 567 (4.20), 656 (3.96).

*2-(pyrrol-1-yl)-3-amino-3-5,10,15-tris(4-tert-butyl-phenyl)corrolato-Cu (**12**)*

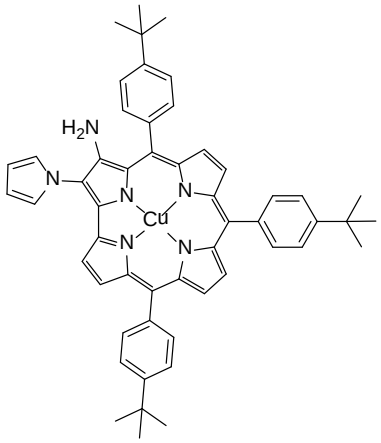

Corrole **11** (30 mg, 0.035 mmol) was dissolved in a mixture of CH_2Cl_2 (12 mL) and CH_3OH (3 mL) and allowed to stir under nitrogen at room temperature for 10 min. 10% Pd on activated carbon (30 mg, 0.282 mmol) and $NaBH_4$ (65 mg, 1.731 mmol) were added and the mixture was stirred under nitrogen for 15 min. The solution immediately turned bright green and TLC monitoring showed almost quantitative consumption of the substrate. The reduction was considered complete when a Soret band at 421 nm was evident and the shoulder at 378 nm had disappeared. Once the reaction was complete, the mixture was filtered through Celite; the filtrate was collected and evaporated under reduced pressure. The crude product was taken up in $CHCl_3$; the solution was washed 3 times with water, dried over anhydrous Na_2SO_4 and evaporated to dryness. The residue obtained was dissolved in CH_2Cl_2 and applied to a silica gel column for chromatographic purification using CH_2Cl_2 as eluent.
Yield: 83%, 24 mg, brown solid, mp >300 °C. ^{1}H NMR (300 MHz, $CDCl_3$, δ ppm): 1.39 (s, 9H, *p*-*t*Bu), 1.41 (s, 9H, *p*-*t*Bu), 1.41 (s, 9H, *p*-*t*Bu), 2.96, (s, 2H, NH2), 6.22 (br d, 1H, *β*-pyrr), 6.33 (br m, 2H, pyrr), 6.95 (br m, 2H, pyrr), δ 7.16-7.18 (br m, 4H, *meso*-Ar), 7.38 (d, 2H, *J* = 6 Hz, *meso*-Ar), 7.60 (d, 2H, *J* = 9 Hz, *meso*-Ar), δ 7.67-7.76 (br m, 6H, *meso*-Ar + *β*-pyrr), 7.91 (br d, 1H, *β*-pyrr), 8.10 (br d, 1H, *β*-pyrr), 8.27 (br d, 1H,*β*-pyrr). ^{13}C NMR (300 MHz, CDCl3, δ ppm): 31.45, 31.75, 31.98, 34.27, 34.48, 34.82, 109.38, 120.30,122.15, 124.51, 125.00, 126.15, 133.45, 152.61, 152.90, 154.14.Anal. Calcd for $C_{53}H_{51}CuN_6$: C, 76.18; H,6.15; N, 10.06; found: C, 76.30; H, 5.96; N, 10.01; MS (FAB, *m/z*): 836 (M+); UV-vis (CH2Cl2): λ_{max} nm (log ε): 421 (5.01), 635 (3.90).

General procedure for the synthesis of β,β′-fused pyrrolo[1,2-a]pyrazinocorrolato-Cu

To a mixture of corrole **12** (35 mg, 0.042 mmol) and aldehyde (0.50 mmol) in 1,4-dioxane (5 mL), DBSA (1.32 μL, 0.004 mmol) was added. The reaction mixture was stirred at room temperature and the course of the reaction was monitored by TLC and UV-vis measurements. After 120 min the mixture was treated with 10% aqueous

$NaHCO_3$ and the organic phase was extracted with $CHCl_3$ and washed with water (3 times). The crude product was dried over anhydrous $NaSO_4$ and then the solvent was removed under reduced pressure. The mixture was purified by column chromatography over silica gel using CH_2Cl_2/hexane (3:1) as eluent. The characterization data of all the newly prepared compounds are given below.

*β,β′-fused pyrrolo[1,2-a]pyrazinocorrolato-Cu (**13**)*

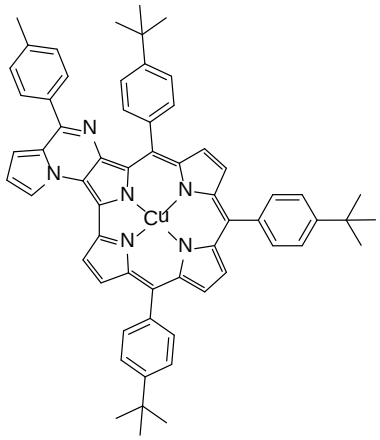

Yield: 32%, 12 mg, brown solid, mp >300 °C. ^{1}H NMR (300 MHz, CDCl3, δ ppm): 1.42 (s, 9H, *p-t*Bu), 1.45 (s, 9H, *p-t*Bu), 1.49 (s, 9H, *p-t*Bu), 2.43 (s, 3H, CH3), 6.99 (br m, 2H, pyrr), 7.10 (d, 1H, *J* = 3 Hz, pyrr), δ 7.17-7.20 (br m, 5H, *meso*-Ar + pyrr), 7.28 (br d, 1H, pyrr), δ 7.42-7.53 (br m, 8H, *meso*-Ar), δ 7.62-7.66 (br m, 4H, tolyl), 7.71 (br m, 2H, pyrr), 7.74 (br d, 1H, pyrr), 8.12 (br d, 1H, pyrr), 8.15 (br d, 1H, pyrr) Anal. Calcd for $C_{61}H_{55}CuN_6$: C, 78.30; H, 5.92; N, 8.98; found: C, 78.12; H, 5.87; N, 9.04; MS (FAB, *m/z*): 934 (M+); UV-vis (CH_2Cl_2): λ_{max} nm (log ε): 433 (5.07), 644 (4.15).

*β,β′-fused pyrrolo[1,2-a]pyrazinocorrolato-Cu (**14**)*

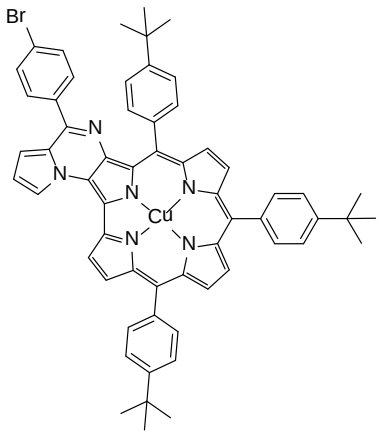

Yield: 21%, 9 mg, brown solid, mp >300 °C. ^{1}H NMR (300 MHz, CDCl3, δ ppm): 1.40 (s, 9H, *p*-*t*Bu), 1.43 (s, 9H, *p*-*t*Bu), 1.47 (s, 9H, *p*-*t*Bu), 6.99 (br d, 1H, pyrr), 7.10 (br d, 1H, pyrr), 7.20 (d, 2H, *J* = 3 Hz, pyrr), δ 7.42-7.49 (br m, 11H, *meso*-Ar + pyrr), δ 7.62-7.71 (br m, 8H, *meso*-Ar + Ar), 8.81 (br d, 1H, pyrr), 8.16 (br d, 1H, pyrr). ^{13}C NMR (300 MHz, CDCl3, δ ppm): 29.71, 31.30, 31.54, 125.08, 125.30, 130.02, 130.58, 131.16, 131.56. Anal. Calcd for $C_{60}H_{52}BrCuN_6$: C, 72.02; H, 5.24; N, 8.40; found: C, 71.93; H, 5.11; N, 8.58; MS (FAB, *m/z*): 1000 (M+); UV-vis (CH_2Cl_2): λ_{max} nm (log ε): 433 (4.90), 553 (4.04), 647 (3.92).

*β,β′-fused pyrrolo[1,2-a]pyrazinocorrolato-Cu (**15**)*

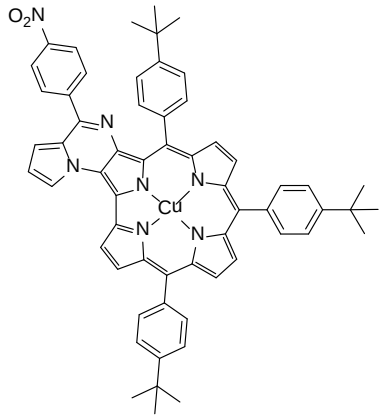

Yield: 29%, 12 mg, brown solid, mp >300 °C. ^{1}H NMR (300 MHz, $CDCl_3$, δ ppm): 1.39 (s, 9H, *p*-*t*Bu), 1.42 (s, 9H, *p*-*t*Bu), 1.45 (s, 9H, *p*-*t*Bu), 6.87 (br d, 1H, pyrr), 6.97 (br d, 1H, pyrr), 7.07 (br d, 1H, pyrr), 7.10 (brd, 1H, pyrr), 7.14 (br d, 1H, pyrr), 7.20 (br d, 1H, pyrr), δ 7.40-7.45 (br m, 8H, *meso*-Ar), δ 7.49-7.52 (br m, 5H, *meso*-Ar + pyrr), 7.84 (d, 2H, *J* = 6 Hz, Ar), 7.92 (br d, 1H, pyrr), 8.03 (br d, 1H, pyrr), 8.10 (d, 2H, *J* = 9 Hz, Ar). ^{13}C NMR (300 MHz, $CDCl_3$, δ ppm): 29.72, 31.29, 31.55, 34.95, 106.27, 123.07, 124.24, 125.00, 125.19, 129.63. Anal. Calcd for $C_{60}H_{52}CuN_7O_2$: C, 74.55; H, 5.42; N, 10.14; found: C, 74.38; H, 5.14; N, 10.23; MS (FAB, *m/z*): 969 (M+); UV-vis (CH_2Cl_2): λ_{max} nm (log ε): 425 (4.81), 655 (4.02).

*β,β′-fused pyrrolo[1,2-a]pyrazinocorrolato-Cu (**16**)*

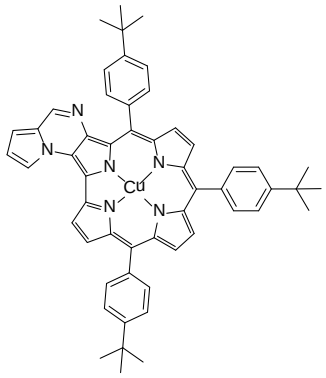

Yield: 19%, 7 mg, brown solid, mp >300 °C. ^{1}H NMR (300 MHz, $CDCl_3$, δ ppm): 1.41 (s, 9H, *p*-*t*Bu), 1.43 (s, 9H, *p*-*t*Bu), 1.45 (s, 9H, *p*-*t*Bu), 6.94 (d, 1H, *J* = 3 Hz, pyrr), 7.00 (br d, 1H, pyrr), δ 7.43-7.50 (br m, 7H, *meso*-Ar), 7.56 (br d, 1H, pyrr), 7.59 (br d, 1H, pyrr), δ 7.64-7.71 (br m, 5H, *meso*-Ar), 7.76 (d, 1H, *J* = 3 Hz, pyrr) 8.15 (br m, 2H, pyrr), 8.58 (s, 1H, pyrazino). ^{13}C NMR (300 MHz, CDCl3, δ ppm): 29.72, 31.28, 124.66, 125.09, 125.38. Anal. Calcd for $C_{54}H_{49}CuN_6$: C, 76.70; H, 5.84; N, 9.94; found: C, 76.89; H, 5.96; N, 9.86; MS (FAB, *m/z*): 849 (M+); UV-vis (CH_2Cl_2): λ_{max} nm (log ε): 430 (4.93), 633 (3.85).

*Formylation of 2-(pyrrol-1-yl)-3-nitro-3-5,10,15-tris(4-tert-butyl-phenyl)corrolato-Cu (**17**)*

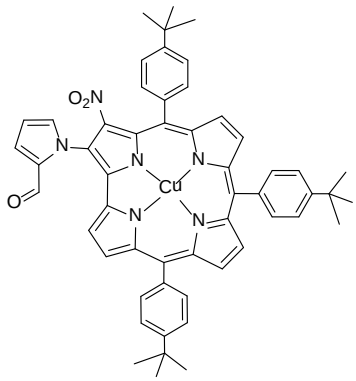

The Vilsmeier reagent was prepared by cooling DMF (0.6 mL, 7.8 mmol) to 0 °C and adding $POCl_3$ (0.6 mL, 6.4 mmol) under nitrogen; the reagent was then added dropwise to a solution of **11** (20 mg, 0.023 mmol) in CH_2Cl_2 (7 mL). The resulting mixture was allowed to reach room temperature and stirred under nitrogen. The progress of the reaction was monitored by UV/Vis spectroscopy; after three hours there was no

evidence of the absorptions of the starting material. A saturated solution of $NaHCO_3$ (15 mL) was then added and the mixture stirred overnight. The organic phase was then separated, washed with water, dried on Na_2SO_4, and the solvent evaporated. The crude mixture was dissolved in CH_2Cl_2, and column chromatography (silica gel, CH_2Cl_2 eluent) afforded **17** as a brown solid. Yield: 48%, mp >300 °C.
^1H NMR (300 MHz, $CDCl_3$, δ ppm): 1.41 (s, 9H, *p*-*t*Bu), 1.45 (s, 18H, *p*-*t*Bu), 6.56 (t, 1H, *J* = 3 Hz, pyrr),7.25 (br t, 2H, pyrr), 7.36 (d, 1H, *J* = 3 Hz, *β*-pyrr), δ 7.47 (br m, 4H, pyrr), δ 7.53-7.55 (br m, 6H, *meso*-Ar), 7.62 (d, 1H, *J* = 3 Hz, pyrr), δ 7.66-7.68 (br m, 6H, *meso*-Ar);Anal. Calcd for $C_{54}H_{49}CuN_6O_3$: C, 72.58; H, 5.53; N, 9.41; found: C, 72.61; H, 5.50; N, 9.48; MS (ESI, *m/z*): 892 (M+); UV-vis (CH_2Cl_2): λ_{max} nm (log ε): 376 (4.58), 435 (4.86), 574 (4.18), 673 (3.89).

References

(1) Sessler, J. L.; Gebauer, A.; Vogel, E. Expanded Porphyrins. In *The Porphyrin Handbook*; Kadish, K. M.; Smith, K. M.; Guilard, R., 2000; Vol. II.

(2) Saegusa, Y.; Ishizuka, T.; Komamura, K.; Shimizu, S.; Kotani, H.; Kobayashi, N.; Kojima, T. Ring-Fused Porphyrins: Extension of π-Conjugation Significantly Affects the Aromaticity and Optical Properties of the Porphyrin π-Systems and the Lewis Acidity of the Central Metal Ions. *Phys. Chem. Chem. Phys.* **2015**, *17* (22), 15001–15011.

(3) Tomé, A. C.; Neves, M. G. P. M. S.; Cavaleiro, J. A. S. Porphyrins and Other Pyrrolic Macrocycles in Cycloaddition Reactions. *J. Porphyr. Phthalocyanines* **2009**, *13* (04n05), 408–414.

(4) Barata, J. F. B.; Silva, A. M. G.; Faustino, M. A. F.; Neves, M. G. P. M. S.; Tomé, A. C.; Silva, A. M. S.; Cavaleiro, J. A. S. Novel Diels-Alder and Thermal [4+4] Cycloadditions of Corroles. *Synlett* **2004**, No. 7, 1291–1293.

(5) Li, C.; Fechtel, M.; Feng, Y.; Kräutler, B. Corroles Programmed for Regioselective Cycloaddition Chemistry — Synthesis of a Bisadduct with C60-Fullerene. *J. Porphyr. Phthalocyanines* **2012**, *16* (05n06), 556–563.

(6) M. Santos, C. I.; Oliveira, E.; B. Barata, J. F.; F. Faustino, M. A.; S. Cavaleiro, J. A.; S. Neves, M. G. P. M.; Lodeiro, C. Corroles as Anion Chemosensors: Exploiting Their Fluorescence Behaviour from Solution to Solid-Supported Devices. *J. Mater. Chem.* **2012**, *22* (27), 13811–13819.

(7) Santos, C. I. M.; Oliveira, E.; Barata, J. F. B.; Faustino, M. A. F.; Cavaleiro, J. A. S.; Neves, M. G. P. M. S.; Lodeiro, C. New Gallium(III) Corrole Complexes as Colorimetric Probes for Toxic Cyanide Anion. *Inorganica Chim. Acta* **2014**, *417*, 148–154.

(8) Vale, L. S. H. P.; Barata, J. F. B.; Neves, M. G. P. M. S.; Faustino, M. A. F.; Tomé, A. C.; Silva, A. M. S.; Paz, F. A. A.; Cavaleiro, J. A. S. Novel Quinone-Fused Corroles. *Tetrahedron Lett.* **2007**, *48* (50), 8904–8908.

(9) Vale, L. S. H. P.; Barata, J. F. B.; Santos, C. I. M.; Neves, M. G. P. M. S.; Faustino, M. A. F.; Tomé, A. C.; Silva, A. M. S.; Paz, F. A. A.; Cavaleiro, J. A. S. Corroles in 1,3-Dipolar Cycloaddition Reactions. *J. Porphyr. Phthalocyanines* **2009**, *13* (03), 358–368.

(10) Finikova, O. S.; Chernov, S. Y.; Cheprakov, A. V.; Filatov, M. A.; Vinogradov, S. A.; Beletskaya, I. P. New Selective Synthesis of Substituted Tetrabenzoporphyrins. *Dokl. Chem.* **2003**, *391* (4–6), 222–224.

(11) Ito, S.; Murashima, T.; Ono, N.; Uno, H. A New Synthesis of Benzoporphyrins Using 4,7-Dihydro-4,7-Ethano-2H-Isoindole as a Synthon of Isoindole. *Chem. Commun.* **1998**, *0* (16), 1661–1662.

(12) Vicente, M. G. H.; Tomé, A. C.; Walter, A.; Cavaleiro, J. S. Synthesis and Cycloaddition Reactions of Pyrrole-Fused 3-Sulfolenes: A New Versatile Route to Tetrabenzoporphyrins. *Tetrahedron Lett.* **1997**, *38* (20), 3639–3642.

(13) Remy, D. E. A Versatile Synthesis of Tetrabenzporphyrins. *Tetrahedron Lett.* **1983**, *24* (14), 1451–1454.

(14) Pomarico, G.; Nardis, S.; Paolesse, R.; Ongayi, O. C.; Courtney, B. H.; Fronczek, F. R.; Vicente, M. G. H. Synthetic Routes to 5,10,15-Triaryl-Tetrabenzocorroles. *J. Org. Chem.* **2011**, *76* (10), 3765–3773.

(15) Wu, F.; Liu, J.; Mishra, P.; Komeda, T.; Mack, J.; Chang, Y.; Kobayashi, N.; Shen, Z. Modulation of the Molecular Spintronic Properties of Adsorbed Copper Corroles. *Nat. Commun.* **2015**, *6*, ncomms8547.

(16) Jiao, L.; Hao, E.; Fronczek, F. R.; Vicente, M. G. H.; Smith, K. M. Benzoporphyrins via an Olefin Ring-Closure Metathesis Methodology. *Chem. Commun.* **2006**, *0* (37), 3900–3902.

(17) Setsune, J. Palladium Chemistry in Recent Porphyrin Research. *J. Porphyr. Phthalocyanines* **2004**, *08* (01), 93–102.

(18) Vestfrid, J.; Botoshansky, M.; Palmer, J. H.; Durrell, A. C.; Gray, H. B.; Gross, Z. Iodinated Aluminum(III) Corroles with Long-Lived Triplet Excited States. *J. Am. Chem. Soc.* **2011**, *133* (33), 12899–12901.
(19) Nardis, S.; Pomarico, G.; Mandoj, F.; Fronczek, F. R.; Smith, K. M.; Paolesse, R. One-Pot Synthesis of Meso-Alkyl Substituted Isocorroles: The Reaction of a Triarylcorrole with Grignard Reagent. *J. Porphyr. Phthalocyanines* **2010**, *14* (8), 752–757.
(20) Du, R.-B.; Liu, C.; Shen, D.-M.; Chen, Q.-Y. Partial Bromination and Fluoroalkylation of 5,10,15-Tris(Pentafluorophenyl) Corrole. *Synlett* **2009**, No. 16, 2701–2705.
(21) Nardis, S.; Monti, D.; Paolesse, R. Novel Aspects of Corrole Chemistry. *Mini-Rev. Org. Chem.* **2005**, *2* (4), 355–374.
(22) Pomarico, G.; Nardis, S.; Stefanelli, M.; Cicero, D. O.; Vicente, M. G. H.; Fang, Y.; Chen, P.; Kadish, K. M.; Paolesse, R. Synthesis and Characterization of Functionalized Meso - Triaryltetrabenzocorroles. *Inorg. Chem.* **2013**, *52* (15), 8834–8844.
(23) Barata, J. F. B.; Santos, C. I. M.; Neves, M. G. P. M. S.; Faustino, M. A. F.; Cavaleiro, J. A. S. Functionalization of Corroles. In *Synthesis and Modifications of Porphyrinoids*; Topics in Heterocyclic Chemistry; Springer, Berlin, Heidelberg, 2013; pp 79–141.
(24) Barata, J. F. B.; Neves, M. G. P. M. S.; Faustino, M. A. F.; Tomé, A. C.; Cavaleiro, J. A. S. Strategies for Corrole Functionalization. *Chem. Rev.* **2017**, *117* (4), 3192–3253.
(25) Mastroianni, M.; Zhu, W.; Stefanelli, M.; Nardis, S.; Fronczek, F. R.; Smith, K. M.; Ou, Z.; Kadish, K. M.; Paolesse, R. β-Nitro Derivatives of Germanium(IV) Corrolates. *Inorg. Chem.* **2008**, *47* (24), 11680–11687.
(26) Smith, K. M.; Barnett, G. H.; Brian, E.; Zoya, M. Novel Meso-Substitution Reactions of Metalloporphyrins. *J. Am. Chem. Soc.* **1979**, *101* (20), 5953–5961.
(27) Stefanelli, M.; Shen, J.; Zhu, W.; Mastroianni, M.; Mandoj, F.; Nardis, S.; Ou, Z.; Kadiah, K. M.; Fronczek, F. R.; Smith, K. M.; et al. Demetalation of Silver(III) Corrolates. *Inorg. Chem.* **2009**, *48* (14), 6879–6887.
(28) Serra, V. I. V.; Pires, S. M. G.; Alonso, C. M. A.; Neves, M. G. P. M. S.; Tomé, A. C.; Cavaleiro, J. A. S. Meso-Tetraarylporphyrins Bearing Nitro or Amino Groups: Synthetic Strategies and Reactivity Profiles. In *Synthesis and Modifications of Porphyrinoids*; Topics in Heterocyclic Chemistry; Springer, Berlin, Heidelberg, 2013; pp 35–78.
(29) Collman, J. P.; Decréau, R. A. 5,10,15-Tris(o-Aminophenyl) Corrole (TAPC) as a Versatile Synthon for the Preparation of Corrole-Based Hemoprotein Analogs. *Org. Lett.* **2005**, *7* (6), 975–978.
(30) Collman, J. P.; Kaplun, M.; Decréau, R. A. Metal Corroles as Electrocatalysts for Oxygen Reduction. *Dalton Trans.* **2006**, *0* (4), 554–559.
(31) Barbe, J.-M.; Canard, G.; Brandès, S.; Guilard, R. Organic-Inorganic Hybrid Sol-Gel Materials Incorporating Functionalized Cobalt(III) Corroles for the Selective Detection of CO. *Angew. Chem. - Int. Ed.* **2005**, *44* (20), 3103–3106.
(32) Barbe, J.-M.; Canard, G.; Brandès, S.; Guilard, R. Synthesis and Physicochemical Characterization of Meso-Functionalized Corroles: Precursors of Organic–Inorganic Hybrid Materials. *Eur. J. Org. Chem.* **2005**, *2005* (21), 4601–4611.
(33) Stefanelli, M.; Mandoj, F.; Mastroianni, M.; Nardis, S.; Mohite, P.; Fronczek, F. R.; Smith, K. M.; Kadish, K. M.; Xiao, X.; Ou, Z.; et al. Amination Reaction on Copper and Germanium β-Nitrocorrolates. *Inorg. Chem.* **2011**, *50* (17), 8281–8292.
(34) Crossley, M. J.; Govenlock, L. J.; Prashar, J. K. Synthesis of Porphyrin-2,3,12,13- and -2,3,7,8-Tetraones: Building Blocks for the Synthesis of Extended Porphyrin Arrays. *J. Chem. Soc. Chem. Commun.* **1995**, No. 23, 2379–2380.
(35) Cho, S.; Lim, J. M.; Hiroto, S.; Kim, P.; Shinokubo, H.; Osuka, A.; Kim, D. Unusual Interchromophoric Interactions in β,β' Directly and Doubly Linked Corrole Dimers: Prohibited Electronic Communication and Abnormal Singlet Ground States. *J. Am. Chem. Soc.* **2009**, *131* (18), 6412–6420.
(36) Barata, J. F. B.; Silva, A. M. G.; Neves, M. G. P. M. S.; Tomé, A. C.; Silva, A. M. S.; Cavaleiro, J. A. S. β,B′-Corrole Dimers. *Tetrahedron Lett.* **2006**, *47* (46), 8171–8174.

(37) Barata, J. F. B.; Silva, A. M. G.; Faustino, M. A. F.; Neves, M. G. P. M. S.; Tomé, A. C.; Silva, A. M. S.; Cavaleiro, J. A. S. Novel Diels-Alder and Thermal [4+4] Cycloadditions of Corroles. *Synlett* **2004**, *2004* (07), 1291–1293.
(38) Santos, C. I. M.; Oliveira, E.; Barata, J. F. B.; Faustino, M. A. F.; Cavaleiro, J. A. S.; Neves, M. G. P. M. S.; Lodeiro, C. Corroles as Anion Chemosensors: Exploiting Their Fluorescence Behaviour from Solution to Solid-Supported Devices. *J. Mater. Chem.* **2012**, *22* (27), 13811–13819.
(39) Zhao, S.; Neves, M. G. P. M. S.; Tomé, A. C.; Silva, A. M. S.; Cavaleiro, J. A. S.; Domingues, M. R. M.; Ferrer Correia, A. J. Reaction of Meso-Tetraarylporphyrins with Pyrazine Ortho-Quinodimethanes. *Tetrahedron Lett.* **2005**, *46* (13), 2189–2191.
(40) Lindsey, J. S.; Hsu, H. C.; Schreiman, I. C. Synthesis of Tetraphenylporphyrins under Very Mild Conditions. *Tetrahedron Lett.* **1986**, *27* (41), 4969–4970.
(41) Mandoj, F.; Nardis, S.; Pomarico, G.; Paolesse, R. Demetalation of Corrole Complexes: An Old Dream Turning into Reality. *J. Porphyr. Phthalocyanines* **2008**, *12* (01), 19–26.
(42) Lu, G.; Lin, W.; Fang, Y.; Zhu, W.; Ji, X.; Ou, Z. Synthesis and Electrochemical Properties of Meso-Phenyl Substituted Copper Corroles: Solvent Effect on Copper Oxidation State. *J. Porphyr. Phthalocyanines* **2011**, *15* (11n12), 1265–1274.
(43) Stefanelli, M.; Mastroianni, M.; Nardis, S.; Licoccia, S.; Fronczek, F. R.; Smith, K. M.; Zhu, W.; Ou, Z.; Kadish, K. M.; Paolesse, R. Functionalization of Corroles: The Nitration Reaction. *Inorg. Chem.* **2007**, *46* (25), 10791–10799.
(44) Fisher, T. E.; Kim, B.; Staas, D. D.; Lyle, T. A.; Young, S. D.; Vacca, J. P.; Zrada, M. M.; Hazuda, D. J.; Felock, P. J.; Schleif, W. A.; et al. 8-Hydroxy-3,4-Dihydropyrrolo[1,2-a]Pyrazine-1(2H)-One HIV-1 Integrase Inhibitors. *Bioorg. Med. Chem. Lett.* **2007**, *17* (23), 6511–6515.
(45) Rault, S.; Lancelot, J. C.; Prunier, H.; Robba, M.; Renard, P.; Delagrange, P.; Pfeiffer, B.; Caignard, D. H.; Guardiola-Lemaitre, B.; Hamon, M. Novel Selective and Partial Agonists of 5-HT3 Receptors. Part 1. Synthesis and Biological Evaluation of Piperazinopyrrolothienopyrazines. *J. Med. Chem.* **1996**, *39* (10), 2068–2080.
(46) Dawidowski, M.; Chońska, J.; Mika, W.; Turło, J. Novel Fluorinated Pyrrolo[1,2-a]Pyrazine-2,6-Dione Derivatives: Synthesis and Anticonvulsant Evaluation in Animal Models of Epilepsy. *Bioorg. Med. Chem.* **2014**, *22* (19), 5410–5427.
(47) Arban, R.; Bianchi, F.; Buson, A.; Cremonesi, S.; Fabio, R. D.; Gentile, G.; Micheli, F.; Pasquarello, A.; Pozzan, A.; Tarsi, L.; et al. Pyrrolo[1,2-a]Pyrazine and Pyrazolo[1,5-a]Pyrazine: Novel, Potent, and Selective Series of Vasopressin1b Receptor Antagonists. *Bioorg. Med. Chem. Lett.* **2010**, *20* (17), 5044–5049.
(48) Micheli, F.; Bertani, B.; Bozzoli, A.; Crippa, L.; Cavanni, P.; Di Fabio, R.; Donati, D.; Marzorati, P.; Merlo, G.; Paio, A.; et al. Phenylethynyl-Pyrrolo[1,2-a]Pyrazine: A New Potent and Selective Tool in the MGluR5 Antagonists Arena. *Bioorg. Med. Chem. Lett.* **2008**, *18* (6), 1804–1809.
(49) Singh, D. K.; Nath, M. Ambient Temperature Synthesis of β,β′-Fused Nickel(II) Pyrrolo[1,2-a]Pyrazinoporphyrins via a DBSA-Catalyzed Pictet-Spengler Approach. *Org. Biomol. Chem.* **2015**, *13* (6), 1836–1845.
(50) Elming, N.; Clauson-Kaas, N. The Preparation of Pyrroles from Furans. *Acta Chem. Scand.* **1952**, No. 6, 867–874.
(51) Pictet, A.; Spengler, T. Über Die Bildung von Isochinolin-Derivaten Durch Einwirkung von Methylal Auf Phenyl-Äthylamin, Phenyl-Alanin Und Tyrosin. *Berichte Dtsch. Chem. Ges.* **1911**, *44* (3), 2030–2036.
(52) Whaley, W. M.; Govindachari, T. R. The Pictet-Spengler Synthesis of Tetrahydroisoquinolines and Related Compounds. In *Organic Reactions*; John Wiley & Sons, Inc., 2004.
(53) Singh, D. K.; Nath, M. Ambient Temperature Synthesis of β,B′-Fused Nickel(II) Pyrrolo[1,2-a]Pyrazinoporphyrins via a DBSA-Catalyzed Pictet–Spengler Approach. *Org. Biomol. Chem.* **2015**, *13* (6), 1836–1845.
(54) Paolesse, R.; Jaquinod, L.; Senge, M. O.; Smith, K. M. Functionalization of Corroles: Formylcorroles. *J. Org. Chem.* **1997**, *62* (18), 6193–6198.

(55) Paolesse, R.; Nardis, S.; Venanzi, M.; Mastroianni, M.; Russo, M.; Fronczek, F. R.; Vicente, M. G. H. Vilsmeier Formylation of 5,10,15-Triphenylcorrole: Expected and Unusual Products. *Chem. – Eur. J.* **2003**, *9* (5), 1192–1197.
(56) Sudhakar, K.; Giribabu, L.; Salvatori, P.; Angelis, F. D. Triphenylamine-Functionalized Corrole Sensitizers for Solar-Cell Applications. *Phys. Status Solidi A* **2015**, *212* (1), 194–202.
(57) Fulmer, G. R.; Miller, A. J. M.; Sherden, N. H.; Gottlieb, H. E.; Nudelman, A.; Stoltz, B. M.; Bercaw, J. E.; Goldberg, K. I. NMR Chemical Shifts of Trace Impurities: Common Laboratory Solvents, Organics, and Gases in Deuterated Solvents Relevant to the Organometallic Chemist. *Organometallics* **2010**, *29* (9), 2176–2179.

Chapter II

Design and synthesis of new Phthalocyanine-Corrole hybrid conjugates

The Energy Issue

Human activity is continuing to affect the Earth's energy budget by changing the emissions and resulting atmospheric concentrations of greenhouse gases and aerosols and by modifying land surface properties.

Previous assessments have already shown through multiple lines of evidence that the climate is changing across our planet, largely as a result of human activity. The most compelling evidence of climate change comes from observations of the atmosphere, land, oceans and cryosphere. Unequivocal evidence from *in situ* observations and ice core records show that the atmospheric concentrations of important greenhouse gases such as CO_2, CH_4 and N_2O have increased over the last few centuries.[1] It is certain that global mean surface temperature has increased since the late 19th century. The temperature of the Earth surface has been successively warmer in each of the past three decades than all the previous decades in the instrumental record, and the first decade of the 21st century has been the warmest. Overall, the global annual temperature has increased at an average rate of 0.17°C per decade since 1970.[2]

Fossil fuels, including coal, oil and natural gas, are currently the world's primary energy sources and the principal cause of global warming. Moreover, it is estimated that in the next two decades energy consumption will increases by 5.0 per cent, with the bulk of the demand coming from developing countries. Oil, coal and gas together account for the majority of global primary energy consumption. Fossil fuels are non-renewable sources; they draw on finite resources that will eventually dwindle, becoming too expensive and too environmentally damaging to retrieve. On the contrary, many types of renewable energy resources are naturally replenished on a human timescale, existing over wide geographical areas. Among them, solar energy is one of the most promising in the long term. Every hour, the Earth receives enough solar power to supply humans' energy consumption for one year.[3,4]

In answer to this need, organic photovoltaics has emerged as a major topic in contemporary research,[5] using photosynthetic systems found in nature as a major source of inspiration.

During photosynthesis, energy from sunlight is first captured by photosynthetic π-pigments such as chlorophylls and carotenoids, which cover a wide spectral range of solar irradiation. (**Figure 2.1**).[6–8]

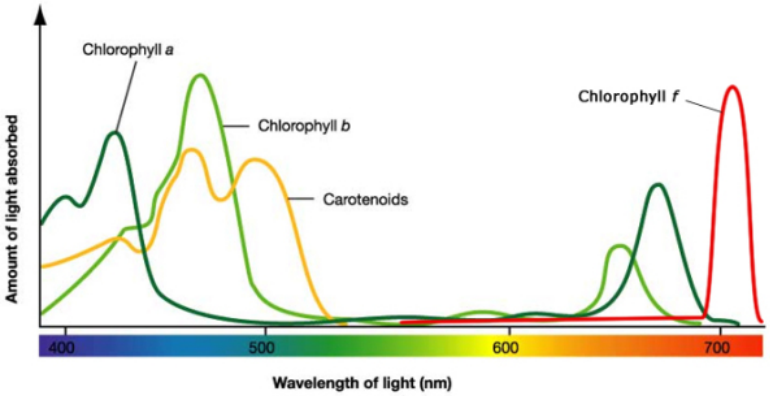

Figure 2.1. UV-vis absorption spectra of chlorophylls (green and red lines) and carotenoids (yellow line).

The captured light energy is transferred to chlorophylls that are in a special protein environment where the actual energy conversion event starts *via* electron transfer processes.[8]Pigments and proteins involved in this actual primary electron transfer event together are called the reaction centre. A large number of π-pigments molecules (100-5000), collectively referred to as antennas, harvest light and transfer the light energy to the same reaction centre. The purpose of such antenna molecules is to maintain a high rate of electron transfer in the reaction centre, even at lower light intensities. The success of this process relies on the effectiveness of these electron transfers and the lack of recombination reactions that would interrupt the process and cause a waste of the absorbed energy. The importance and the complexity of energy transfer and electron transfer processes in the photosynthetic reaction centre, have prompted the design and the preparation of a variety of donor-acceptor (D-A) covalently and non-covalently linked ensembles, including dyads, triads, tetrads and pentads, which are able to mimic the energy transfer and electron transfer processes in the photosynthetic reaction centre.[9–11]

Basic theory of photoinduced Electron Transfer (PET) and Excited Energy Transfer(EET)

A molecule in the excited state can relax to the ground state either by fluorescence, internal conversion, intersystem crossing, non-radiative decay or by two main physical mechanisms, electron transfer (PET) or energy transfer (EET) to another molecule. PET

and EET constitute the base of artificial photosystems, that are constituted by an electron donor unit (D) connected to an electron acceptor moiety (A) through a linker (L). This linker can connect both units either by covalent or supramolecular interactions. Both processes are depicted in **Figure 2.2**.

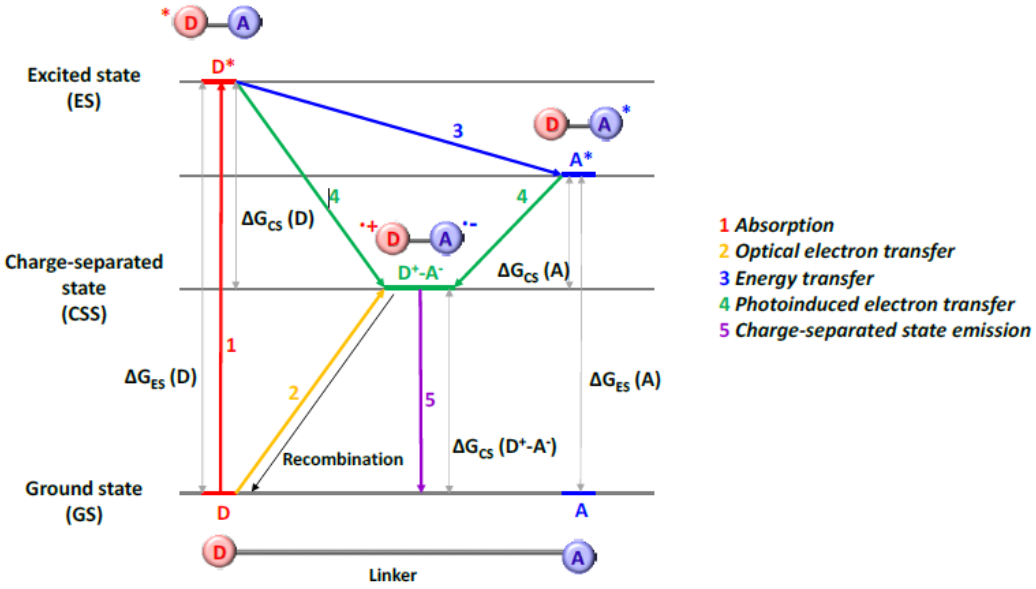

Figure 2.2. Schematic representation of photoinduced electron transfer (4) and energy transfer (3) between a donor and an acceptor connected through a linker.[12]

In the case of energy transfer reaction, upon photoexcitation, the energy of the excited state is transferred to the acceptor, leaving the donor molecule in the ground state and the acceptor molecule in the excited state. This type of reaction is likely to occur if the acceptor moiety has a low-energy excited state available and is not amenable to oxidation or reduction.

In the electron transfer process, an excited electron is transferred from a donor to an acceptor, and in can take place in two different ways, leading to photoinduced electron transfer or photoinduced hole transfer (PHT).[13,14] In PET mechanism, the electron donor is photoexcited, and an electron is promoted from its highest occupied molecular orbital (HOMO) to its lowest unoccupied molecular orbital (LUMO); it is subsequently transferred to the energetically lower-lying LUMO of the electron acceptor.

In the case of PHT, the electron acceptor is the part of the molecule being photoexcited, thus a hole appears in its HOMO, which is filled with an electron originating from the higher-lying HOMO of the electron donor.

In both cases, a charge separate donor-acceptor pair or charge separated state (CSS) is formed, involving a radical cation ($D^{\bullet+}$) and a radical anion ($A^{\bullet-}$), which will subsequently recombine to the electronic ground state (**Figure 2.3**).

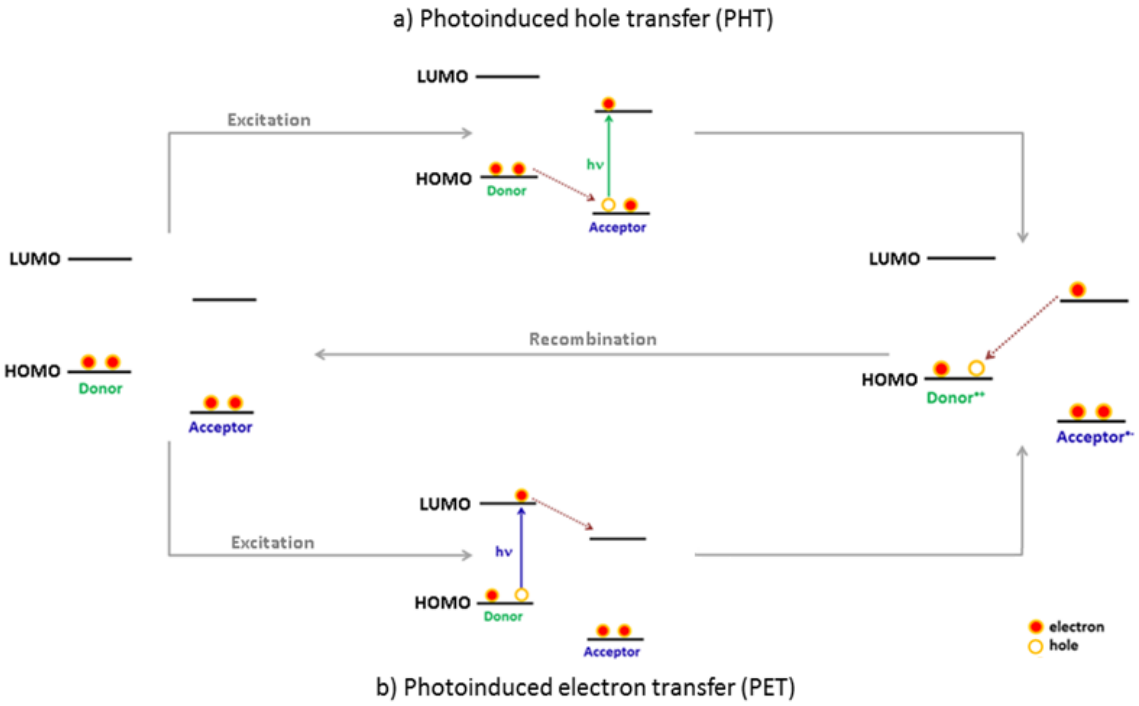

Figure 2.3. Schematic representation of the PHT (**a**) and PET (**b**) mechanisms.

This absorbed energy will be efficiently converted into electrical or chemical energy if these charged species are utilized as electrons and holes to drive electrical current or promote chemical reactions before back electron transfer leads to the initial ground states of the donor-acceptor species.

Specifically, an ideal (supra)molecular efficient artificial solar energy conversion system should be endowed with the following features:

- antenna molecules that capture light, absorbing in the visible range of the spectrum with high extinction coefficients, and form an "excited state species";
- the excited state species must transfer electron(s)/energy to acceptor entities;
- the energetic level of the CSS must be high and close to the energy level of the initial excited state, to minimize de energy loss;

- the electron transfer must be directional;
- the rates of the energy/electron transfer should be faster than those of the deactivation processes in order to achieve efficient energy or electron transfer.

Marcus theory of electron transfer

Marcus theory is the most successful description of electron transfer both for explaining and predicting electron transfer rates.[15,16] According to the theory, the rate constant of non adiabatic intramolecular electron transfer (k_{ET}) in an electron donor-acceptor-linked molecule at a fixed distance is given by the following equation:

$$\boldsymbol{k_{ET} = \left(\frac{4\pi^3}{h^2 \lambda k_B T}\right)^{1/2} V^2 \, exp\left[\frac{(\Delta G_{ET} + \lambda)^2}{4\lambda k_B T}\right]} \qquad \textbf{(Eq. 1)}$$

Here, h is Planck's constant, λis the reorganization energy (i.e. the required energy to structurally reorganize the electron donor and acceptor and their solvation spheres upon electron transfer), k_B is the Boltzmann constant, T is the absolute temperature, V is the electronic coupling constant and ΔG_{ET} is the free energy change of electron transfer.

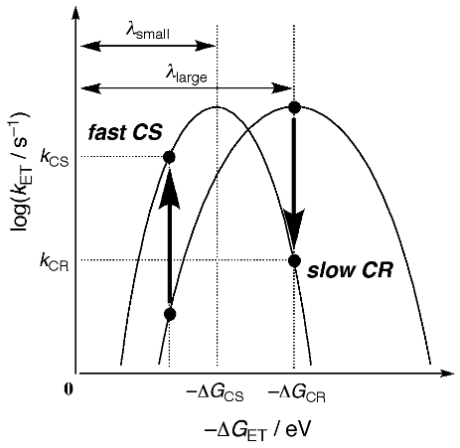

Figure 2.4. Schematic representation of Marcus curve.[17]

This parabolic dependence of log k_{ET} on $-\Delta G_{ET}$ is the result of two main factors: the electronic coupling element V, which determines the maximum k_{ET} value, and the reorganization energy (λ).In the 'normal region' of the Marcus curve (-$\Delta G°$ <λ), the rate

constant of an electron transfer reaction increases with increasing thermodynamic driving force. This relationship is maintained until the driving force equals the reorganization energy ($-\Delta G^\circ \sim \lambda$).In this case, the k_{ET} value reaches a maximum, and the reaction rate is mainly governed by the magnitude of the electronic coupling (V) between the donor and the acceptor subunits (**Figure 2.4**). Beyond this thermodynamic maximum, in the highly exothermic region of the parabola ($-\Delta G^\circ > \lambda$),the rates of electron transfer decrease with increase in the free energy changes. This latter range is generally referred to as the Marcus "inverted region".[18,19]

The smaller the reorganization energy, the faster the forward photoinduced charge separation (CS) process of an electron donor–acceptor dyad (D–A), but the charge recombination (CR) process becomes slower when the CR driving force ($-\Delta G_{CR}$) is larger than the reorganization energy (λ) of the electron transfer event.

Due to their structural similarity with naturally occurring chlorophylls, porphyrinoids have been the preferred chromophores for biomimetic photosynthesis.[11,20]

Within the family of porphyrinoids, phthalocyanines enjoy a privileged position, possessing unique physico-chemical properties, which render these macrocycles valuable building blocks in materials science.[21–24]

A brief introduction to the synthesis and the main properties of these compounds will be discussed in the following section.

Phthalocyanines

Among the huge variety of organic compounds that can be used as molecular components in artificial photosynthetic systems, tetrapyrrolicmacrocycles enjoy a privileged position. Out of all proportion, Phthalocyanines (Pcs), together with Porphyrins (Pors), are among the most studied chromophores.

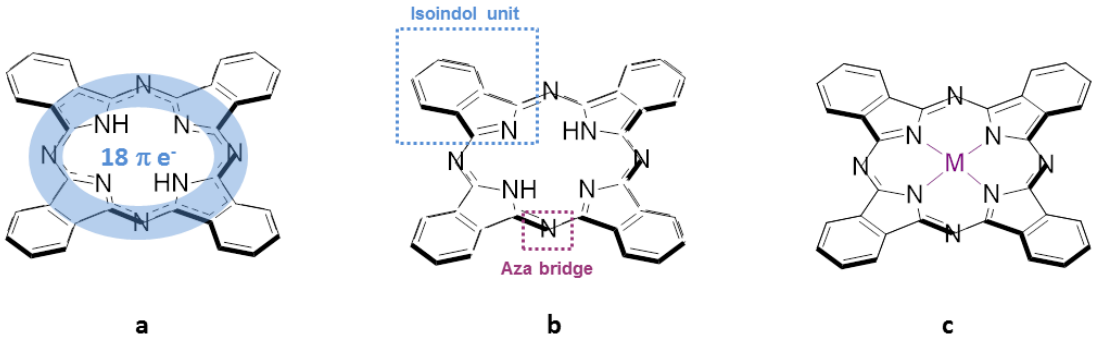

Figure 2.5. Electronic delocalization (**a**), free-base (**b**), and metallophthalocyanine(**c**).

Phthalocyanines[25,26] (**Figure 2.5**) are planar aromatic macrocycles consisting of four isoindole units presenting an 18 π –electron aromatic cloud delocalized over an arrangement of alternated carbon and nitrogen atoms. Therefore, Pcs can be referred to as tetrabenzotetraazaporphyrins. For many years, Pcs have been an important article of trade, i.e., dyestuffs for textiles and inks, as a consequence of their dark green-blue colour: their absorption spectra show, in fact, an intense Q-band in the visible region, usually centred at 620–700 nm (**Figure 2.6**).[23]

This single main band is associated to $\pi - \pi^*$ HOMO-LUMO transitions from doubly degenerated orbitals. In the case of metallophthalocyanines, having lower symmetry (D_{4h}), the LUMO is degenerated and only one band is observed. Parallel to that observed for porphyrins, the electronic spectrum of free-base phthalocyanines is characterized by a split Q-band, which occurs as a result of the reduction of symmetry from D_{4h} to D_{2h} on going from the metal complexes to the free base macrocycles. The Soret band is situated at higher energies in the spectrum and is related to $\pi - \pi^*$ transitions from lower-energy molecular orbitals.[23]

The chemical versatility of Pcs is associated to the versatility of their electronic and optical properties. Peripheral substituents play an important role in the tuning of the absorption bands of both phthalocyanine free base and the metal complexes. The Q-band can be shifted with the same additivity when the same kind of substituents are introduced at the same position of each benzene ring in a Pc macrocycle. Moreover, the Q-band of unsymmetrical metallated Pcs, generally leads to a splitting of the band due to a reduction of the symmetry.[27]

Metallophthalocyanines exhibit a fluorescence emission, which is characterized by a narrow band at long wavelengths (between 670 and 710 nm). This emission originates from an excited state which is localized on the tetrapyrrolic ring. Its maximum is red-shifted by only 8-20 nm from the absorption band, due to the high rigidity of the tetrapyrrolic ligand (**Figure 2.7**).[28]

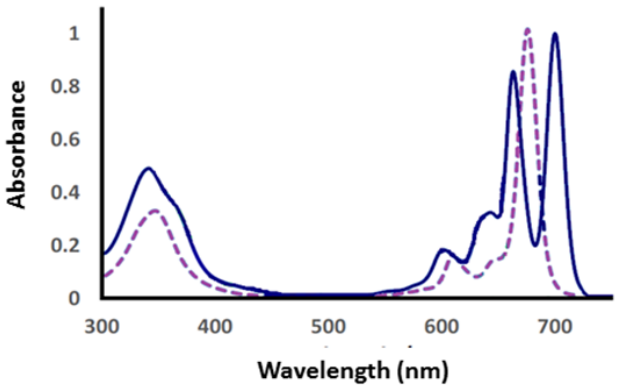

Figure 2.7.UV-vis spectra of free-base PcH_2 (blue solid line), and metallatedMPc (purple dashed line).

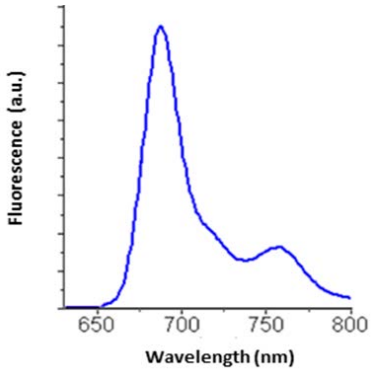

Figure 2.6. Emissionspectrumof MPc

The above mentioned systems can host more than 70 metals in their inner cavity and support different types, either donor or acceptor, of peripheral and axial substituents. However, as the coordination number of the macrocycle is four, according to the size and oxidation state of the metal, one or two ions (in the case of alkaline ions) can be inserted into the Pc core. When the metal demands a higher coordination number, one or two axial ligands are needed, resulting in pyramidal or octahedral structures

Unsubstituted phthalocyanines are highly insoluble in most of organic solvents. In order to increase their solubility, a wide variety of substituents can be attached at the axial positions and/or at the periphery of the macrocycle itself.[29] All these changes allow the

tailoring of the electrophysical parameters over a broad range, thus modulating their electronic properties and optical features.

Synthesis of phthalocyanines

Synthesis of symmetrically substituted phthalocyanines

The synthesis of Pcs usually involves the reaction of either phthalonitrile or 1,3-diiminoisoindoline precursors that assemble to form the macrocyclic structure (**Scheme 2.1**).[29,30]

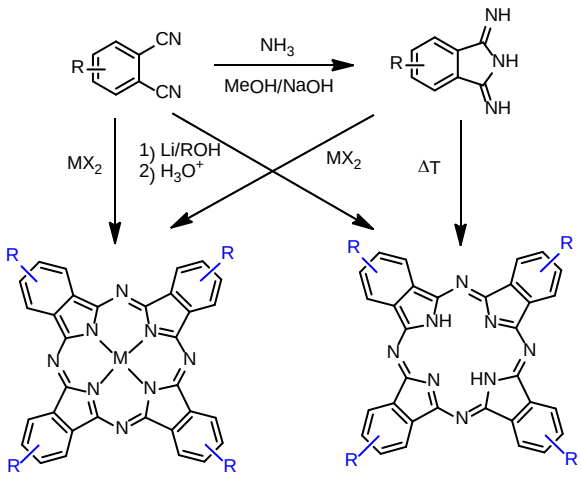

Scheme 2.1. General synthetic procedures to obtain H_2Pc and MPcs.

MPcs can be synthesized by means of a metal template reaction in which the appropriate precursor and the metal salt are heated to reflux in a high boiling solvent (DMF, *o*-DCB, DMAE etc). For the latter, they can be synthesized starting from 1,3-diiminoisoindolines using the above mentioned reaction conditions, or by using a phthalonitrile and a basic catalyst (as DBU or hydroquinone) in the presence of alcohols, such as DMAE or 1-penthanol.[31]

Another synthetic approach involves the use of lithium or magnesium alkoxides as metal templates, giving rise to the corresponding MPcs, that can be easily demetallated by treatment with a mineral or organic acid (namely AcOH, TFA) thus affording the corresponding free base derivative.[32]

More recently, alternative procedures to prepare Pcs have been described, such as the treatment of phthalonitriles with metal salts and hexamethyldisilazane in DMF,[33] the double-addition of oximes to phthalonitriles[34] and microwave-assisted synthesis.[35,36]
When non symmetric phthalonitriles are used as starting materials, the resulting Pcs are obtained as mixtures of four structural isomers with C_{4h}, D_{2h}, $C_{2v}$and C_{2s}symmetries (**Figure 2.8**).[37] These regioisomers have been separated in a few cases by chromatographic techniques[38,39]or obtained separately employing a regioselective synthesis of Pcs.[40–42]

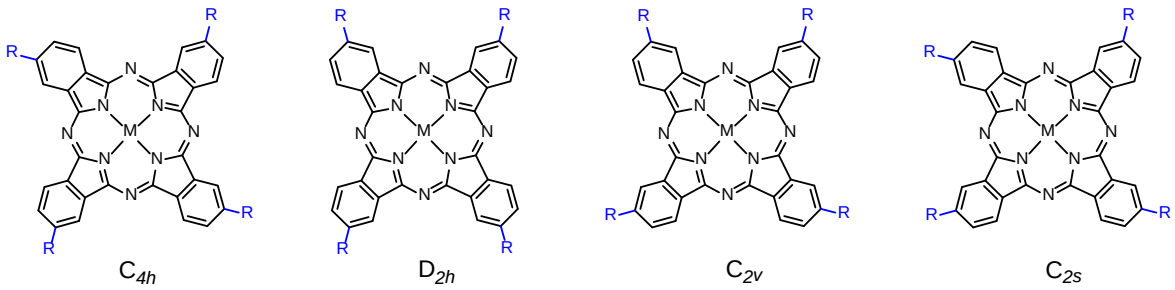

Figure 2.8. Structures of the constitutional isomers of 2(3)-tetrasubstitutedMPcs.

Synthesis of asymmetrically substituted phthalocyanines

Among the various strategies for the synthesis of monofunctionalized A3B-type Pcs, the approach relying on the statistical reaction of two different phthalonitrile or diiminoisoindoline precursors A and B in ratios of 3:1 equivalents (or a slight excess of A), appears to be the most commonly applied.[30,43]
However, the concomitant presence of different substituted Pcs, obtained in a statistical manner, represents the nuisance in this procedure (**Figure 2.9**).

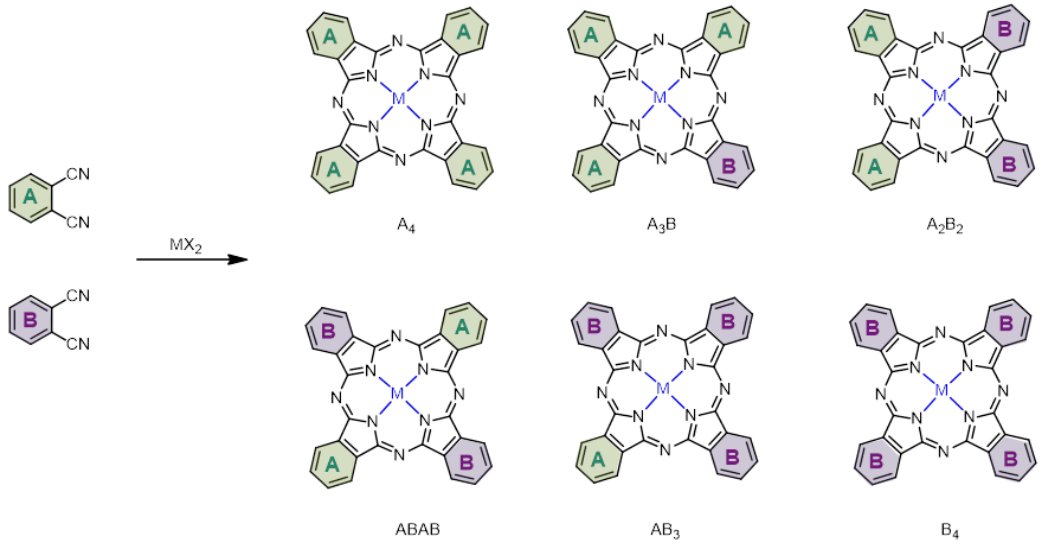

Figure 2.9. Representation of the set of Pc compounds obtained *via* statistical cyclotetramerization of two differently functionalized phthalonitriles, or diiminoisoindolines, A and B in a 1:1 ratio.

In order to maximize the yield of the unsymmetrically substituted derivative, different approaches have been reported;[44–46] however they will not be detailed here as this lies outside the scope of the present thesis.

Phthalocyanines as organic synthetic artificial photosystems

As previously discussed, a wide variety of donor-acceptor systems have been designed and employed to study and understand photo-induced electron and energy transfer reactions.

Among these different systems, those involving phthalocyanines have been widely used in recent years. The extensively π-conjugated systems of Pcs increase their electron donating ability and make them suitable candidates as light harvesting building blocks in the construction of artificial photosynthetic systems.

The great interest in Pcs as active material in biomimetic systems has led to the synthesis and the study of a wide range of covalent and non-covalent Pc-based D-A systems incorporating electroactive acceptor units of diverse nature and redox character such as fullerene, carbon nanotubes, graphene, perylenediimide, anthraquinone, ferrocene, ruthenium bypyridine complexes, flavin, porphyrin and others.

In recent years, several hetero-oligomeric Pc-Porf systems have been synthesized, thanks to the possibility to tune their redox properties. This allowed to employ them as donor or acceptor in multicomponent arrays. Their photophysical properties have been studied in solution and/or in solid state, revealing the occurrence, in the majority of the cases, of PET events. In such systems, the nature of the bridging spacer has been varied both from the electronic (i.e., conjugated/non-conjugated) and/or structural (i.e., rigid/flexible) point of view, with the aim of identifying to which extent these changes could influence the PET dynamics.[47]

To the best of our knowledge, no multicomponent systems based on corrole-phthalocyanine (Corr-Pc) conjugates have been described. Indeed, since Corr and Pc display complementary absorption with high absorption coefficients, they appear ideal light-harvesting partners as they can cover together a large range of the solar spectrum (UV, visible and near IR).

Herein, the different synthetic strategies that have been pursued so far for the preparation of D-A Corr-Pc nanostructure systems, have been resumed.

This Chapter is aimed to describe the synthesis of unreported electron-donor photosensitizers based on Corr-Pc framework and their study as photoactive systems. In these new conjugates, the donor and the acceptor units are connected either covalently (**Figure 2.10**,**a**) or by using supramolecular interactions (**Figure 2.10**,**b**).

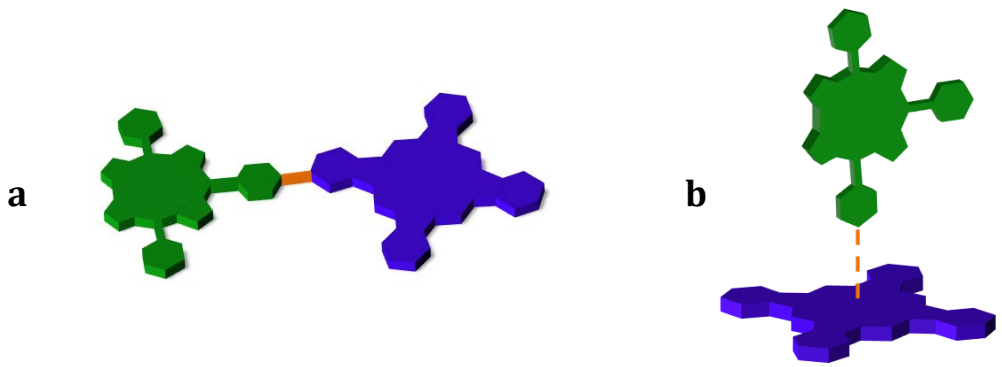

Figure 2.10. Schematic representation covalently (**a**)and supramolecular (**b**) conjugated Corr-Pc dyads.

Results and discussion

Pthalocyanine-Corrole covalent systems

During the last years several studies have been focused on the synthesis of metalloPor-Pc heteroarrays, in which the two chromophores are linked through the *meso* or *β*-position of the porphyrin (**Figure 2.11**).[48,49]

Given the lower symmetry of corrole, all the functionalizations on its *β*-positions lead to the potential formation of a huge number of different regioisomers.

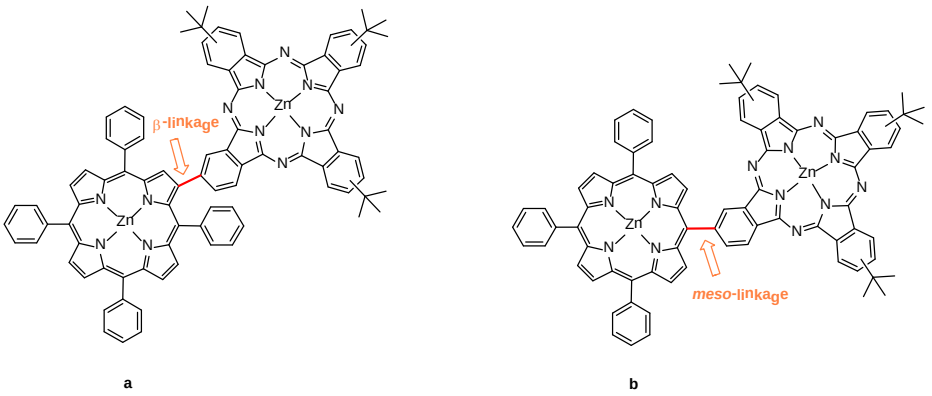

Figure 2.11. Molecular structure of (**a**): a *β*-linked ZnPor-ZnPc dyad, (**b**): *meso*-linked ZnPor-ZnPc dyad

We decided to connect the two units through the corrole *meso* position.

The choice to use a *meso*-linkage was twinfold: first, we wanted to exploit simple synthetic procedures avoiding low yielding steps and tricky purifications. Moreover, several works on porphyrins described in the literature bring clear evidence that *meso* carbons exhibit a larger electronic density than the *beta*-ones, thus enhancing faster rates of energy transfer. Moreover it was shown that in *meso*-substituted porphyrins the energy transfer proceeds via a through-bond mechanism, and in many cases an improvement of the efficiency was achieved by increasing the distance from the donor to the acceptor units. [50]

For this reason, we decided to prepare different (*meso*)Corr-ZnPc arrays, in which the Pc is linked to the 10-*meso* position of the corrole, using an ethynylphenyl spacer in between (**Figure 2.12**). This further spatial separation between the electron and the hole is expected to decreases the coupling between opposite charges and increases the

CS lifetime. To achieve this goal, we decided to prepare *trans*-A_2B corroles bearing an ethynylphenyl group in their position 10, and different A_3B phthalocyanine derivatives with a iodo functionality in one annulated benzene ring. This synthetic design allows the preparation of new dyads through a cross-coupling reaction. As already mentioned before, low oxidation potentials of corroles make them particularly suitable species in energy/electron transfer. Thus, at first, we prepared two different corroles with electron donor character covalently linked to a phthalocyanine with a strong electron-acceptor ability.

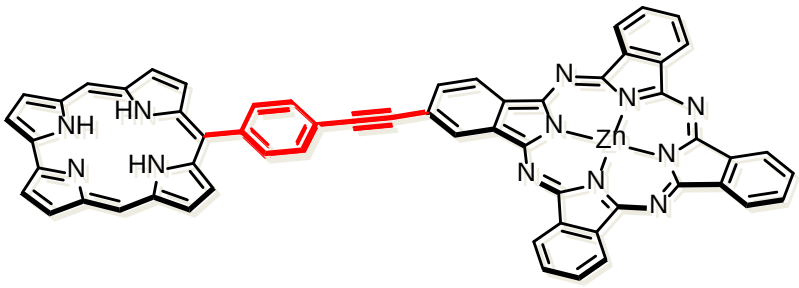

Figure 2.12. Schematic representation of a covalently conjugated Corr-Pc system, bearing an ethynylphenyl spacer in between

Synthesis of ethynylphenyl-substituted corroles

As already described in the introduction of the present thesis, a widely extended method to obtain *trans*-A_2B corroles relies on the synthesis starting from aldehydes and dipyrromethanes. We tackled the synthesis of DPM following a widely used procedure reported by Lindsey in 2003.[51] The procedure entails reaction of an aldehyde in a 100 molar excess of pyrrole as the solvent containing $InCl_3$as a mild Lewis acid at room temperature. We prepared two different types of DPMs, bearing a different numbers of methoxy moieties at the phenyl group, namely *p*-anisaldehyde and 3,4,5-trimethoxybenzaldehyde. All the desired dipyrromethanes were obtained with high yields (**Scheme 2.2**).

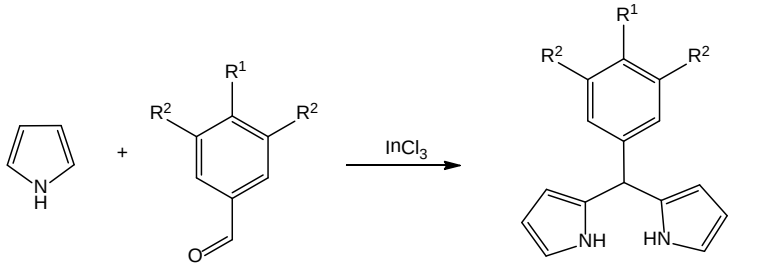

a) R^1= OCH_3, R^2= H
b) R^1= R^2= OCH_3

18a) R^1= OCH_3, R^2= H 60%
18b) R^1= R^2= OCH_3 42%

Scheme 2.2. Synthesis of dipyrromethanes **18a-b**

Subsequently, DPMs were reacted with trimethylsilylacetylene to achieve the desired *trans*-A_2B corroles. A specific approach reported in the literature, particularly efficient for aldehydes bearing electron-donating groups, was used. It involves the reaction of aldehydes with DPM in a water–methanol mixture in the presence of HCl, using chloranil as the oxidizing agent.[52] Further treatment with TBAF in dry CH_2Cl_2 removed the trimethylsilyl group affording corroles **20a-b** in high yields (**Scheme 2.3**).

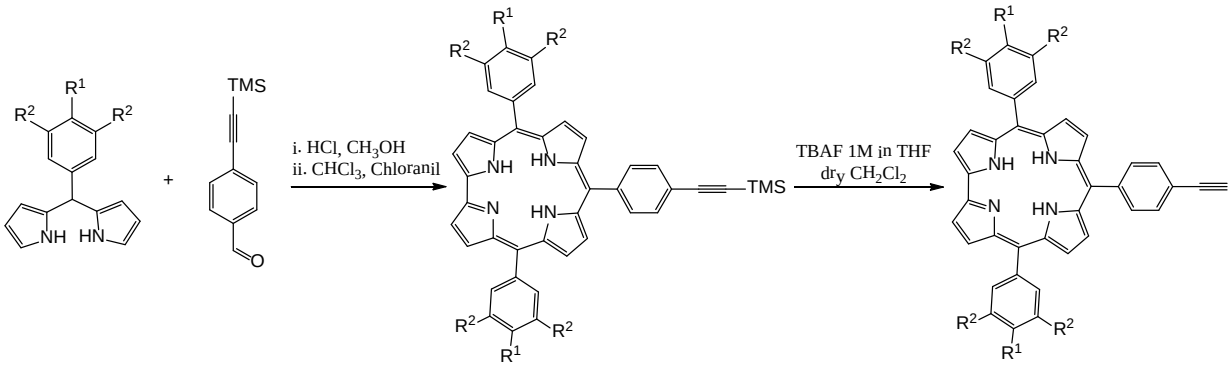

18a) R^1= OCH_3, R^2= H
18b) R^1= R^2= OCH_3

19a) R^1= OCH_3, R^2= H 12%
19b) R^1= R^2= OCH_3 17%

20a) R^1= OCH_3, R^2= H 57%
20b) R^1= R^2= OCH_3 70%

Scheme 2.3. Synthesis of corroles **20a-b**

The structure of **20a,b** was established on the basis of its spectroscopic features, namely, UV-Vis , ^{1}H-NMR and mass analyses. UV-vis comparison of **20a,b** is shown in Figure 2.13. Both compounds showed a pattern comparable, with the typical trend of free base aryl corroles.[53]

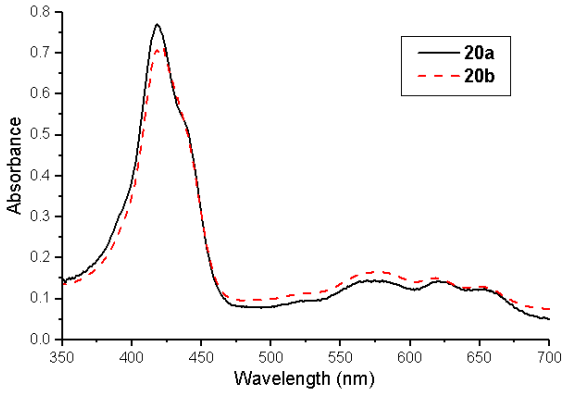

Figure 2.13. UV-vis spectra of **20a** (black solid line) and **20b** (red dashed line)

Comparing the ^{1}H-NMR spectra of the corroles (**Figure 2.14**), the main differences between the different substitution pattern can be easily spotted. In all cases the peak at δ 3.32-3.35 revealed the presence of an acetylene proton. A different set of doublets between 7.4 and 8.4 ppm indicate the presence of a different number of protons in *meso*-phenyl positions. Moreover, in the case of **20a**, it has been possible to observe a 6H integration signal in the aliphatic zone, which underscores the presence of a methoxy moiety in *para*-position of phenyl groups. Corrole **20b** shows two signals with different integration values in the same zone, which is consistent with the presence of a trimethoxy functionality.

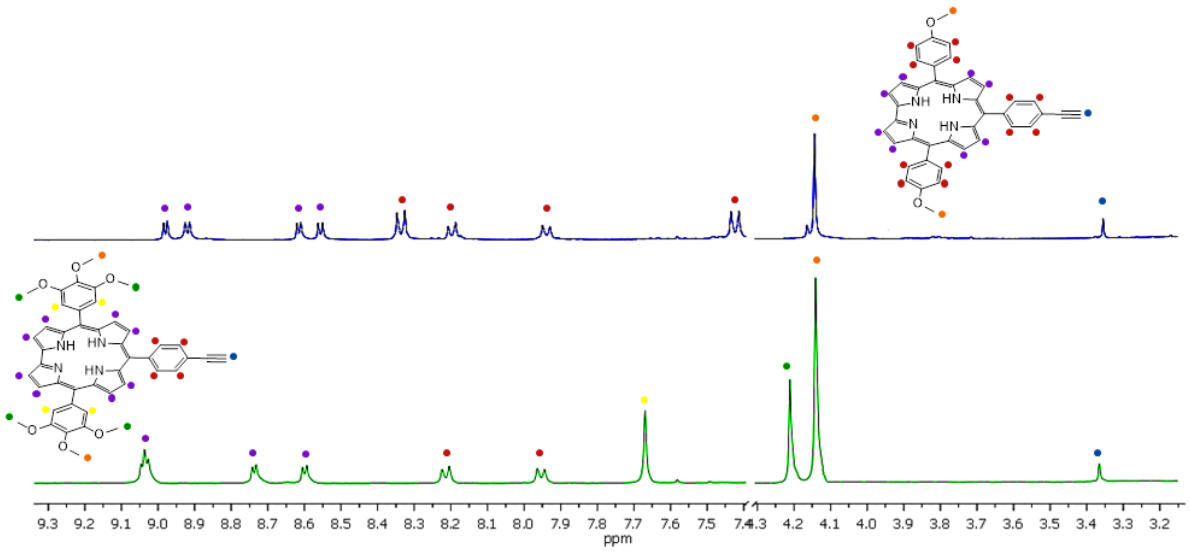

Figure 2.14. ^{1}H NMR spectra of **20a** and **20b**

Synthesis of monoiodo-phthalocyanine derivative

A widely extended method to obtain new phthalocyanine derivatives relies on the employment of palladium catalysed cross-coupling reactions (such as Suzuki, Heck, Stille, Sonogashira, etc.).[54] On this regard, an A_3B phthalocyanine, bearing electron withdrawing peripheral substituents (i.e. alkylsulfonyl groups) was prepared. Also, the incorporation of a reactive functional group (i.e. a iodo moiety) is necessary to perform the cross-coupling reaction with corrole terminal alkynyl group.

The selection of an alkylsulfonyl functionality as the electron withdrawing group has been twinfold: several Pc derivatives with strong electron withdrawing substituents such as, F, Cl, CN, CO_2R, $NO_2$and SO_2R groups, have been reported in the literature.[55] Among them, the alkylsulfonyl group plays an important role, not only promoting a considerable stabilization of the HOMO and the LUMO level of Pc, but also increasing the solubility due to the flexible alkyl chains. Therefore, the strong electron accepting 2-ethylhexylsulfonyl group was chosen in our research project to increase the solubility in the final material.

The preparation 4,5-bis(2-ethylhexylsulfonyl)phthalonitrile (**26**) represent a multistep synthesis. However, almost every step is high-yielding and in many cases it does not require chromatographic purification.

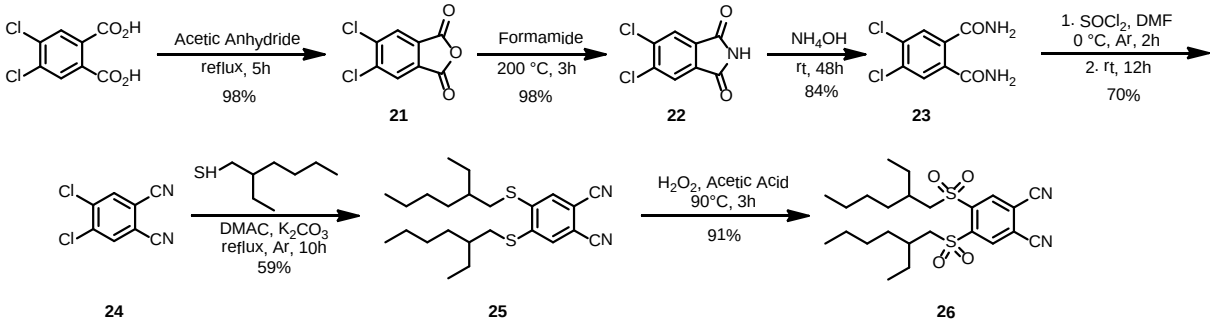

Scheme 2.4. Synthesis of 4,5-bis(2-ethylhexylsulfonyl)phthalonitrile (**26**)

The first step involved the quantitative dehydration of 4,5-dichlorophthalic acid yielding the dichlorophthalyc anhydride **21**,which was then reacted with formamide, affording 4,5-dichlorophthalimide (**22**) with 98% yield. Further treatment with ammonium hydroxide gave the analogous phthalamide (**23**). Its dehydratation with thionyl chloride led to 4,5-dichlorophthalonitrile (**24**).[56] Reaction of **24** with 2-ethylhexane-1-thiol and

the subsequent oxidation gave 4,5-bis(2-ethylhexylsulfonyl)phthalonitrile (**26**) in high 91 % yield (**Scheme 2.4**).[57,58]

Next, Zn-Phthalocyanine **27** was obtained by cyclotetramerization reaction of 4-iodophthalonitrile with the desired 1,2-dicyanobenzene derivative in a *o*-DCB/DMF refluxing mixture , in the presence of $Zn(OAc)_2$ as a template (**Scheme 2.5**), following a procedure already reported in the literature.[58]

To maximize the yield of the A_3B derivative, a 1.2:3 molar ratio (4-iodophthalonitrile/4,5-bis(2-ethylhexylsulfonyl)phthalonitrile) was employed, leading to a statistical mixture of Pcs that was then purified by column chromatography. The first fraction corresponded to traces of poli-halogenated species, followed by the desired compound mono-iodoPc **27a,** as the major component. Lastly**,** a discrete amount of the symmetric Pc was obtained. This reaction allowed to isolate Pcs **27a** in 23% yield.

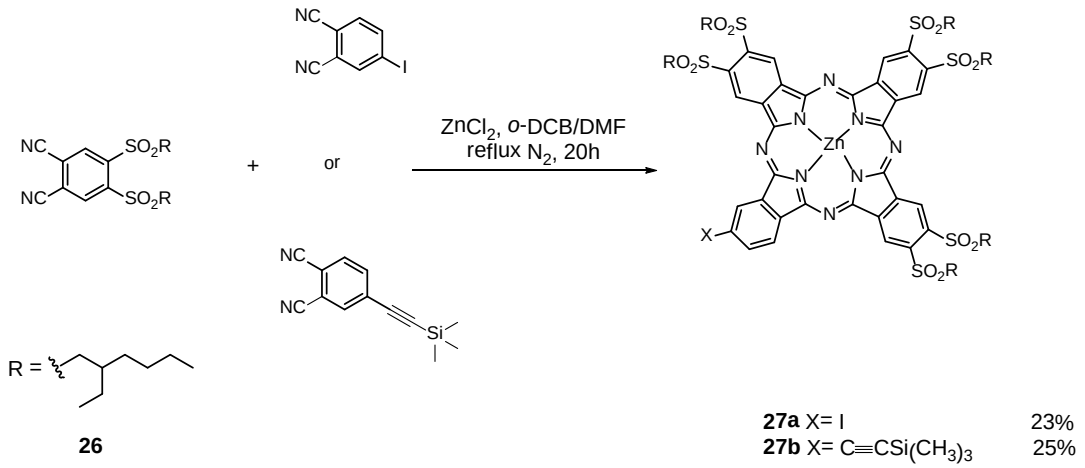

Scheme 2.5. Synthesis of Pcs **27a,b**

Assembly of Corr-ZnPc dyads

A Sonogashira cross-coupling reaction was identified as the means to form the link between Corr and ZnPc. We used the copper-free methodology to prevent metal insertion in the corrole ring during the reaction.

With a view to create different D-A arrays, and to investigate the generality of this reaction and the relative influence of the different number of methoxy moieties on the product pattern, two new covalent dyads were prepared, as depicted in **Scheme 2.6**.

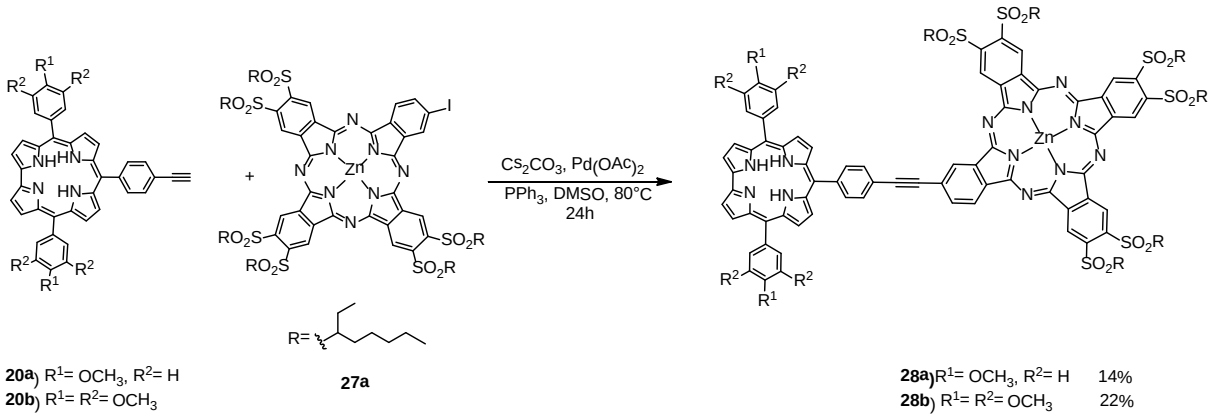

Scheme 2.6. Synthesis of Dyads **28a** and **28b**

The reaction has been carried out in dry DMSO in presence of Cs_2CO_3, $Pd(OAc)_2$ and triphenylphosphine, with a Corr/Pc 1:1.2 molar ratio. The reaction mixture was stirred in argon atmosphere at 80 °C for 20 hours. When no more corrole derivative was detected by TLC analysis, the reaction was stopped and purified on column chromatography. ^{1}H NMR analysis of both dyads was not able to provide decisive information in structural identification, since all the signals in the aromatic range showed a strong line broadening. This can be explained by the high aggregation tendency of Pcs derivatives. Nonetheless, in both cases we were able to observe a peak in MALDI-TOF, which corresponds to the desired dyads. Mass spectra with isotopic distribution of dyads **28a** and **28b** can be found in the appendix section.

Electrochemical Studies

Electrochemical measurements were employed to determine the energies of their frontier orbitals – HOMO and LUMO – and the band gap between them corresponding to the energy of the first singlet excited state. These are crucial parameters for the study of photoinduced transfer processes.[59]

The measurements were carried out using a three electrode cell in N_2 saturated CH_2Cl_2 solution containing 0.1 M tetrabutylammonium perchlorate (TBAP) as supporting electrolyte. A standard calomel electrode was used (SCE) as the reference electrode, a platinum wire as the auxiliary electrode and a platinum disk (1 mm diameter) as working electrode. All data are represented vs SCE.

The electrochemical properties of derivatives **28a,b** were investigated by cyclic voltammetry (CV) and compared with the redox values of their references, that are, the monomeric Corr and Pc.

Due to the great tendency of terminal alkynes to polymerize, we decided to carry out CV analyses on corroles **19a,b**. The presence of a trimethylsilyl group should protect the triple bond thus preventing side reactions during the measurement. Regarding the Pc, is well known that a halide functionality strongly influences redox properties of the macrocycle. In order to deepen electrochemical properties of the single Pc unit, we decided to use a phthalocyanine bearing a trimethylsilylacetylene group (**27b**), in lieu of the iodide moiety. This could also provide to the Pc a chemical environment similar to that in dyads. Their corresponding redox potentials are summarized in **Table 2.1**.

Figure 2.15 shows CV of the building blocks. Cyclic voltammogram of corrole **19a** presents a reversible first oxidation process and a successive redox event at more positive potentials, which is electrochemically quasi-reversible. Compound **19b** shows an irreversible first oxidation potential, at more positive values if compared with **19a**. Two other oxidation peaks exhibit a reversible and quasi-reversible behaviour. As expected, either one of **19a,b** display a reduction peak at low negative potentials. This represents an additional confirmation of the fact that corroles could represent a suitable donor system. In the case of Pc, the first oxidation wave is shifted towards higher potentials if compared with corrole counterparts. Moreover, two reversible reduction peaks were evident (**Figure 2.15**).

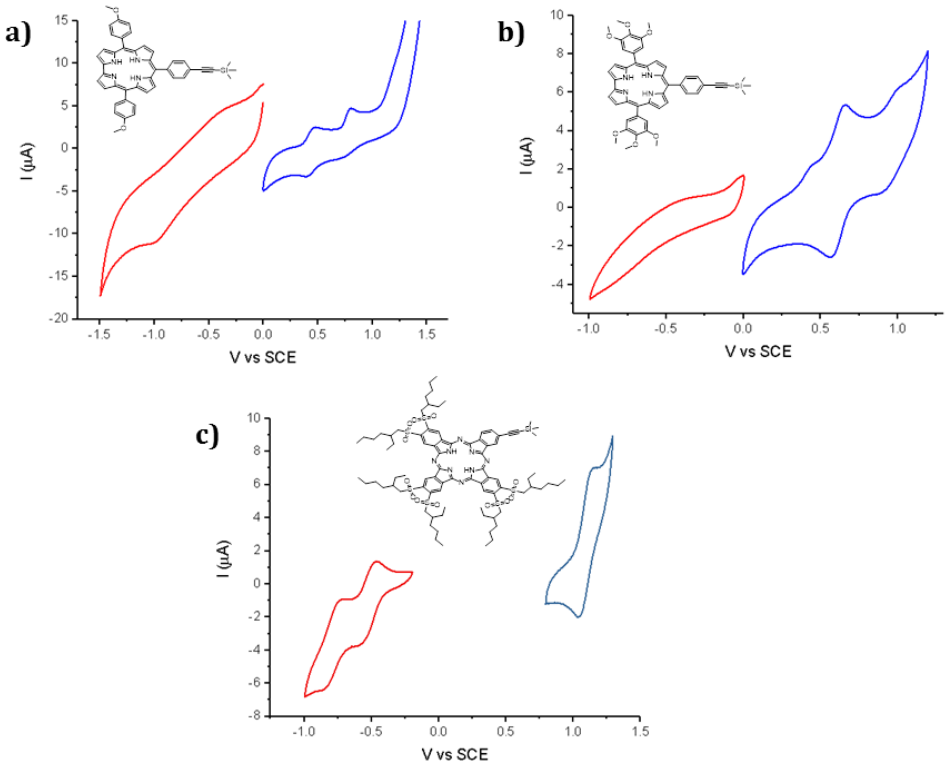

Figure 2.15. Cyclic voltammograms of **19a** (**a**), **19b** (**b**) and **27b** (**c**) in CH_2Cl_2 (0.1M TBAP) at room temperature, using a Pt electrode and measuring at 100mV s^{-1}. Potentials vs SCE

To inspect the nature of the interactions between phthalocyanine and corrole, CV measurements of dyads **28a**,**b** were also, performed, as shown in **Figure 2.16**.

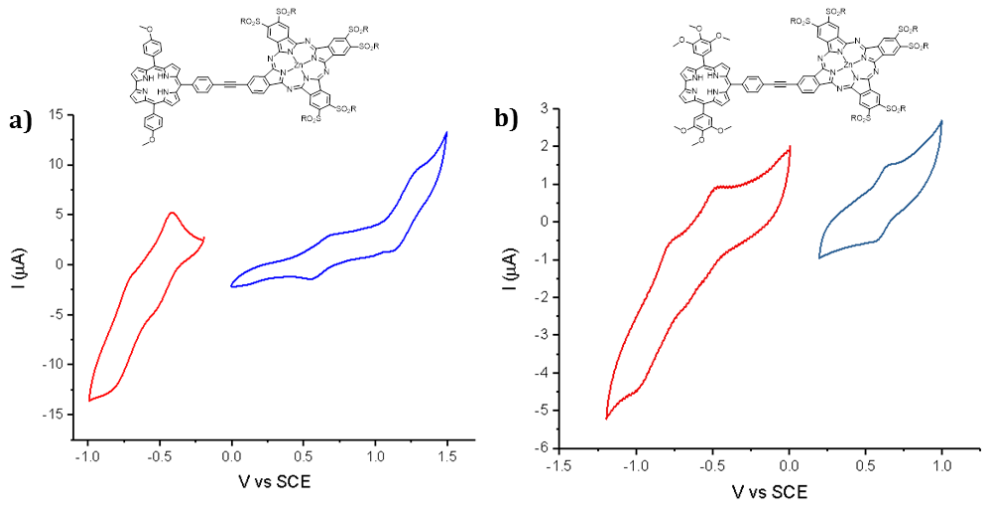

Figure 2.16. Cyclic voltammograms of **28a** (**a**) and **28b** (**b**) in CH_2Cl_2 (0.1M TBAP) at room temperature, using a Pt electrode and measuring at 100mV s^{-1}. Potentials vs SCE

CVs of both dyads exhibit shifts of redox potential, if compared with the corresponding monomers. **28b** shows more evident variation in the number of peaks and in their values. Indeed, only one oxidation peak, and a severe shift in all other peaks is observed. This could be ascribable to a ground state interaction between the two chromophores.

The corresponding data are summarized in **Table 2.1**.

Table 2.1. Redox potentials of dyads **28a,b** and their reference compounds, Ep *vs* SCE, V.

Compound		E_{red2}	E_{red1}	E_{ox1}	E_{ox2}	E_{ox3}
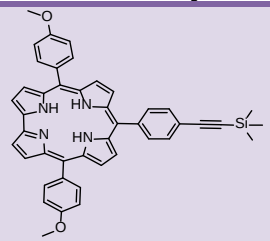	**19a**	-	-1.01[a]	0.48	0.81	-
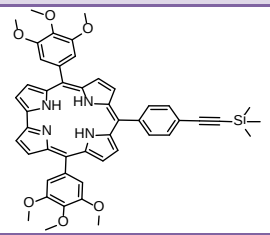	**19b**	-	-	0.44[a]	0.66	0.99
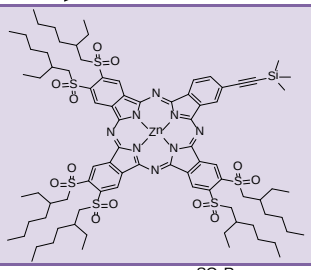	**27b**	-0.86	-0.58	1.14	-	-
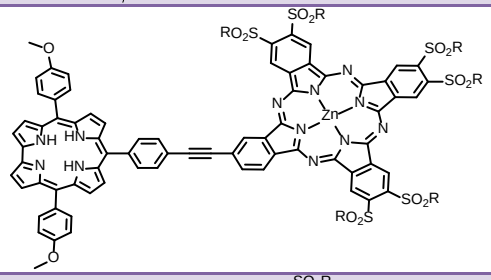	**28a**	-0.83	-0.52	0.68	1.28	-
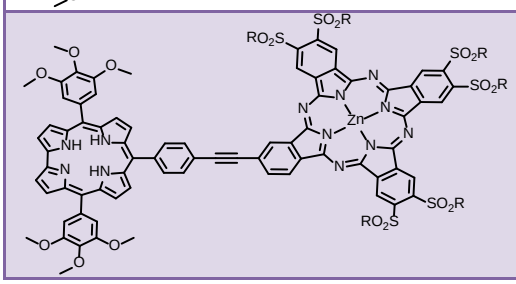	**28b**	-1.01	-0.66	0.64	-	-

[a] irreversible

Calculation of HOMO-LUMO levels

The energy of the LUMO can be approximated by the electron affinity, which is the energy change when an electron is accepted by an atom or molecule in the gaseous state to form an anion. In a similar way, the energy of the HOMO can be connected to the ionization potential, which is the minimum energy required to remove an electron from an isolated atom or molecule in the gas phase. Cyclic voltammetry (CV) constitutes a means of obtaining the HOMO and LUMO levels starting from oxidation and reduction potentials.

While the HOMO/LUMO energies are scaled in vacuum, the reduction/oxidation potentials are measured in solution. This implies a series of unavoidable approximations that must be taken into account when comparing these different values.

Cyclic voltammetry provided useful data to determine energy level values. In order to scale the obtained values in vacuum, we used the following approximation:[60,61]

$$E_{HOMO/LUMO} = -4.68 - E^{1}_{ox/red}\ (vs\ \mathbf{SCE})\ (\mathbf{eV}) \qquad \textbf{(Eq. 2)}$$

Using equation 2, HOMO and LUMO energy values of both dyads **28a,b** were determined. This conversion *vs* vacuum was mandatory in order to compare the values obtained by CV with the ones obtained by computational analysis in vacuum.

Table 2.2. Experimental and theoretical HOMO-LUMO energy levels data (in eV) of dyads **28a** and **28b**.

Dyad	Experimental data			Computational data		
	E_{LUMO} (eV)	E_{HOMO} (eV)	E_{gap} (eV)	E_{LUMO} (eV)	E_{HOMO} (eV)	E_{gap} (eV)
28a	-4.16	-5.36	1.2	-4.15	-4.97	0.82
28b	-4.68	-5.32	1.3	-4.16	-5.02	0.86

DFT B3LYP/3-21G(*) Calculations

To visualize the geometry and electronic structure of the phthalocyanine-corrole dyads, computational studies were performed using JAGUAR applying density functional theory (DFT) at the B3LYP level in conjunction with the 6-31G (d,p) basis set. Both geometry optimization and energy level calculations were performed in vacuum. As expected, the corrole unit attained a twisted configuration in the optimized structures. The distances of "center to center", calculated from the geometrical structure of **28a** and **28b** are, in both cases, 18.5 Å, with the linker having 8,4 Å length (**Figure 2.17**).

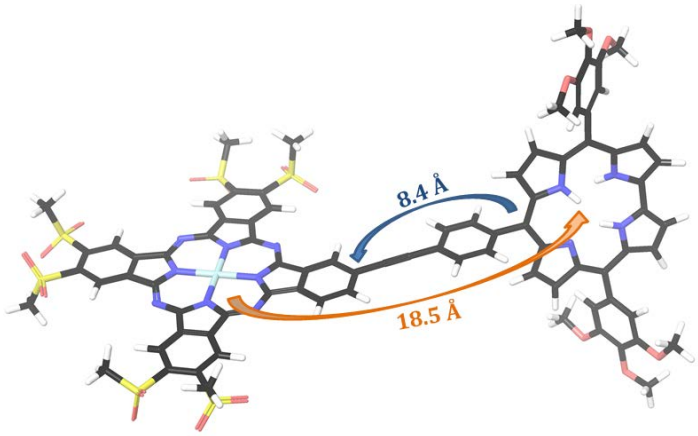

Figure 2.17. Optimized geometry of **28b** showing linker and "center to center" distances (alkyl chains omitted for clarity)

All the data obtained about the HOMO-LUMO energy levels are summarized in **Table 2.2** and are shown schematically in **Figure 2.18**and **Figure 2.19**. For both dyads **28a** and **28b** the HOMO (5.02 and 4.97 eV, respectively) and the HOMO -1 locate on the corrole moiety, while HOMO -2 resides almost entirely on the phthalocyanine framework and in the ethynylphenyl spacer, according to what observed in the cyclic voltammetry analysis. LUMO orbitals are totally located on the phthalocyanine p-system. Moreover, the ethynylphenyl spacer does not contribute to the HOMO or LUMO energy levels, suggesting no considerable interaction between the donor and acceptor entities in the ground state.

Thus, the calculated distribution of MO manifested the proposed intramolecular electron transfer from the excited corrole to the phthalocyanine in gaining of charge-separated state corrole$^{\bullet+}$ - phthalocyanine$^{\bullet-}$.

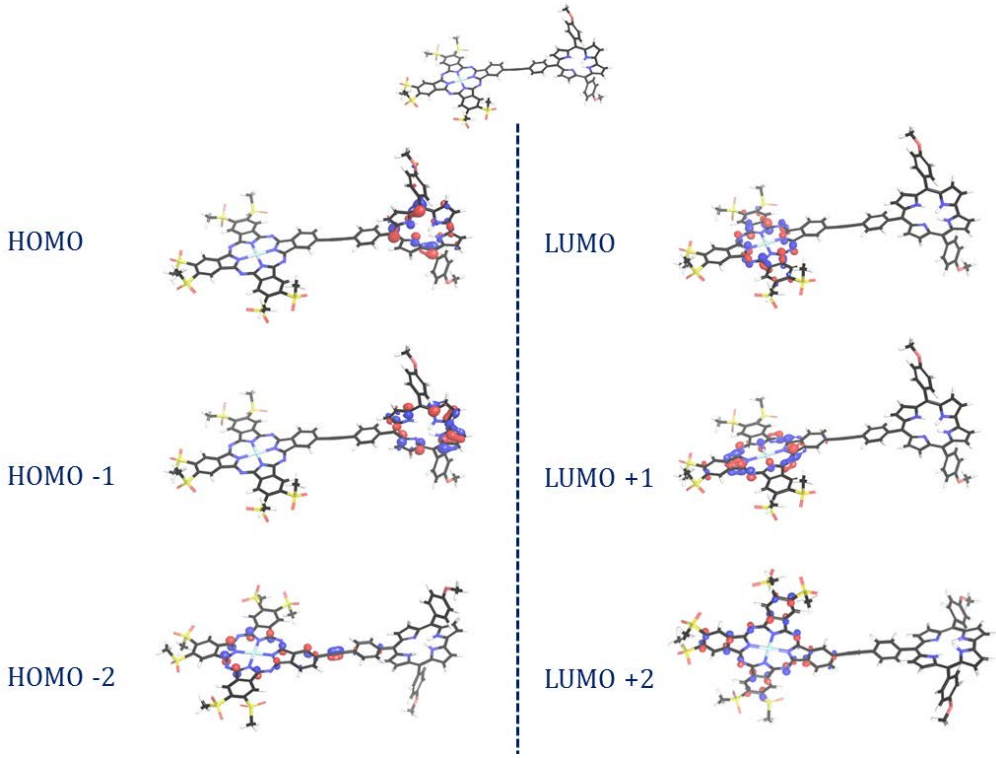

Figure 2.18. B3LYP/6-31G(*)-calculated frontier HOMO and LUMO of the corrole-phthalocyanine dyad **28a**. The red and blue colours in indicate the negative and positive electrostatic potentials.

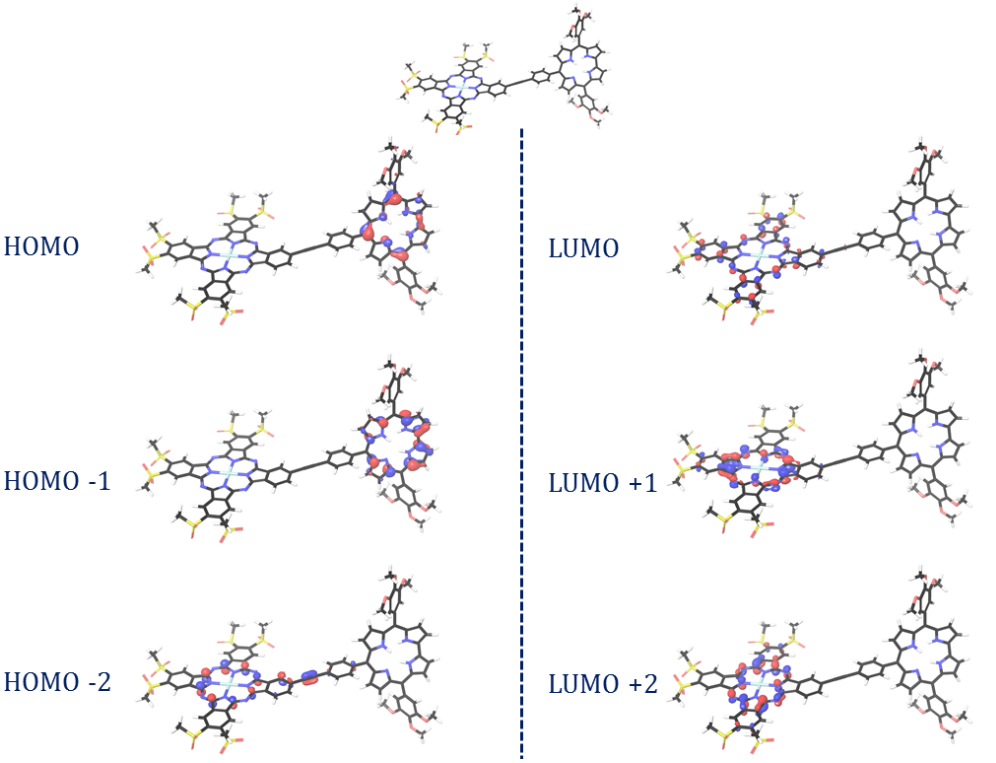

Figure 2.19. B3LYP/6-31G(*)-calculated frontier HOMO and LUMO of the corrole-phthalocyanine dyad **28b**. The red and blue colours in indicate the negative and positive electrostatic potentials.

Photophysical studies

The photophysical studies of this chapter were carried out during a predoctoral stay in the laboratory of Prof. Dirk Guldi at the Friederich-Alexander University in Erlangen, Germany.

Steady State Absorption and Emission Spectroscopy

To elucidate the electronic interactions between the different photoactive components, the model compounds (*meso*-tetraphenylporphyrinato)zinc(II) (ZnTPP) and *meso*-tetraphenylporphyrin (H_2TPP), were compared with those of compounds **19a,b**, and **27b.**

Figure 2.20 shows UV/vis spectra of dyads **28a,b** in THF compared to the spectra of the monomeric Corr and Pc. Both dyads **28a** and **28b** display similar absorption spectra, with characteristic absorptions of the individual macrocyclic components, namely strong absorptions assigned to the corrole and phthalocyanine Soret and Q bands. The small red shift (ca. 3 nm) experienced by the phthalocyanine Q-band in dyad **28a** suggests that the electronic interaction between the two chromophores in the ground state is weak or negligible. The same trend was observed in the UV/vis spectrum of **28b**.

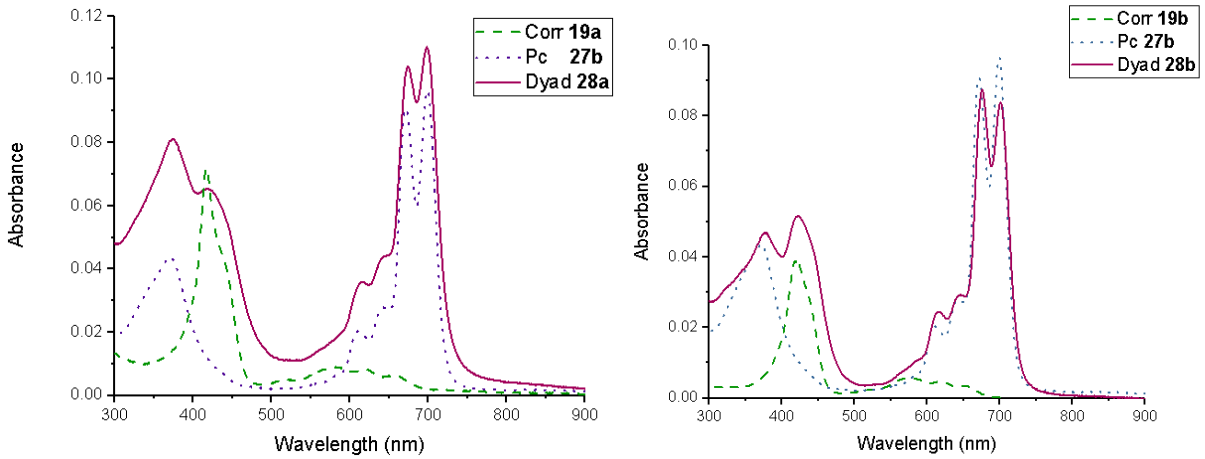

Figure 2.20. UV/vis spectrum of dyad **28a** (left) and **28b** (right) in THF, compared to the ones of the Corr-Pc building blocks

Insights into the excited-state interactions within the Corr-Zn(II)Pc ensembles were obtained from steady-state fluorescence measurements in chlorobenzene, THF and toluene. Fluorescence of Zn(II)Pc derivative (**27b**), was monitored upon photoexcitation at 676 nm, that correspond to its Q band absorption maximum. Corroles **19a** and **19b**, were studied using a 450 nm excitation wavelength. Dyads **28a,b** were monitored upon photoexcitation at either 450 or 676 nm, in order to see if a communication between the excited states of Corr and Pc is present, thus confirming an energy transfer process.

Both corroles exhibited emission maxima at 676 nm, 38 nm blue shifted if compared with the emission spectrum of phthalocyanine **27b** (**Figure 2.21**). Phthalocyanine derivative exhibited a higher fluorescence quantum yields than corroles in apolar or slightly polar solvents. The situation changes in polar solvents as THF, when the relative quantum yield of **27b** decreases, while that of corroles rises. **Figure 2.21** shows a comparison of dyads emission spectra at 450 and 676 nm. In both dyads, upon excitation whether at 460 or 676 nm, only one peak, corresponding to phthalocyanine emission, is evident. On the basis of the fluorescence spectra, it can be deduced that an energy transfer from Corr to Pc occurred. In this process, upon photoexcitation at 450 nm, corrole subunit rises to the excited state, and its energy is transferred to the phthalocyanine counterpart. As result, corrole is left in the ground state, as shown by the absence of any florescence signal, while excited phthalocyanine rises to the excited state, thus relaxing through radiative decay (i.e. fluorescence).

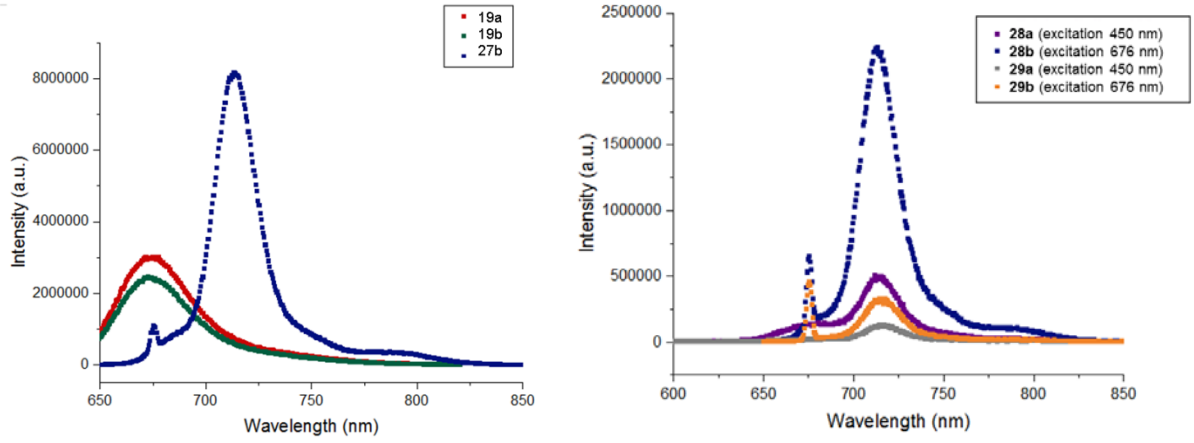

Figure 2.21. Left: emission spectra of corroles **19a,b** (excitation wavelength: 450 nm), of phthalocyanine **27b** (excitation wavelength: 676 nm). Right: emission spectra of dyads **28a,b** at two different excitation wavelength (450, 676 nm)

Fluorescence quantum yields (Φ_F) in different solvents are summarized in **Table 2.3**.

Table 2.3. Fluorescence quantum yields (Φ_F) of dyads **28a,b** and their reference compounds in THF, PhCl and toulene

Compound	Φ_F (toluene)	Φ_F (PhCl)	Φ_F (THF)
19a	13%[a]	18%[a]	17%[a]
19b	11%[a]	21%[a]	20%[a]
27b	19%[b]	29%[b]	16%[b]
28a	0.3%[a] 0.8%[b]	2.8%[a] 8%[b]	2.7%[a] 7%[b]
28b	1.9%[a] 6.9%[b]	0.6%[a] 1.5%[b]	0.6%[a] 2.6%[b]

Excitation: [a] 450 nm [b] 676 nm

Transient Absorption spectroscopy

At this stage, preliminary studies using transient absorption spectroscopy were performed. In transient absorption spectroscopy, a fraction of the molecules is promoted to an electronically excited state by means of an excitation (or pump) pulse. Differential absorption spectra are then calculated, i.e., the absorption spectra of the excited sample minus the absorption spectrum of the sample in the ground state (ΔAbs). ΔAbs spectra contain contributions from various processes and allow investigating the generation of ultra-short-lived species.[62] Once the sample is excited with a femtosecond pulse, differential vis-NIR spectra are recorded at different delay times, from 2 ps up to 7500 ps, in order to observe the temporal evolution of excited states.

First, we performed transient absorption measurements of corrole and phthalocyanine, in order to see their behaviour toward photoexcitation and obtain information for the study of our dyads. All measurements were performed in THF with a concentration of dye of $5 \cdot 10^{-6}$ M.

Right after conclusion of the 150 fs laser pulse (λ_{ex} = 676 nm), reference Pc **27b** showed the typical transient absorption features of ZnPc,[57] with transient maxima at 517, 592, 629 and 839 nm accompanied by ground state bleaching around 672 and 701 nm, which indicated formation of the ZnPc singlet excited state (^{1}***Pc**). This state deactivated *via*

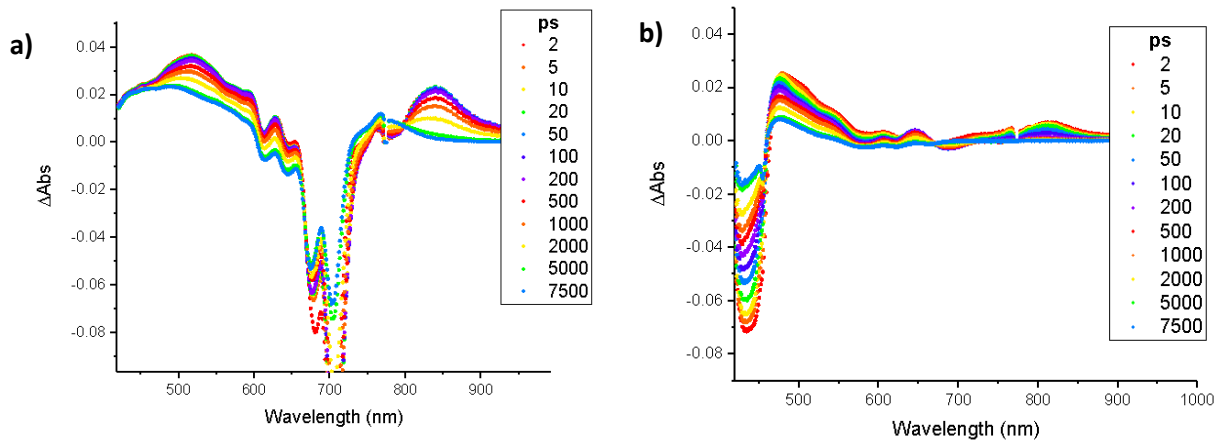

Figure 2.22. Transient absorption spectra of ZnPc **27b** upon 676 nm photoexcitation (a) and Corr **19b** upon 450 nm photoexcitation (b) in THF .

intersystem crossing within ~2.5 ns to the lower lying triplet excited state ^{3}***Pc**, which exhibited a transient maximum at 767 nm (**Figure 2.22,a**).

In order to analyse the excited states features of corroles toward photoexcitation, transient absorption measurement was conducted only on corrole **19b**.

Upon excitation of derivative **19b** with a 450 nm laser pulse, differential absorption peaks arose, at 479, 607 and 812 nm, which are attributed to the population of the singlet excited state of corrole.[63] Moreover, a bleaching at 433 nm was observed. The singlet excited state features underwent quantitative intersystem crossing with a lifetime of ~ 65 ps to afford the triplet manifold with a characteristic maximum at 645 nm (**Figure 2.22,b**).

On this basis, dyads **28a** and **28b** were studied, using both 450 and 676 nm laser pulses, to selectively excite corrole (450 nm) or phthalocyanine (676 nm) macrocycles. When exciting **28a** at 450 nm, new intense peaks appeared, namely at 501, 592 and 758 nm. The latter value is not clearly visible because of instrument limitations. A bleach at 438 and 680 nm was also present (**Figure 2.23,a**).

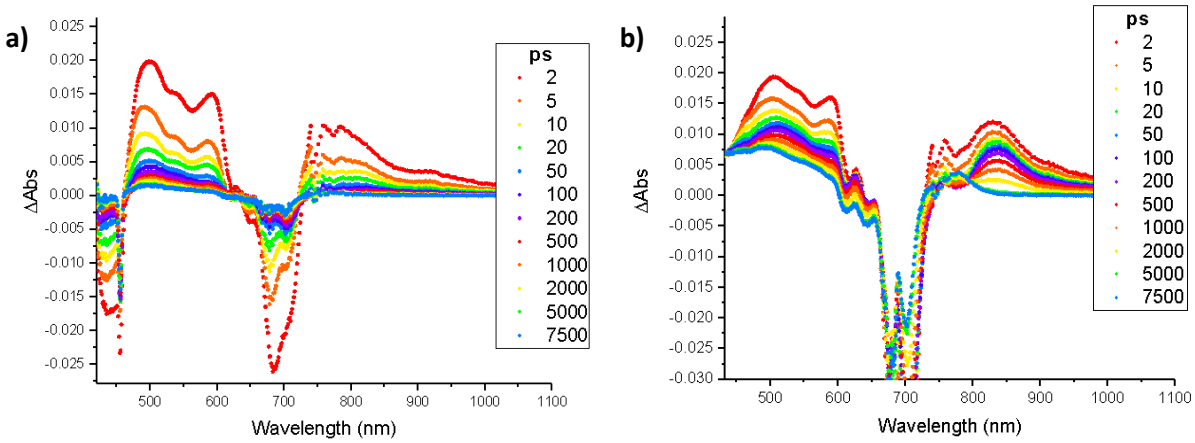

Figure 2.23. Transient absorption spectra of Dyad **28a** upon 450 nm photoexcitation (**a**) and upon 676 nm photoexcitation (**b**) in THF.

After a 676 nm photoexcitation, dyad **28a** showed similar transient maxima, already observed in the previous case, exciting at 450 nm. Nevertheless, both peaks at 501 and 757 nm exhibited lower relative intensities if compared with the peak observed at 592 nm. Furthermore, the associated states have a shorter lifetime, as it can be seen in **Figure 2.23,b**. A ground state bleaching minimizing at 676 and 702 nm was present, accompanied by the peak corresponding to phthalocyanine triplet state ^{3}***Pc at** 770nm**.**

In the case of dyad **28b**, both excitation at 450 and 676 nm resulted in a similar spectral behaviour. Photoexcitation of THF solution of **20b** with a 450 nm laser pulse (**Figure 2.24,a**) led to different absorption changes that include strong transient maxima at 495, 592 and around 757 nm, as well as transient minima at 433 and 684 nm. Likewise, the differential absorption spectra of **20b** upon 676 laser irradiation revealed transient maxima at 503, 588 and around 757 nm, and transient minima at 683 and 705 nm.

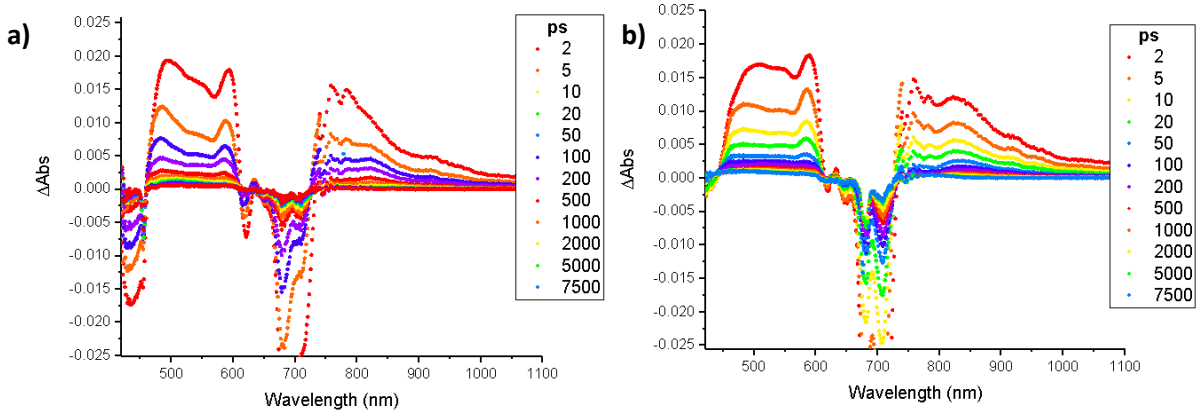

Figure 2.24. Transient absorption spectra of Dyad **28b** upon 450 nm photoexcitation (**a**) and upon 676 nm photoexcitation (**b**) in THF.

To assist in the interpretation of the excited-state spectral features of the two dyads, we deemed necessary to perform spectroelectrochemical experiments. To this end, the formation of the one-oxidized form of corrole **19b** and the one-electron reduced form of phthalocyanine **27b** were monitored upon spectroelectrochemical oxidation and reduction in THF.

In the case of corrole **19b**, a growing potential up to 0.3 V was applied, recording at the same time absorption spectra of the solution. The differential absorption spectrum of **19b** upon spectroelectrochemical oxidation at 0.3 V displayed a broad peak centred at 495 nm, and other two maxima at 612 and 693 nm (**Figure 2.25,a**). These features are in keeping with the general behaviour of corroles upon oxidation. It was found that corrole cations have a distinct, red shifted spectrum with respect to the ground state.[53,64]

2

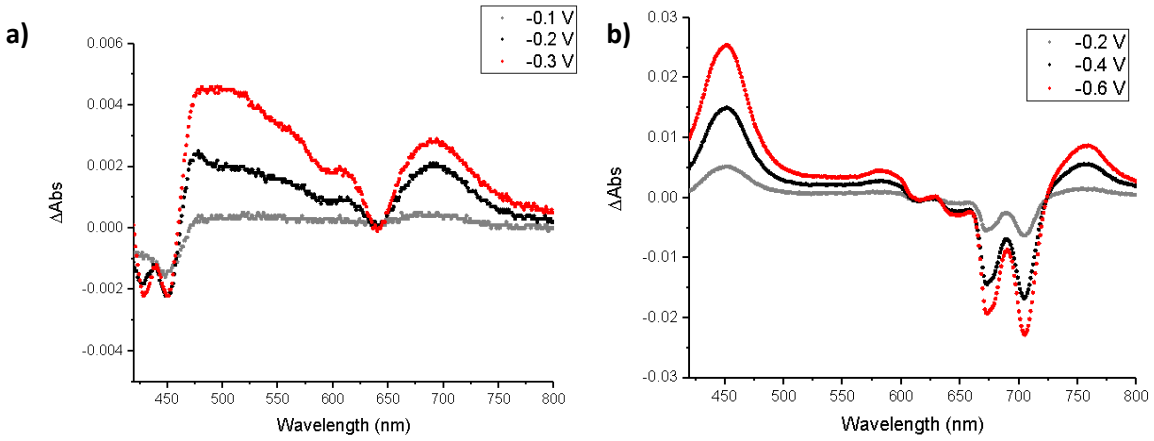

Figure 2.25. Differential absorption spectra obtained upon **a**) electrochemical oxidation of Corr **19b** (applying a growing bias up to 0.3 V) and **b**) electrochemical reduction of Pc **27b** (applying a decreasing bias up to -0.6 V).

On the other hand, spectroelectrochemistry of phthalocyanine **27b** under reductive conditions revealed different sets of maxima at 450, 585 and 757 nm, as well as minima at 673 and 705 nm (**Figure 2.25,b**).

From a comparison of spectra obtained from the spectroelectrochemical reduction of Pc with those obtained from transient absorption analyses of **28a** and **28b**, it is possible to assign the peak at 757 nm to the radical anion of phthalocyanine. Similarly, the features of the corrole **19b** radical cation species could also be identified by comparing the spectra obtained upon spectroelectrochemical oxidation with those of the two dyads. The peak with maximum at 501 nm (in the case of **28a**) and 495 nm (in the case of **28b**) can be ascribed to the formation of the one-electron oxidized form of the corrole counterpart.

Further studies are needed to assess more precisely the energetic pathways of charge separation and charge recombination, as well as their lifetimes. This represents an ongoing study in our laboratories.

Pthalocyanine-Corrole supramolecular systems

Synthesis of the precursors

In this study, a corrole derivative, bearing electron donating group, was prepared and connected to an electron accepting Zn(II) phthalocyanine by metal-ligand, axial coordination of the pyridyl moiety of the corrole molecule to the zinc metal centre in the Pc macrocycle (**Scheme 2.7**).

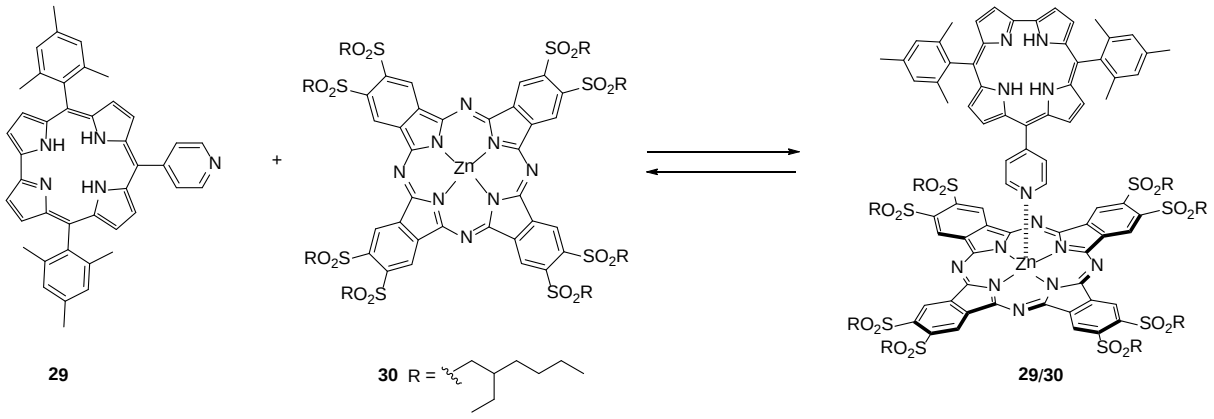

Scheme 2.7. Metal-ligand, axial coordination of a *N*-(*p*-pyridyl)-substituted corrole **29** to Zn(II)Pc **30** leading to supramolecular complexe **29/30**

As already discussed in the introduction of the present thesis, a widely extended method to obtain *trans*-A_2B corroles derivatives relies on the synthesis of the desired dypirromethane and letting it react with a suitable aldehyde.

Starting from mesitylbenzaldehyde, the analogue dipyrromethane was synthesized, using the method already reported in the literature.[51]

Moreover, 10-*meso*-pyridyl-substituted corrole **29** was obtained following an already reported procedure, aimed to the synthesis of *trans*-A_2B-corroles bearing substituents with basic nitrogen atoms at *meso* positions. The corrole formation reaction involves the acid-catalyzed condensation of a dipyrromethane (DPM) and an aldehyde followed by oxidation with DDQ.[65] Corrole **29** was obtained with 18% yield.

Octakis(2-ethylhexylsulfonyl) Zn(II)Pc **30** was prepared as already reported in the literature.[57] Cyclotetramerization reaction of 4,5-bis(2-ethylhexylsulfonyl)phthalonitrile **26** in a *o*-DCB/DMF mixture at 145 °C in the presence of zinc(II) acetate led to the formation of **30** in 25% yield.

Compounds **29** and **30** were characterized by UV-vis, ^{1}H NMR and mass analyses.

UV-vis spectra of the two species are shown in **Figure 2.26**. In the case of **29**, a splitted Soret band was evident, in concordance with data already reported in the literature.[65] ZnPc **30** showed only one sharp Q band, due to the high symmetry of the complex, as already reported.[66]

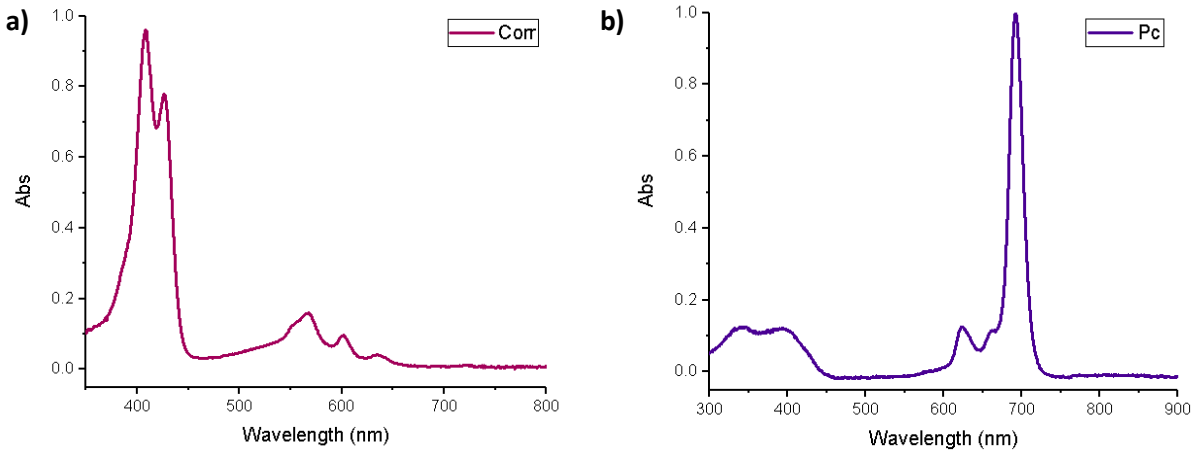

Figure 2.26. Normalized UV-vis spectra of a) Corr **29**, b)Pc **30**

With the aim of studying the coordination interaction between pyridine in the corrole and zinc in the phthalocyanine macrocycle, NMR and photophysical studies were performed.

Host-guest interactions

NMR studies

We decided to further study the Corr-ZnPc interaction by performing ^{1}H NMR titrations. The binding of a guest G to a host H, generally causes a change in the environment of the nuclear spins on the host, the guest, or both. Since a change in environment usually results in a change in chemical shift, ligand binding corresponds to the chemical exchange between two environments. In dealing with the study of ligand binding kinetics, it is worth mentioning the term of "chemical exchange". Chemical exchange refers to a dynamic process that exposes a NMR probe to at least two distinct chemical environments, or states, in a time-dependent manner.

This dynamic process leads to an interconversion between two states, i.e. host-free (H) and host-bound (HG) states of a species. For NMR, the two states have resonance frequencies δ_A and δ_B and chemical shift difference $\Delta\delta=|\delta_A-\delta_B|$ (**Figure 2.27**). Importantly, the appearance of different peaks in the NMR spectrum depends on the population of each state, H and HG, and the relative values of the exchange rate constant k_{ex} and the chemical shift difference $\Delta\delta$. k_{ex} quantifies the average number of stochastic exchange events per unit time and is therefore expressed in s^{-1}. Knowing that, k_{ex} and $\Delta\delta$ can be compared directly, since they have the same unit of measurement.[67,68]

NMR spectra affected by chemical exchange are segregated into three distinct exchange regimes:[69]

- **Slow exchange** ($k_{ex} \ll |\Delta\delta|$): if the equilibrium is slower than ^{1}H-NMR spectroscopy timescale, then each spectrum will show the signals of the free host and guest, as well as the signals of all the complexes formed. As the complexation process advances with the titration, we expect to observe a change in the proportion of the integrals of the different species present in the reaction media.
- **Intermediate Exchange** ($k_{ex} \approx |\Delta\delta|$): in the intermediate exchange time regime, the resonance line becomes very broad as the ligand is added and it slowly migrates from the unliganded position towards the position of the fully liganded host. Under some conditions, the line can disappear completely during the titration.

- **Fast Exchange** ($k_{ex} \gg |\Delta\delta|$): In the case of fast exchange, the exchange is sufficiently fast that the chemical shift of the observed line, δ, is essentially equal to the weighted average of the initial and final states.

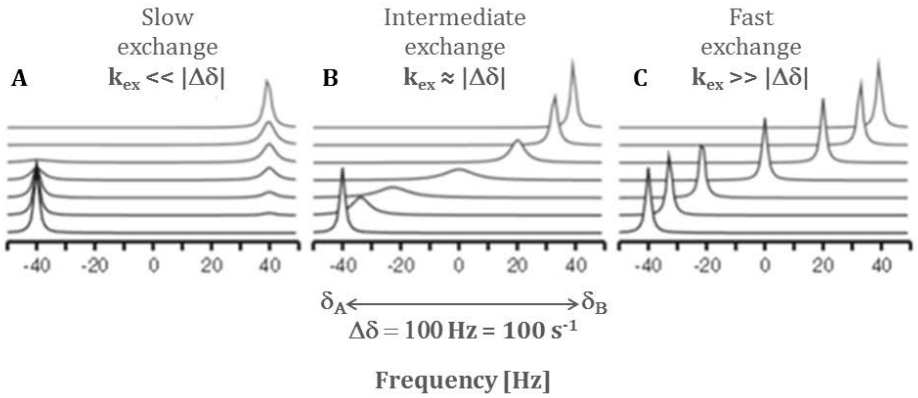

Figure 2.27. Effect of slow (**A**), intermediate (**B**), or fast (**C**) exchange on the spectrum of a resonance whose frequency is changed as a result of ligand binding.

With the aim of proving the formation of the supramolecular complex and to determine both the stoichiometry and the association constants of the binding, a titration experiment was performed.
Measurements were carried out in $CDCl_3$ at 20 °C, keeping a constant concentration of 100 μM of **29** (host) and adding known quantities of **30** (guest).

In order to appreciate the change in the chemical shift of the 1:1 species (Δδ), a complete assignment of the ^1H NMR spectrum of the host and of the **29/30** complex was necessary. ^1H NMR spectrum of **29** is shown in **Figure 2.28**. Resonances belonging to the methyl moieties were assigned thanks to their different integration values in the aliphatic range, at 1.98 and 2.66 ppm. Assignment of protons in the *β*-pyrrolic positions has been possible thanks to the combination of COSY and ROESY spectra.

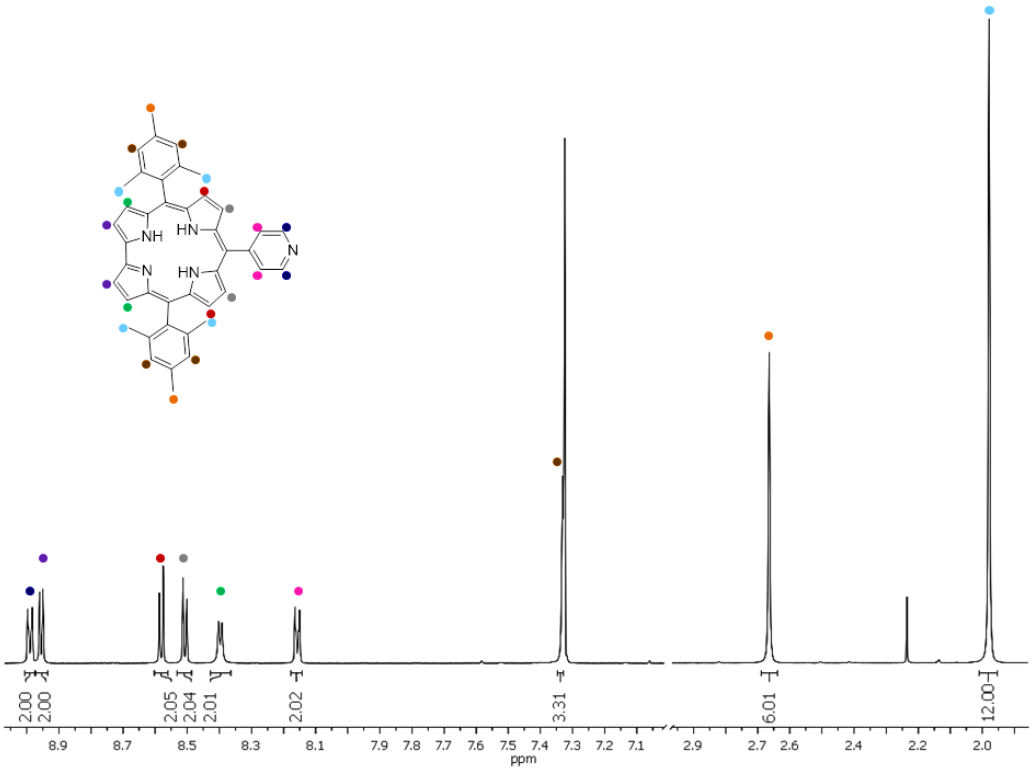

Figure 2.28. ^{1}H NMR of **29**

Protons at position 2 and 18 of the corrole macrocycle were assigned unambiguously at 8.95 ppm, being that signal the only one that didn't result in a cross peak using ROESY analysis. This occurs because only these protons are not subject to dipolar interactions with CH_3 *ortho*-functionalities of the *meso*- phenyl groups (**Figure 2.29**).

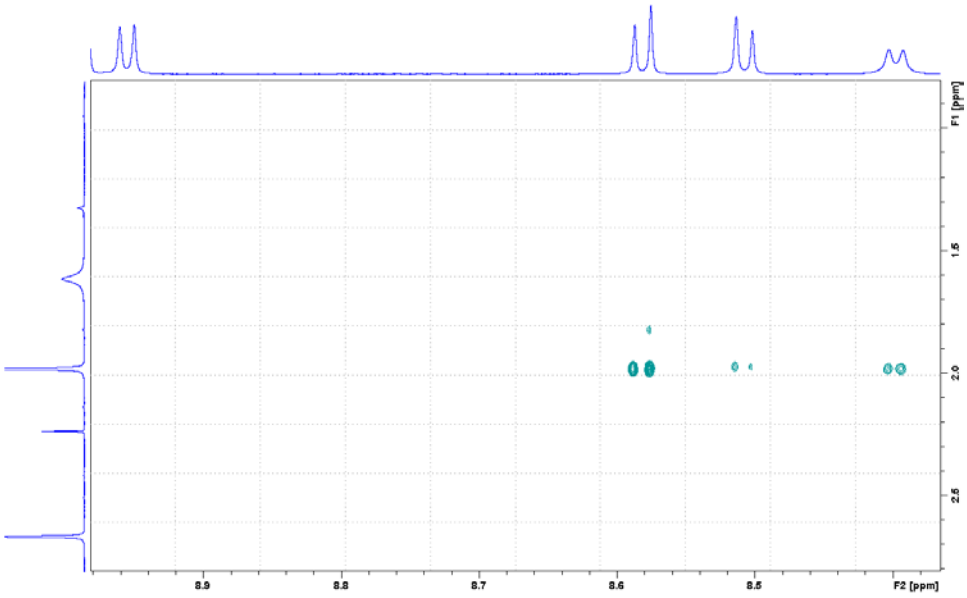

Figure 2.29. Assignment of the doublet 2,18 using ROESY analysis

Combining COSY and ROESY, the assignment of the other aromatic protons becomes more clear: **Figure 2.30** shows the scalar coupling between protons 2,18 and 3,17, and a cross-peak due to a dipolar correlation of 8,12 β-pyrrolic protons with two protons of the pyridine moiety. All spectra and additional data can be found in the appendix section.

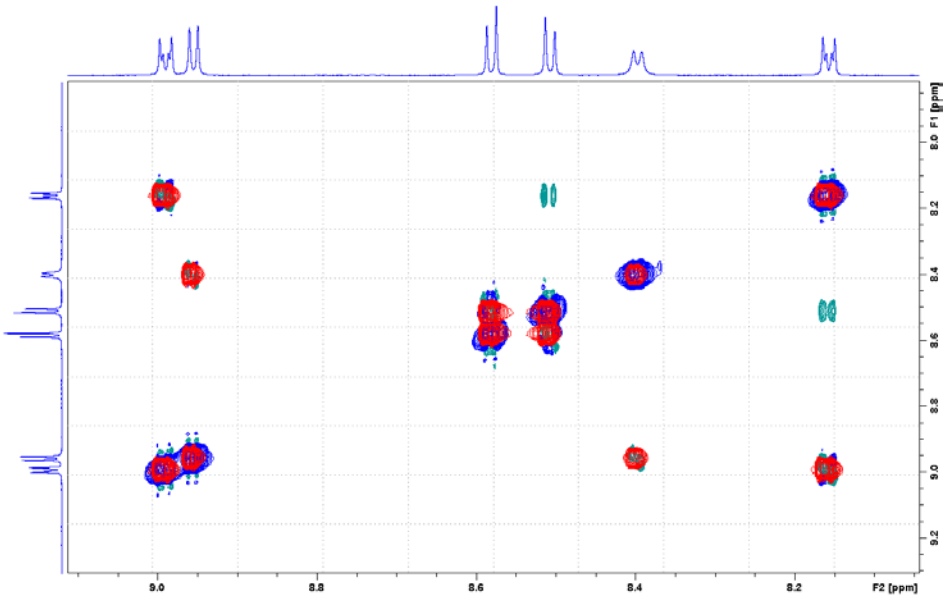

Figure 2.30. Combination of COSY (blue dots) and ROESY (green dots) analyses

Titration of **29** with **30** is shown in **Figure 2.31**. Upon addition of Pc, peak linewidths are "exchange broadened", making the assignment of several protons almost impossible. All peaks experienced different magnitudes shifts toward upper fields. The closer protons to the Pc-zinc centre are the most affected by the aromatic current. Protons corresponding to the pyridine moiety and positions 8,12 of the corrole macrocycle (**Figure 2.31**, red, orange and light orange dots) rapidly coalescenced and disappeared. This behaviour was already observable from the first addition of Pc (0.25 equivalents). The saturation point appears around 0.75 eq. of added **30**.

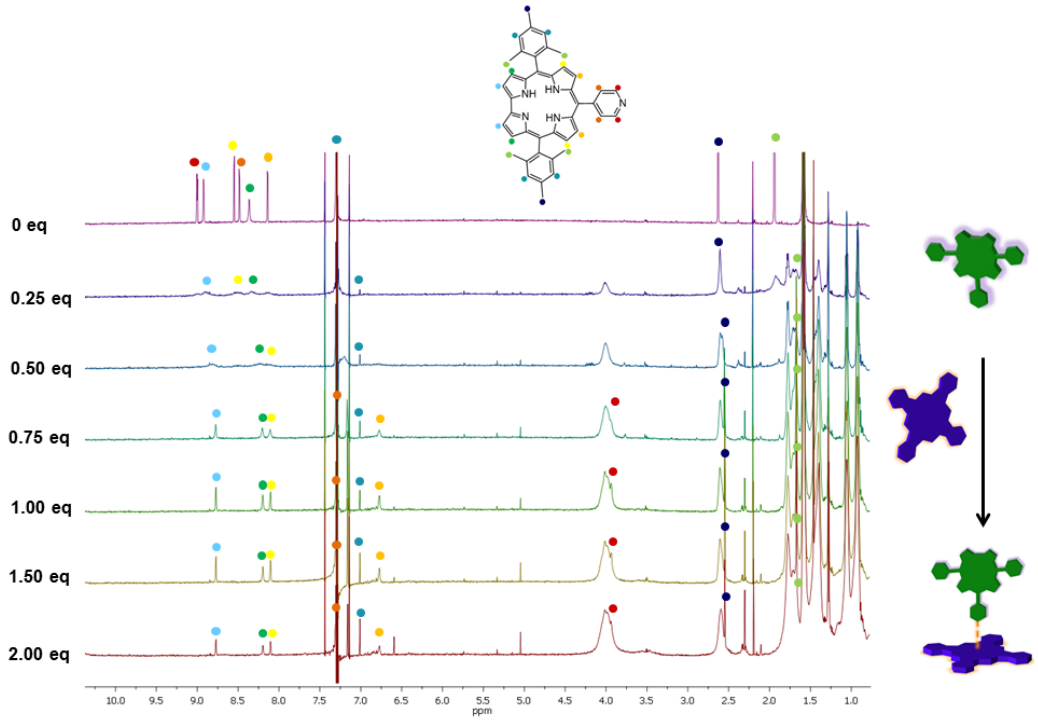

Figure 2.31. ^{1}H-NMR titration of Pc **30** with Corr **29** in $CDCl_3$

After the saturation point, all the signals sharpened and recovered their multiplicity. In order to appreciate the Δδ from corrole to the complex, bidimensional analyses of complex **29/30** were performed using the same concentration of the two dyes, that is 2.5 mM. All bidimensional spectra and additional data can be found in the appendix section.

Initial and final step of the titration experiment are shown in **Figure 2.32**. A table with chemical shifts experienced by all signals is also included (**Figure 2.32**, **inset**). After complexation of corrole with phthalocyanine, chemical shifts vary in a range from Δδ ≈ 0.082 ppm to Δδ ≈ 5.006 ppm.

All the data obtained from experiments were used to estimate kinetic and thermodynamic constants.

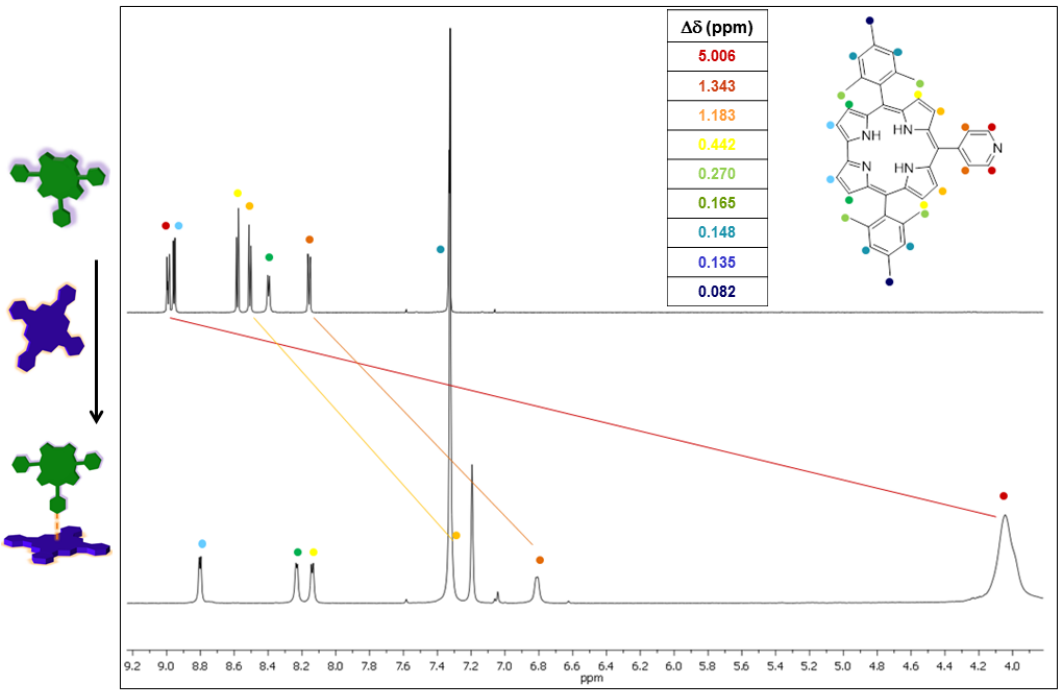

Figure 2.32. First and last spectrum of the titration performed between Corr **29** and ZnPc **30**

According to the mass law, binding constant can be represented as:

$$H + G \rightleftharpoons HG \qquad K_D = \frac{[H][G]}{[HG]} \qquad \textbf{(Eq. 3)}$$

The value of the equilibrium dissociation constant (K_D) is obtained by fitting a plot of a general response (obtained by different techniques) at equilibrium (R_{eq}) against the concentration of the guest (**Figure 2.33**).

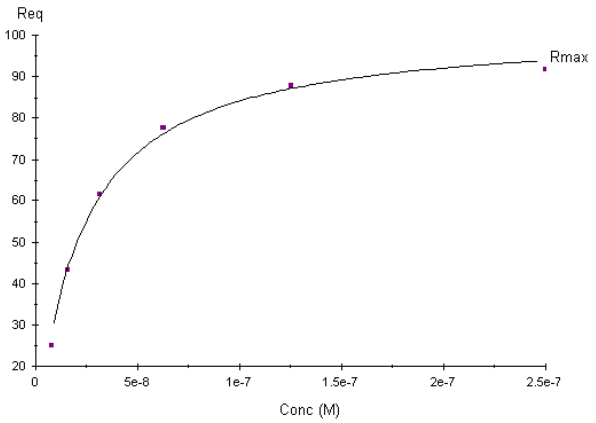

Figure 2.33. General plot of response at equilibrium (R_{eq}) against the concentration

Table 2.4. Correlation between K_D and molar values

K_D value	Molar concentration
10^{-1} to 10^{-3}	mM
10^{-4} to 10^{-6}	μM
10^{-7} to 10^{-9}	nM
10^{-10} to 10^{-12}	pM
10^{-13} to 10^{-15}	fM

To obtain a reliable fit to a plot of R_{eq} against C for the determination of the binding constant, it is important that the range of Host/Guest concentration is wide enough to reveal the curvature of the plot in full. If the concentration range is too low, the plot R_{eq} against C will not approach to a maximum value and the determination of K_D will be uncertain. In the same way, if the concentration range is too high, the plot R_{eq} against C will saturate at the very beginning of the measurement, making the determination of K_D unreliable. In relation to the affinity constant for the interaction, the concentration range should ideally cover 0.1-100 times the equilibrium dissociation constant (**Table 2.4**).

In our case, the chosen concentration to perform the experiment is too high to determine the effective value of K_D. As shown in **Figure 2.31**, the saturation point was obtained upon the addition of 0.75 equivalents of Pc, which is not consistent with a stoichiometric binding. It means that we can only estimate the value of K_D. Since we worked at a corrole concentration of 100µM, we are sure that K_D is less than or equal to 10^{-6}.

Although this data did not allow us to obtain the specific value of the thermodynamic constant, K_D, they represent a useful tool to obtain the exchange constant k_{exc}.

Both kinetic and thermodynamic constants determine the interaction between host and guest, according to the following equilibrium:

$$H + G \underset{k_{on}}{\overset{k_{off}}{\rightleftharpoons}} HG$$

Where k_{on} represents the kinetic association rate constant and governs the velocity of the binding event in solution and k_{off} is the kinetic dissociation rate constant that gives information about the stability of the HG complex.

The relation between the thermodynamic association constant K_D and k_{off}/k_{on} is shown in equation 3.

$$\mathbf{K_D \frac{[H][G]}{[HG]} = \frac{k_{off}}{k_{on}}} \qquad \textbf{(Eq. 4)}$$

Starting from the kinetic association rate constants, the exchange constant k_{exc} can be obtained, according to the following equation:

$$k_{exc} = k_{on}[H]_{free} + k_{off} \qquad \textbf{(Eq. 5)}$$

where H_{free} represents the concentration of the unbounded Host (corrole) in solution. The titration experiment was performed overcoming the saturation point, therefore we can assume that all corrole is bound to phthalocyanine and no free corrole is present. As a result, the exchange constant can be considered equal to k_{off}. In a slow exchange regime, k_{off} will have a much lower value than the observed $\Delta\delta$, while in a fast exchange regime k_{off} will be much higher than $\Delta\delta$. In the case of intermediate exchange conditions, k_{off} can be approximated to the difference of chemical shifts from the H and the HG complex. Different exchange regimes give different values of $\Delta\delta$. The different values of $\Delta\delta$, tabled in the inset of Figure 2.32 stem from different exchange regimes experienced by corrole protons. Aliphatic mesityl protons (blue and light green dots) are barely affected by the electronic changes due to complexation. This results in a fast exchange behaviour, in which the peaks intensity doesn't change during the titrations. Protons belonging to the closest area involved in the complexation (red, orange and light orange dots) seem to display an intermediate exchange behaviour, since they broaden and then disappear. The same behaviour is exhibited by protons in position 2,18 and 3,17 of corrole. However, this behaviour can't be ascribed only to the binding phenomenon, since such protons are far from the coordination center, and their $\Delta\delta$ values largely differ from the ones of the pyridine protons (same exchange regime should give the same $\Delta\delta$ value). This provides an evidence that other processes are involved in the first step of the titration. Probably the presence of Pc changes the rate of tautomeric exchange in corrole inner protons thus changing their lineshapes during the titration. This could explain why *β*-pyrrolic positions are more affected than mesityl ones. We can obtain useful information about how to estimate the exchange constant from the aromatic protons belonging to the mesityl group (light blue dots). Before the addition of Pc, their signal was covered by the solvent peak (**Figure 2.31**). Nevertheless, during the titration experiment, a shift towards upper fields was evident, and the intensity of the new peak directly reported on the population of the complex. This attitude is indicative of a slow exchange regime. This data was used to estimate the exchange constant from the $\Delta\delta$ of phenyl peaks and it was found that $k_{exc} \leq 1 s^{-1}$.

NMR measurements gave us important indication about the binding process. We can conclude that:

- the binding event occurred, as shown by the $\Delta\delta$ observed during the titration;
- the stoichiometry of the binding is 1:1;
- the thermodynamic constant K_D is less than or equal to 10^{-6};
- once formed, the complex is stable, as shown by k_{off} constant;
- other processes probably take place before the binding event.

Photophysical studies

Supramolecular interactions in the ground state between **29** and **30** were investigated performing different titration experiments using visible/near-infrared absorption spectroscopy in chlorobenzene.

Titration experiment was performed maintaining constant the total concentration of Pc and adding variable amounts of **29**. With the aim to avoid Pc aggregation, absorption assays were made with a concentration of $2x10^{-7}$ M of **30**. When adding Corr to the solution of ZnPc in chlorobenzene, no considerable changes in the absorbing features were observed.

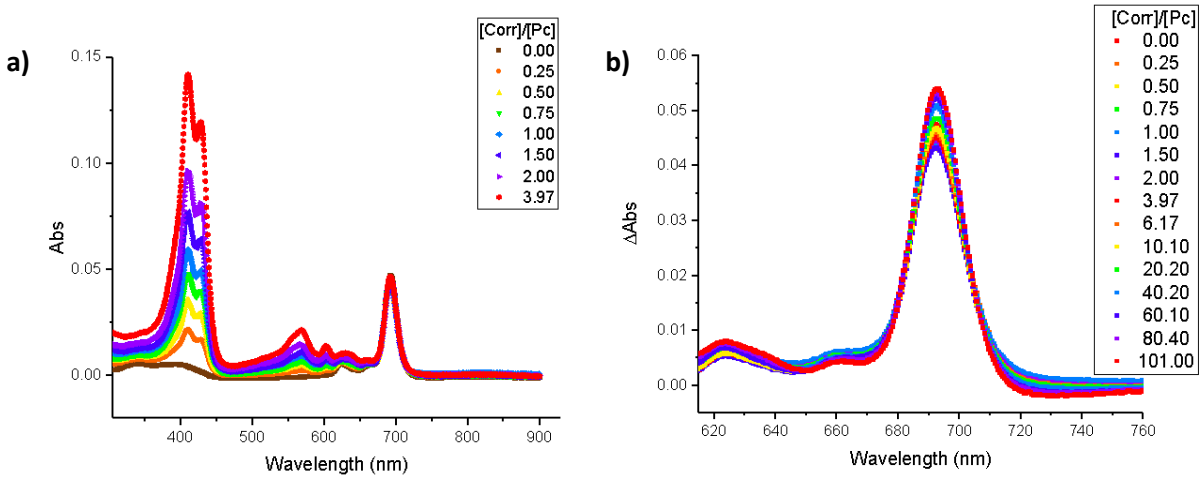

Figure 2.34. **a**)Steady-state absorption spectra of ZnPc **30** upon addition of corrole **29** in chlorobenzene **b**) Differential absorption spectra obtained by subtracting corrole spectra to the Corr/Pc titration solution in chlorobenzene.

The absorption spectra resemble the superimposition of the single Corr and Pc absorptions (**Figure 2.34,a**). Nevertheless, an isosbestic point at 642 nm indicates the formation of ZnPc/Corr supramolecular complex. These observations are more evident if we consider differential absorption spectra (ΔAbs) obtained by subtracting corrole spectra at the relative concentrations to the corrole/phthalocyanine solution (**Figure 2.34,b**).

Further evidence of complexation and electronic interaction came from fluorescence titrations. The ZnPc fluorescence of derivatives **30**, was monitored upon photoexcitation at 675 nm.

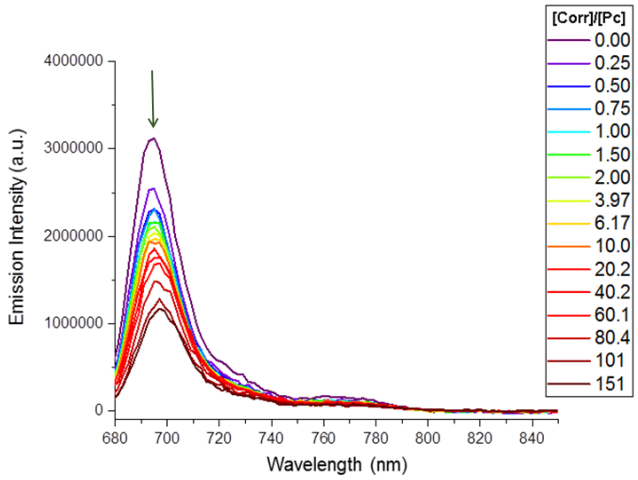

Figure 2.35. Emission spectra (λ_{ex} = 676 nm) of ZnPc **30** (2 x 10^{-7}M) upon addition of different concentrations of Corr **29** (up to 151 equivalents) in chlorobenzene.

Table 2.5. Fluorescence quantum yields (Φ_F) of compounds **29** and **30** in toluene.

Compound	Φ_F (toluene)
29	29%
30	29%

In this case, an exponential decrease of fluorescence emission was observed upon addition of derivative **29.** This was rationalized by the formation of the Corr/Pc conjugate (**Figure 2.35**).

Non-linear curve fitting of the observed spectroscopic changes allowed the determination of the association constant of the formation of Corr-Pc complex. The experimental data points have been fitted by a typical Langmuir type equation (**Figure 2.36**), considering a 1:1 complex formation. The binding constants log K_{ass} was found to be 7.26 ± 0.13 (**29/30**).

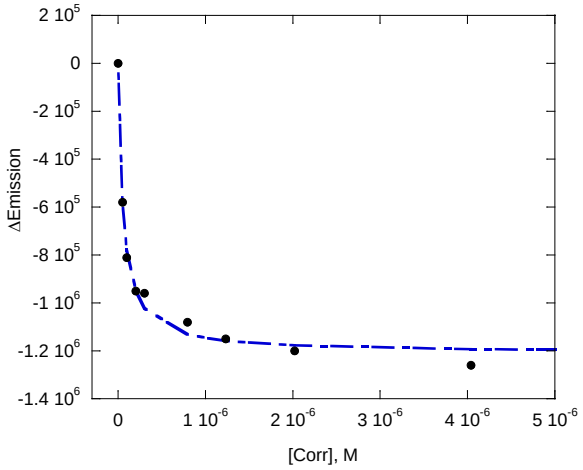

Figure 2.36. Plot of the change in fluorescence intensity of Zn(II)Pc as a ΔEmission *vs* the concentration of corrole.

Photophysical analyses aimed to investigate the excited state energy/electron transfer between the two dyes represent an ongoing study in our laboratories.

Summary and conclusions

In the first section of this Chapter, we have successfully synthesized, for the first time, two different corrole-phthalocyanine covalent dyes. A different number of methoxy moieties present in the corrole framework were expected to improve the electron-donor properties of such a macrocycle and enhance the electron transfer to the linked zinc phthalocyanine bearing electron-withdrawing groups. The structural integrity of the multicomponent system has been confirmed performing spectral, computational and electrochemical studies.

It was found that energy- and electron-transfer reactions compete in both dyads. Upon exciting selectively the corrole macrocycle, only the emission of phthalocyanine counterpart was evidenced. This was ascribed to an intramolecular energy transfer process. Nevertheless a quenching of fluorescence was evidenced upon exciting selectively the corrole (450 nm) or the phthalocyanine (676 nm) macrocycles, as a consequence of other processes that probably take place in the excited states.

Transient absorption spectroscopy showed, upon exciting both at 450 nm and 675 nm, the appearance of a fast-forming and short-living charge separated states constituted by the radical cation of corrole and radical cation of the phthalocyanine.

In the second part of this Chapter, we have prepared a donor-acceptor ensemble built on metal-ligand coordination between a zinc(II) phthalocyanine derivative, bearing electron withdrawing groups at its periphery, and an electron-donor corrole, featuring a pyridyl moiety in position 10. Binding studies were performed by means of NMR and photophysical techniques. The association constant was calculated by emission titration and was found to be $-\log K_{ass} = 7.26 \pm 0.13$. Moreover, the kinetic exchange constant was found to be $k_{exc} \leq 1 s^{-1}$, as evidenced through NMR titrations.

Both works remain an open study since the exact mechanism of energy/electron transfer is not very clear at this stage of investigation. Nevertheless, all this offers food for thought and constitutes a good basis on which to pursue further research in this area.

Experimental section

Materials and Instruments

Chemical reagents and solvents (Sigma-Aldrich, Alfa Aesar, Fluka Chemie and Carlo Erba Reagenti) were of the highest grade available and were used without further purification. Additionally, some solvents were further dried by distillation with $LiAlH_4$ (THF, Toluene), or with previously activated molecular sieves (3 or 4 Å), or with a solvent purifying system by Innovative Technology Inc. MD-4-PS. Air- and moisture sensitive experiments were carried out using standard Schlenk line techniques.

Chromatography: Thin layer chromatography (TLC) analyses were performed on aluminum sheets coated with silica gel 60 F_{254} or neutral alumina 60 F_{254} (Merck).

TLCs analyses were carried out with an UV lamp of 254 and 365 nm.

Column chromatography was carried out using silica gel Merck-60 (230-400 mesh, 60 Å), Sigma-Aldrich (70–230 mesh, 60 Å) and and neutral alumina (Merk, Brockmann Grade III) as the solid support. Eluents and relative proportions are indicated for each particular case.

Nuclear magnetic resonance (NMR): ^{1}H and ^{13}C NMR spectra were measured on a a Bruker AC-300 (300 MHz) or a Bruker AV700 (700MHz) spectrometer, locked on deuterated solvents. Chemical shifts are given in ppm relative to residual solvents using literature reference of δ ppm values.[70]

Mass-spectrometry (MS): Matrix-assisted laser desorption/ionization time of flight (MALDI-TOF) was recorded with a Bruker Ultrareflex III spectrometer. The different matrixes employed are indicated for each spectrum. Fast Atom Bombardment (FAB) mass spectra were recorded with a VG Quattro spectrometer in the positive-ion mode for FAB, using m-nitrobenzyl alcohol (Aldrich) as the matrix. Mass spectrometry data are expressed in *m/z* units.

Ultraviolet-visible spectroscopy: Ground state absorption was recorded with a Cary 5000 UV/Vis/NIR double beam spectrophotometer from VARIAN. Spectra were measured using spectroscopic grade solvents in 1 cm path length quartz cell.

Femtosecond transient absorption spectroscopy: All spectra were obtained with a Ti:sapphire laser system CPA-2101 (Clark-MXR, Inc.) in combination with a Helios

TAPPS-transient absorption pump probe spectroscopy detection unit from Ultrafast Inc. The initial laser output wavelength was 633 nm with a pulse width of 150 fs and 1 kHz repetition. The excitation wavelength was generated using NOPA noncollinear optical parametric amplifier. Transient absorption spectra were measured in THF in a 0.6 mL cuvette with a 0.2 cm path length. Finally, spectra were acquired with a HELIOS (Ultrafast Systems) transient absorption spectrometer.

Electrochemistry: cyclic voltammetry (CV) experiments were performed with a Palmsens potentiostat, using a standard calomel electrode (SCE) as the reference electrode, a platinum wire as the auxiliary electrode and a platinum disk (1 mm diameter) as working electrode. The experiments were performed in anhydrous CH_2Cl_2 and THF using tetrabutylammonium perchlorate (TBAP, Aldrich, electrochemical grade) as supporting electrolyte at 100 mV/s scan rate. Prior to each voltammetric measurement, the cell was degassed by bubbling with nitrogen for about 20 min. Electrochemical measurements were performed using a concentration of approximately 1×10^{-3} M for the compound in question. Compensation for internal resistance was not applied.

Spectroelectrochemistry: Thin-layer UV−visible spectroelectrochemical experiments were performed with a thin-layer cell; a light-transparent platinum net was used as the working electrode and an Ag/AgCl micro-electrode was used as the reference electrode. Potentials were applied through a Palmsens potentiostat. UV-visible absorption spectra were recorded on a Shimadzu 2450 spectrometer equipped with the UV Probe 2.34 program.

Synthetic procedures

Dipyrromethanes **18a,b,**[52]Pcs[57,58] and corrole **29**[65] were prepared following literature procedures.

General procedure for the syntheses of trans-A_2B corroles

Samples of 4-[(trimethylsilyl)ethynyl]benzaldehyde (0.9 mmol) and dipyrromethanes (1.8 mmol) were dissolved in methanol (90mL). Subsequently, a 90 mL solution of HCl (36%) in H_2O was added, and the reaction was stirred at r.t for 90min.

The progress of the reaction was monitored by periodic removal of aliquots from the reaction mixture followed by TLC examination. The crude product was diluted with

$CHCl_3$ (25mL) and washed twice with H_2O. The mixture was dried over Na_2SO_4 and evaporated (in order to remove the residual CH_3OH). Then $CHCl_3$ (450mL) was added, followed by the addition of 2.7 mmol of chloranil. The reaction was stirred at room temperature for 2 hours. The crude product was purified on a silica gel column; different eluent mixtures and characterization data of all the newly prepared compounds are given below.

*5,15-bis (4-methoxyphenyl)-10-[(4-trimethylsilyl)ethynyl]phenylcorrole (**19a**)*

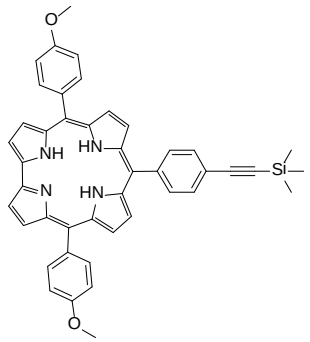

Chromatography using CH_2Cl_2 as eluent. Yield: 12%, green solid, mp >300 °C;
^{1}H NMR ($CDCl_3$, 300 MHz, δ ppm): 0.38 (s, 9H, $SiCH_3$), 4.08 (s, 6H, OCH_3), 7.36 (br d, 4H, *meso*-Ar), 7.86 (br d, 2H, *meso*-Ar), 8.12 (br d, 2H, *meso*-Ar), 8.28 (br d, 4H, *meso*-Ar), 8.48 (br d, 2H, *β*-pyrr), 8.56 (br d, 2H, *β*-pyrr), 8.86 (br d, 2H, *β*-pyrr), 8.93 (br d, 2H, *β*-pyrr); Anal. Calcd for $C_{44}H_{38}N_4O_2Si$: C, 77.39; H, 5.61; N, 8.20; found: C, 77.32; H, 6.68; N, 8.21; MS (FAB, m/z): 684 (M+); UV-vis (CH_2Cl_2): λ_{max} nm (log ε): 420 (5.22), 438 (sh), 583 (4.43), 620 (4.43), 654 (4.34).

*5,15-bis (3,4,5-trimethoxyphenyl)-10-[(4-trimethylsilyl)ethynyl]phenylcorrole (**19b**)*

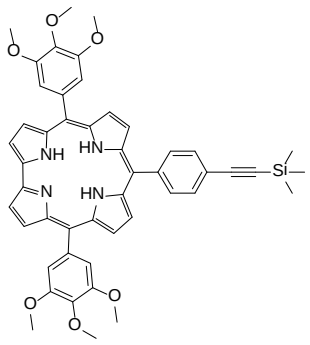

Chromatography using $CHCl_3$ as eluent. Yield: 17%, green solid, mp >300 °C
^{1}H NMR ($CDCl_3$, 300 MHz, δ ppm): 0.43 (s, 9H, $SiCH_3$), 4.14 (s, 12H, OCH_3), 4.20 (s, 6H, OCH_3), 7.66 (s, 4H, *meso*-Ar), 7.92 (d, 2H, J= 6 Hz, *meso*-Ar), 8.16 (d, 2H, J= 6 Hz, *meso*-Ar), 8.57 (d, 2H, J = 3 Hz *β*-pyrr), 8.72 (d, 2H, J = 3 Hz *β*-pyrr), 9.02 (br m, 4 H, *β*-pyrr)
Anal. Calcd for $C_{48}H_{46}N_4O_6Si$: C, 71.80; H, 5.77; N, 6.98; found: C, 71.79; H, 5.83; N, 6.94; MS (MALDI-TOF, matrix DCTB m/z): 802.4 (M+); UV-vis (CH_2Cl_2): λ_{max} nm (log ε): 425 (4.91), 580 (3.96), 623 (4.05), 655 (4.21).

General procedures for the removal of trimethylsilyl group

Corrole (0.14 mmol) was added to a 14 mL solution of dry CH_2Cl_2, then 123 µL of a TBAF solution (1M in THF) were added. The mixture was allow to stir for 2h at rt; until all substrate was consumed. When no more starting material was detected on TLC analysis, the solvent was removed under reduced pressure. The crude was taken up with $CHCl_3$ and washed twice with water; then it was dried on Na_2SO_4. After filtration of the drying agent, the solvent was evaporated. Chromatographic purification of the reaction crude was performed on a silica gel column, eluting with $CHCl_3$. Characterization data of all the newly prepared compounds are given below.

*5,15-bis (4-methoxyphenyl)-10-(4-ethynylphenyl)corrole (**20a**)*

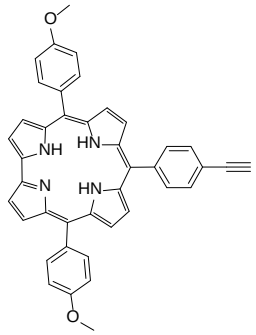

Yield: 57%, green solid, mp >300 °C, ^{1}H NMR ($CDCl_3$, 300 MHz, δ ppm): 3.36 (s, 1H, CH), 4.14 (s, 6H, OCH_3), 7.42 (d, 4H, J=6 Hz, *meso*-Ar), 7.94 (d, 2H, J=6 Hz, *meso*-Ar), 8.20 (d, 2H, J=6 Hz, *meso*-Ar), 8.34 (d, 4H, J=6 Hz, *meso*-Ar), 8.56 (d, 2H, J=3 Hz, *β*-pyrr), 8.62 (d, 2H, J=3 Hz, *β*-pyrr), 8.92 (d, 2H, J=3 Hz, *β*-pyrr), 8.98 (d, 2H, J=3 Hz, *β*-pyrr). Anal. Calcd for $C_{41}H_{30}N_4O_2$: C, 80.63; H, 4.95; N, 9.17; found: C, 80.70; H, 4.93; N, 9.23; MS (MALDI-TOF, matrix DCTB m/z): 610.3 (M+); UV-vis (CH_2Cl_2): λ_{max} nm (log ε): 421 (5.16), 438 (sh), 582 (4.37), 622 (4.39), 655 (4.36).

*5,15-bis (3,4,5-trimethoxyphenyl)-10-(4-ethynylphenyl)corrole (**20b**)*

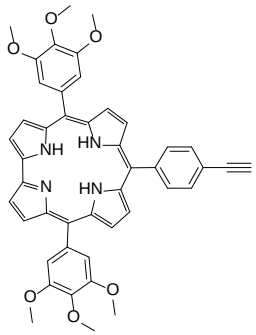

Yield: 70%, green solid, mp >300 °C, ^{1}H NMR ($CDCl_3$, 300 MHz, δ ppm): 3.54 (s, 1H, CH), 4.14 (s, 12H, OCH_3), 4.21 (s, 6H, OCH_3), 7.67 (s, 4H, *meso*-Ar), 7.95 (d, 2H, J=6 Hz, *meso*-

Ar), 8.21 (d, 2H, J=6 Hz, *meso*-Ar), 8.60 (d, 2H, J=3 Hz, *β*-pyrr), 8.74 (d, 2H, J=3 Hz, *β*-pyrr), 9.03 (d, 2H, J=3 Hz, *β*-pyrr), 9.05 (d, 2H, J=3 Hz, *β*-pyrr); Anal. Calcd for $C_{45}H_{38}N_4O_6$: C, 73.96; H, 5.24; N, 7.67; found: C, 73.91; H, 5.29; N, 7.62; MS (FAB, m/z): 733 (M+); UV-vis (CH_2Cl_2): λ_{max} nm (log ε):425 (4.71), 580 (3.88), 621 (3.86), 651 (3.83).

*4,5-Dichlorophthalic anhydride (**21**)*[58]

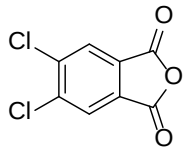

4,5-dichlorophthalic acid (65.0 mmol, 15.3 g) was dissolved in acetic anhydride (25.0 mL) and heated to reflux. After 5 h, the suspended solid was filtered, washed with hexane and stirred in hexane over 12 h. A light grey solid was obtained, that was filtered and thoroughly washed with hexane (100 mL). Yield: 92%, white solid.
^{1}H-NMR (300 MHz, $CDCl_3$, δ ppm) = 8.12 (s, 2H).

*4,5-Dichlorophthalimide (**22**)*[58]

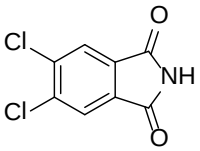

4,5-dichlorophthalic anhydride (**21**) (60.2mmol) and formamide (19.0 mL) were heated to 200 ºC for 3 h. After cooling to room temperature, the solid obtained was filtered, washed with water (40 mL) and vacuum-dried, yielding 12.0 g of 4,5-dichlorophthalamide (**22**). Yield: 93%, white solid.
^{1}H-NMR (300 MHz, $CDCl_3$, δ ppm) = 8.12 (s, 2H).

*4,5-Dichlorophthalamide (**23**)*[58]

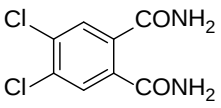

4,5-dichlorophthalimide (**22**) (55.5 mmol) was suspended in a 25% aqueous ammonia solution (168 mL) and was stirred at room temperature for 24 h. Then, a 33% ammonium hydroxide solution (56.0 mL) was added and the mixture was allowed to stir for 24 h. The white solid obtained was filtered, washed with water (50 mL) and vacuum-dried. Yield: 88%, white solid.

^{1}H-NMR (300 MHz, DMSO-d6, δ ppm) = 7.45 (br s, 2H; NH_2), 7.72 (s, 2H; Ar), 7.95 (br s, 2H; NH_2).

*4,5-Dichlorophthalonitrile (**24**)*[58]

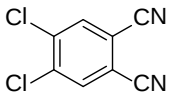

Thionyl chloride (41.0 mL) was cautiously poured over dry DMF (58.0 mL) at 0 ºC under argon atmosphere. The mixture was vigorously stirred at that temperature for 2 h and then 4,5-dichlorophthalamide (**23**) (48.9 mmol) was added. After stirring at room temperature for 12 h, the reaction mixture was poured onto crushed ice (100 mL), resulting in the precipitation of a slightly grey solid which was filtered and washed with water (20 mL). Upon recrystallization from methanol, 8.4 g (42.5 mmol) of compound **24** were obtained. Yield: 87%, white solid.
^{1}H-NMR (300 MHz, $CDCl_3$, δ ppm) = 7.94 (s, 2H).

*4,5-Bis(2-ethylhexylthio)phthalonitrile (**25**)*[58]

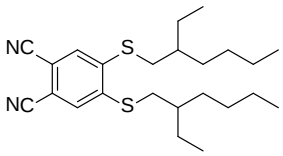

4,5-dichlorophthalonitrile (**24**) (1.27 mmol, 0.25 g,) was poured in a in freshly distilled DMAC (5 mL). The solution was heated to 100ºC, and oven-dry K_2CO_3 (12.3 mmol, 1.7 g) was added in five portions over 30 min. Subsequently, 2-ethylhexane-1-thiol (3.1 mmol, 0.53 mL) was added, and the resulting mixture was stirred at 100 ºC for 10h. After cooling to room temperature, the solution was poured in water (15 mL) and extracted with DCM (3x15 mL). Combined organic layers were dried over $MgSO_4$ and evaporated. The residue was purified by column chromatography (SiO_2, CH_2Cl_2/Heptane 1:1) to give **25** (0.42 g, 1.02 mmol) as a yellowish oil. Yield: 80%.
^{1}H-NMR (300 MHz, $CDCl_3$): δ (ppm) = 0.94 (m, 12H; CH_3), δ1.3-1.4 (m, 16H; $SCH_2CH(CH_2)CH_2CH_2CH_2CH_3$), 1.71 (m, 2H; SCH_2CH), 2.97 (m, 4H; SCH_2), 7.41 (s, 2H; Aryl).

*4,5-Bis(2-ethylhexylsulfonyl)phthalonitrile (**26**)*[58]

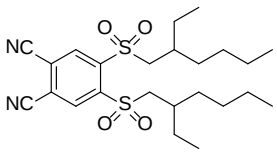

4,5-bis(2-ethylhexylthio)phthalonitrile (**25**) (1.0 eq, 2.4 mmol,1.0 g) was dissolved in acetic acid (20.0 mL) and the solution was heated at 90 ºC. Then, a 33% H_2O_2 solution (11.2 mL) was slowly added and the mixture was stirred at 80 ºC for 3 h. After cooling to room temperature, the solution was poured in water and extracted with CH_2Cl_2 (3x15 mL). Combined organic layers were dried over $MgSO_4$ and evaporated. The residue was purified by column chromatography (SiO_2, Heptane/ ethyl acetate) to give compound **26** as a yellowish oil (1.1 g, 2.3 mmol). Yield: 95%.
^{1}H-NMR (300 MHz, $CDCl_3$): δ (ppm) = 0.88 (m, 12H; CH_3), δ 1.2-1.4 (m, 16H; CH_2), 3.57 (m, 4H; SO_2CH_2), 8.69 (s, 2H; H-3, Aryl).

General procedure for the syntheses of A_3B Pc

A *o*-DCB/DMF (3:1, 2.4 mL, 0.8 mL) solution of 4,5-bis(2-ethylhexylsulfonyl) phthalonitrile (**26**) (0.52 mmol, 250 mg), the appropriate phthalonitrile (0.35 mmol) and Zn(OAc)2 (0.024 mmol, 38.2 mg) was heated at 135 ºC under an argon atmosphere for 12 h. After cooling down to room temperature, the solvent was removed under reduced pressure and the crude was poured on water and extracted with DCM (3x15 mL). Combined organic layers were dried over $MgSO_4$ and evaporated. The mixture of Pcs formed was separated by column chromatography on silica gel using a mixture of THF/Hexane (2:1) as eluent.

*2,3,9,10,16,17-Hexakis(2-ethylhexylsulfonyl)-23-iodo-5,28:14,19-diimino-7,12:21,26-dinitrilo-tetrabenzo[c, h, m, r]-[1, 6, 11, 16]tetraazacycloeicosinato-(2-)-N^{29}, N^{30}, N^{31}, N^{32} zinc (II) (**27a**)*[58]

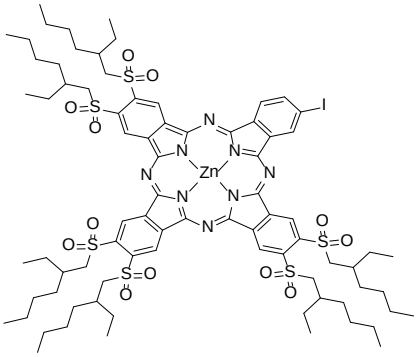

Yield: 23%, dark green solid.^{1}H-NMR (300 MHz, THF-d8): δ (ppm) = δ 0.92-1.15 (m, 36H; CH_3), δ1.35-1.85 (m, 48H; CH_2), δ 2.48-2.73 (m, 6H; SO_2CH_2CHR), δ 3.89-4.23 (m, 12H; SO_2CH_2-R), 8.55 (s, 1H; Pc-H), 9.08 (s, 1H; Pc-H), 9.67 (s, 1H; Pc-H), 9.99 (s, 1H; Pc-H), 10.14 (s, 1H; Pc-H), 10.26 (s, 1H; Pc-H), 10.39 (m, 3H; Pc-H);MS (MALDI-TOF, matrix DCTB m/z) = 1758.5 (M+)UV-Vis (THF): λmax (nm) (log ε) = 701 (5.2), 672 (5.2), 640 (4.7), 608 (4.5), 371 (4.8).

*2,3,9,10,16,17-Hexakis(2-ethylhexylsulfonyl)-23-[(trimethylsilyl)ethynyl)-5,28:14,19-diimino-7,12:21,26- dinitrilo-tetrabenzo[c, h, m, r]-[1, 6, 11, 16]tetraazacycloeicosinato-(2-)-N^{29}, N^{30}, N^{31}, N^{32} zinc (II) (**27b**)*

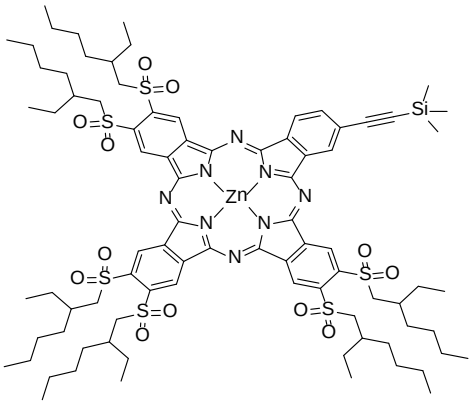

Yield: 25%, dark green solid.^{1}H-NMR (300 MHz, THF-d8): δ (ppm) = 0.41 (s, 9 H, $SiCH_3$), δ 0.8-1.5 (m, 90H; CH, CH_2, CH_3), 2.42 (m, 12H; SO_2CH_2), 10.4 (br s, 2H; Pc-H), 10.7 (br s, 1H; Pc-H), 10.8 (s, 6H; Pc-H); MS (FAB, m/z): 1732 (M+); UV-Vis (THF): λmax (nm) (log ε) = 697 (5.2), 675 (5.1), 640 (4.6), 617 (5.5), 370 (4.8).

*2,3,9,10,16,17,23,24-Octakis(2-ethylhexylsulfonyl)-5,28:14,19-diimino-7,12:21,26-dinitrilo-tetrabenzo[c, h, m, r]-[1, 6, 11, 16]tetraazacycloeicosinato-(2-)- N^{29}, N^{30}, N^{31},N^{32} zinc (II) (**29**)*[58]

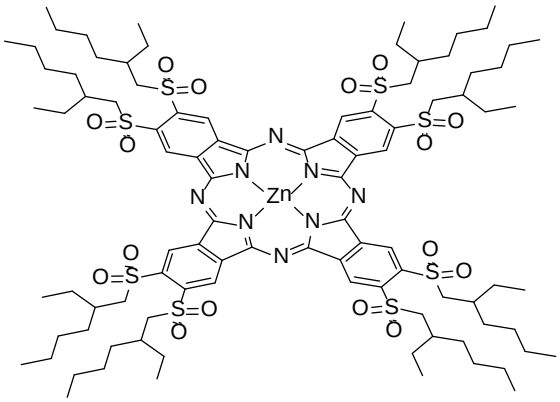

A mixture of of 4,5-Bis(2-ethylhexylsulfonyl)phthalonitrile (61 mg, 0.126 mmol) and 8.5 mg of $Zn(OAc)_2$ (0.046 mmol) was heated to 145 °C in 1.2 mL of a *o*-DCB/DMF (5:1) mixture under argon atmosphere. The reaction completed in 26 h, being followed by TLC analysis. After being cooled to room temperature, the reaction mixture was evaporated to dryness under vacuum purified was by column chromatography (Silica gel, CHCl3/ethyl acetate 100:1) which allowed to obtain Zn(II)Pc as a dark green solid. Yield: 24%; ^{1}H-NMR (300 MHz, $CDCl_3$): δ (ppm) = 0.86 (t, 48 H, J = 7.2 Hz, CH_3), δ 1.1-1.8 (m, 72H; CH_2), δ 3.6-3.9 (m, 16H; SO_2CH_2), 10.5 (m, 8H; Pc-H); MS (MALDI-TOF, matrix DCTB m/z): 1987.8, UV-Vis (THF): λ_{max} (nm) (log ε) = 685 (5.4), 620 (4.6), 377 (4.7).

General procedure for the syntheses of Corr-Pc dyads

Corrole (0.033 mmol), phthalocyanine **27a** (70 mg, 0.040 mmol), Cs_2CO_3 (12 mg, 0.035 mmol), $Pd(OAc)_2$ (2 mg, $8.3\cdot10^{-3}$ mmol), and PPH_3 (2 mg, $8.3\cdot10^{-3}$ mmol) were placed under argon atmosphere in a dry Schlenk flask. Dry DMSO was then added and three Freeze-pump-thaw cycles were performed. The reaction mixture was stirred at 80 °C for 24h. When no more corrole was detected by TLC analysis, the solvent was removed under reduced pressure and the residue was chromatographed (Silica gel, THF/Hexane 2:1). Data of the newly prepared compounds are given below.

*Dyad **28a***

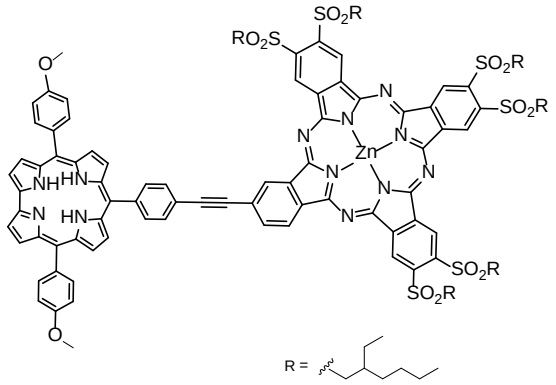

Yield: 14%. Dark blue solid. Anal. Anal. Calcd for $C_{121}H_{140}N_{12}O_{14}S_6Zn$: C, 64.76; H, 6.29; N, 7.49; found: C, 64.84; H, 6.31; N, 7.50; MS (MALDI-TOF, matrix DCTB m/z): 2242.8 (M+); UV-Vis (CH_2Cl_2): λ_{max} (nm) (log ε) = 393 (4.73), 435 (4.70), 628 (sh), 652 (sh), 687 (4.78), 707 (4.77)

*Dyad **29a***

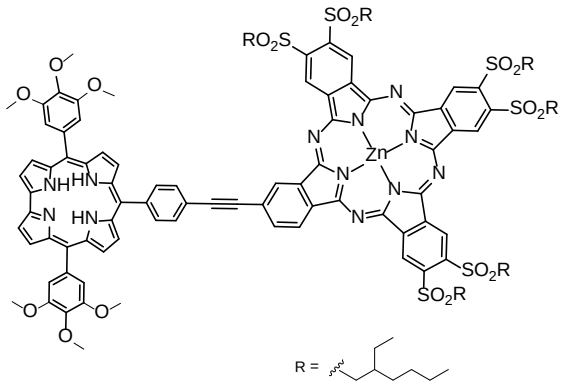

Yield: 22%. Dark blue solid. Anal. Calcd for $C_{125}H_{148}N_{12}O_{18}S_6Zn$: C, 63.50; H, 6.31; N, 7.11; found: C, 63.45; H, 6.33; N, 7.20; MS (MALDI-TOF, matrix Dithranol m/z): 2363.7

(M+); UV-Vis (CH_2Cl_2): λ_{max} (nm) (log ε) =429 (4.56), 628 (sh), 650 (sh), 684 (4.50), 709 (4.53).

References

(1) *IPCC 2013 Work Group I, Chapter 1*; pp 119–158.
(2) Global Climate Report - Annual 2016 - National Centers for Environmental Information (NCEI) https://www.ncdc.noaa.gov/sotc/global/201613 (accessed Sep 25, 2017).
(3) Hoffert, M. I.; Caldeira, K.; Jain, A. K.; Haites, E. F.; Harvey, L. D. D.; Potter, S. D.; Schlesinger, M. E.; Schneider, S. H.; Watts, R. G.; Wigley, T. M. L.; et al. Energy Implications of Future Stabilization of Atmospheric CO2 Content. *Nature* **1998**, *395* (6705), 881–884.
(4) Schiermeier, Q.; Tollefson, J.; Scully, T.; Witze, A.; Morton, O. Energy Alternatives: Electricity without Carbon. *Nature* **2008**, *454* (7206), 816–823.
(5) Hammarström, L.; Hammes-Schiffer, S. Artificial Photosynthesis and Solar Fuels. *Acc. Chem. Res.* **2009**, *42* (12), 1859–1860.
(6) Deisenhofer, J.; Michel, H. The Photosynthetic Reaction Center from the Purple Bacterium Rhodopseudomonas Viridis (Nobel Lecture). *Angew. Chem. Int. Ed. Engl.* **1989**, *28* (7), 829–847.
(7) Hoff, A. J.; Deisenhofer, J. Photophysics of Photosynthesis. Structure and Spectroscopy of Reaction Centers of Purple Bacteria. *Phys. Rep.* **1997**, *287* (1), 1–247.
(8) Nelson, N.; Yocum, C. F. Structure and Function of Photosystems I and Ii. *Annu. Rev. Plant Biol.* **2006**, *57* (1), 521–565.
(9) Fukuzumi, S.; Imahori, H. Biomimetic Electron-Transfer Chemistry of Porphyrins and Metalloporphyrins. In *Electron Transfer in Chemistry*; Balzani, V., Ed.; Wiley-VCH Verlag GmbH, 2001; pp 927–975.
(10) Gust, D.; Moore, T. A. Mimicking Photosynthesis. *Science* **1989**, *244* (4900), 35–41.
(11) Wasielewski, M. R. Photoinduced Electron Transfer in Supramolecular Systems for Artificial Photosynthesis. *Chem. Rev.* **1992**, *92* (3), 435–461.
(12) Fernández Ariza, J. Synthesis and Properties of Photo- and Electroactive Tetraazaporphyrins and Their Performance in Dye-Sensitized Solar Cells, Universidad Autónoma de Madrid, 2016.
(13) Nelsen, S. F. Electron Transfer Reactions in Organic Chemistry. In *Electron Transfer in Chemistry*; Balzani, V., Ed.; Wiley-VCH Verlag GmbH, 2001; pp 342–392.
(14) Fox, M. A. Photoinduced Electron Transfer. *Photochem. Photobiol.* **1990**, *52* (3), 617–627.
(15) Marcus, R. A. On the Theory of Electron-Transfer Reactions. VI. Unified Treatment for Homogeneous and Electrode Reactions. *J. Chem. Phys.* **1965**, *43* (2), 679–701.
(16) Marcus, R. A.; Sutin, N. Electron Transfers in Chemistry and Biology. *Biochim. Biophys. Acta BBA - Rev. Bioenerg.* **1985**, *811* (3), 265–322.
(17) Fukuzumi, S. Artificial Photosynthetic Systems Composed of Porphyrins and Phthalocyanines. In *Handbook of Porphyrin Science*; Handbook of Porphyrin Science; World Scientific Publishing Company, 2010; Vol. Volume 10, pp 183–243.
(18) Marcus, R. A. Electron Transfer Reactions in Chemistry: Theory and Experiment (Nobel Lecture). *Angew. Chem. Int. Ed. Engl.* **1993**, *32* (8), 1111–1121.
(19) Closs, G. L.; Miller, J. R. Intramolecular Long-Distance Electron Transfer in Organic Molecules. *Science* **1988**, *240* (4851), 440–447.
(20) Gust, D.; Moore, T. A.; Moore, A. L. Molecular Mimicry of Photosynthetic Energy and Electron Transfer. *Acc. Chem. Res.* **1993**, *26* (4), 198–205.
(21) McKeown, N. B. *Phthalocyanine Materials: Synthesis, Structure and Function*; Cambridge University Press, 1998.
(22) de la Torre, G.; Nicolau, M.; Torres, T. Chapter 1 - Phthalocyanines: Synthesis, Supramolecular Organization, and Physical Properties. In *Supramolecular Photosensitive and Electroactive Materials*; Nalwa, H. S., Ed.; Academic Press: San Diego, 2001; pp 1–111.
(23) Rio, Y.; Rodríguez-Morgade, M. S.; Torres, T. Modulating the Electronic Properties of Porphyrinoids: A Voyage from the Violet to the Infrared Regions of the Electromagnetic Spectrum. *Org. Biomol. Chem.* **2008**, *6* (11), 1877–1894.

(24) *Functional Phthalocyanine Molecular Materials | Jianzhuang Jiang | Springer*.
(25) Ishii, K.; Kobayashi, N. The Photophysical Properties of Phthalocyanine and Related Compounds. In *The Porphyrin Handbook*; Kadish, K. M.; Smith, K. M.; Guilard, R., 2003; Vol. 16, pp 1–40.
(26) Martínez-Díaz, M. V.; Torres, T. On the Significance of Phthalocyanines in Solar Cells. In *Handbook of Porphyrin Science*; World Scientific, 2010; Vol. 10, pp 141–181.
(27) Kobayashi, N.; Ogata, H.; Nonaka, N.; Luk'yanets, E. A. Effect of Peripheral Substitution on the Electronic Absorption and Fluorescence Spectra of Metal-Free and Zinc Phthalocyanines. *Chem. – Eur. J.* **2003**, *9* (20), 5123–5134.
(28) Chahraoui, D.; Valat, P.; Kossanyi, J. Fluorescence of Phthalocyanines: Emission from an Upper Excited State. *Res. Chem. Intermed.* **1992**, *17* (3), 219–232.
(29) Claessens, C. G.; Hahn, U.; Torres, T. Phthalocyanines: From Outstanding Electronic Properties to Emerging Applications. *Chem. Rec. N. Y. N* **2008**, *8* (2), 75–97.
(30) Rodríguez-Morgade; de la Torre, G.; Torres, T. Design and Synthesis of Low-Symmetry Phthalocyanines and Related Systems. In *The Porphyrin Handbook*; Kadish, K. M.; Smith, K. M.; Guilard, R., 2003; Vol. 15, p 125.
(31) Tomoda, H.; Saito, S.; Ogawa, S.; Shiraishi, S. Synthesis of Phthalocyanines from Phthalonitrile with Organic Strong Bases. *Chem. Lett.* **1980**, *9* (10), 1277–1280.
(32) Leznoff, C. C.; Hu, M.; Nolan, K. J. M. The Synthesis of Phthalocyanines at Room Temperature. *Chem. Commun.* **1996**, *0* (10), 1245–1246.
(33) Uchida, H.; Tanaka, H.; Yoshiyama, H.; Reddy, P. Y.; Nakamura, S.; Toru, T. Novel Synthesis of Phthalocyanines from Phthalonitriles under Mild Conditions. *Synlett* **2002**, *2002* (10), 1649–1652.
(34) Kopylovich, M. N.; Kukushkin, V. Y.; Haukka, M.; Luzyanin, K. V.; Pombeiro, A. J. L. An Efficient Synthesis of Phthalocyanines Based on an Unprecedented Double-Addition of Oximes to Phthalonitriles. *J. Am. Chem. Soc.* **2004**, *126* (46), 15040–15041.
(35) Acar, İ.; Kantekin, H.; Bıyıklıoğlu, Z. The Synthesis, Using Microwave Irradiation and Characterization of Novel, Metal-Free and Metallophthalocyanines. *J. Organomet. Chem.* **2010**, *695* (2), 151–155.
(36) Kantar, C.; Akal, H.; Kaya, B.; Islamoğlu, F.; Türk, M.; Şaşmaz, S. Novel Phthalocyanines Containing Resorcinol Azo Dyes; Synthesis, Determination of PKa Values, Antioxidant, Antibacterial and Anticancer Activity. *J. Organomet. Chem.* **2015**, *783* (Supplement C), 28–39.
(37) Sommerauer, M.; Rager, C.; Hanack, M. Separation of 2(3),9(10),16(17),23(24)-Tetrasubstituted Phthalocyanines with Newly Developed HPLC Phases. *J. Am. Chem. Soc.* **1996**, *118* (42), 10085–10093.
(38) Hanack, M.; Schmid, G.; Sommerauer, M. Chromatographic Separation of the Four Possible Structural Isomers of a Tetrasubstituted Phthalocyanine: Tetrakis(2-Ethylhexyloxy)Phthalocyaninatonickel(II). *Angew. Chem. Int. Ed. Engl.* **1993**, *32* (10), 1422–1424.
(39) Rodríguez-Morgade, S.; Hanack, M. Synthesis, Separation and Characterization of the Structural Isomers of Octa-Tert-Butylphthalocyanines and Dienophilic Phthalocyanine Derivatives. *Chem. – Eur. J.* **1997**, *3* (7), 1042–1051.
(40) Ranta, J.; Kumpulainen, T.; Lemmetyinen, H.; Efimov, A. Synthesis and Characterization of Monoisomeric 1,8,15,22-Substituted (A3B and A2B2) Phthalocyanines and Phthalocyanine–Fullerene Dyads. *J. Org. Chem.* **2010**, *75* (15), 5178–5194.
(41) Leznoff, C. C.; Drew, D. M. The Synthesis of Pure 1,11,15,25-Tetrasubstituted Phthalocyanines as Single Isomers Using Bisphthalonitriles. **1994**.
(42) Lv, W.; Zhang, X.; Lu, J.; Zhang, Y.; Li, X.; Jiang, J. Synthesis and Hollow-Sphere Nanostructures of Optically Active Metal-Free Phthalocyanine. *Eur. J. Inorg. Chem.* **2008**, *2008* (27), 4255–4261.
(43) de la Torre, G.; Claessens, C. G.; Torres, T. Phthalocyanines: The Need for Selective Synthetic Approaches. *Eur. J. Org. Chem.* **2000**, *2000* (16), 2821–2830.

(44) Sastre, A.; Torres, T.; Hanack, M. Synthesis of Novel Unsymmetrical Monoaminated Phthalocyanines. *Tetrahedron Lett.* **1995**, *36* (46), 8501–8504.
(45) Zhao, L.; Wang, K.; Shang, H.; Jiang, J. Novel Chiral ABBB-Type Unsymmetrical Phthalocyanine. Ring-Expansion Synthesis, Spectroscopic, and Electrochemical Properties. *Dyes Pigments* **2015**, *120* (Supplement C), 52–56.
(46) Mudyiwa, M.; Ndinguri, M. W.; Soper, S. A.; Hammer, R. P. Microwave Assisted Solid-Phase Synthesis of Substituted Tetraazaporphyrins and a Phthalocyanine-Peptide Conjugate. *J. Porphyr. Phthalocyanines* **2010**, *14* (10), 891–903.
(47) Araki, Y.; Ito, O. Factors Controlling Lifetimes of Photoinduced Charge-Separated States of Fullerene-Donor Molecular Systems. *J. Photochem. Photobiol. C Photochem. Rev.* **2008**, *9* (3), 93–110.
(48) Pereira, A. M. V. M.; Hausmann, A.; Tomé, J. P. C.; Trukhina, O.; Urbani, M.; Neves, M. G. P. M. S.; Cavaleiro, J. A. S.; Guldi, D. M.; Torres, T. Porphyrin–Phthalocyanine/Pyridylfullerene Supramolecular Assemblies. *Chem. – Eur. J.* **2012**, *18* (11), 3210–3219.
(49) Urbani, M.; Osati, S.; Kuhri, S.; Guldi, D. M.; Torres, T. Photoinduced Electron Transfer in a Meso-Linked Zn(II)Porphyrin-Zn(II)Phthalocyanine/C60-Pyridyl Supramolecular System. *J. Porphyr. Phthalocyanines* **2013**, *17* (06n07), 501–510.
(50) Faure, S.; Stern, C.; Guilard, R.; Harvey, P. D. Role of the Spacer in the Singlet−Singlet Energy Transfer Mechanism (Förster vs Dexter) in Cofacial Bisporphyrins. *J. Am. Chem. Soc.* **2004**, *126* (4), 1253–1261.
(51) Laha, J. K.; Dhanalekshmi, S.; Taniguchi, M.; Ambroise, A.; Lindsey, J. S. A Scalable Synthesis of Meso-Substituted Dipyrromethanes. *Org. Process Res. Dev.* **2003**, *7* (6), 799–812.
(52) Koszarna, B.; Gryko, D. T. Efficient Synthesis of Meso-Substituted Corroles in a H2O−MeOH Mixture. *J. Org. Chem.* **2006**, *71* (10), 3707–3717.
(53) Shen, J.; Shao, J.; Ou, Z.; E, W.; Koszarna, B.; Gryko, D. T.; Kadish, K. M. Electrochemistry and Spectroelectrochemistry of Meso-Substituted Free-Base Corroles in Nonaqueous Media: Reactions of (Cor)H3, [(Cor)H4]+, and [(Cor)H2]-. *Inorg. Chem.* **2006**, *45* (5), 2251–2265.
(54) *Metal-Catalyzed Cross-Coupling Reactions*, 2nd Edition.; A. de Meijere, F. Diederich: Weinheim, Germany, 2004.
(55) Melville, O. A.; Lessard, B. H.; Bender, T. P. Phthalocyanine-Based Organic Thin-Film Transistors: A Review of Recent Advances. *ACS Appl. Mater. Interfaces* **2015**, *7* (24), 13105–13118.
(56) Wöhrle, D.; Eskes, M.; Shigehara, K.; Yamada, A. A Simple Synthesis of 4,5-Disubstituted 1,2-Dicyanobenzenes and 2,3,9,10,16,17,23,24-Octasubstituted Phthalocyanines. *Synthesis* **1993**, *1993* (02), 194–196.
(57) Trukhina, O.; Rudolf, M.; Bottari, G.; Akasaka, T.; Echegoyen, L.; Torres, T.; Guldi, D. M. Bidirectional Electron Transfer Capability in Phthalocyanine–Sc3N@Ih–C80 Complexes. *J. Am. Chem. Soc.* **2015**, *137* (40), 12914–12922.
(58) Ruiz Ganivez, C. Novel Single Molecule Magnets and Photosensitizers for Molecular Photovoltaics Based on Customized Phthalocyanines, Universidad Autónoma de Madrid, 2015.
(59) *Wiley: Electrochemical Methods: Fundamentals and Applications, 2nd Edition - Allen J. Bard, Larry R. Faulkner*.
(60) Cardona, C. M.; Li, W.; Kaifer, A. E.; Stockdale, D.; Bazan, G. C. Electrochemical Considerations for Determining Absolute Frontier Orbital Energy Levels of Conjugated Polymers for Solar Cell Applications. *Adv. Mater.* **2011**, *23* (20), 2367–2371.
(61) The Absolute Electrode Potential: An Explanatory Note (Recommendations 1986). *J. Electroanal. Chem. Interfacial Electrochem.* **1986**, *209* (2), 417–428.
(62) Berera, R.; Grondelle, R. van; Kennis, J. T. M. Ultrafast Transient Absorption Spectroscopy: Principles and Application to Photosynthetic Systems. *Photosynth. Res.* **2009**, *101* (2–3), 105–118.
(63) Raavi, S. S. K.; Yin, J.; Grancini, G.; Soci, C.; Soma, V. R.; Lanzani, G.; Giribabu, L. Femtosecond to Microsecond Dynamics of Soret-Band Excited Corroles. *J. Phys. Chem. C* **2015**, *119* (52), 28691–28700.

(64) Ventura, B.; Esposti, A. D.; Koszarna, B.; Gryko, D. T.; Flamigni, L. Photophysical Characterization of Free-Base Corroles, Promising Chromophores for Light Energy Conversion and Singlet Oxygen Generation. *New J. Chem.* **2005**, *29* (12), 1559–1566.
(65) Gryko, D. T.; Piechota, K. E. Straightforward Route to Trans-A2B-Corroles Bearing Substituents with Basic Nitrogen Atoms. *J. Porphyr. Phthalocyanines* **2002**, *06* (02), 81–97.
(66) Langmar, O.; Ganivet, C. R.; Lennert, A.; Costa, R. D.; De, L. T.; Torres, T.; Guldi, D. M. Combining Electron-Accepting Phthalocyanines and Nanorod-like CuO Electrodes for p-Type Dye-Sensitized Solar Cells. *Angew. Chem. - Int. Ed.* **2015**, *54* (26), 7688–7692.
(67) Hirose, K. A Practical Guide for the Determination of Binding Constants. *J. Incl. Phenom. Macrocycl. Chem.* **2001**, *39* (3–4), 193–209.
(68) Kleckner, I. R.; Foster, M. P. An Introduction to NMR-Based Approaches for Measuring Protein Dynamics. *Biochim. Biophys. Acta BBA - Proteins Proteomics* **2011**, *1814* (8), 942–968.
(69) *Fundamentals of Protein NMR Spectroscopy | Gordon S. Rule | Springer*.
(70) Fulmer, G. R.; Miller, A. J. M.; Sherden, N. H.; Gottlieb, H. E.; Nudelman, A.; Stoltz, B. M.; Bercaw, J. E.; Goldberg, K. I. NMR Chemical Shifts of Trace Impurities: Common Laboratory Solvents, Organics, and Gases in Deuterated Solvents Relevant to the Organometallic Chemist. *Organometallics* **2010**, *29* (9), 2176–2179.

Appendix

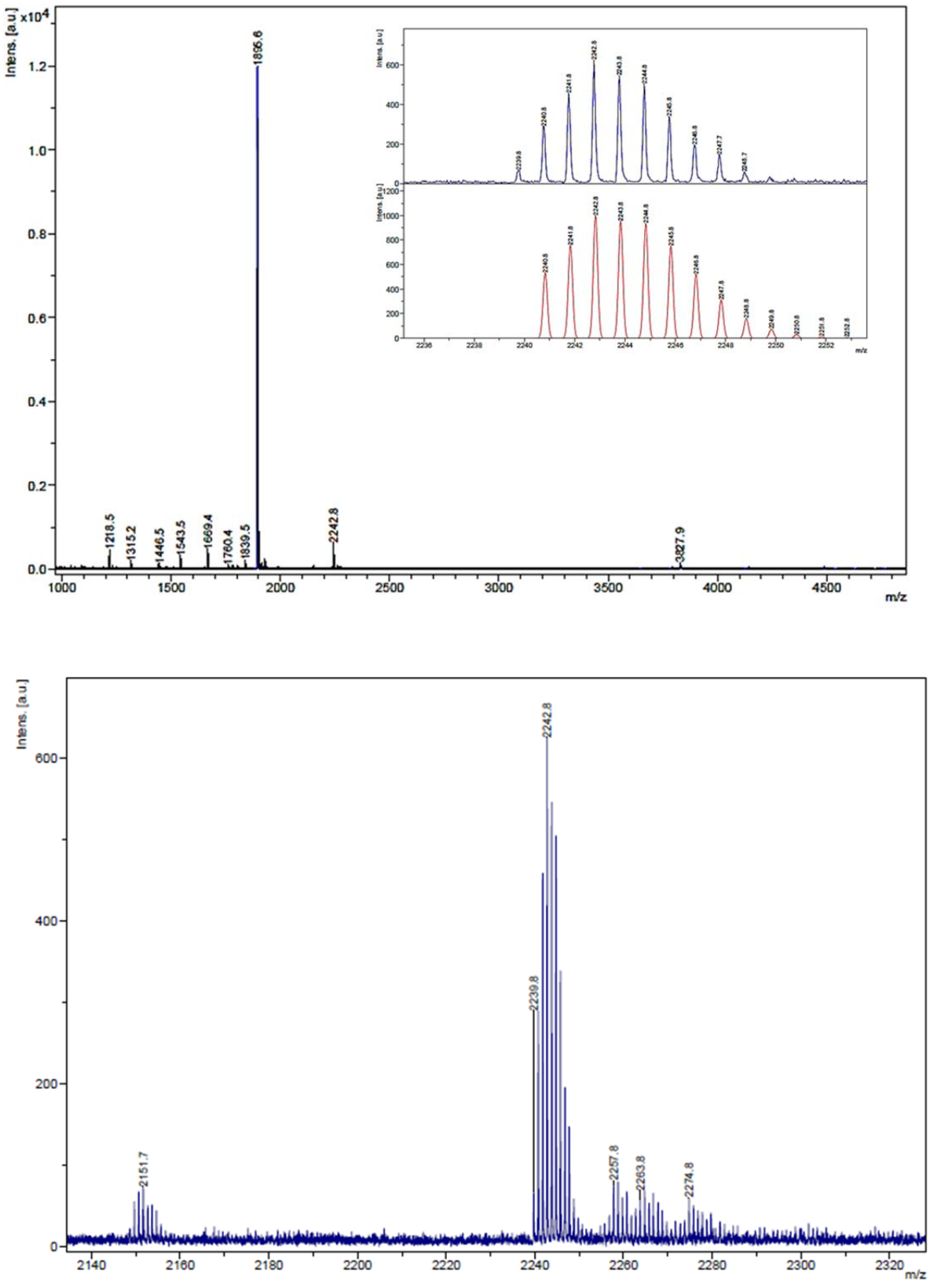

Figure 1. MALDI-TOF spectrum of dyad **28a.**

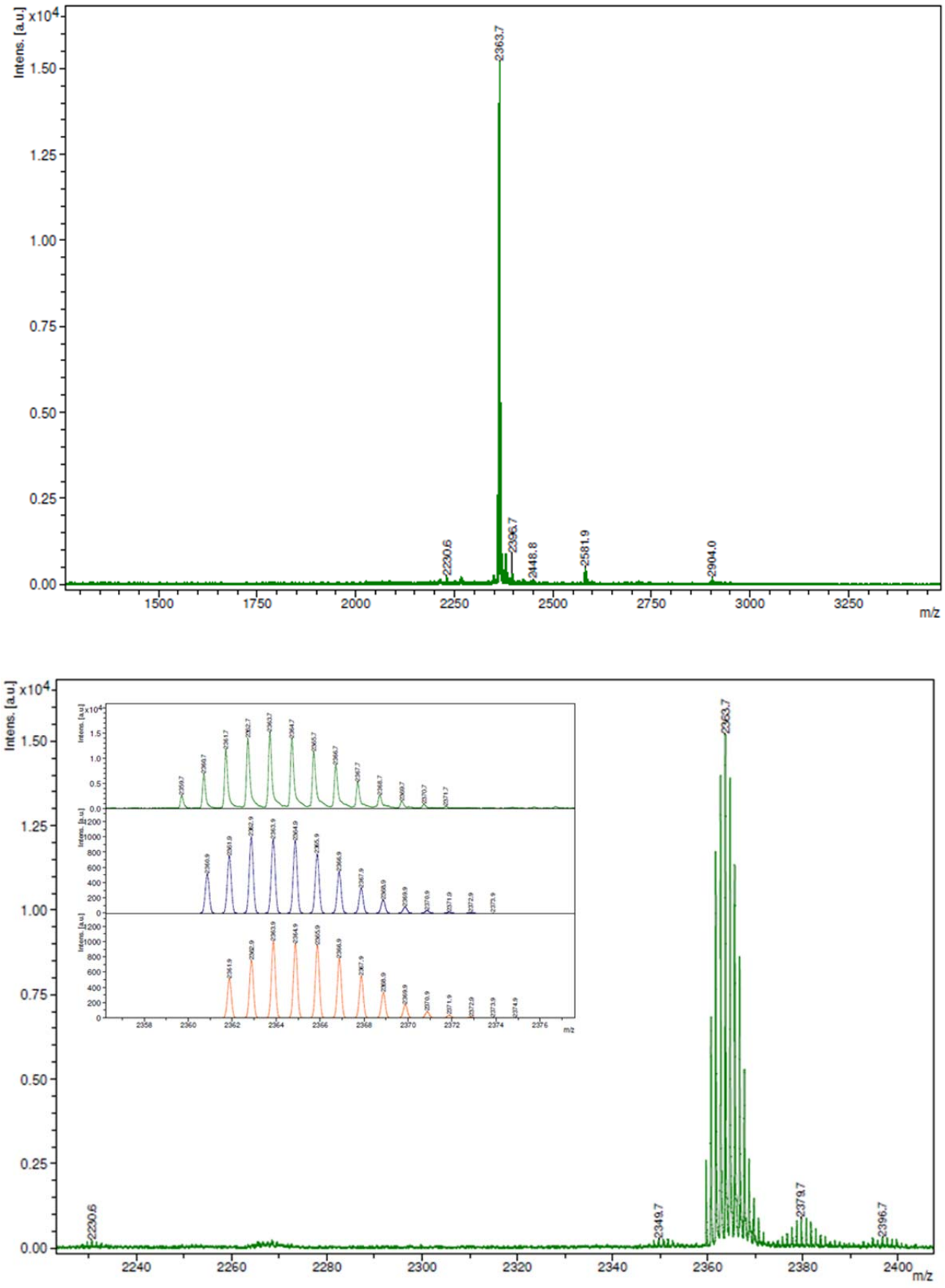

Figure 2. MALDI-TOF spectrum of dyad **29a.**

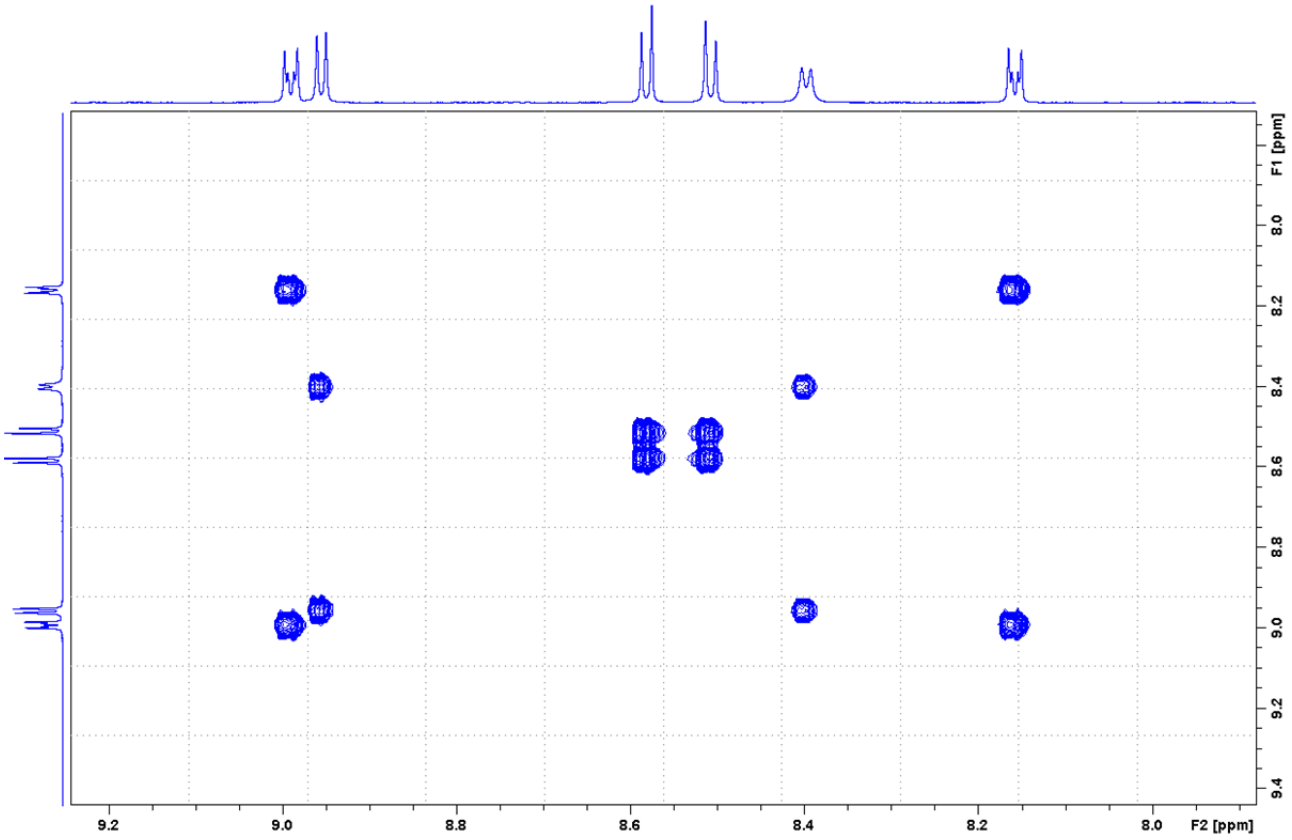

Figure 3. COSY spectrum of corrole **29** (focus on the β-pyrrolic signals).

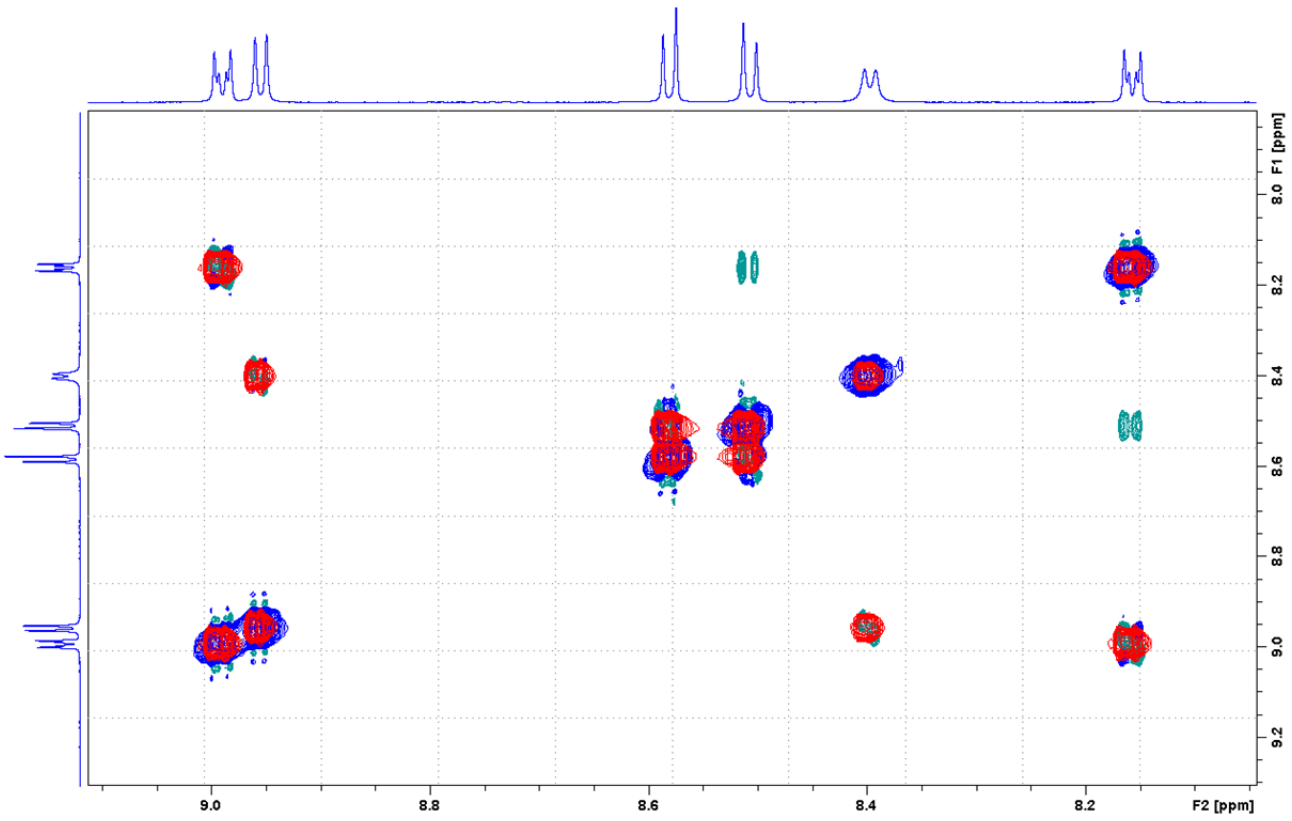

Figure 4. Overlapping of COSY and ROESY spectra of corrole **29** (focus on the β-pyrrolic signals)

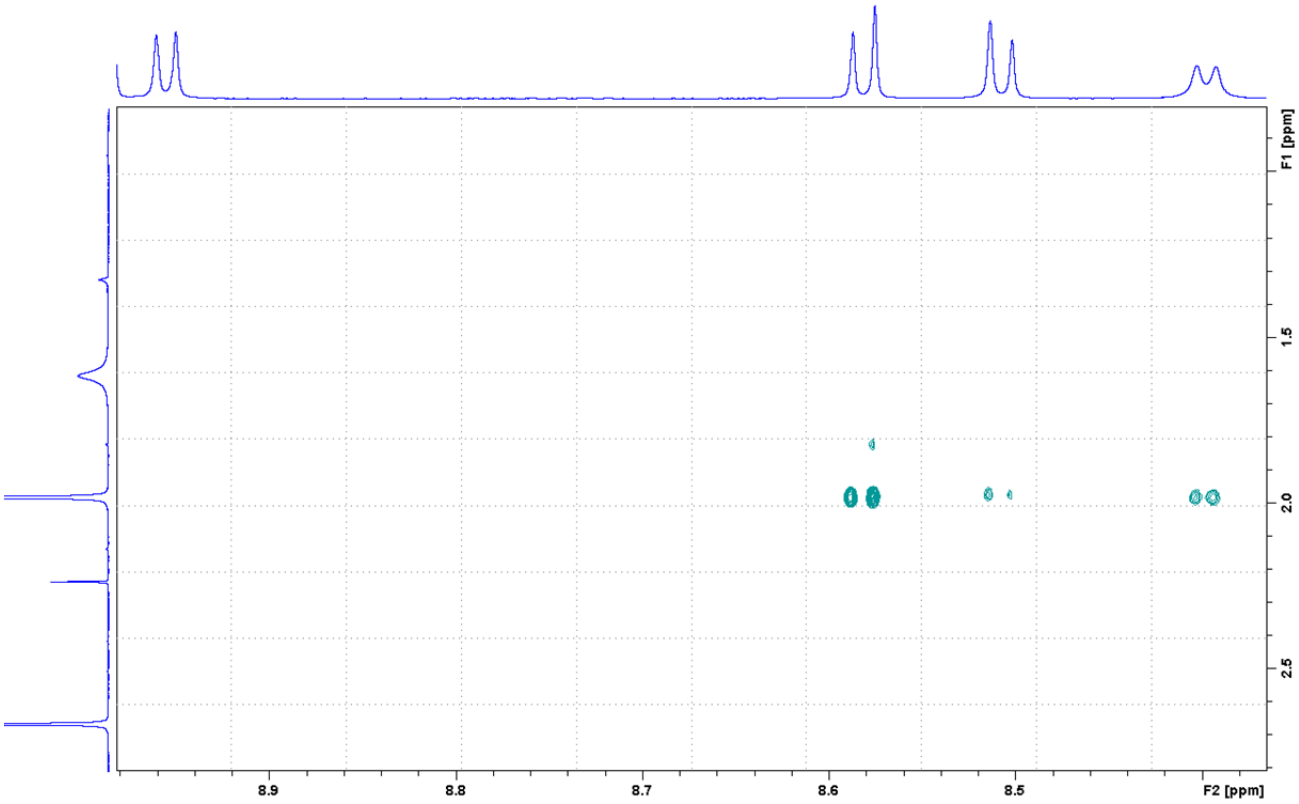

Figure 5. ROESY spectrum of corrole **29** (focus on the β-pyrrolic signals).

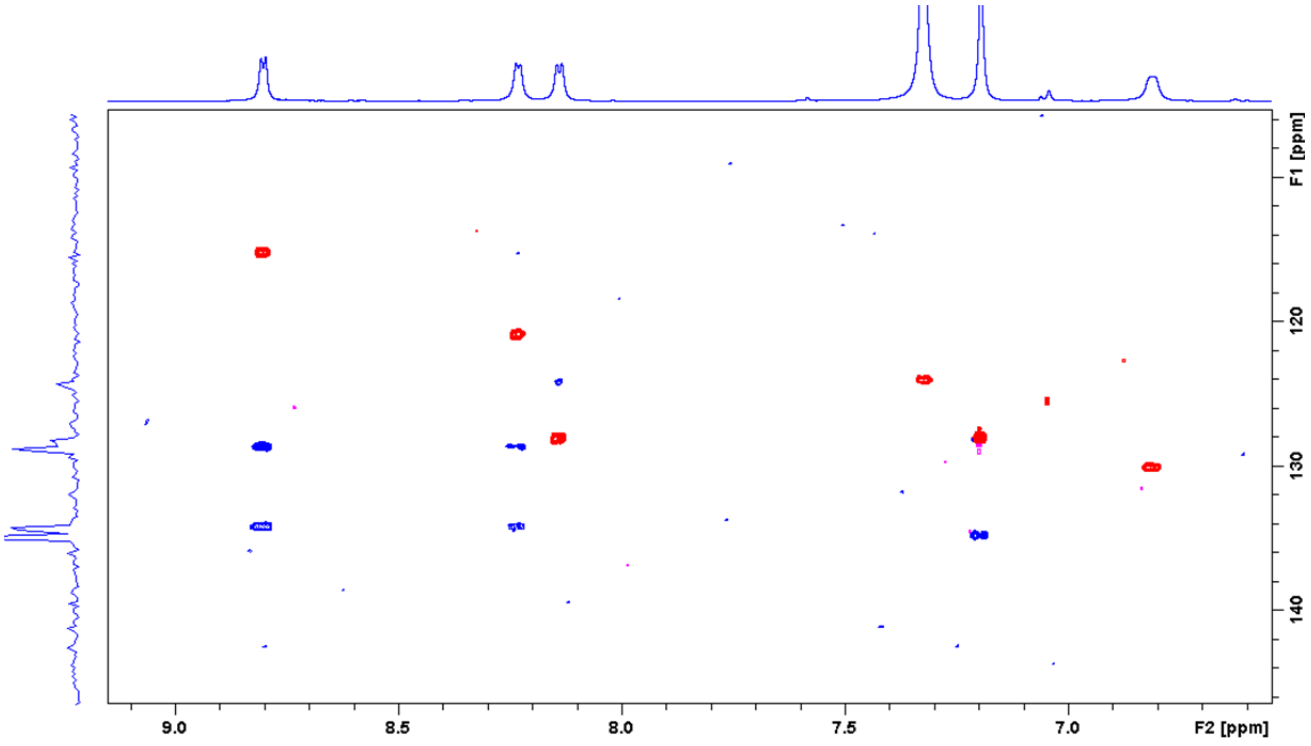

Figure 6. HSQC spectrum of complex **29/30** (focus on the *β*-pyrrolic signals).

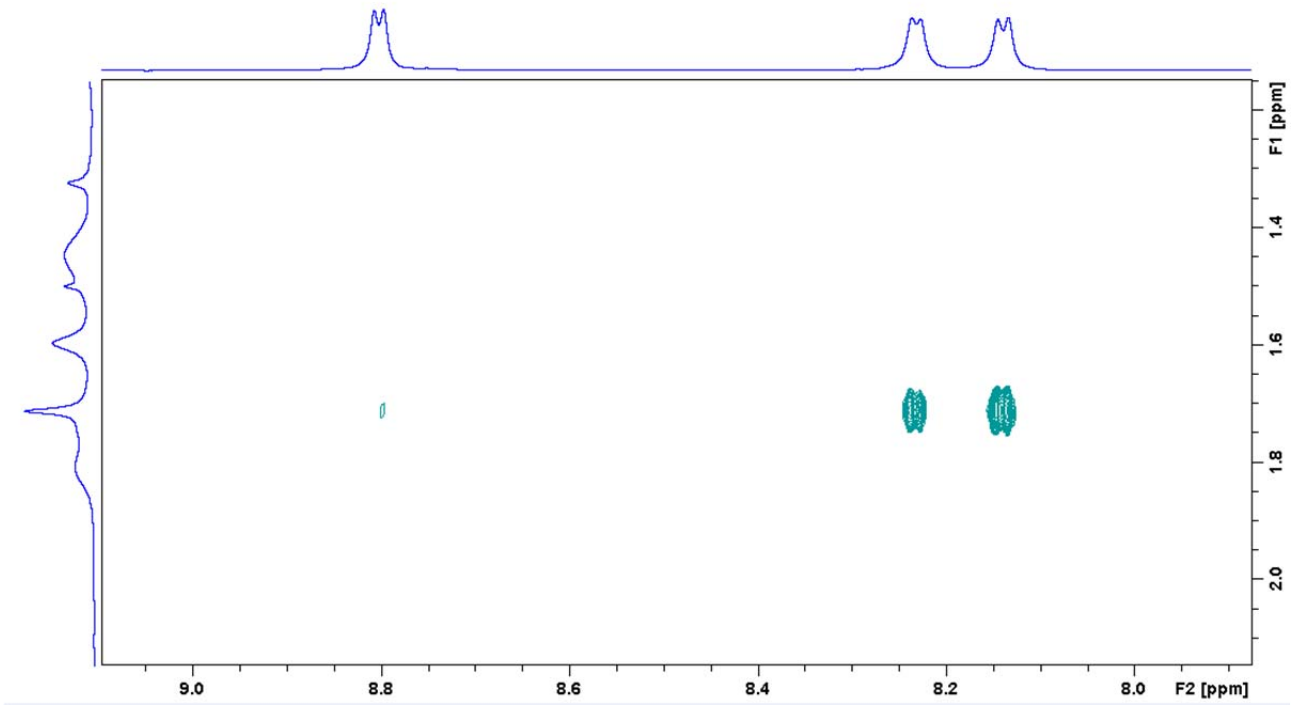

Figure 7. ROESY spectrum of complex **29/30** (focus on *β*-pyrrolic peaks).

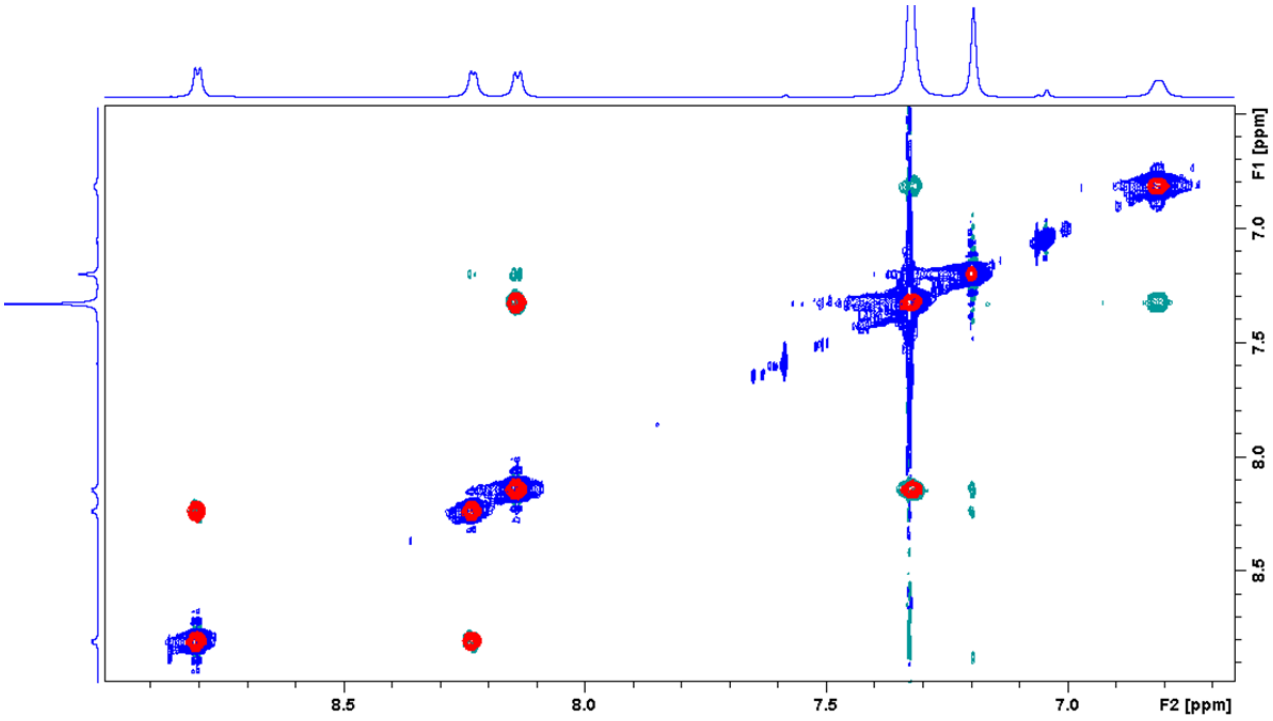

Figure 8. Overlapping of COSY and ROESY measurement of complex **29/30** (focus on β-pyrrolic peaks).

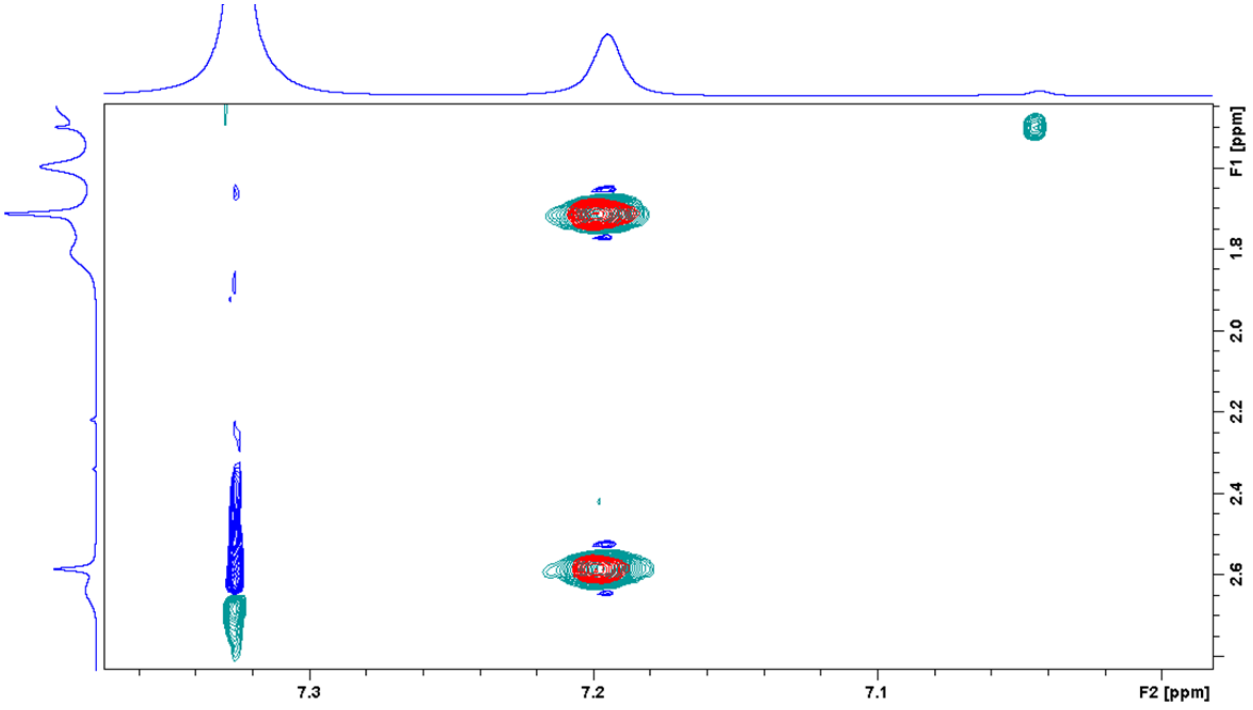

Figure 9. Overlapping of COSY and ROESY measurement of complex **29/30** (focus on aromatic mesityl peaks).